Chemistry of Transition Metal Fluoride Complexes

Ruqia Nazir

A thesis submitted for the degree of PhD

The University of York
Department of Chemistry

June 2012

ABSTRACT

Metal fluoride complexes that are extremely sensitive to air and water have been characterized by liquid injection field desorption/ionization (LIFDI) mass spectrometry. Dilute solutions of fluoride complexes of nickel, rhodium, titanium, zirconium, hafnium and ruthenium in toluene and tetrahydrofuran were examined by LIFDI methods on a time-of-flight mass spectrometer. All the spectra of nickel, titanium zirconium and hafnium complexes exhibited the molecular ion as base peak. The ruthenium and rhodium complexes showed $[M\text{-}HF]^+$ as base peaks but the molecular ions were easily detected.

Two new nickel fluoride complexes are formed by C-F activation reactions with 2,3,5,6-tetrafluoro-4-dimethylaminopyridine and 2,3,5,6-tetrafluoro-4-methoxypyridine yielding $NiF\{2\text{-}C_5NF_3(4\text{-}NMe_2)\}(PEt_3)_2$ and $NiF\{2\text{-}C_5NF_3(4\text{-}OMe)\}(PEt_3)_2$, respectively. The crystal structure of $NiF\{2\text{-}C_5NF_3(4\text{-}NMe_2)\}(PEt_3)_2$ shows typical square planar coordination at nickel with an Ni-F distance of 1.8521(9) Å. $(Cp^*)_2MF_2$ (Cp* = pentamethylcyclopentadienyl and M = Ti, Zr, Hf) complexes were synthesized from the reaction corresponding metal dichloride with NaF. $(DMEA)_2MF_2$ (DMEA = N,N-dimethylethylene-1,2-diamine and M= Zn, Co, Ni) were synthesized from the reaction of MF_2 with DMEA. $Ru(PMe_3)_4F_2$ was prepared from the reaction of $Ru(PMe_3)_4(FHF)_2$ with TMAF. The compounds were characterized by multinuclear NMR spectroscopy and LIFDI mass spectrometry.

The nickel monofluoride complexes do not provide useful mass spectra by EI or ESI methods. Only the difluoride complexes of titanium, zirconium, hafnium, ruthenium, zinc, cobalt and nickel species showed evidence of the fluoride ligands in the ESI spectra. Collision induced dissociation (CID) was used to investigate the fragmentation pattern of the ions formed in the ESI mass spectrum. It was observed that the ligand attached to the metal has an effect on the fragmentation pattern of complex and the presence of phosphine strengthens the metal fluoride bond.

A modified quadrupole mass spectrometer was used to carry out gas phase ion molecule (I-M) reaction of metal ions with liquid and gaseous neutral molecule. Transition metal fluoride complexes did not show evidence of I-M reactions while Re and Mn tricarbonyl complexes have shown 100% conversion to the product.

The decay pathway of multiply charged anions (MCAs) of Ti and Zr was also investigated and it was found that these ions decay through ionic fragmentation rather than electron detachment.

Hydrogen bonding of pentamethyl cyclopentadienyl difluoride complexes of Ti and Zr with indole and 1,1,1,3,3,3 hexafluoroisopropanol was studied using ^{19}F NMR spectroscopy. ΔS° and ΔH° were calculated from the equilibrium constant values (K) using Van't Hoff's equation.

TABLE OF CONTENTS

LIST OF FIGURES

Chapter 1

Chapter 2

Chapter 3

Chapter 4

Chapter 5

Chapter 6

LIST OF TABLES

ACKNOWLEDGEMENTS

I am very thankful to my supervisor Professor Robin Perutz for his guidance, encouragement and support thoughout my work. I would also like to thank to Dr Carroline Dessent for her advice and cooperation. I would especially acknowledge to Dr Naser Jasim who helped me a lot during experimental work.

A special thanks to Dr Ed Bergstrom, Dr Karl Heaton and Dr Trevor Dransfield for their help with the mass spectrometry. Thanks to Heather Fish for training and help with NMR experiments, Adrian. C. Whitwood for X-ray crystallography and Graeme Mcallister for CHN analysis. I will also thank to members of technical and workshop staff for providing an excellent service. Thanks to my lab fellows Barbara Procacci, Dr Olga Torres, Marius Câmpian, Dr Jacob Schneider, Dr Torsten Beweries, Christopher Windle, and David Taylor for their help and support through out my work.

Special acknowledgement goes to my husband Muslim Khan for being very patient and cooperative during all my PhD time. I am also very thankful to my family without their encouragement and support it would not be possible to complete my work successfully. I would like to acknowledge that all my higher education was the dream of my father (late) and I always got inspiration from his love and being very kind to me.

I am very grateful to Kohat University of Science and Technology, the Wild Fund of the University of York and EPSRC for financial support.

AUTHOR'S DECLARATION

I hereby declare that this is a true copy of my thesis and to the best of my knowledge it is my original work or otherwise acknowledged within the text. The work described in this thesis was carried out at the University of York and has not been submitted to any university for a degree.

Ruqia Nazir

June 2012

Dedicated to my family

INTRODUCTION

The research area of transition metal fluoride complexes has greatly developed during the last few decades. The characterization of transition metal fluoride complexes with mass spectrometry is of current interest because in the gas phase intrinsic properties and reactivity of ions can be studied without the influence of other factors like solvent or counter ions.

This chapter will be focussed on the synthesis, characterization and applications of transition metal fluoride complexes (1.1-1.3), different ionization techniques in mass spectrometry and use of these techniques for the characterization of transition metal halides, mass analysers and their applications (1.4), multiply charged anions and their fragmentation pathways (1.5), transition metal fluoride complexes as hydrogen and halogen bond acceptors (1.6).

1.1 Transition metal fluoride complex

Fluorine has become of great importance after the realization that fluorine containing compounds have many applications in everyday life like crop protection, non-stick cookware, refrigeration, textiles and toothpaste etc. About 30% of agrochemical compounds and 10% of pharmaceutical compounds are composed of fluorine containing compounds.[1-3]

The first reaction involving the formation of a C–F bond was reported in 1830s. During the last few decades considerable attention was paid not only towards the coordination and activation of C–F bonds at the metal centre but also towards their selectivity.[1,4] Several reviews have been devoted to the formation of C–F bonds.[5,6]

The fluorinated alkene can coordinate to metal through the double bond (C=C) and fluorinated arenes can bind by η^6-, η^4- and η^2- coordination.

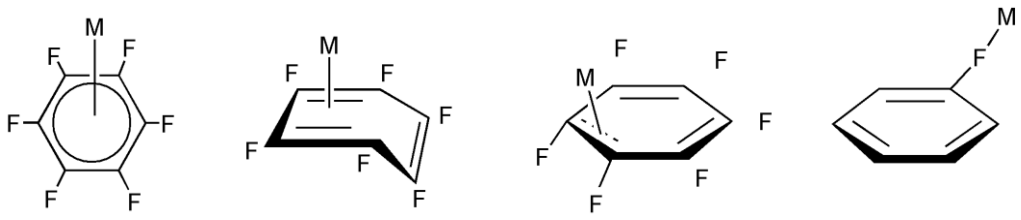

η^6 η^4 η^2

Scheme 1. 1 Coordination of the fluorinated arenes to the metal centre[4]

The C–F bond activation involves the following fundamental processes.[4]

(i) Oxidative addition

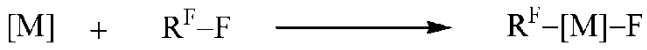

(ii) M-C bond formation and HF elimination

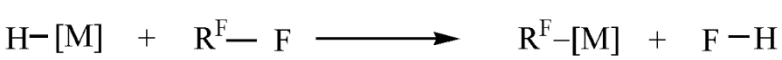

(iii) M-C bond formation and SiF bond elimination

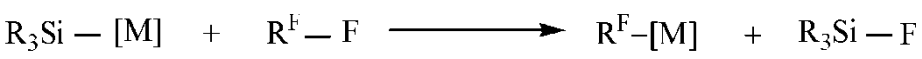

(iv)Hydrofluorination and M-F bond formation

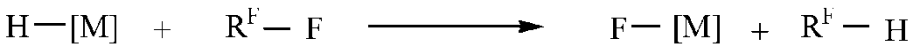

(v) Nucleophilic attack

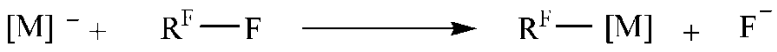

(vi)Defluorination

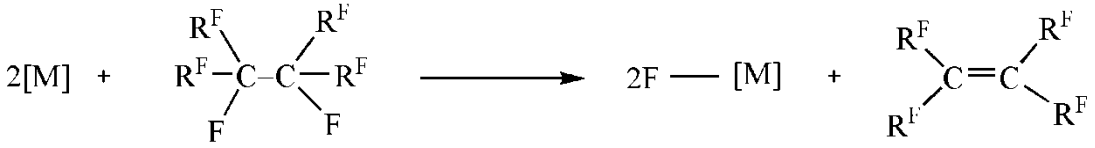

Activation of C–F bonds by metal complexes is selective, employing mild conditions (eq 1.1) and gives isolable products. Stone and co-workers activated a C–F bond using the d^0 metal complex.[7,8]

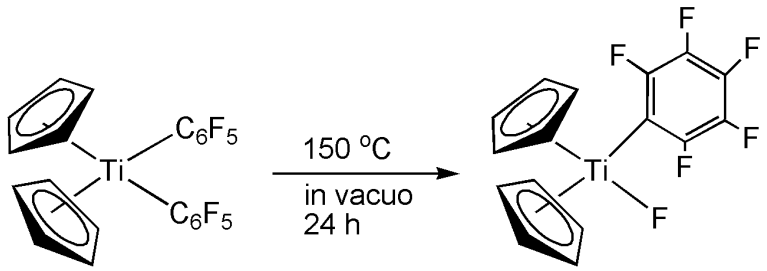

---------- 1.1

Zirconocene difluoride and alkylmonofluoride complexes have been synthesized from zirconocene dimethyl complexes using NH_4BF_4 and $NEt_3.3HF$ as fluorinating agents (eq 1.2).[9]

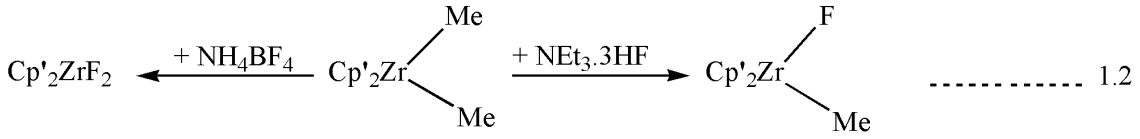

1.2

$Cp'_2 = Me_2Si(\eta^5\text{-}C_9H_{10})_2$

Zirconocene difluoride complexes were prepared from zirconocene 2-vinylpyridine complexes by acidolysis reaction using HBF_4 etherate as a fluorinating but the reproducibility was low. NEt_3.3HF proved to be a better reagent and can also give the monofluoride complexes like Cp`$_2$Zr(F)(CH_2CH_2-2-Py) if used in careful stoichiometric amounts (reaction 1.4). 2-vinylpyridine complexes were prepared from bis (trimethylsilyl)acetylene complexes which in turn were prepared from the dichloride complex (reaction 1.3).[9]

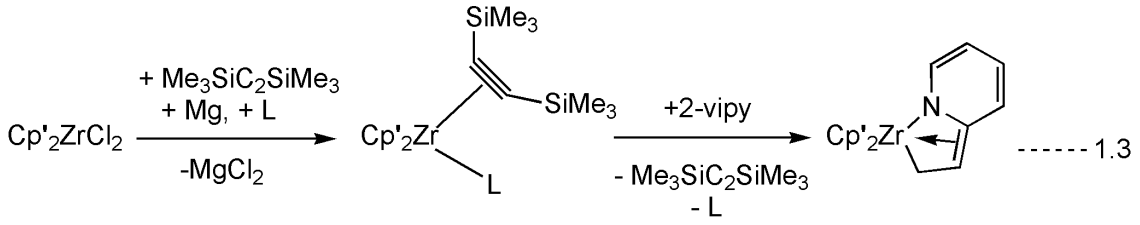

1.3

$Cp'_2 = Me_2Si(\eta^5\text{-}C_5H_4)_2$
L = THF

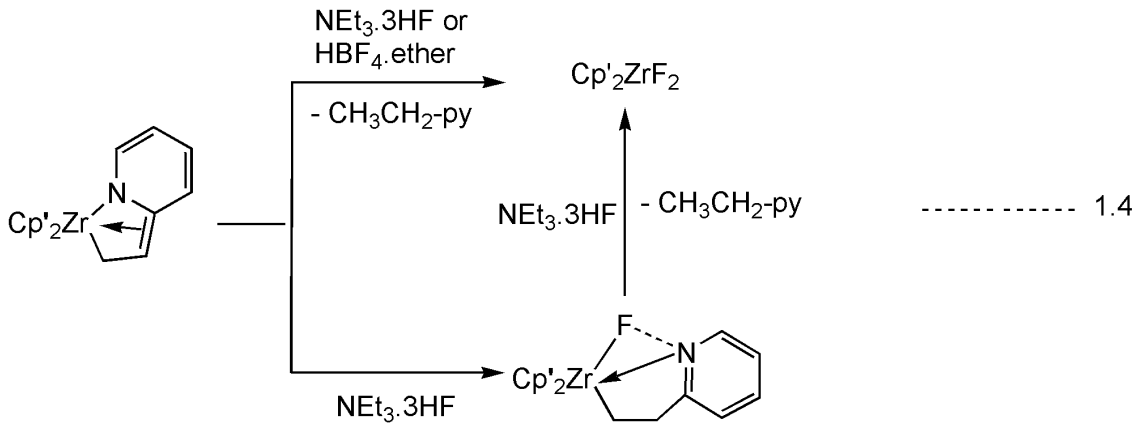

1.4

Perutz et al. studied the effect of metal centre on the C–F and C–H activation. It was observed that perfluorinated arenes undergo C–F bond activation at the metal centre (Scheme 1. 2). Depending upon the metal centre, competition occurs between C–H and C–F activation upon addition of partially fluorinated arenes and pyridine.[10-12]

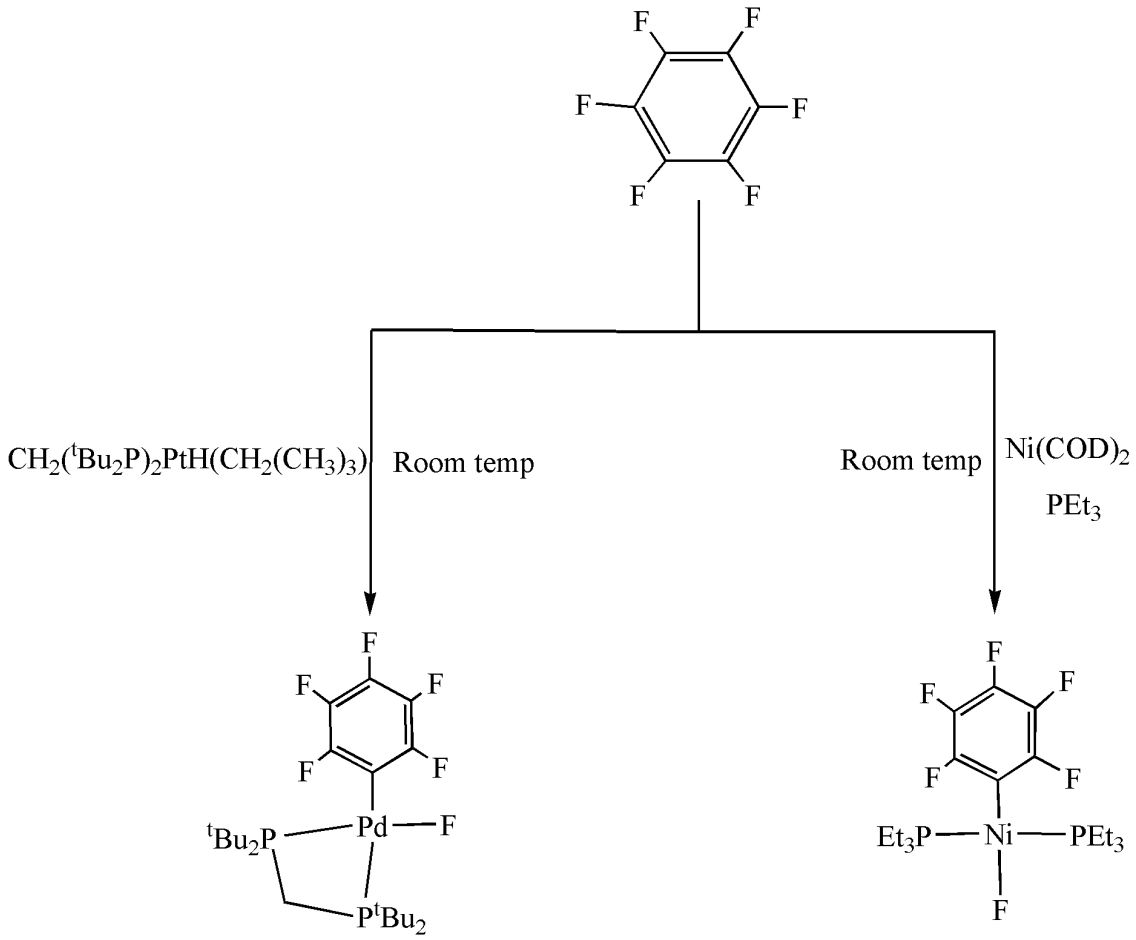

Scheme 1. 2 Reactivity of Ni^0 and Pt^0 Precursor towards C_6F_6[10,12]

The addition of fluorinated pyridines to the Ni^0 occurs through C–F activation at the position ortho to the nitrogen. The addition of fluorinated pyridine and arenes occur through η^2 coordination before oxidative addition. Palladium behaves in a similar way but it is activated at the para position to nitrogen. Fluoropyridines behave differently with $Pt(PR_3)_2$. Instead of C–F activation there is rearrangement between fluorine and the alkyl group (Scheme 1. 3).[11,12]

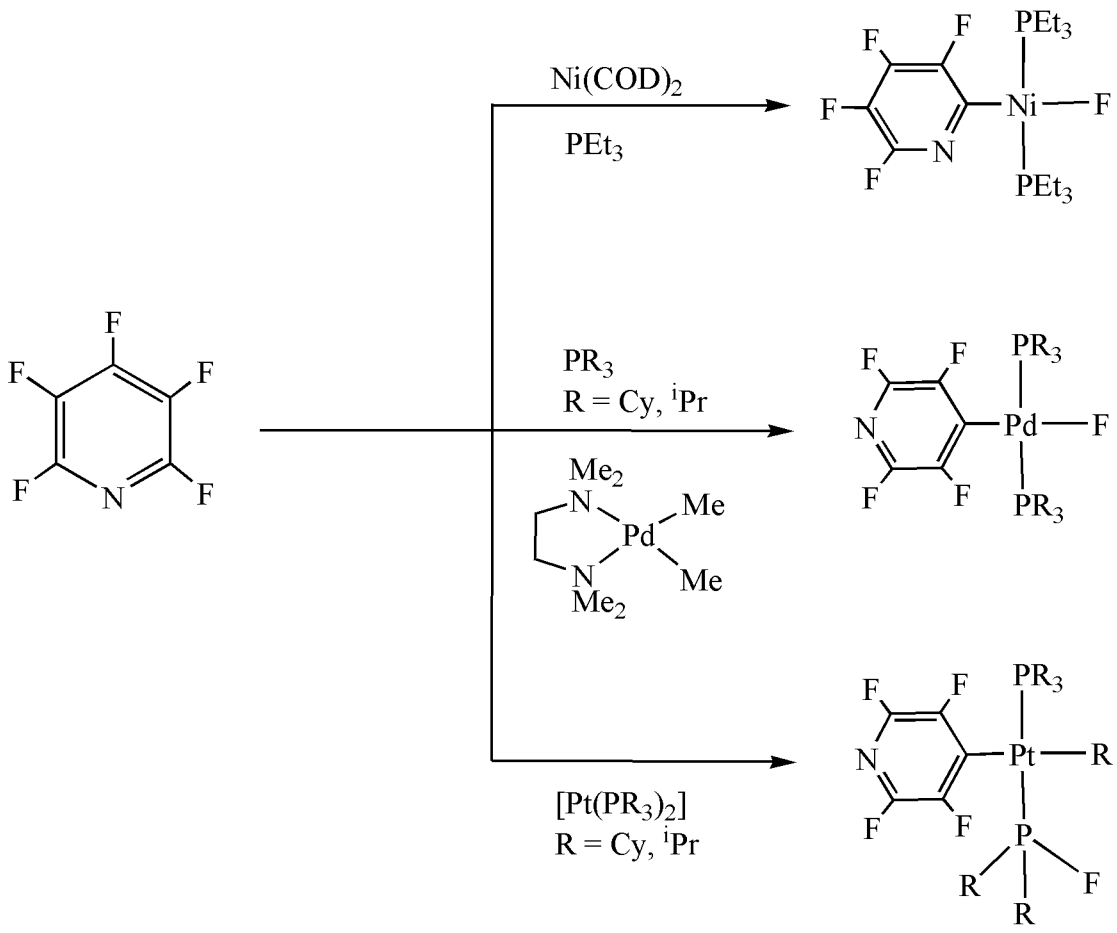

Scheme 1. 3 Activation of C-F during the addition of fluorinated pyridine to the Ni^0 and C-H bond activation at $Pt(PR_3)$ with pentafluoropyridine[12]

More attention was paid towards the metal-mediated formation of C–F bonds. Vigalok et al. investigated electrophilic oxidative fluorination reactions upon treatment of the late transition metals with fluorinating reagents.[13-15] $(R_2P(CH_2)_nPR_2)M(Ar)_2$ (where R= alkyl, aryl, n= 2, 3, M= Pd, Pt) were reacted with XeF_2 and metal difluoride complexes were obtained (Fig 1. 1).[13] Electrophile fluorinating reagents such as XeF_2, F_2, or halogen fluoride can be used for the metal mediated C-F transformation reaction.[15]

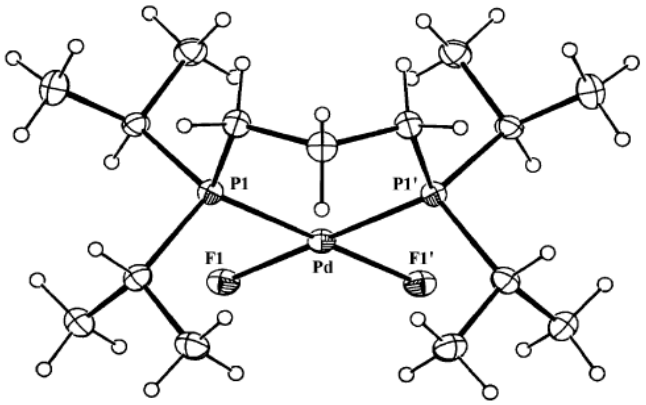

Fig 1. 1 Crystal structure of di(*i*-propylphosphino)propane palladium difluoride[13]

In order to see the intermediates involved in the above reaction, the platinum diaryl precursor was modified by making one of the aryl groups a part of a five-membered chelate ring (Scheme 1. 4).

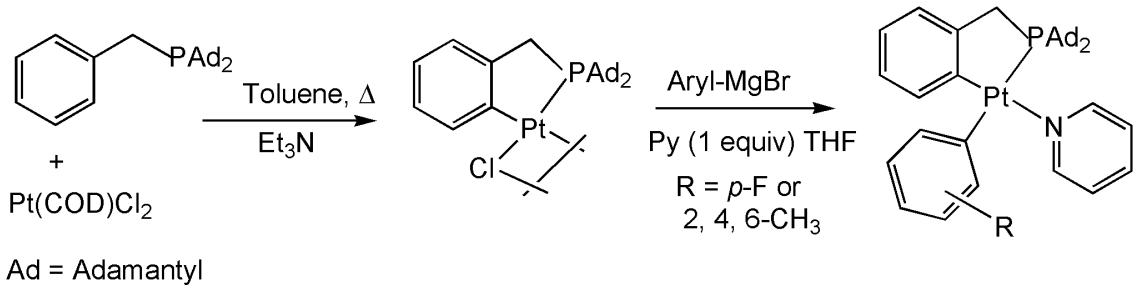

Scheme 1. 4 Synthesis of Pt diaryl precursor

The Pt diaryl precursor was reacted with XeF_2 (used as electrophilic fluorinating agent) to give the platinum difluoride product which is well characterized by NMR and X-ray crystallography. One of the fluorides from the platinum difluoride was removed by Me_3Si-OTf led to C-C coupling followed by ligand rotation and cyclometalation and the other fluorine ligand eliminated as HF. The same product was obtained by reacting the Pt (II) precursor with *N*-fluoro-2,4,6-trimethylpyridinium tetrafluoroborate followed by addition of pyridine or PPh_3 (Scheme 1. 5). It is concluded that these complexes go through the formation of Pt(IV) species followed by reductive elimination. This can be used for designing catalytic process using electrophilic fluorinating agents.[14]

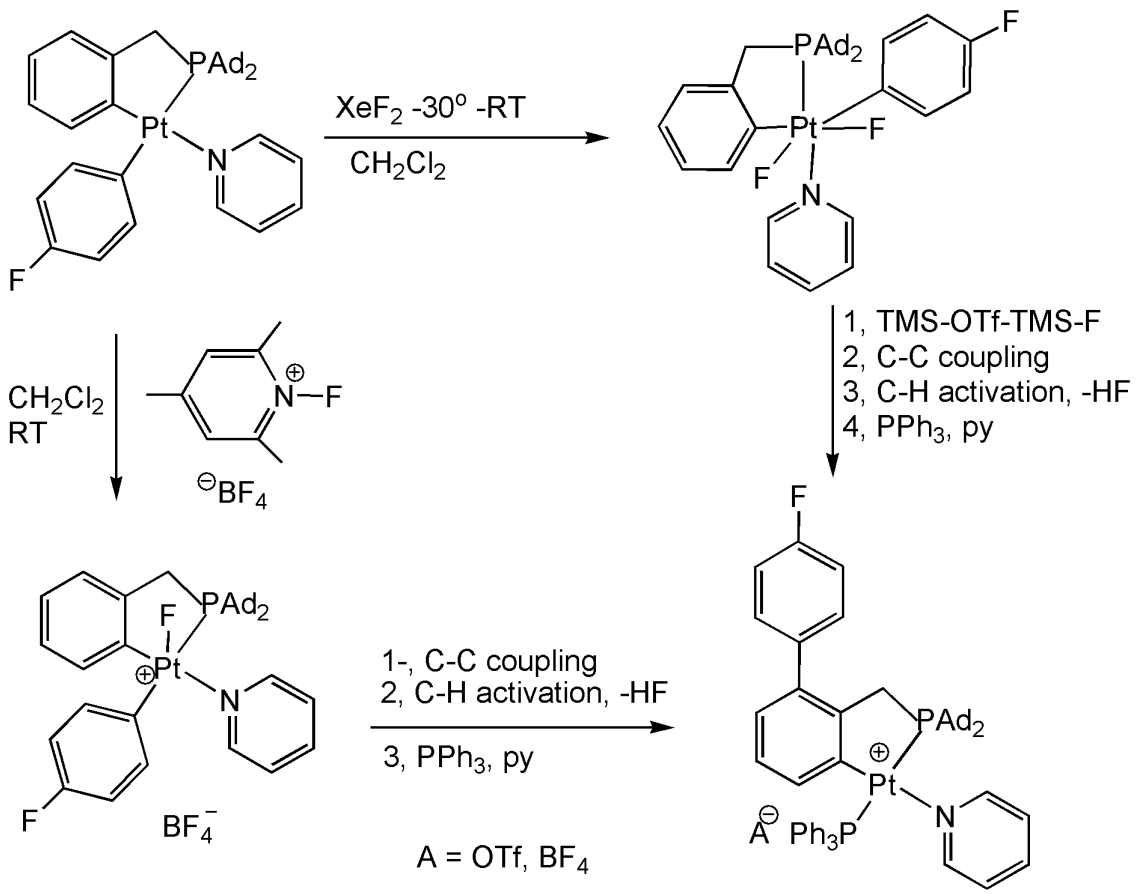

Scheme 1. 5 Electrophilic Fluorination of cyclometalated Pt (II) Aryl Complexes[14]

Further more research has concentrated upon the C-F bond forming reductive elimination in the last decade. The palladium catalysed reaction of electrophilic fluorinating reagents causing C-F bond formation by reductive elimination involves the formation of Pd^{IV} alkyl/aryl intermediates. The Pd^{IV} alkyl fluoride species was observed directly in the system using a cyclometalated bipyridine-Pd^{II} complex as a precursor. The reaction of the precursor with the electrophilic fluorinating agent N-fluoro-2,4,6-trimethylpyridinium triflate resulted in formation of the Pd^{IV} complex (b). The triflate ligand is very labile and can be easily displaced by water or pyridine. The difluoride complex is obtained by reaction of the monofluoride complex with tetramethylammonium fluoride.[16]

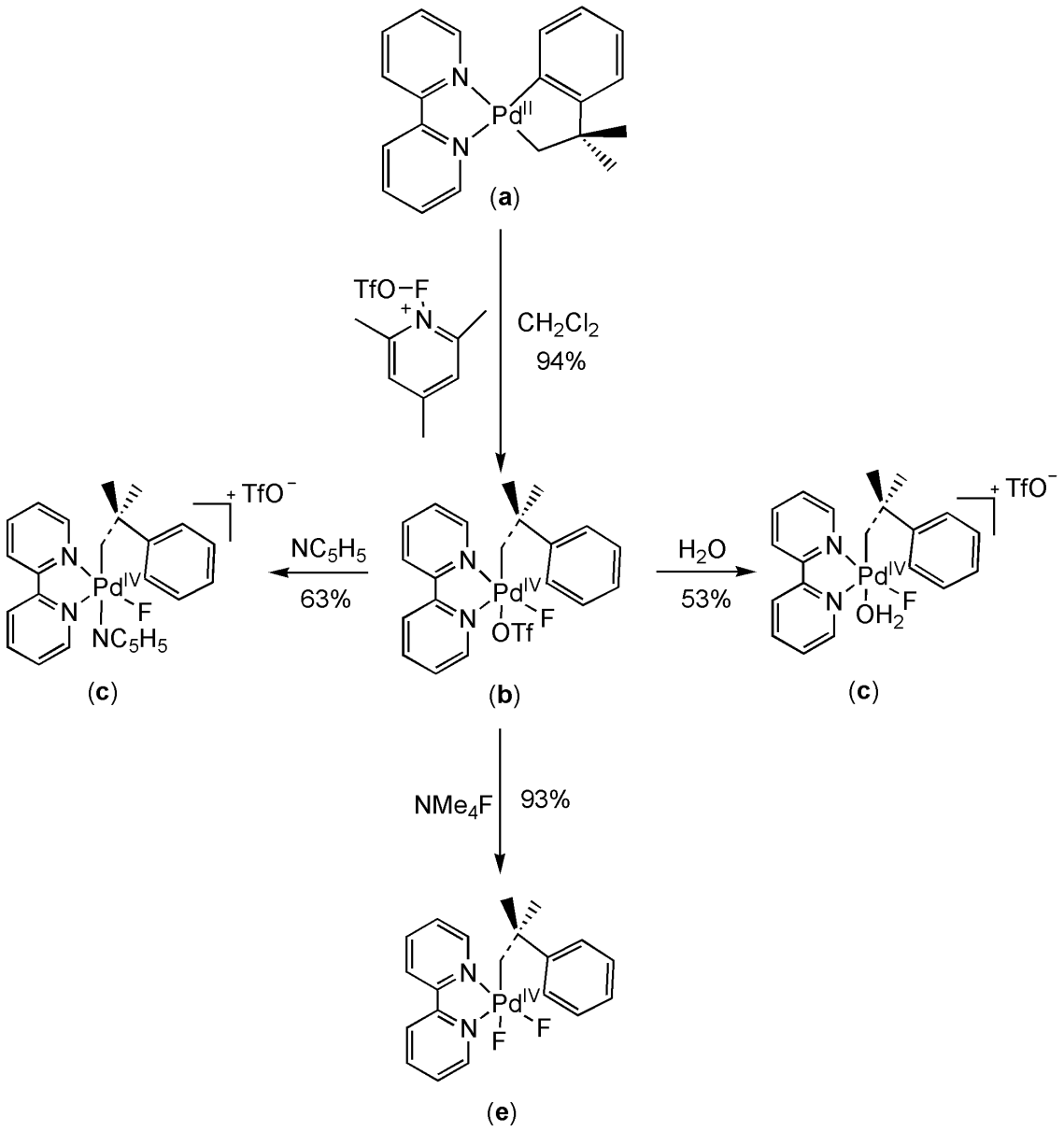

Scheme 1. 6 Synthesis of Pd^{IV} monofluoride and difluoride complexes[16]

Many transition metal fluoride complexes which are of critical importance in the field of agrochemicals and pharmaceuticals have been synthesized using different fluorinating reagents. The scheme 1.7(a) lists important nucleophilic fluorinating reagents.[17]

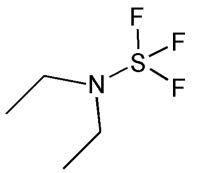

Diethylaminosulfur trifluoride
DAST

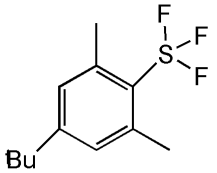

4-tert-butyl-2,6-dimethylphenylsulfur trifluoride

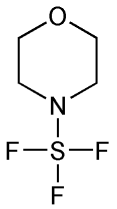

Morpholinosulfur trifluoride

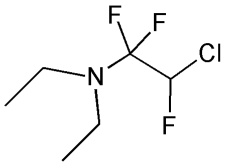

N,N-Diethyl-2-chloro-1,1,2-trifluoroethylamine

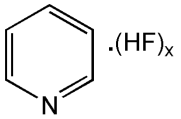

Hydrogen fluoride pyridine

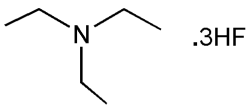

Triethylamine trihydrofluoride

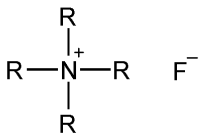

Tetraalkylammonium fluoride
TMAF

KF

Potassium fluoride

NaF

Sodium fluoride

CsF

Cesium fluoride

AgF

Silver fluoride

Scheme 1. 7 (a) List of nucleophilic fluorinating reagents[18,21]

Currently electrophlic fluorinating reagents have received great importance. Following is the list of electrophilic fluorinating reagents.[16,18-20]

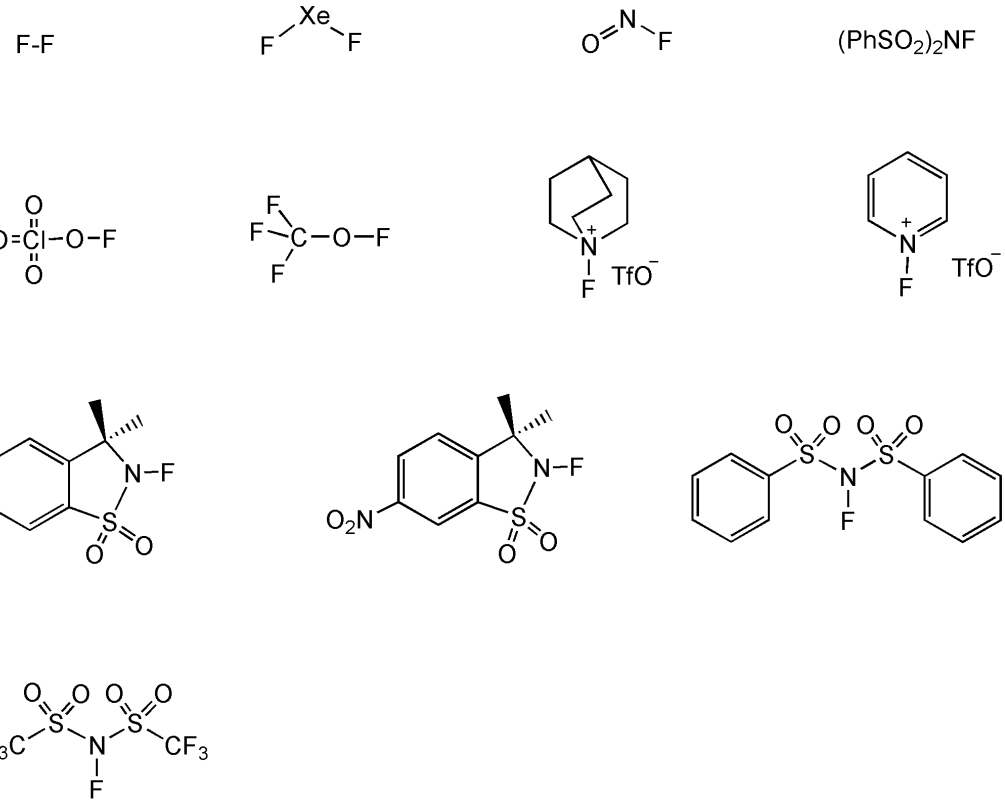

Scheme 1. 8 (b) List of electrophilic or oxidizing fluorinating reagents[18,21]

1.2 Anhydrous HF, bifluoride anion and bifluoride complexes

Anhydrous HF has proved to be a versatile solvent. It can be used to do many inorganic reactions. Sometimes it as used as a source of ligand for the synthesis of organofluorine complexes.[22,23] It is has also been used as a solvent and catalyst with Friedel-Craft activity. Silver forms complexes with arenes in anhydrous HF.[23-25] XeF_2 in anhydrous HF has been used for the oxidative fluorination of metal carbonyls. $Os(CO)_5F$ has been prepared as a major product from the reaction of $Os_3(CO)_{12}$ with XeF_2 in anhydrous HF. This method is expensive and difficult to control. [26,27]

$$Os_3(CO)_{12} + XeF_2 \xrightarrow{\text{anhydrous HF}} \underset{\text{Major}}{Os(CO)_5F^+} + \underset{\text{minor}}{Os_2(CO)_7F_3^+} + \underset{\text{minor}}{Os_2(CO)_8F_4^+}$$

Elemental fluorine in anhydrous HF has also been used as a source of fluorination for the synthesis of $[MF(\mu\text{–}F)(CO)_3]$ where M= Os, Ru. This method is convenient and gives clean product.[28] Iridium fluorocomplexes have been synthesized by the same method. $Ir_4(CO)_{12}$ was reacted with elemental fluorine in anhydrous HF which resulted in the formation of $Ir(CO)_3F_3$. Addition of phosphines to $Ir(CO)_3F_3$ in THF replaced the carbonyl ligands and gave $IrF_3(CO)L_2$ or $IrF(CO)L_2$.[29]

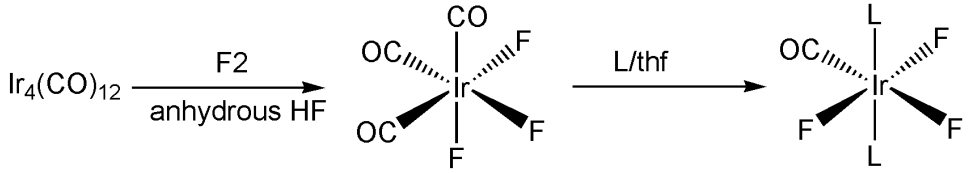

L = PPh_3, PMe_3, PEt_3, PMe_2Ph, $PMePh_2$, $PEtPh_2$, PCy_3

The bifluoride complexes came to be known a decade ago. In the free bifluoride ion, the hydrogen bonding is explained by a three-centre four electron interactions and is an example of the strongest type of hydrogen bonding.[30,31] A series of ruthenium bifluoride complexes including *trans*-$[Ru(depe)_2H(FHF)]$, *trans*-$[Ru(dppe)_2H(FHF)]$, *trans*-$[Ru(dppp)_2H(FHF)]$ and *cis*-$[Ru(PMe_3)_4(FHF)_2]$ (where depe = $Et_2PCH_2CH_2PEt_2$, dppe = $Ph_2PCH_2CH_2PPh_2$, dppp = $Ph_2PCH_2CH_2CH_2PPh_2$) were prepared by Perutz et al. from the corresponding dihydride complexes, using $Et_3N.3HF$ as a source of HF. These complexes were well characterized by NMR spectroscopy. ^{19}F NMR spectra showed resonances at ca. δ –300 for the proximal fluorine and ca. δ –165 distal fluorine. The spectra are obtained at low temperature because the resonances are broad at room temperature probably due to exchange with free HF in the solution. The

resonance for the acidic protons is at *ca.* δ 13. The value of the coupling constant (*J*) for the distal fluorine lies in the range 300–400 Hz.[32]

The NMR spectra of *trans*-[Ru(dppe)$_2$H(FHF)] are explained in more detail here. The acidic proton shows a broad resonance at δ 12.5-13.3 (room temperature) which splits into a doublet at low temperature (Fig 1. 2).[32]

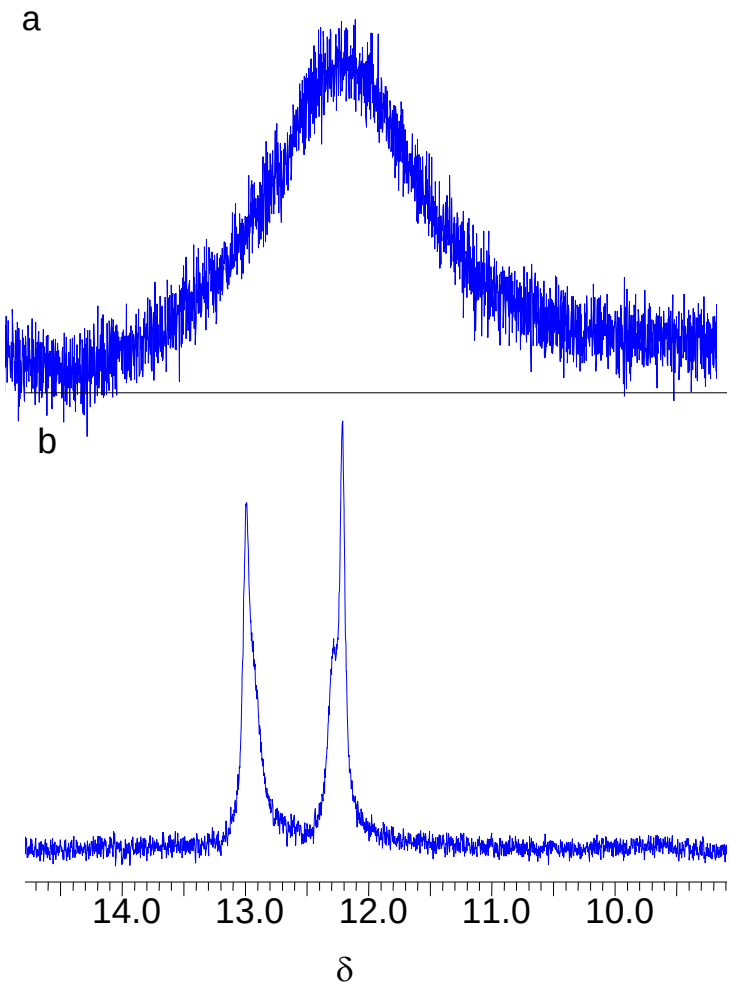

Fig 1. 2 ^{1}H NMR spectra (500.13 MHz) of the acidic region of [*trans*-Ru(dppe)$_2$H(FHF)] in deuterated THF (a) at room temperature (b) at 193 K.

The ^{19}F NMR spectrum shows a resonance for the proximal fluorine at −353 (Fig 1. 3) while another resonance at −166.5 to −168 splits into a doublet of doublets at low temperature (Fig 1. 4). The crystal structures for some of these compounds have also been obtained, providing further insight into these bifluoride complexes.

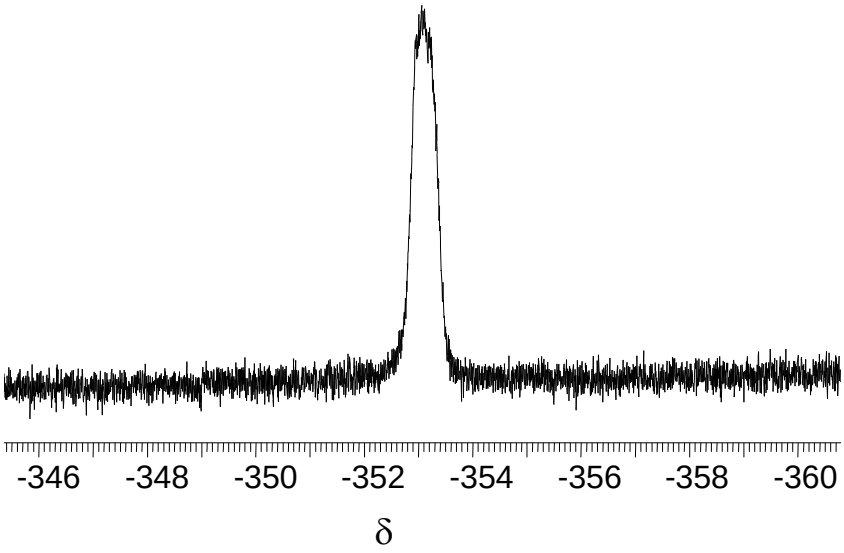

Fig 1. 3 ^{19}F NMR spectra (470.4 MHz) for *trans*-[Ru(dppe)$_2$H(FHF)] in deuterated THF at room temperature.

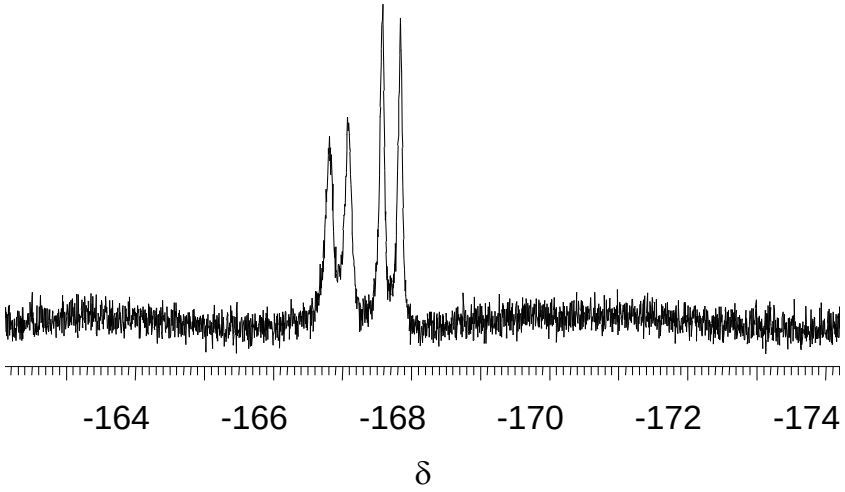

Fig 1. 4 ^{19}F NMR spectra (470.4 MHz) for *trans*-[Ru(dppe)$_2$H(FHF)] in deuterated THF showing the terminal fluorine at 193 K.

The fluoride bridged ruthenium dimers were synthesized by reacting the corresponding dihydride complexes of monophosphines with $Et_3N.3HF$.

$$cis\text{-}[RuH_2(PR_3)_4] + NEt_3.3HF \xrightarrow{THF} [Ru_2(\mu\text{-}F)_3(PR_3)_6][F(HF)_n] \text{ ------ } 1.5$$

R = Et, Pr and Bu

The crystals were obtained by reacting the bridged complex from the reaction of the compound with salts such as like NH_4OTf. The crystal structure showed that Ru–F distances in the range 2.132 – 2.170 Å which are longer that the terminally bonded fluoride and Ru–F–Ru angles in the range 91.72–93.02.

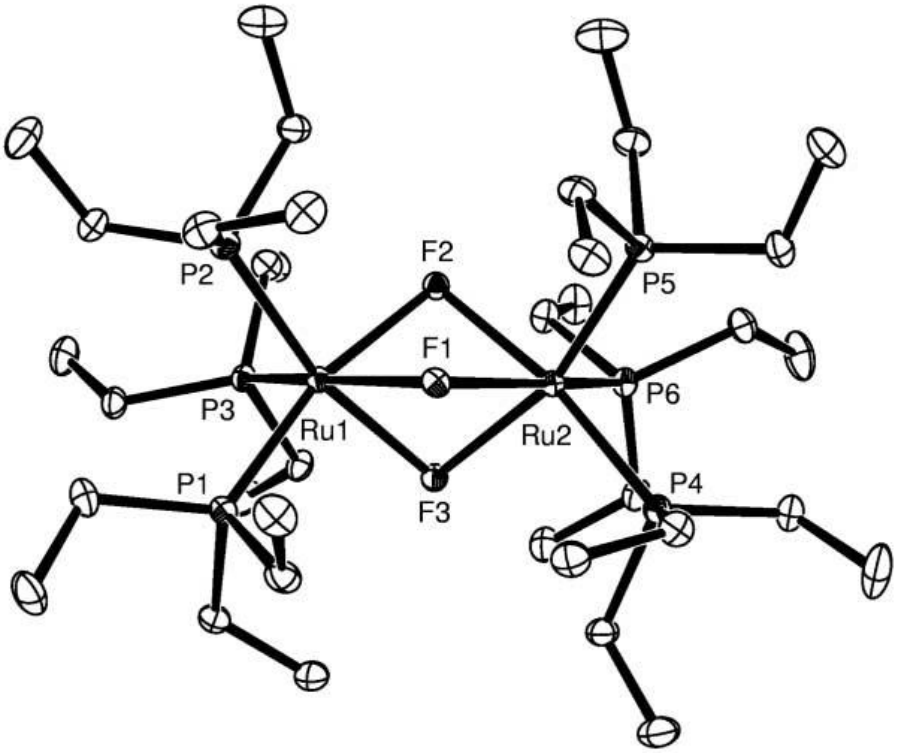

Fig 1. 5 Crystal structure of $[Ru_2(\mu\text{-}F)_3(PEt_3)_6]$. Ellipsoids are drawn at the 30% level.[33]

Platinum bifluoride complexes were prepared from the reaction of platinum dihydride with $Et_3N.3HF$ as well by C-F activation. *trans*-$[Pt(PR_3)_2H(FHF)]$ (R = Cy, iPr) was synthesized from the reaction of *trans*-$[Pt(PR_3)_2H_2$ with $Et_3N.3HF$ (equation 2.7). *trans*-$Pt(PR_3)_2H(FHF)]$ (R = Cy, iPr) was also obtained from the reaction of the dihydride complex with hexafluorobenzene in the presence of $[Me_4N]F$ by C–F activation. It was proved by control experiments that $[Me_4N]F$ is not directly involved in the reaction.[34]

$$\text{trans-Pt(PCy}_3)_2\text{H}_2 \xrightarrow[\text{THF/50 }^{o}\text{C}]{\text{C}_6\text{F}_6,\ \text{NMe}_4\text{F}} \text{trans-Pt(PCy}_3)_2\text{H(C}_6\text{F}_5) + \text{trans-Pt(PCy}_3)_2\text{H(FHF)} \quad \text{----- 1.6}$$

The nickel bifluoride complexes have been prepared from the nickel fluoride complexes. The NiF complexes have been prepared by C-F activation which in turn can coordinate with HF via hydrogen bonding.[35]

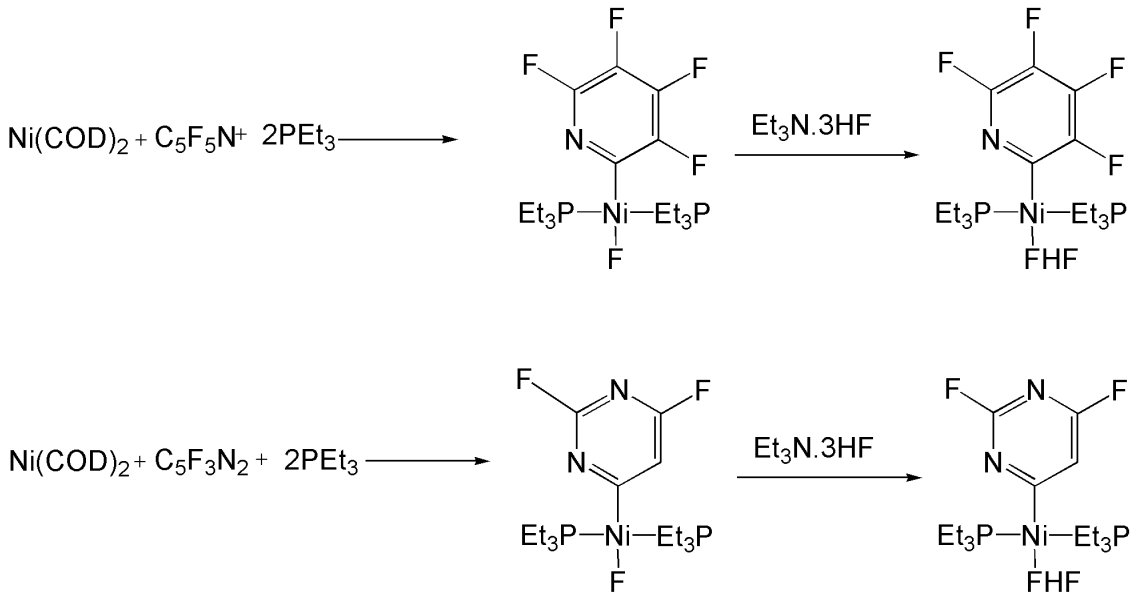

Scheme 1. 9 Formation of nickel bifluorides by C–F activation.[35]

1.3 Applications of transition metal fluoride complexes:

Organometallic fluoride complexes have many applications in synthesis and catalysis.

1. The synthesis of optically active, chiral catalysts is highly desirable. The efficiency of enantioselectivity is more difficult to achieve than the efficiency of the cycle. Titanium fluoride complexes can be used as catalysts for the addition of nucleophiles to aldehydes. Binaphtholtitanium difluoride has been used to catalyse the addition of allylsilane to aldehyde.[36]

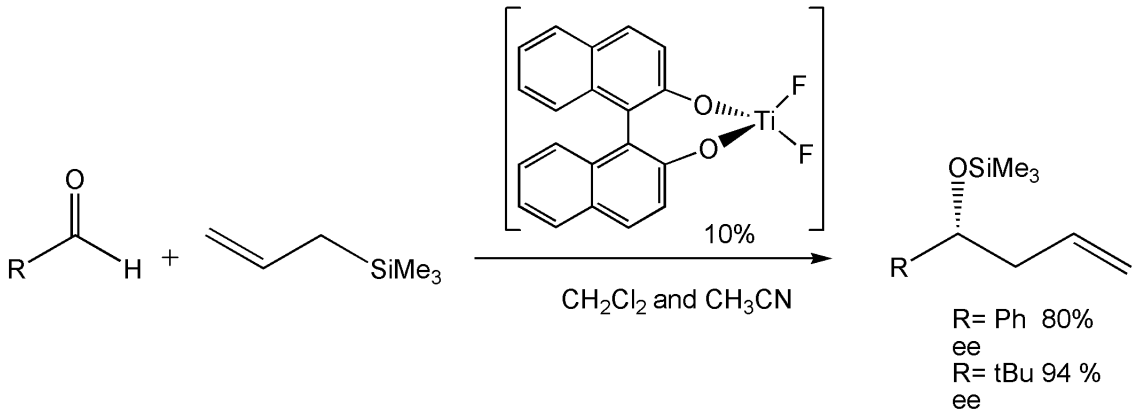

Similarly chiral dialkoxy cyclopentadienyltitanium fluorides possess catalytic properties for the conversion of benzaldehyde to 2-phenylethanol. At -78 ^{o}C using 2.0 mole of the catalyst, 77% of product is obtained with 90% ee.[36]

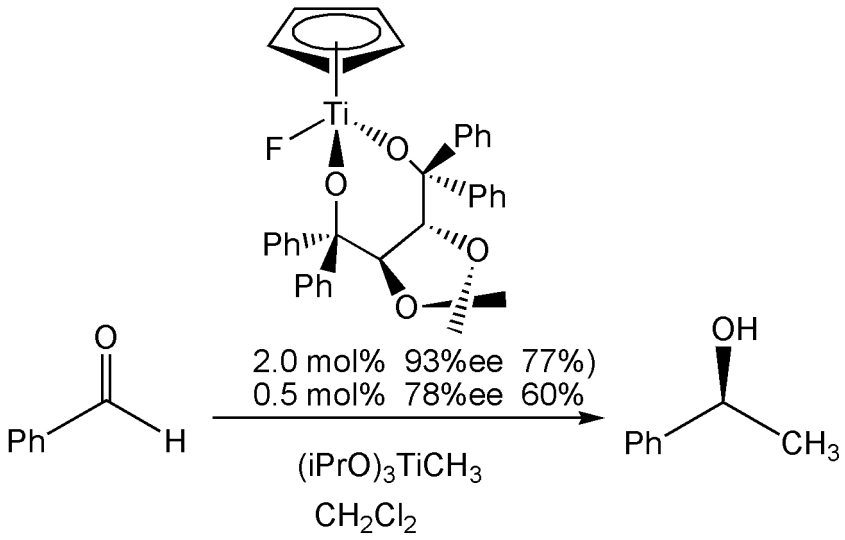

Scheme 1. 10 Synthesis of 2-phenylethanol from benzaldehyde using chiral titanium catalyst

2. Transition metal fluoride complexes also form hydrogen and halogen bonds which have lots of applications in supramolecular chemistry and crystal engineering.
3. Metallocene difluoride complexes of Ti and Zr can be used as catalysts for olefin polymerization, reduction of perfluorocarbons and transamination of group 4 fluorides.[37]
4. Alkylgold(III) fluoride complexes play an important role in Au(I)/Au(III) catalytic cycles resulting in the C(sp^3)–F reductive elimination. The relatively long lifetime of alkylgold(III) fluoride intermediates compared to their iodide analogues makes the C–C coupling possible.[38]

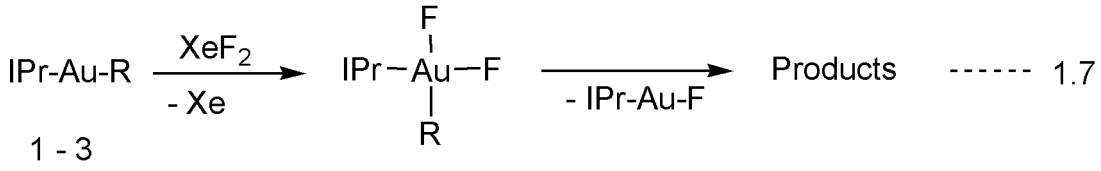

(IPr = 1,3-bis(2,6-diisopropylphenyl)imidazol-2-ylidene

The following table shows the products obtained with different R.

Number	R	Product mixture
1	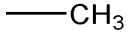	None
2	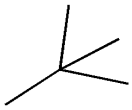	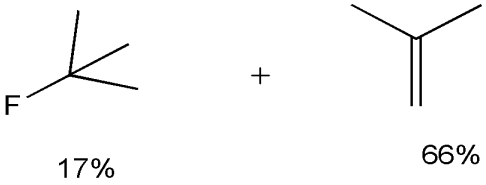 17% 66%
3	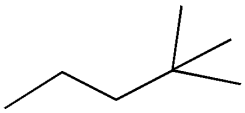	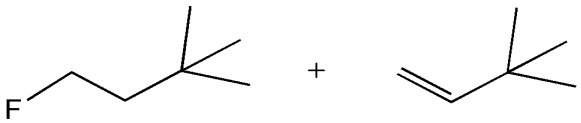 11% 56%

5. Synthesis of unactivated aryl halides: Vigalok used palladium (II) complexes to activate the unactivated aryl fluoride bond of fluoroquinoline by simply stirring with sodium methoxide in THF at room temperature.[39]
6. Fluorine containing compounds are mostly synthetic and have found many applications in the agrochemical and pharmaceutical industry. Transition metal fluorinating reagents are used in the catalysis of nucleophilic fluorination by transition metals.[17,20]
7. ^{18}F (an isotope of fluorine having half-life of 110 minutes) is used in Positron Emission Tomography (PET) imaging. Ritter et al. synthesized palladium based electrophilic fluorinating reagents which can be used to for the synthesis of ^{18}F labelled aryl fluoride through late stage of fluorination. This late stage fluorination can be used for the synthesis of PET tracers not available in the past for clinical use.[20]
8. Aryl fluorides can be selectively synthesized from thermolysis of palladium difluoride complexes in the presence of electrophilic fluorinating reagents (eq. 1.8).[40,41]

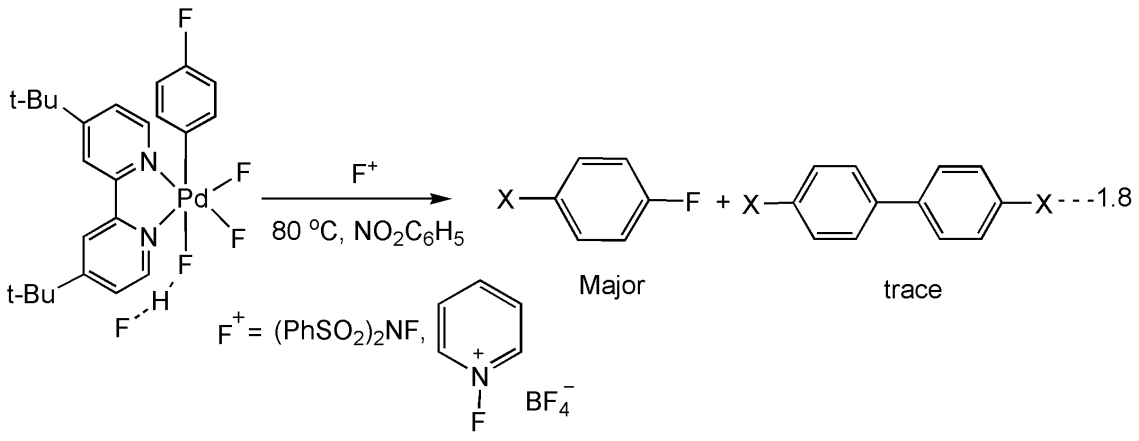

9. Iron and palladium catalysts have been used for the trifluoromethylation of potassium vinyltrifluoroborates[42] and vinyl sulfonates[43] and conversion of aryl triflates to aryl fluorides.[44]

1.4 Mass spectrometry

Mass spectrometry [45] is an analytical technique used to generate ions in the gas phase, separate them according their m/z using either electric or magnetic fields or a combination of both. These ions are detected and counted by a detector. A mass spectrometer consists of the following parts.

I. Inlet source syringe pump
II. Ionization source
III. Mass analyser
IV. Detector

1.4.1 Electron impact (EI)

EI is a hard ionization technique and involves high energy electrons to generate ions and is very popular in organic chemistry. It works best on small, volatile, neutral, thermally robust molecules and is extremely suitable for simple organic compounds, often simple ligands but has restricted use in organometallic and coordination chemistry. This ionization method is mostly used to observe the fragmentation pattern as the molecular ion is not observed or if it is present its intensity is low. However there are some organometallic complexes which do show intense molecular ions using EI. For example cyclopentadienyl complexes of iron which are volatile and thermally stable, give the molecular ion as base peak.[45]

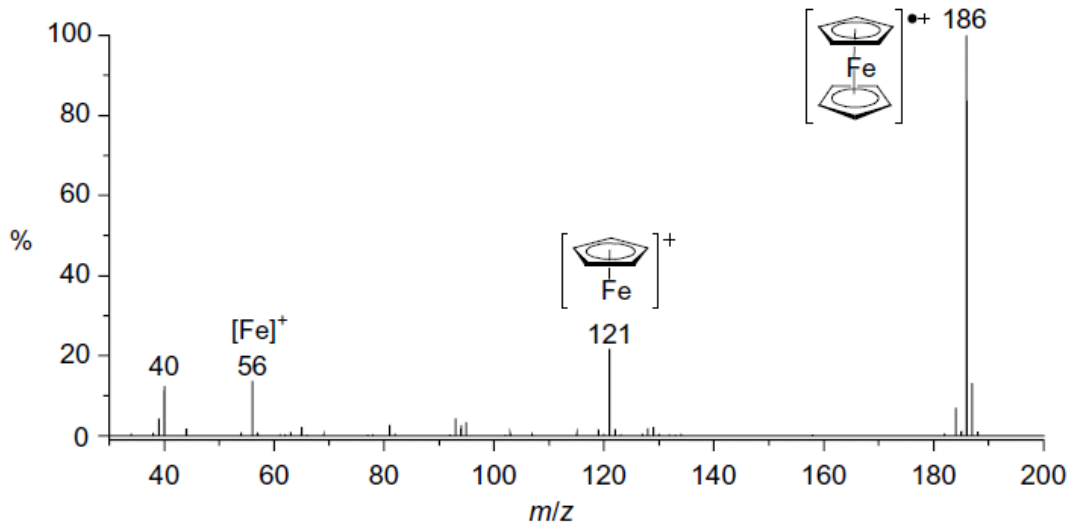

Fig 1. 6 EI mass spectrum of ferrocene showing the molecular ion peak as base peak[45]

1.4.2 Electrospray ionization (ESI)

ESI was developed in 1960's by Dole and co-workers. During standard electrospray ionization, the solution of interest is passed through a stainless steel capillary (75 - 150 micrometers) having a high voltage of 3 or 5 kV at the tip. The charged droplets are produced after passing through the charged capillary and this process is called nebulization. These charged droplets undergo columbic explosion and the solvents are removed with the dry gas and nebulization gas (nitrogen). This gas, usually nitrogen, helps to direct the spray emerging from the capillary tip towards the mass spectrometer.

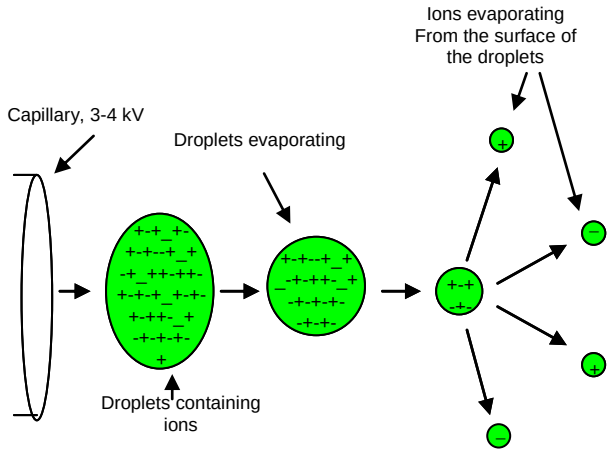

Fig 1. 7 Droplet production in the electrospray interface[46]

The charged ions released from the droplets are moved from the sampling cone or orifice through an intermediate vacuum region and from there through a small aperture into the analyser of the mass spectrometer, which is held under high vacuum. The lens and skimmer voltages can be optimized for different samples individually (Fig 1. 8).[45,47,48]

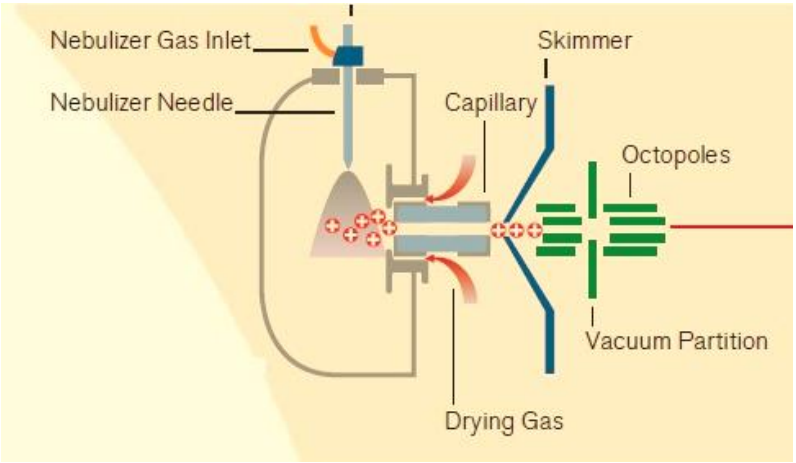

Fig 1. 8 Essential features of the electrospray interface instrument having ion trap analyser[46]

1.4.3 **Cone voltage**:

The extent of ion excitation can be controlled in the ESI by changing the potential between the electrospray capillary and skimmer. This is called the cone voltage or skimmer potential. Increasing the cone voltage can cause some insource CID (CID is discussed in detailed in chapter 4).[49-51]

In electrospray ionization, the process of desolvation occurs at different points depending upon the type of instrument used. In instruments with a quadrupole mass analyser, the effective voltage for declustering is controlled by the cone voltage and in an ion trap mass spectrometer an important role is played by the skimmer voltage.[52]

Certain dihalide complexes like cis-$[PtCl_2(PPh_3)_2]$, $[PtCl_2(dppe)]$, cis $[Cp^*IrCl_2(PPh_3)]$ and $[(p\text{-cymene})RuCl_2]_2$ were analysed by ESI-MS in positive ion mode. At low cone voltages (5-20 V) the dominant resonance is found for ions formed by the loss of halide ligand and coordination of solvent molecule $[M\text{-halide} + solvent]^+$. At higher cone voltages (>50 V) spectra were dominated by ions formed by loss of halide ligand only $[M\text{-halide}]^+$. Upon addition of pyridine to the mobile phase, replacement of solvent molecule by pyridine giving $[M\text{-halide} + pyridine]^+$ was observed.[53]

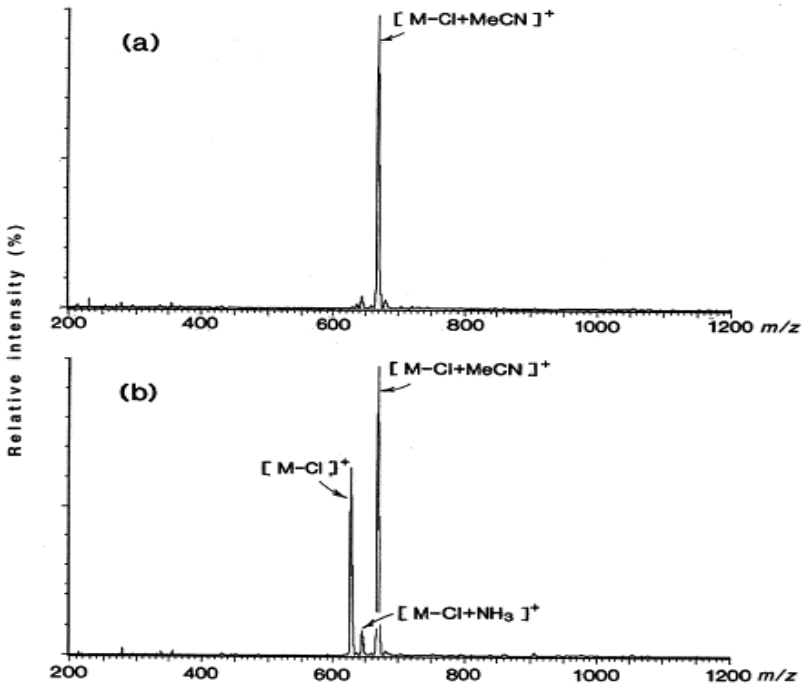

Fig 1. 9 Positive ion ESMS spectra of complex $[PtCl_2(dppe)]$ recorded in MeCN solution (a) Cone voltage 10 V (b) 50 V[53]

Potential antitumour drugs and analogous platinum (II) and platinum (IV) complexes with the eddp ligand have been studied by negative-mode ESI-MS.

Complexes with different oxidation states of Pt show different behaviour under the same experimental conditions. The mass spectra of (**a**) and (**b**) are different from (**c**) as the oxidation state of Pt in (**c**) is different from the oxidation state of Pt in (**a**) and (**b**). The spectra of (**a**) and (**b**) seem to be dominated by a resonance for $(M+X)^-$ adduct ions while quasimolecular ion $(M–H)^-$ appears to be dominant signal in the spectrum of (**c**).[54]

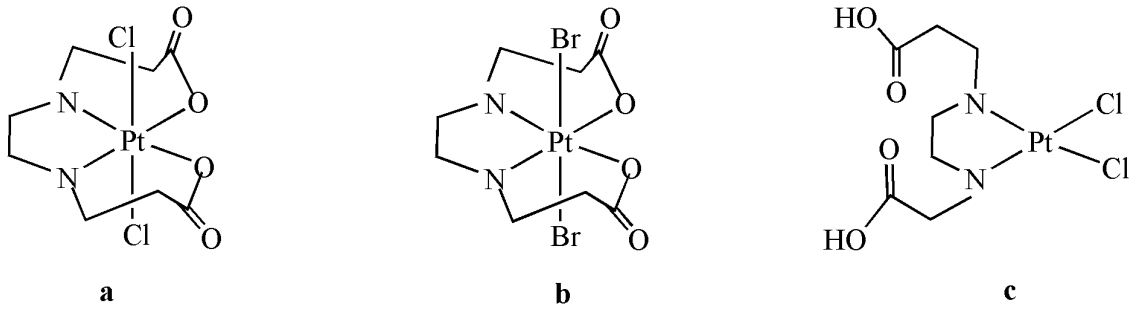

a **b** **c**

Fig 1. 10 Complexes of Pt(II) and Pt(IV) with eddp ligand and its dibutyl ester[54]

1.4.4 Liquid injection field desorption ionization (LIFDI)

LIFDI is a soft ionization technique (its principle and working are discussed in detail in chapter 3) and is very suitable for air/water sensitive, nonpolar, non-volatile, neutral compounds. It has been successfully applied to characterize highly reactive nickel and rhodium complexes. Fig 1. 11 shows the LIFDI mass spectrum of [acetylacetonato-k^2O,O'][1,8-bis(diphenylphosphino)-9,10-ethano-9,10-dihydroanthracene-k^2P,P'] rhodium(I). The molecular ion is observed at m/z 776. The observed isotopic pattern is in good agreement with the calculated. Some impurities can also be observed in the spectrum (Fig 1. 11).[55]

LIFDI has also been used to characterize ionic liquids and fluoride complexes of nickel and platinum.[56-58]

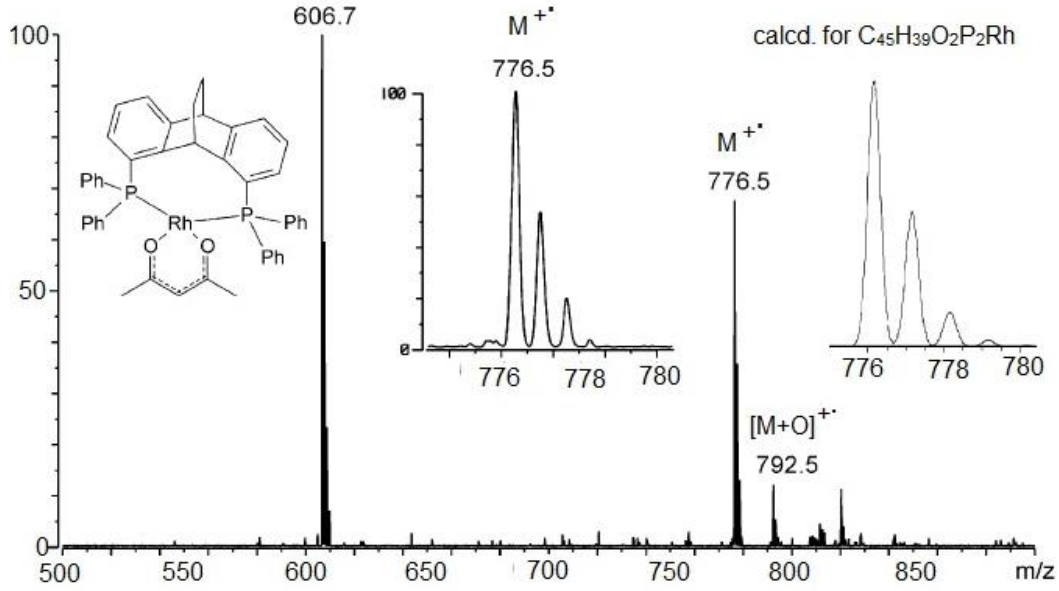

Fig 1. 11 LIFDI mass spectrum of [acetylacetonato- k^2O,O'][1,8-bis(diphenylphosphino) -9,10-ethano-9,10-dihydroanthracene-k^2P,P']rhodium (I) from THF reveals the presence of the molecular ion at m/z 776.5 and some side-products.[55]

1.4.5 Mass analyser

The ions are separated according to the charge-to-mass ratio in the mass analyser. Different types of analysers are available including magnetic sector, time of fight (TOF), quadrupole ion–trap, fourier transform ion cyclotron resonance mass spectrometer. Two analysers can be combined together in one spectrometer called hybrid mass spectrometer. Time–of–fight (TOF) and quadrupole ion–trap (QIT) will be discussed in detail in chapters 3 and 4, respectively.

Different mass analysers can be combined with ionization sources depending upon the compatibility and requirements. The combination of electrospray with quadrupole ion–trap analyser has revolutionized the field of mass spectrometry. The quardrupole ion–trap has been called the "complete chemical laboratory" by O'Hair et al. and can be used to study the structure and chemical reactivity of complexes/molecules in gas phase. ESI/QIT mass spectrometers can be used to study transition metal-mediated reactions like activation of C–H, C–C bonds and C–C coupling reactions. The conversion of alcohol to aldehyde is an example of a functional group transformation that has been studied by mass spectrometry. Methanol is converted to formaldehyde using molybdenum (VI) trioxide catalyst. The mechanism of the catalytic cycle was understood using QIT mass spectrometer. Fig 1. 12 shows two

cycles, both of which use a Mo catalyst but the only difference is a change in the sequence. $[Mo_2O_6(OCH_3)]_2$ is collisionally activated and H_2CO is formed.[59]

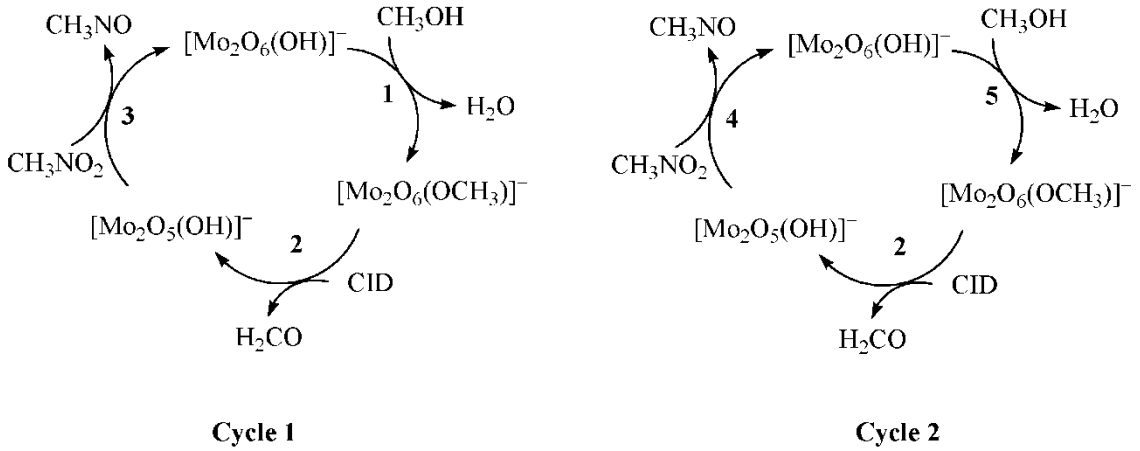

Fig 1. 12 Mechanism for the catalytic conversion of methanol to formaldehyde. Second step in both cycles shows the formation of $[Mo_2O_6(OCH_3)]_2$. Both cycles differ only in the sequence of reaction with CH_3NO_2 and CH_3OH.[59]

The structures of the products of fragmentation of chemical isomers e.g CH_3CH_2SH/CH_3SCH_3 have been identified through CID.[60] Gas–phase studies have also been used to determine mechanism the C-H bond activation.[61,62] Chen et al. observed the reaction of platinum (II) complexes with benzene in the gas phase using the modified octopole tandem mass spectrometer. TFE was used as a solvent which has no effect on the C-H activation step.[62]

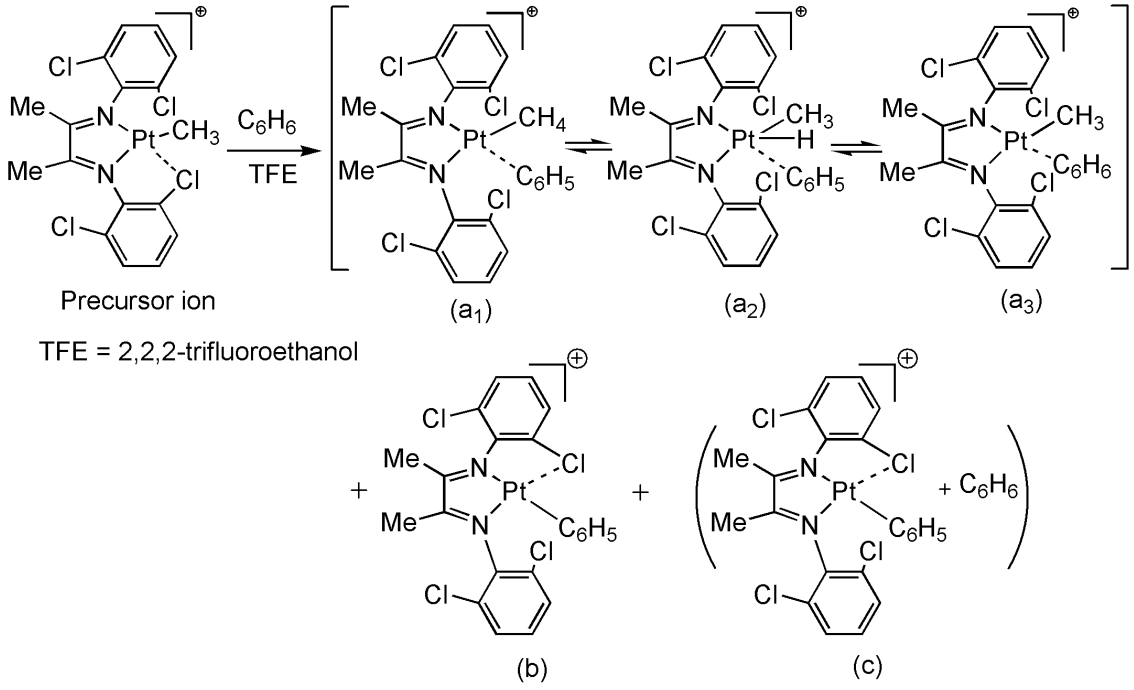

Scheme 1. 11 The precursor ion was isolated and subjected to collision with benzene in the octopole[62]

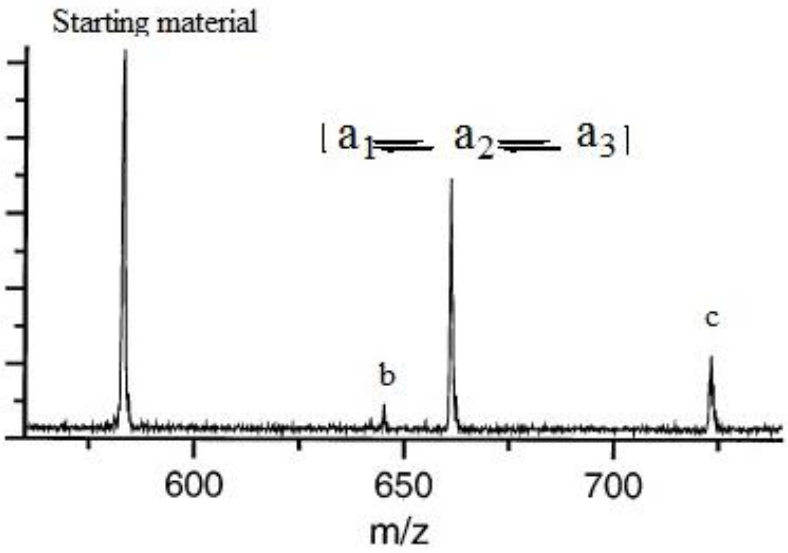

Fig 1. 13 Mass spectrum showing the starting material and the daughter ions formed from the gas phase reaction (scheme 1.10)[62]

The molecular requirements for activation of the C-I bond of aryl iodide by Au^1 ion was established through CID and gas–phase ion–molecule reactions of gold cations with iodobenzene. $(R_3P)Au^+$ (R = Me, Ph) ions were produced from the CID of $(R_3P)_2Au^+$ which in turn were produced from the CID of $(R_3P)AuCl_3$. $[Au_3L^n]^+$ (L^n=Ph_2P-$(CH_2)_n$$PPh_2$; n=3–6) ions were produced by CID of larger gold clusters. From the experimental observations it became clear that the reactivity depends upon the number of the gold atoms present and also upon the type of the ligand attached. Reaction (i) works at 100% efficiency while reaction (ii) did not give any product. In order to make sure that C–I bond activation occurred the product was subjected to CID and the fragmentation pattern confirmed the activation of the C–I bond.[63]

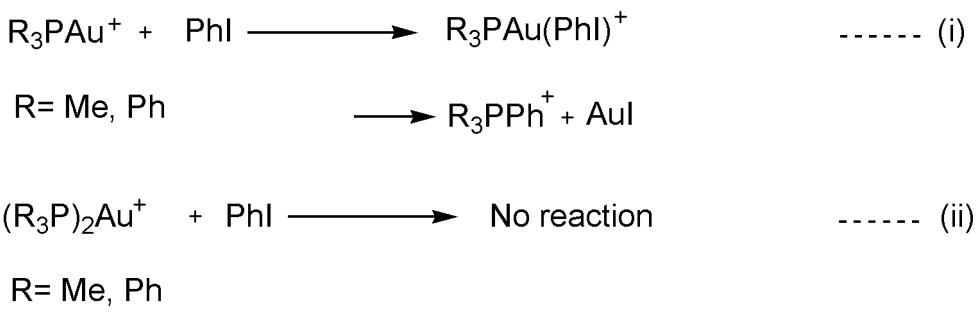

$[Au_3L^n]^+$ showed a single product $[Au_3L^nPhI]^+$ but the reaction efficiency is reduced. The efficiency is dependent upon the -CH_2- linker and it is observed that the reaction efficiency is at a minimum when n=3.

$$[Au_3L^n]^+ + PhI \longrightarrow [Au_3L^nPhI]^+ \quad \text{------ (iii)}$$

$L^n = Ph_2P\text{-}(CH_2)_nPPh_2$; n=3-6)

Currently there is a demand to understand how fluorine containing compounds work as catalysts for a large number of chemical reactions. For example, CF_3CuI helps in C-C cross coupling reactions but the exact mechanism of the decarboxylation of the trifluoroacetic acid compounds is still unknown. O'Hair et al. investigated the competition between decarboxlation and C–F activation for trifluoracetate complexes of the coinage metals (Cu, Ag, and Au).[64]

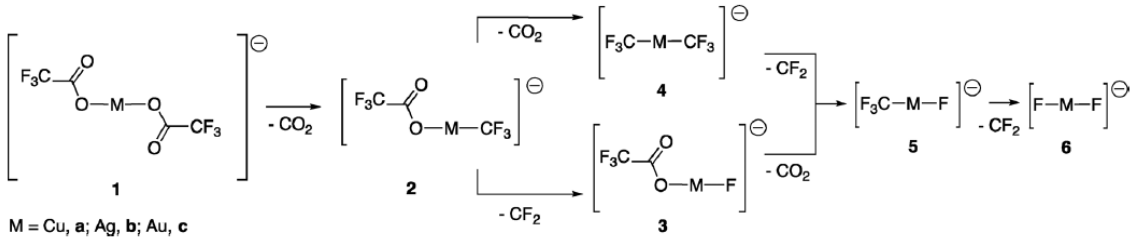

Scheme 1. 12 Proposed mechanism for the collisionally activated decomposition products of coinage metals trifluoroacetate complexes $[CF_3CO_2MO_2CCF_3]^-$ through multistage CID[64]

From Fig 1. 14 it can be seen that during MS^1, $[CF_3CO_2CuO_2CCF_3]^-$ and $[CF_3CO_2AgO_2CCF_3]^-$ dissociate mainly through decarboxylation, while during MS^2 the fragmentation occurs through C–F activation. MS^3 is again followed by decarboxylation. $[CF_3CO_2CuO_2CCF_3]^-$ behaves in a different way and the fragmentation mainly goes through the loss of lactone.

From the above investigation, it is possible to make a comparison between diacetate complexes of coinage metals $[CH_3CO_2MO_2CCH_3]^-$ and their perfluorinated analogues:

- $[CH_3CO_2ML]^-$ complexes (where L = CH_3CO_2 and CH_3) only fragment via decarboxylation and acetate ligand loss while their perfluorinated analogues undergo a much richer range of reactions. CID of $[CF_3CO_2ML]^-$ results in losses of CO_2, CF_2, and "CF_2CO_2" along with $CF_3CO_2^-$
- It was also be observed that $[CF_3MF]^-$ where M = Cu, Ag and Au were successfully generated in the gas phase and sequential C–F bond activation reactions also gave rise to the previously experimentally unknown difluorides $[FMF]^-$,[64] while the decarboxylation of the $[CH_3CO_2MO_2CCH_3]^-$ gives the dimethylmetallates.[65,66]

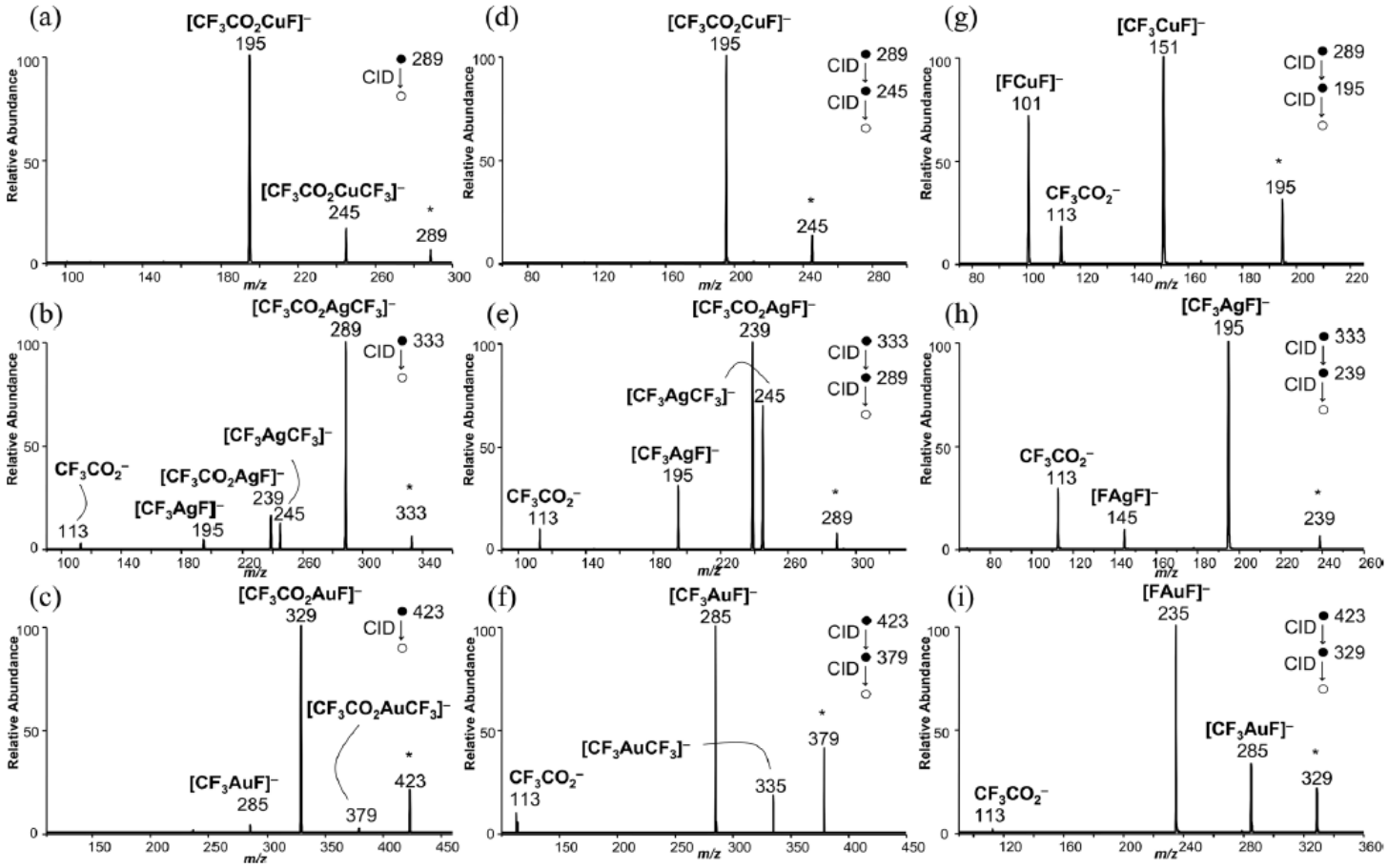

Fig 1. 14 3D quadrupole ion trap MS^2 and MS^3 mass spectra of the collision induced dissociation of (a) $[CF_3CO_2CuO_2CCF_3]^-$, (b) $[CF_3CO_2AgO_2CCF_3]^-$ and (c) $[CF_3CO_2AuO_2CCF_3]^-$.[64]

1.5 Multiply charged anions (MCAs)

Multiply charged anions are highly energetic species and are particularly unstable in gas phase.[67] As these ions have excess charges and in the absence of counter ion or solvent, they experience a columbic repulsive interaction. Dessent et al. showed that they mostly fragment by electron decay or ionic fragmentation (discuss in detail in chapter 4).[68,69]

The nature of the multiply charged anions has also been studied by photodetachment spectroscopy.[70,71] The electron affinity of ZrF_6^{2-} was calculated using photodetachment photoelectron spectroscopy and it was found that the second electron affinity is much greater than the first. It is in agreement with the observation that ZrF_6^{2-} is very unstable towards the loss of F^- ion.[72]

The decay pathway of transition metal dianions ($IrCl_6^{2-}$, $OsCl_6^{2-}$, $ReCl_6^{2-}$, $IrBr_6^{2-}$ and $PtBr_6^{2-}$) was investigated through mass spectrometry. The negative ion ESI spectrum gave major resonances for KMX_6^{2-}, MX_6^{2-} and MX_5^- (where M = Ir, Os, Re and X = Cl, Br). The parent dianion (MX_6^{2-}) was isolated and subjected to CID. It was observed that with increasing collision energy the parent dianion decayed and the daughter ion MX_5^- increased in intensity. No peak for MX_6^- was observed. It was concluded that transition metal dianions decay by ionic fragmentation rather than electron detachment upon low energy collision activation in the gas phase and therefore the repulsive columbic barrier for ionic fragmentation lies below the electron detachment (discussed in detail in chapter 4).[68]

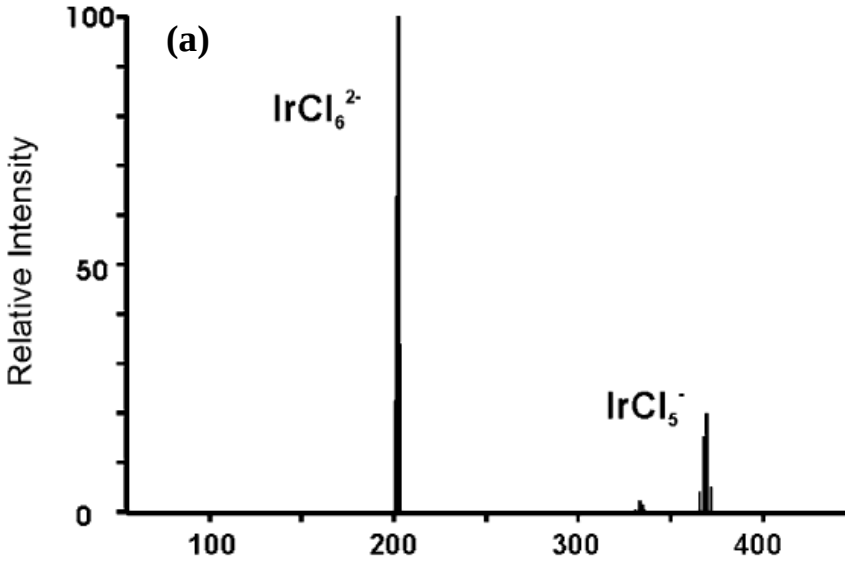

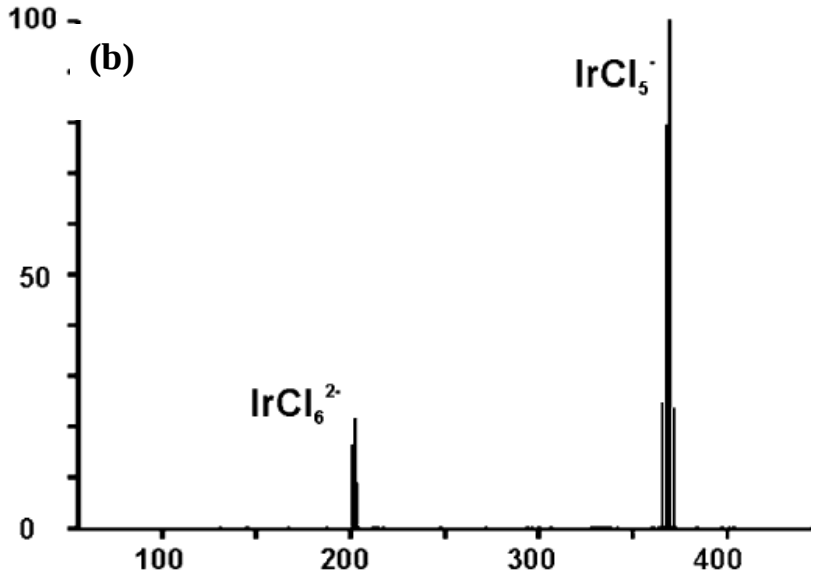

Fig 1. 15 Low energy collision induced dissociation of $IrCl_6^{2-}$ at (a) 0% collision energy and (b) 7% collision energy[68]

As solvent molecules can stabilize the excess charges by reducing the columbic interaction, it is important to understand how the solvent molecules are attracted and what their effect is on the stability of the MCAs. Descent et al. have studied the structure and stability of microsolvated clusters of $Pt(CN)_4^{2-}$, i.e. $Pt(CN)_4^{2-}.(H_2O)_n$ n = 1–4, $Pt(CN)_4^{2-}.(MeCN)_m$ m = 1, 2 and $Pt(CN)_4^{2-}.(H_2O)_3.MeCN$ through low-energy collision induced dissociation.[73]

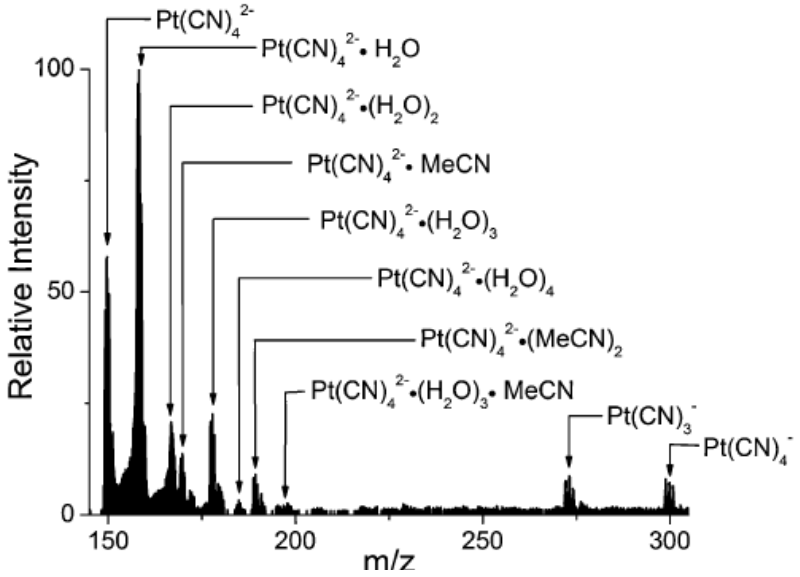

Fig 1. 16 Negative-ion ESI-MS of the potassium $K_2Pt(CN)_4^{2-}$ (MeCN solution) of recorded with a capillary temperature of 70 ºC and water enriched nitrogen auxiliary gas.[73]

The negative ion ESI spectrum of $K_2Pt(CN)_4^{2-}$ shows solvated clusters of $Pt(CN)_4^{2-}$ with H_2O_n or $(MeCN)_m$ or having both (n = 0-4, m = 0-2) (Fig 1. **16**). All these ions were isolated and subjected to CID one by one. It was observed that $Pt(CN)_4^{2-}$ fragments by ionic fragmentation as the repulsive columbic barrier for ionic fragmentation RCB_{if} lies below the repulsive columbic barrier for electron detachment RCB_{ed}.

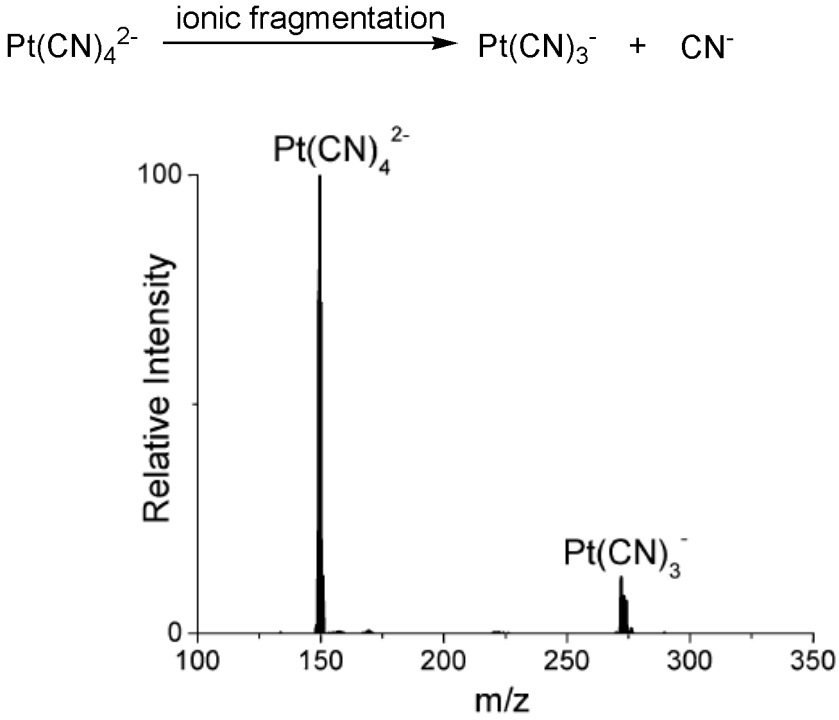

Fig 1. 17 Low energy collision induced dissociation of $Pt(CN)_4^{2-}$ showing the formation of daughter ion $Pt(CN)_3^{-}$ [73]

From the CID of the solvated cluster ion i-e $Pt(CN)_4^{2-}.(H_2O)_n$ n = 1–3, $Pt(CN)_4^{2-}.(MeCN)_m$ m =1, 2 and $Pt(CN)_4^{2-}.(H_2O)_n.MeCN_m$ (n + m < 4), it was observed that fragmentation occurs through the loss of solvent cluster in one step and no sequential loss was observed, resulting in the formation of $Pt(CN)_4^{2-}$ daughter ion (major). This observation leads to the conclusion that the solvent molecules are attached on the surface and the hydrogen bonding interaction between the solvent molecules is stronger than the interaction between anion and solvent. It can be further concluded that cluster solvent molecule increase the stability of the MCAs towards fragmentation.[73]

1.6 Hydrogen bonding

Hydrogen bonding was first recognized by two young scientists W.M. Latimer and W.H. Rodebush in 1920. They realized for the first time the reason for association of water molecules. After their discovery many people paid attention to the concept of the shared proton. For hydrogen bonding interactions one group should act as a weak acid (proton donor) and the other group as weak base (proton acceptor).

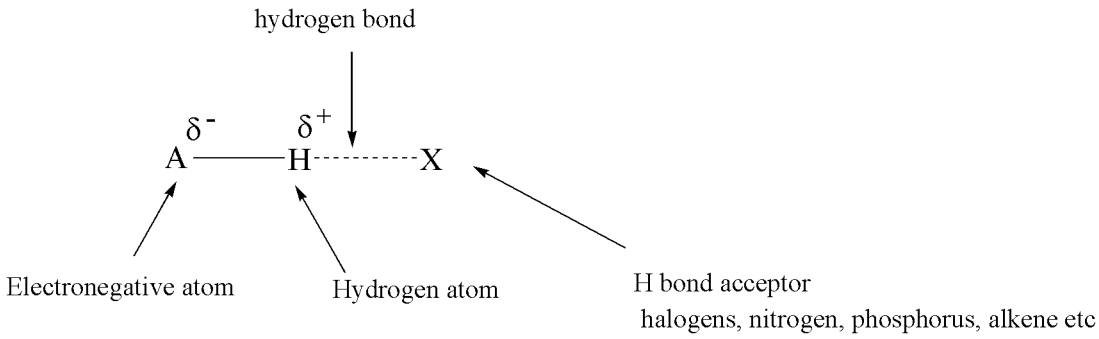

Fig 1. 18 Schematic representation of hydrogen bonding

Hydrogen bonding plays an important role in the chemistry of transition metal complexes. The role of hydrogen bonding is essential in the chemical behaviour of metal based-drugs and their interaction with biochemical molecules or in other words their biological activities.[74] Hydrogen bonding can occur between two molecules (two centre) or three molecules (three centre).[75,76]

An unconventional type of intramolecular hydrogen bonding was observed in iridium hydride complexes having IrH as a weak base and N-H as a weak acid. The H···H distances were about 1.7-1.9 ºA and strength of hydrogen bond was about 12-25 kJ mol^{-1}.[77,78]

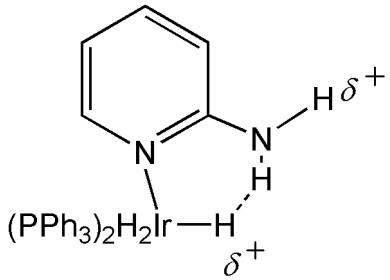

More confirmation for this type of unconventional bonding was provided by the neutron diffraction studies of [$ReH_5(PPh_3)_3$.indole]. The rhenium hydride crystallizes together with indole as large yellow crystals and the hydrogen bond involves 3 centres. Indole does not undergo self-association and is a good proton donor for hydrogen bonding. The distance $H_l \cdots H_{IA}$ is 2.212 (9) ºA and $H_{lA} \cdots H_2$ is 1.734 (8) ºA. The bond length of the short bond is very similar to that mentioned in the above example.[79]

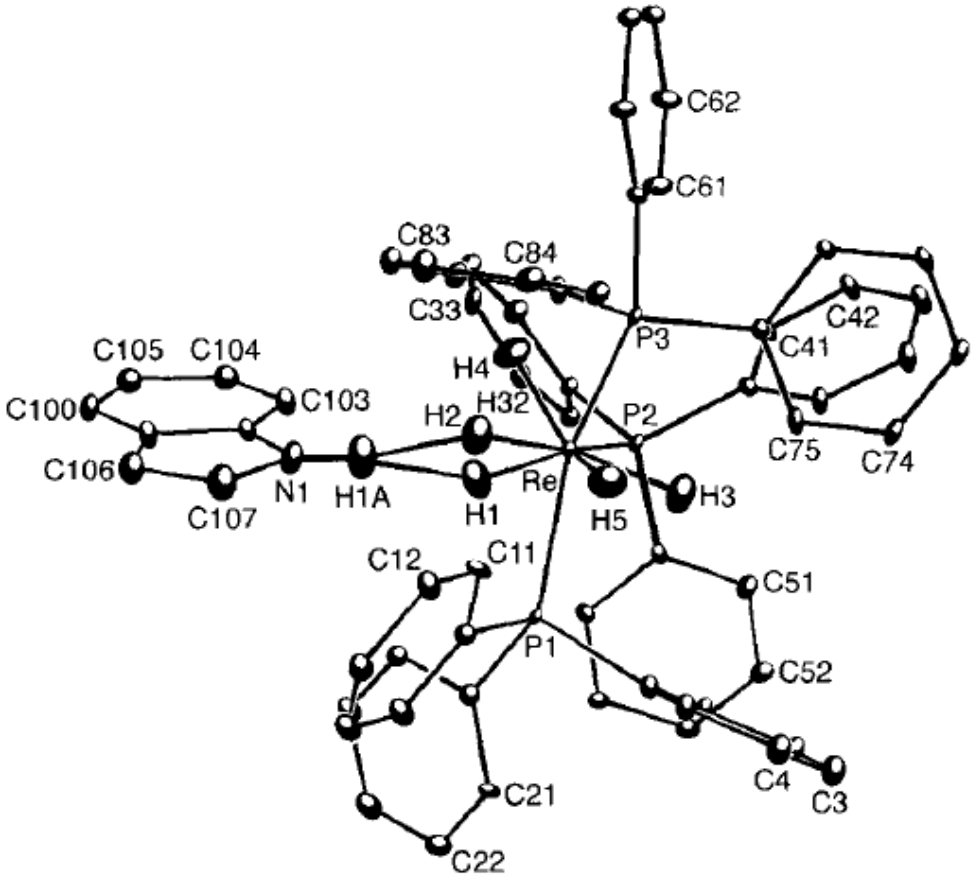

Fig 1. 19 ORTEP diagram of neutron diffraction of [$ReH_5(PPh_3)_3$.indole][79]

[$ReH_5(PPh_3)_3$.indole] has been characterized by IR spectroscopy and it is seen that in both the IR spectrum and neutron diffraction, the vibration for NH of indole has shifted to lower energy. IR spectroscopy has also been used to calculate the strength of intermolecular hydrogen bonds between a variety of weak proton acids such as indole and 2,4,6-$Me_3C_6H_2OH$ and the transition-metal hydrides like [$ReH_5(PPh_3)_3$, [$ReH_7(Ph_2PCH_2CH_2PPh_2)$ and [$WH_4(PMePh_2)$ and quantitatively correlated with the enthalpy of interaction with the vibration for NH of indole.[80]

The hydrogen bond acceptor capabilities of metal halides (M–X) are of specific interest. Halide ions (X^-) and transition metal halides (M–X) are strong acceptors of hydrogen bonds and carbon bound halide (C–X) are weak acceptors. Comparative investigations have been made on the behaviour of hydrogen bond acceptors having fluoride ligand (X=F) and the heavier analogues. (M–F) complexes form much shorter hydrogen bonds and also quite different in directionality. The general trend followed is H····F–M stronger than H····X–M. for all the donor-acceptor pairs. The hydrogen bond distances (DH····X–M) have been compared using normalized distance functions R_{HX} = $d(H\cdots X)/r_H + r_X)$ where D= C, N, O, X= F, Cl, Br, I and M= transition metal. [81,82]

Most important is the directionality of the transition metal fluoride acceptor with which the donor approach towards them. The H····F–M angle is greater (130-160º) than the H····X–M angles (90-130º) where X= Cl, Br and I. Fig 1. 20 shows the angular preferences in terms of percentage.

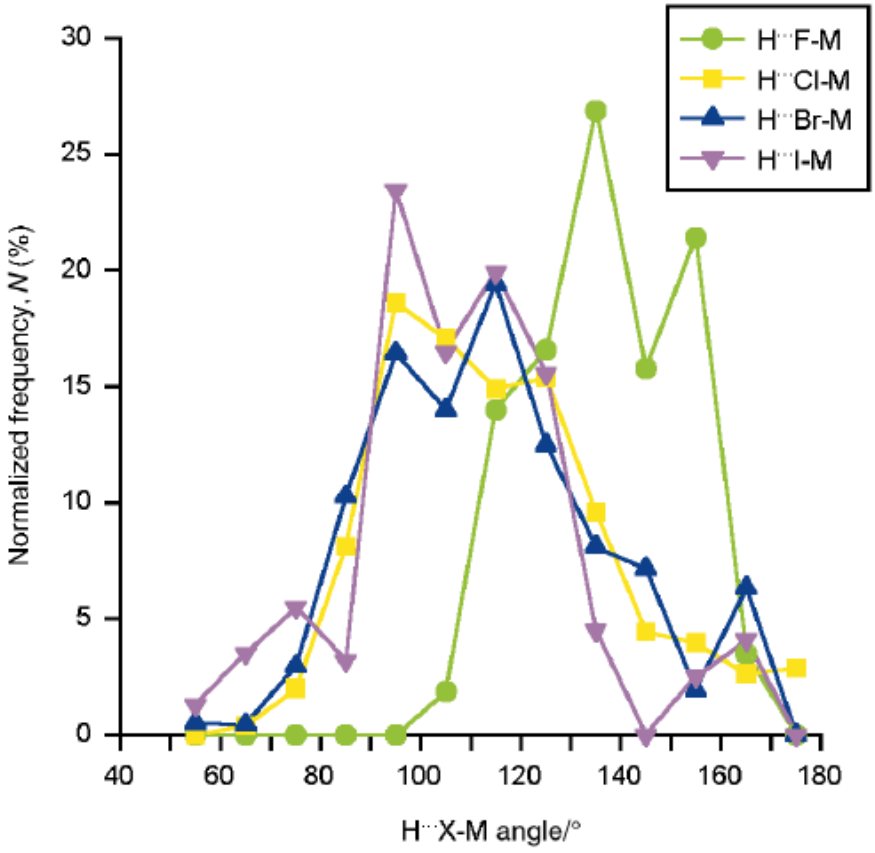

Fig 1. 20 Normalized distribution of H····X–M angles expressed as percentages of total number of observed N–H····X–M hydrogen bonds.[82]

The electrostatic potentials of Cl, Br and I in CH_3X show well resolved minima while in CH_3F it is not resolved. There is a negative charge accumulation around the fluorine. This also clarifies the reason for the anisotropic behaviour of fluorine containing acceptors (Fig 1. 21).

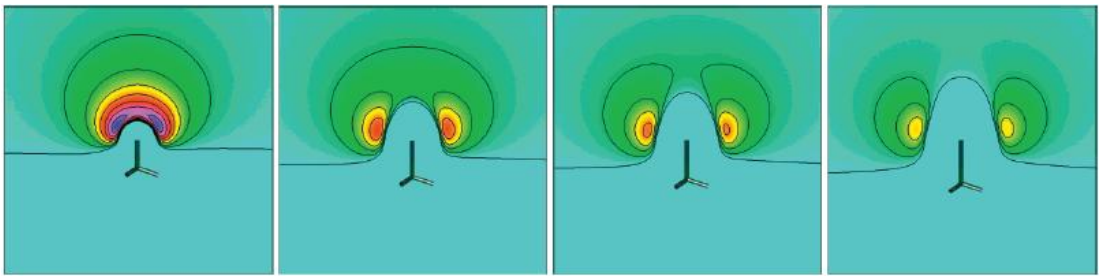

a **b** **c** **d**

Fig 1. 21 Electrostatic potentials of CXH_3, where X= (a) F, (b) Cl, (c) Br and (d) I. The contours are separated by 4 kcal·mol^{-1} intervals.[83]

The hydrogen bond formation capabilities of all the above groups i-e X^-, C–X and M–X with D–H have also been investigated in terms of geometrical data from crystal structures. The correlation between the normalized distance vs angles were expressed in unbiased normalized plots and these results also confirm that all the acceptor groups X^-, C–X and M–X (X = F, Cl, Br, I) can form hydrogen bonds with D–H donors (D= C, N and O) (Fig 1. 22).

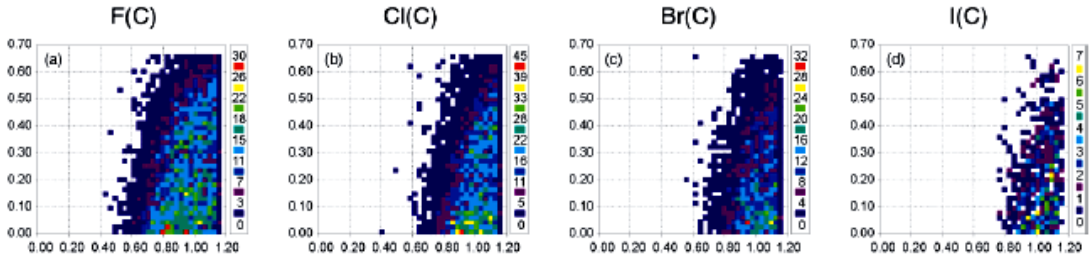

Fig 1. 22 Normalised distribution of C–H···X contact lengths (R^3_{HX}) vs angles (1−Cos(180−θ)).[83]

From all of the above discussion it is clear that terminally bound halogens exhibit anisotropic behaviour. Fluorine favours larger angles than its heavier analogues and the behaviour of metal fluorides is distinctly different.[83]

Hydrogen bonding has been used as tool in assembling supramolecular architecture.[84,85] For example, cyanuric acid and melamine form a complex in a ratio of 1:1 that can attain the structure of super graphite (Fig 1. 23).[86]

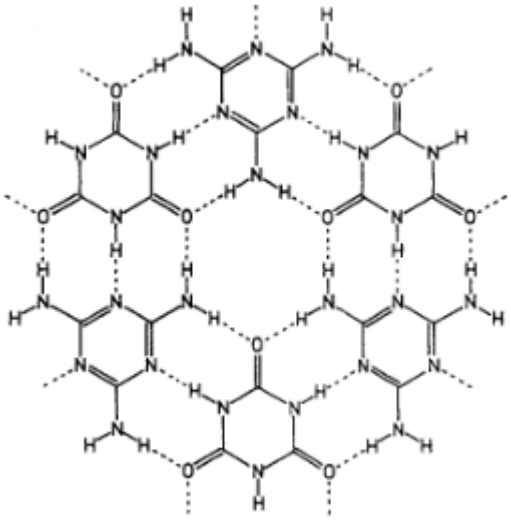

Fig 1. 23 Probable triply H-bonded 2D sheet architecture of the 1 : 1 complex between melamine and cyanuric acid.[86]

SYNTHESIS AND CHARACTERIZATION OF TRANSITION METAL FLUORIDE COMPLEXES

2.1 Introduction

Recent developments in the field of fluorine chemistry were inspired by the dramatic change in the physical properties, chemical reactivity and physiological activities of organic molecules by incorporation of fluorine or fluorine containing substituents. Transition metal complexes bearing fluoro ligand are of great importance in the field of organometallic chemistry, playing important roles in catalysis, synthesis, C-H activation, material science, and the generation of highly reactive "naked" fluoride. Late transition metal fluoride complexes have received attention due to their uncommon chemical properties and bonding features. Fluoro transition-metal complexes exhibit remarkable reactivity patterns compared to their chloro, bromo and iodo counterparts. This is strongly supported by the fluoro congener of Wilkinsons catalyst [$(PPh_3)_3RhF$]. [1-3] The chemistry of transition–metal fluoro complexes is relatively unexplored. Their lack of study is due in part to the instability of low valent metal centers and fluoride ions by hard acid/base rules and the tenacity with which the fluoride reagent holds onto water molecules and other protic reagents due to strong hydrogen bonding. These factors make the preparation and introduction of clean fluoride reagents difficult.[4]

Activation of carbon-fluorine bonds received a much greater amount of attention in the last few decades because of the greater strength of the C–F bond (418 kJ mol^{-1}). Selective activation of the carbon-fluorine bond is more than an idle curiosity and a variety of methods of activating carbon-fluorine bonds by transition-metal centers have been established in the last few decades.[5] However, the formation of new organofluorine compounds via C-F activation, followed by functionalization within the coordination sphere remains less developed.[6] However Perutz et al reported several examples of nickel fluoride complexes where nickel attacks at the heterocycle and selectively activates the C-F bond in preference to C-H bonds (scheme 2.1).[7-9]

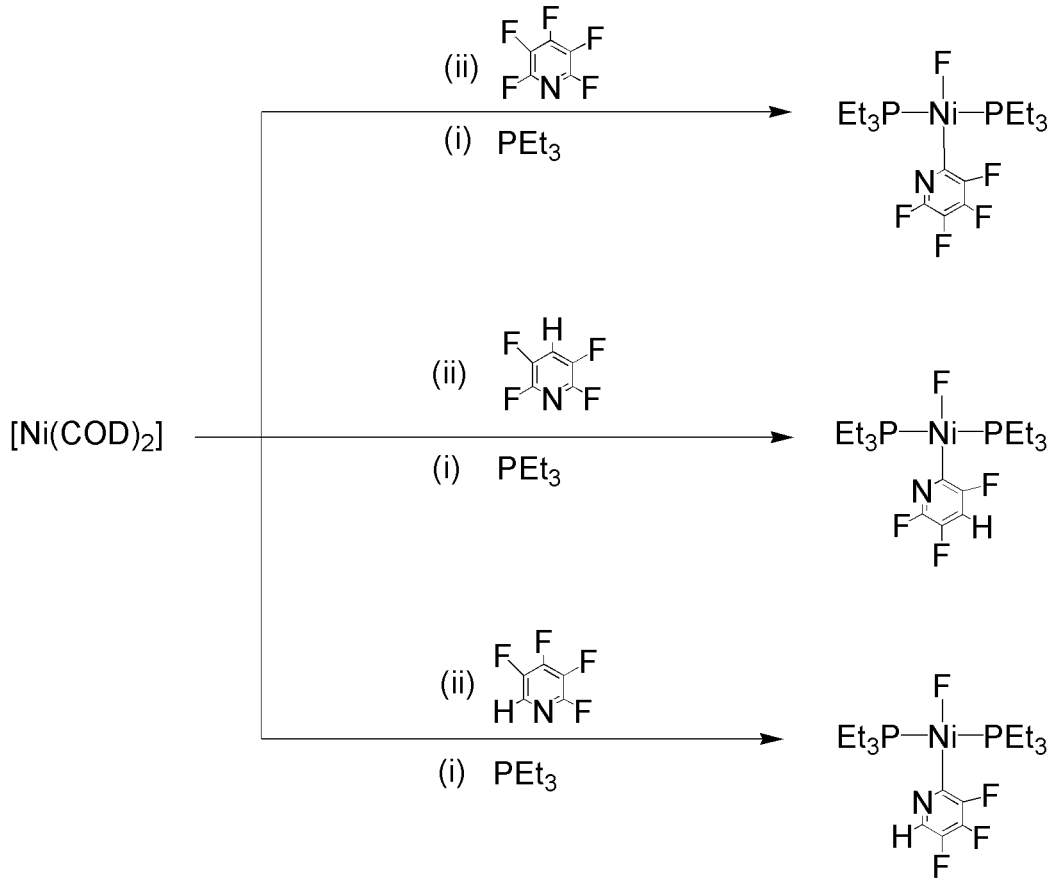

Scheme 2. 1 Reactivity of $Ni(COD)_2$ with pentafluoropyridine and 2,3,5,6-tetrafluoropyridine in the presence of triethylphosphine.[8]

The group 10 transition metal complexes are of current interest due to their role in catalysis, reductive elimination, oxidative addition and ligand transfer reactions. Fluoro complexes of platinum and palladium were previously considered to be inaccessible due to incompatibility of soft late trasition metals and the hard fluorine base.[10-13] However, difluoro complexes of palladium were prepared by treating dimethyl complexes of palladium with an equivalent amount of XeF_2 in dry dichloromethane and the quantitative formation of the product was observed. L represents ligands which can be di(*i*-propylphosphino)propane (dippp) and di(cyclohexylphosphino)propane (dcpp) in the following reaction.[14]

$$L_2Pd(CH_3)_2 + XeF_2 \xrightarrow{CH_2Cl_2\ \ -30^{o}\text{- RT}} L_2PdF_2 \quad \text{----------} \quad (2.1)$$

(L_2 = dippp; depp)

Recently difluoro platinum and palladium complexes bearing phosphine ligands have been fully characterized by A. Vigalok.[10]

It was considered that phosphines may be essential to stabilize the M–F bond but a recent report by Sanford and Grushin suggested that sp^2 nitrogen-donors can also support a stable $Pd^{II}(Ar)(F)$ species. (2-Phenylpyridine)palladium(lutidine) fluoride complexes were prepared from a palladium (II) iodide reaction with silver fluoride.[12]

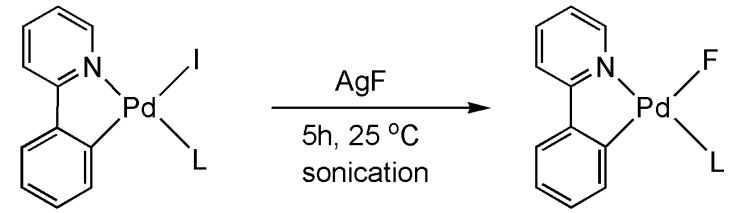

(2.2)

L = 2,5-lutidine
L = 4-tBu-pyridine

Currently, organometallic fluorides are being successfully applied in many areas of synthesis and catalysis. This is exemplified by the pioneer work of Roesky who use Me_3SnF and AsF_3 in the preparation of group 4 metallocene fluorides.[15]

$$Cp_2TiCl_2 + 2Me_3SnF \longrightarrow Cp_2TiF_2 + 2Me_3SnCl \quad \text{2.3}$$

Many biologically active molecules including pharmaceuticals, agrochemicals, positron emission tomography (PET) imaging agents etc contain aryl fluorides. A lot of attention has been paid towards the synthesis of these aryl fluorides (Ar-F) but they still remained challenging for the scientist.[11,16,17] Several recent reports have shown that these aryl fluorides can be prepared by Pd catalyzed cross–coupling reactions.

Recently Sanford and Ball reported the synthesis of aryl fluorides (Ar–F) from the reaction of (t-Bu-Py)$(Pd^{II}(p\text{-}FC_6H_4)(X)$ with XeF_2. Biaryl was also obtained as a minor species.

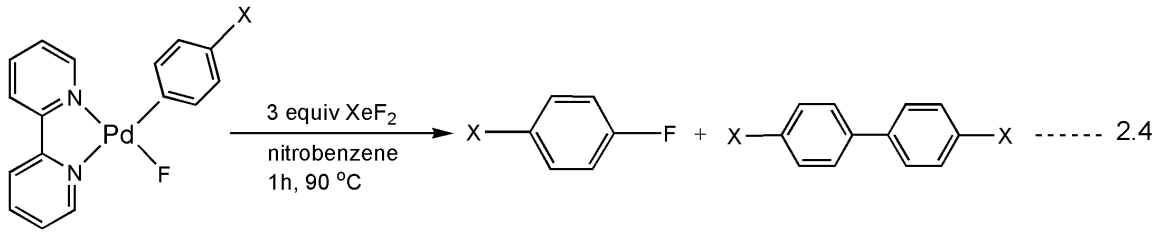

2.4

X = F, CF3, OMe Major Minor

The reactive intermediate was observed at lower temperature and characterized by NMR and X-ray crystallography. ^{19}F NMR spectroscopy showed clear resonances for F–H–F at –117.6 ppm and for Pd–F at –204.5 ppm.[11]

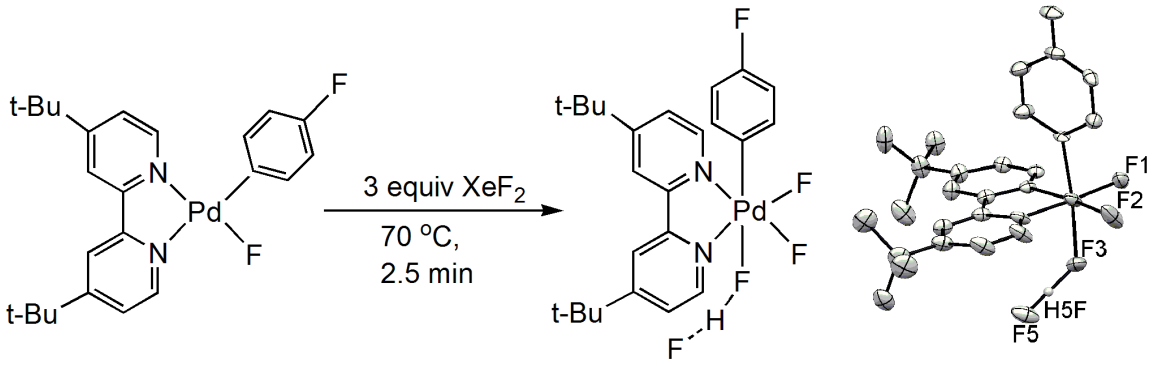

Bifluoride complexes

The bifluoride complexes were first reported during the last decades of the 20th century although few reports have appeared on the isolation and reliable characterization of these complexes. For example, Parkin and Murphy reported the synthesis of $Mo(PMe_3)_4H_2F(FHF)$ from its dihydride complex (scheme 2.2) and characterized it by X-ray diffraction.(Fig 2. 1).[18]

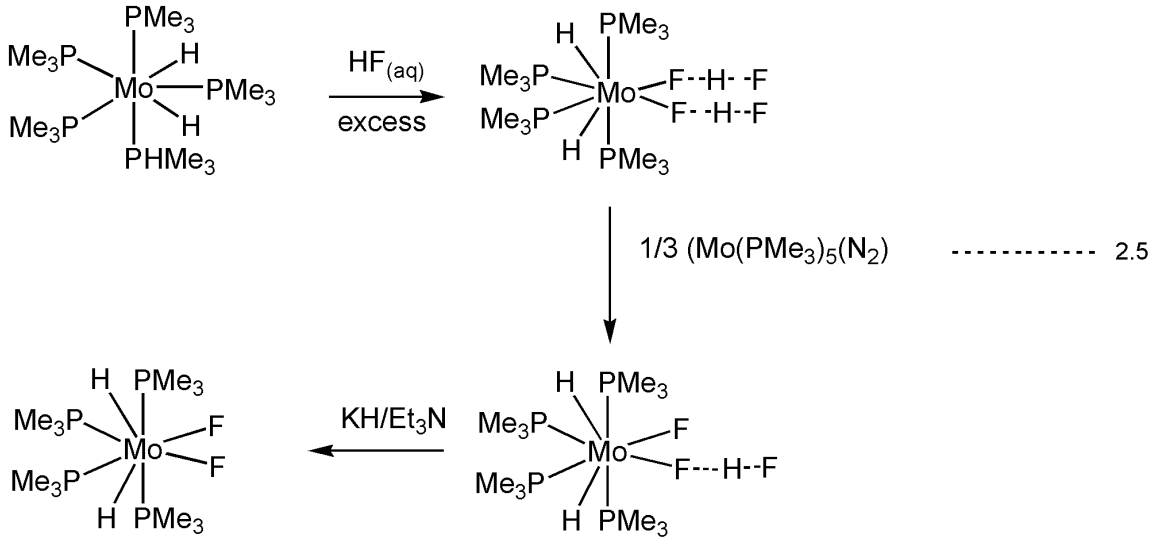

Scheme 2.2 synthesis of $Mo(PMe_3)_4H_2F(FHF)$[18]

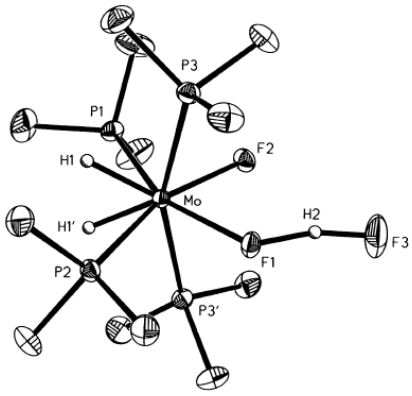

Fig 2. 1 Molecular structure of $Mo(PMe_3)H_2F(FHF)$[18]

Perutz et al. reported the synthesis of $Ru(dmpe)_2H(FHF)$ and characterization by NMR spectroscopy in solution and in the solid state by crystallography. They prepared the compound by reacting the dihydride complex with either $Et_3N.3HF$ or fluoroarenes.[19]

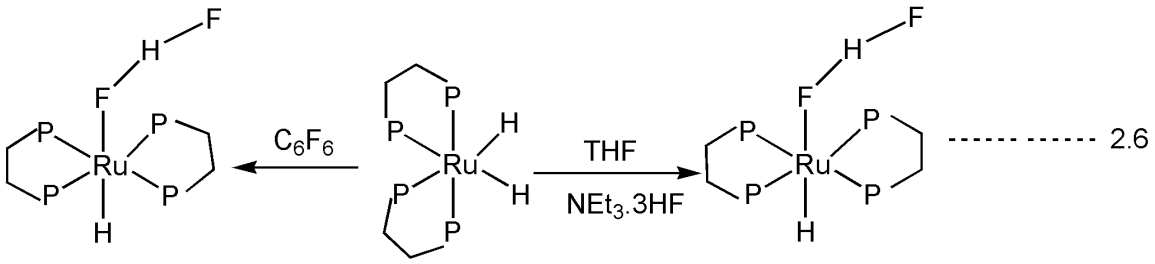

Scheme 2.3 Synthesis of $Ru(dmpe)_2H(FHF)$[19]

Platinum bifluoride complexes were synthesized from the reaction of platinum dihydride complexes with $Et_3N.3HF$ which is a mild source of HF and can be handled without any special techniques.

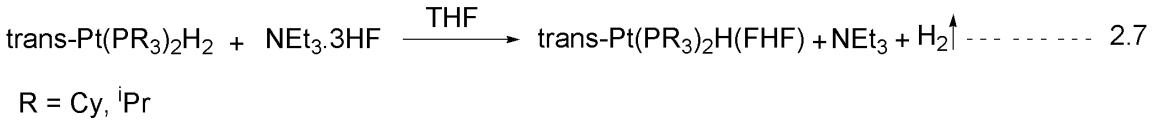

^{I}H NMR spectra of platinum bifluoride complexes showed a doublet with platinum satellites at –26 to –28 assigned to the hydride. The acidic proton gave a broad resonance at 11.5. In the ^{19}F NMR spectra for trans-$Pt(PR_3)_2H(FHF)$ a resonance appeared at δ –283 to –281, assigned to the proximal fluorine and another resonance at δ –179 to –182 corresponding to the distal fluorine. Both these resonance showed platinum satellites.[20]

2.2 Results

2.2.1 Synthesis of Mono fluoride complexes

2.2.1.1 Complexes of Nickel

Nickel fluoride complexes were made by C-F oxidative addition of hexafluorobenzene and of fluorinated pyridines (Scheme 1).

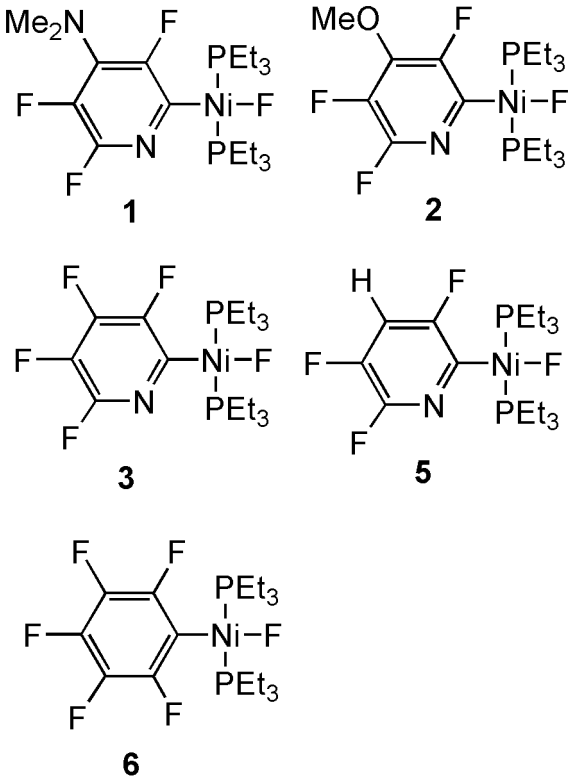

Scheme 2.2 Nickel fluoride complexes

Trans-NiF{2-C_5NF_3(4-NMe_2)}$(PEt_3)_2$ **1** was prepared from the reaction of 4-dimethylamino-2,3,5,6-tetrafluoropyridine[21] with Ni(1,5-cyclooctadiene)$_2$ and PEt_3. The ^{31}P NMR spectrum shows a doublet at δ 12.7 (J_{PF} = 48.2 Hz), indicative of coupling with a single fluorine nucleus. The ^{19}F NMR spectrum shows a triplet at δ –367.8 (J_{PF} = 47.4 Hz), which provides evidence for the presence of the metal fluoride (Fig 2. 2). The other three resonances at δ –91.3, –121.2 and –164.3 confirm the presence of the C_5F_3N group.

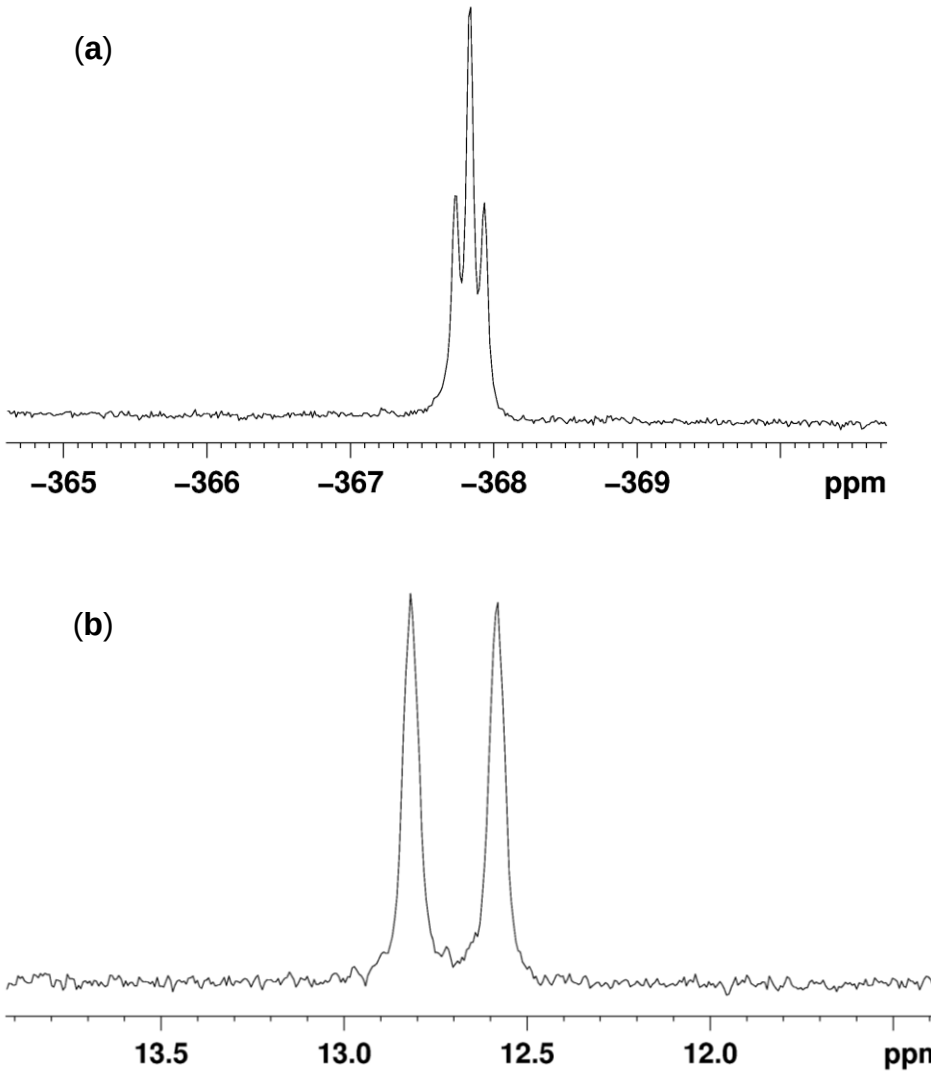

Fig 2. 2 (a) ^{19}F NMR spectra (407.4 MHz) of **1**, metal fluoride region and (b) ^{31}P NMR spectra (202.46 MHz) in C_6D_6 at room temperature,

Complex **1** was further studied by mass spectrometry using LIFDI and ESI techniques. LIFDI gave the $[M]^+$ as base peak at m/z 488, while ESI gave decomposition.[22]

The molecular structure of **1** was confirmed by X-ray diffraction (Fig 2. 3, Table 2.1), The Ni-F distance of 1.8521(9) Å compares with 1.836(5) Å in trans-$NiF(C_6F_5)(PEt_3)_2$, 1.856(7) Å in trans-$NiF(C_5NHF_3)(PEt_3)_2$[24] 1.916(3) Å in trans-$NiF(C_6HF_4)(PEt_3)_2$,[25] 1.8589(15) Å in trans-$NiF(C_6F_5)((iPrNC_5H_4NMe)_2$[26] and 1.856(4) Å in $NiF(4\text{-}(CF_3)C_6F_4)(i Pr_2Im)_2$. [27]

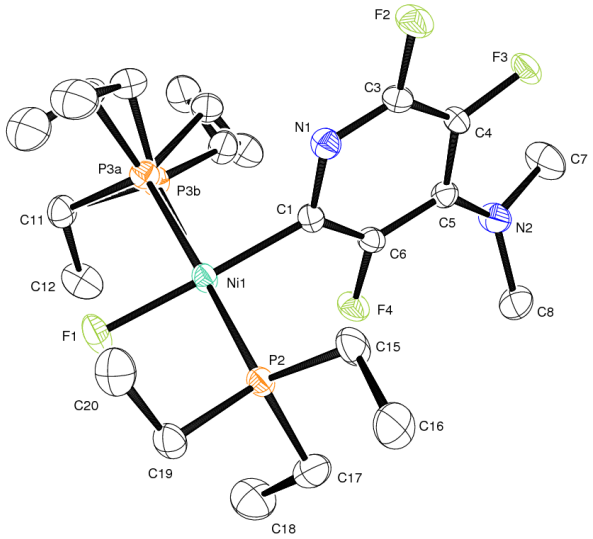

Fig 2. 3 Molecular structure of trans-NiF{2-C_5NF_3(4-NMe_2)}(PEt_3)$_2$.[22] Ellipsoids set at 50% probability, hydrogen atoms not shown. Note the disorder in the position of one PEt_3 group.

Table 2.1 Principal bond lengths (Å) and angles (deg) of **1**

Ni–F(1)	1.8521(9)
Ni–P(2)	2.1920(4)
Ni–P(3B)	2.194(2)
Ni–P(3A)	2.201(2)
C(1)–Ni	1.8749(13)
F(1)–Ni–C(1)	178.11(5)
F(1)–Ni–P(2)	90.21(3)
F(1)–Ni–P(3A)	88.01(9)
F(1)–Ni–P(3B)	90.94(8)
C(1)–Ni–P(2)	91.62(4)
C(1)–Ni–P(3A)	90.11(10)
C(1)–Ni–P(3B)	87.23(9)

Trans-NiF{2-C_5NF_3(4-OMe)}(PEt_3)$_2$[22] was prepared from the reaction of 2,3,5,6-tetrafluoro-4-methoxypyridine with Ni(1,5-cyclooctadiene)$_2$ and PEt_3. The ^{31}P NMR spectrum shows a doublet at δ 13.05 (J_{PF} = 48.1 Hz), indicative of coupling with a single fluorine nucleus. The ^{19}F NMR spectrum shows a triplet at δ –368.78 which provides

evidence for the presence of metal fluoride, with coupling to both phosphorus nuclei (J_{PF} = 45.7 Hz). The other three resonances at δ –170.1, –128.3 and –88.7 confirm the presence of the C_5F_3N group.

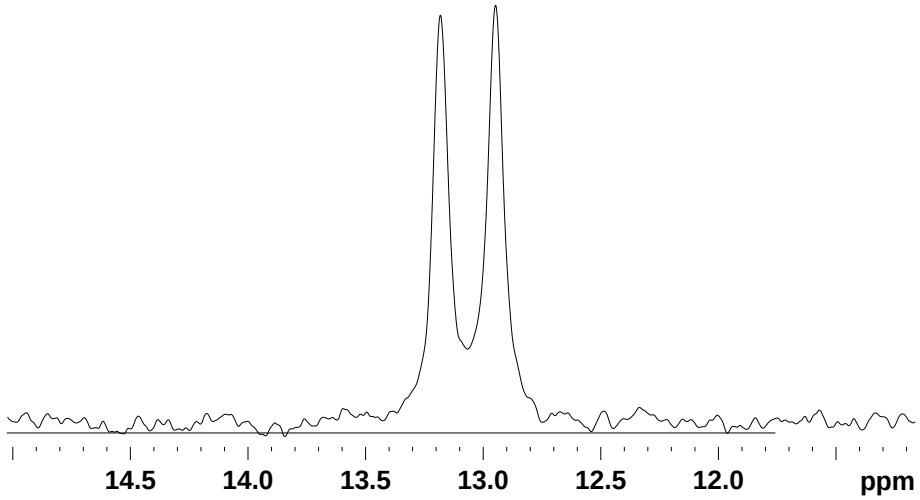

Fig 2. 4 ^{31}P NMR spectra (202.46 MHz) of **2** in C_6D_6 at room temperature

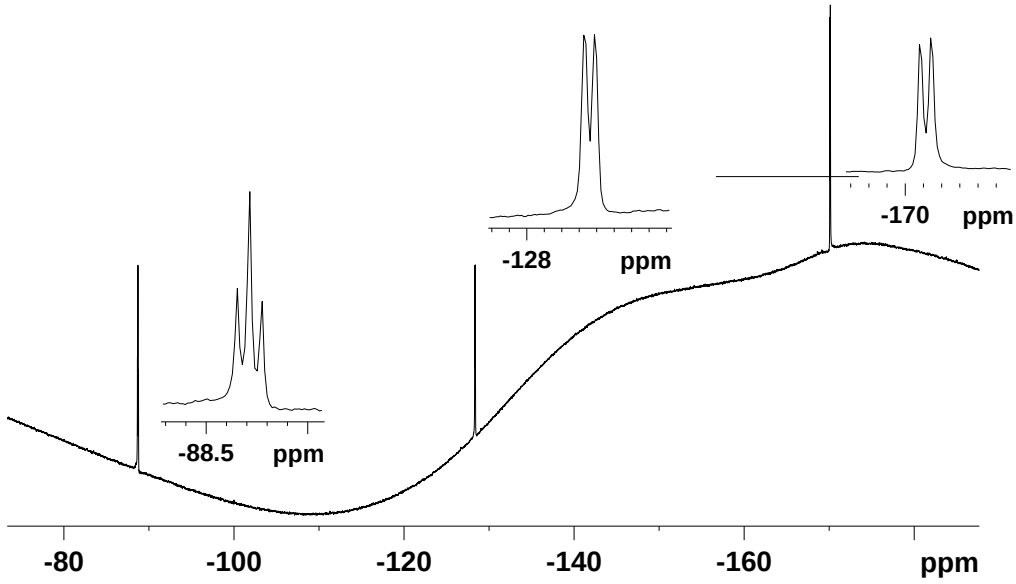

Fig 2. 5 ^{19}F NMR spectra (407.4 MHz) of **2** in C_6D_6 at room temperature

The LIFDI mass spectrum of complex **2** gave the molecular ion peak $[M]^+$ at 475 as base peak (100%, (chapter 3, Fig 3.6), whereas the compound showed decomposition with ESI.

$Ni(PEt_3)_2(C_5F_4N)F$ (**3**) has been already reported in the group but it was reinvestigated in order to see its reaction F^- with in solution.

2.2.1.1.1 Reaction $Ni(PEt_3)_2(C_5F_4N)F$ with F^- donating reagent

The target of this work was to prepare NiF complexes bearing negative charge. Tetramethyl ammonium fluoride (TMAF), cesium fluoride (CsF) and tetrabutyl ammonium fluoride (TBAF) were used to provide F^- in the solution. Benzene, THF, acetonitrile and DMSO were used as solvent. Tetramethyl ammonium fluoride (TMAF) was added to the solution of **3** in benzene and left stirring overnight at 25°C, but no reaction was observed. The progress of the reaction was followed by NMR spectroscopy.

The reaction of $Ni(PEt_3)_2(C_5F_4N)F$ with TMAF in THF was also followed by NMR spectroscopy. TMAF is only sparingly soluble in THF and acetonitrile (even at 50°C) but seems to be insoluble in benzene.

For the complex obtained from reaction of $Ni(PEt_3)_2(C_5F_4N)F$ with TMAF in THF, the ^{19}F NMR spectrum shows a resonance for starting material at δ –373.3 (Fig 2. 6a).[24] On standing a new product grew in with very similar spectroscopic characteristics, showing a triplet for nickel fluoride at δ –370.4 coupled to two phosphorus nuclei (J_{PF} = 44.0 Hz) (table 1) which provides evidence for the presence of metal fluoride and two equivalent ^{31}P nuclei. The ^{31}P NMR spectrum shows two doublets for starting material at δ 13.8 and for the new product at δ 13.2 (J_{PF} = 47.7 for both) (Fig 2. 6b).

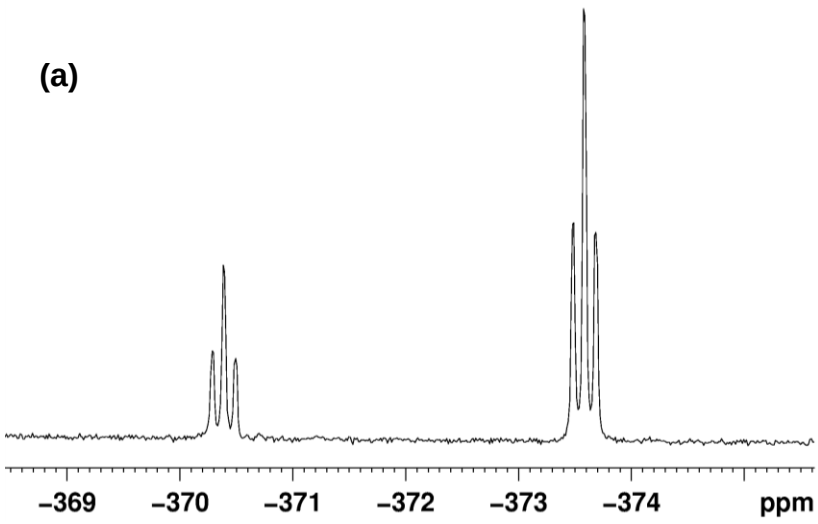

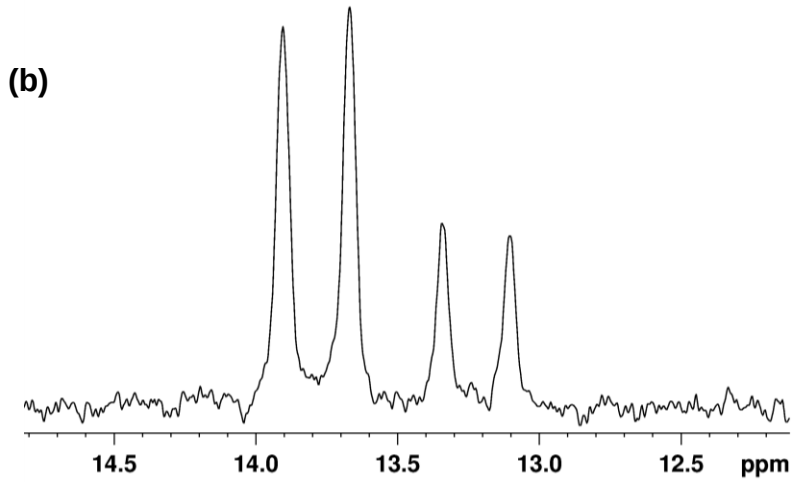

Fig 2. 6 (a) ^{19}F NMR spectra (407.4 MHz) in metal fluoride region of [3 + TMAF] in THF locked on C_6D_6 at room temperature (b). ^{31}P NMR spectra (202.46)

The ^{19}F NMR spectrum also displays some peaks in addition to those for the reactant in the organic fluorine region see table (2.2) at δ –172.5 (b), δ –164.0 (d, J_{PF}= 19.9 Hz), δ –160.4 (b), δ –148.3 (d, J= 18.71 Hz) and δ –130.7(m). The total conversion to the product was about 30%.

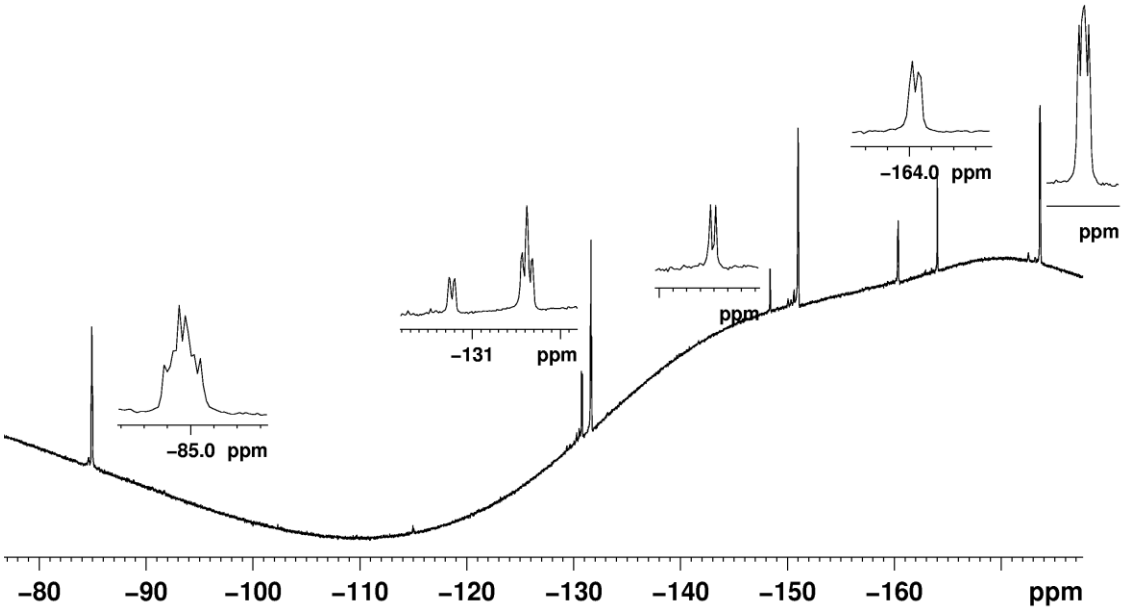

Fig 2. 7 ^{19}F NMR (407.4 MHz) of [$NiF(C_5F_4N)(PEt_3)_2$ + TMAF] in THF locked on C_6D_6 at room temperature in organic fluorine region

The effect of time and temperature was also studied. With the passage of time there was increase in the amount of the new product (Fig 2. 8) but after one week the reaction stopped and later on decomposition was observed.

The reaction mixture was heated at 50°C, the same reaction was observed but the rate of the reaction was increased. It reaches its maximum conversion by heating overnight and then decomposition was observed (Fig 2. 9).

From all the above observation it is suggested that the product (**3`**) is formed by halogen type interaction between **3** and the Me_4NF. The observation was further strengthening by mass spectrometric evidence obtained for the reaction of **1** with TMAF.

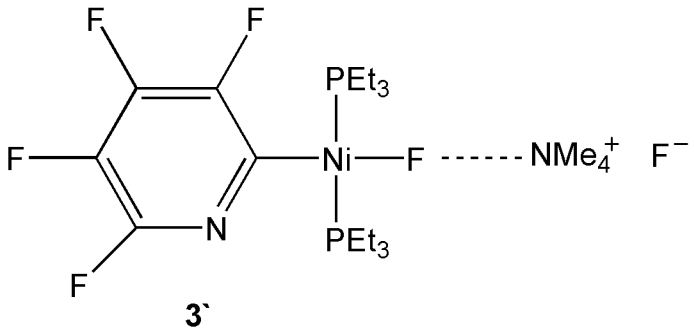

3`

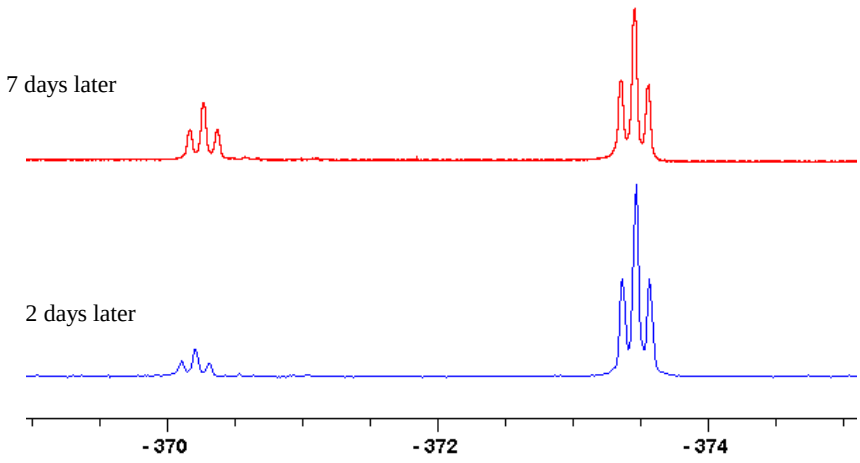

Fig 2. 8 ^{19}F NMR (407.4 MHz) of [**3** + TMAF] in THF locked on C_6D_6 at room temperature in metal fluoride region showing the effect of time on the product formation

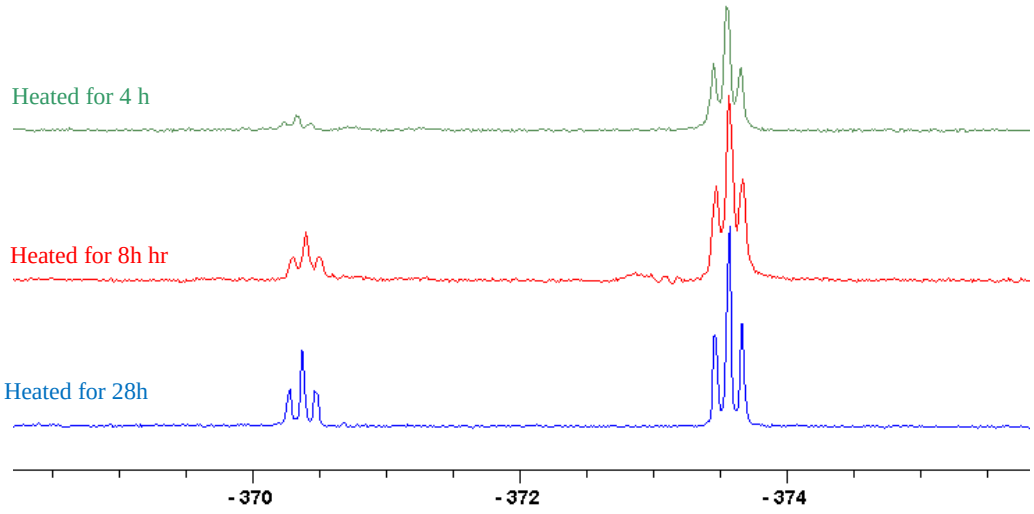

Fig 2. 9 ^{19}F NMR (407.4 MHz) of [**3** + TMAF] in THF locked on C_6D_6 at room temperature in metal fluoride region showing the effect of temperature on the product formation

The same experiment was repeated by reacting **1** with TMAF. The reaction mixture was heated at 50°C and the same results as in the above experiments were observed after 28 h and 100 % conversion to product was observed after 2 week and the TMAF was completely dissolved.

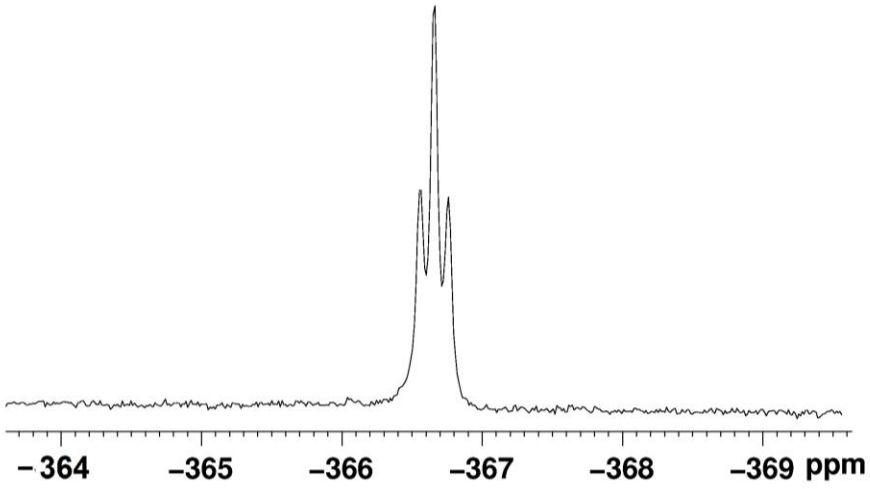

Fig 2. 10 ^{19}F NMR (407.4 MHz) of [**1** + TMAF] in THF at room temperature in metal fluoride lower spectrum is after 28 h and upper is after 2 weeks.

The product was observed by LIFDI mass spectrometry. In the LIFDI mass spectrum a peak at 488 corresponds to the starting material (**1**) while another peak at 562 is assigned to the product.

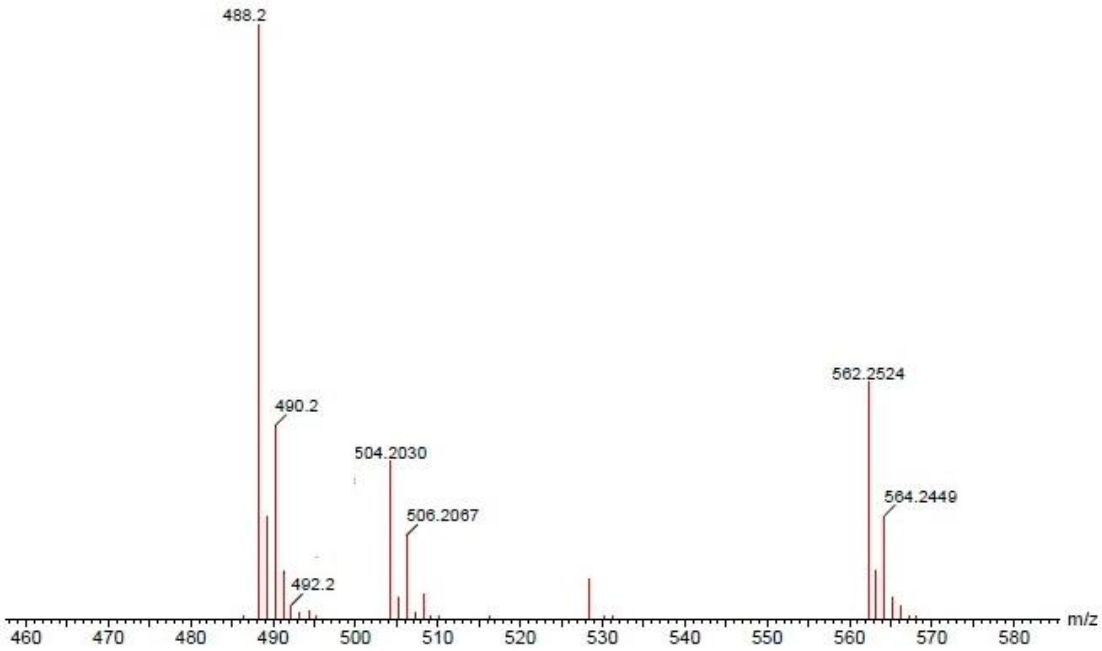

Fig 2. 11 LIFDI mass spectra of $[Ni(PEt_3)_2(C_5F_3NNMe_2)F^{\cdots}NMe_4^+F^-]$ in methanol

From the NMR and mass spectra observation it is concluded that the product formed is $[Ni(PEt_3)_2(C_5F_3NNMe_2)F^{\cdots\cdots}NMe_4^+F^-]$ (**1`**). It was further concluded that the bond between $NiF^{\cdots\cdots}NMe_4$ is not very stable in LIFDI mass spectrometry, that why some of it decomposes and is converted back to the starting material (Fig 2. 11).

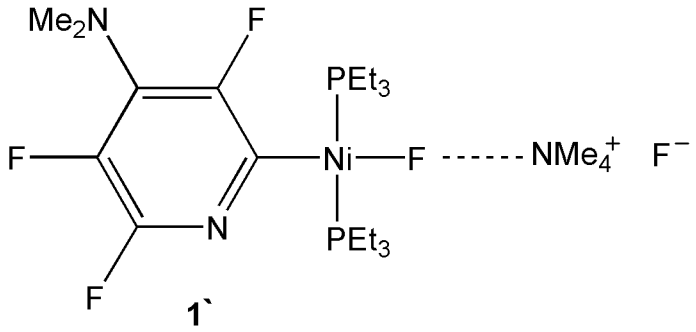

1`

When acetonitrile was used as a solvent instead of THF for the reaction of $Ni(PEt_3)_2(C_5F_4N)F$ and TMAF, the ^{19}F NMR spectrum showed two resonances, a triplet at $\delta -362.4$ (reactant) and a doublet at $\delta -324.5$ (product) characteristic of metal fluoride (Fig 2. 12). Its doublet coupling J_{PF} = 52.4 Hz, shows that it is coupling to one phosphorus and

there were some free phosphine. Most probably one of the phosphines is replaced by the acetonitrile as acetonitrile is a good coordinating agent (table 2.2). The formation of compound **4** was further confirmed by ESI mass spectrometry.

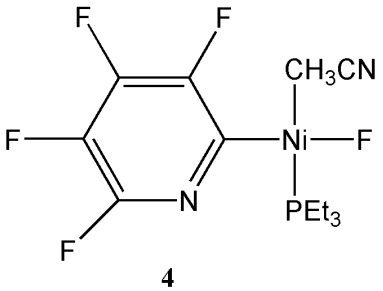

4

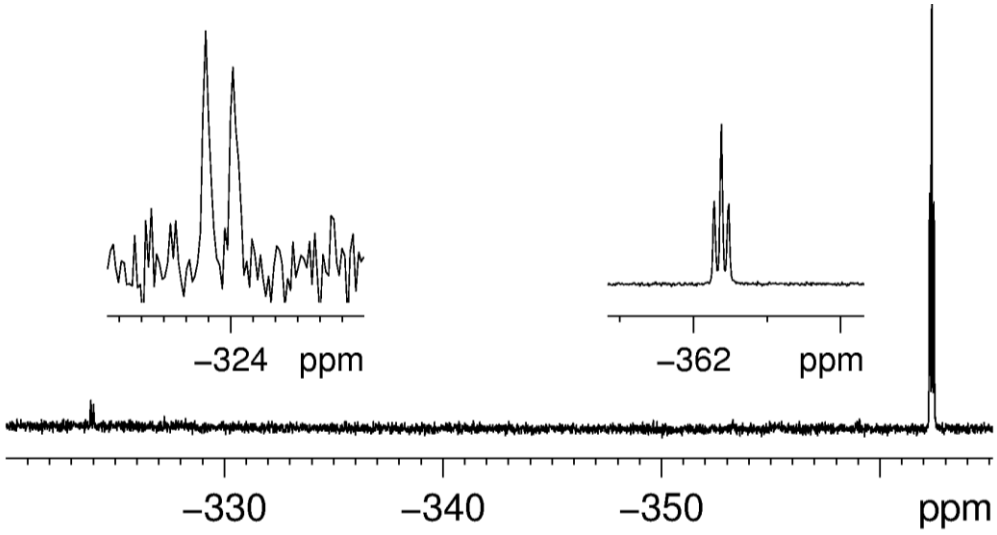

Fig 2. 12 ^{19}F spectra (407.4 MHz) of [**3** + TMAF] in CD_3CN at room temperature in metal fluoride region.

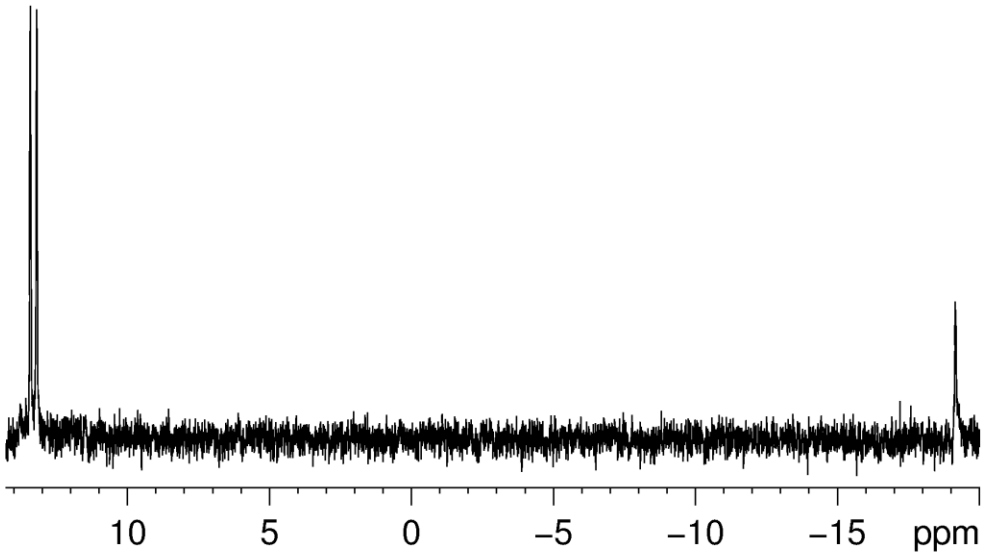

Fig 2. 13 ^{31}P NMR spectra (407.4 MHz) of [**3** + TMAF] in CD_3CN at room temperature

The reaction of **3** with CsF gave the same results as TMAF in all the solvents. For ^{31}P NMR and ^{19}F NMR spectrum see table 2.2.

18-Crown-6 was added to the reaction mixture in order to increase the rate of reaction of dissolved fluoride. The ^{19}F NMR spectrum showed three resonances at δ –362.53 (t), δ –359.16 (not clear) and δ –359.67 (t) (see table 2.2) which gives an indication for the formation of two new products but still nothing could be identified.

No reaction was observed for **3** when TBAF was used as source of F^-.

2.2.1.2 Complexes of rhodium

$Rh(PPh_3)_3F$ (8) was prepared by stirring the solution of $Rh_2(1,5\text{-}COD)_2\mu(OH)_2$ in ether with $Et_3N.3HF$. the complex was recrystallized from warm benzene and hexane mixture[3] The progress of the reaction was followed by NMR spectroscopy. The ^{19}F NMR spectrum shows a broad peak at δ 285.0 and the ^{31}P NMR spectrum shows two peaks at δ 31.5 and δ 56.3 which provides evidence for the formation of $Rh(PPh_3)_3F$ by comparison with literature values. There are some other peaks both in ^{19}F NMR and ^{31}P NMR spectra which indicate the presence of impurities. One of them may be the $[Rh(PPh_3)_2(PPh_2F)C_6H_5]$ because **8** can convert to its isomer at room temperature.[3] LIFDI mass spectrum of the complex **8** gave molecular ion $[M^+]$ at m/z 908 (10%). ESI mass spectrum showed $[M–F]^+$ at m/z 888 as base peak.

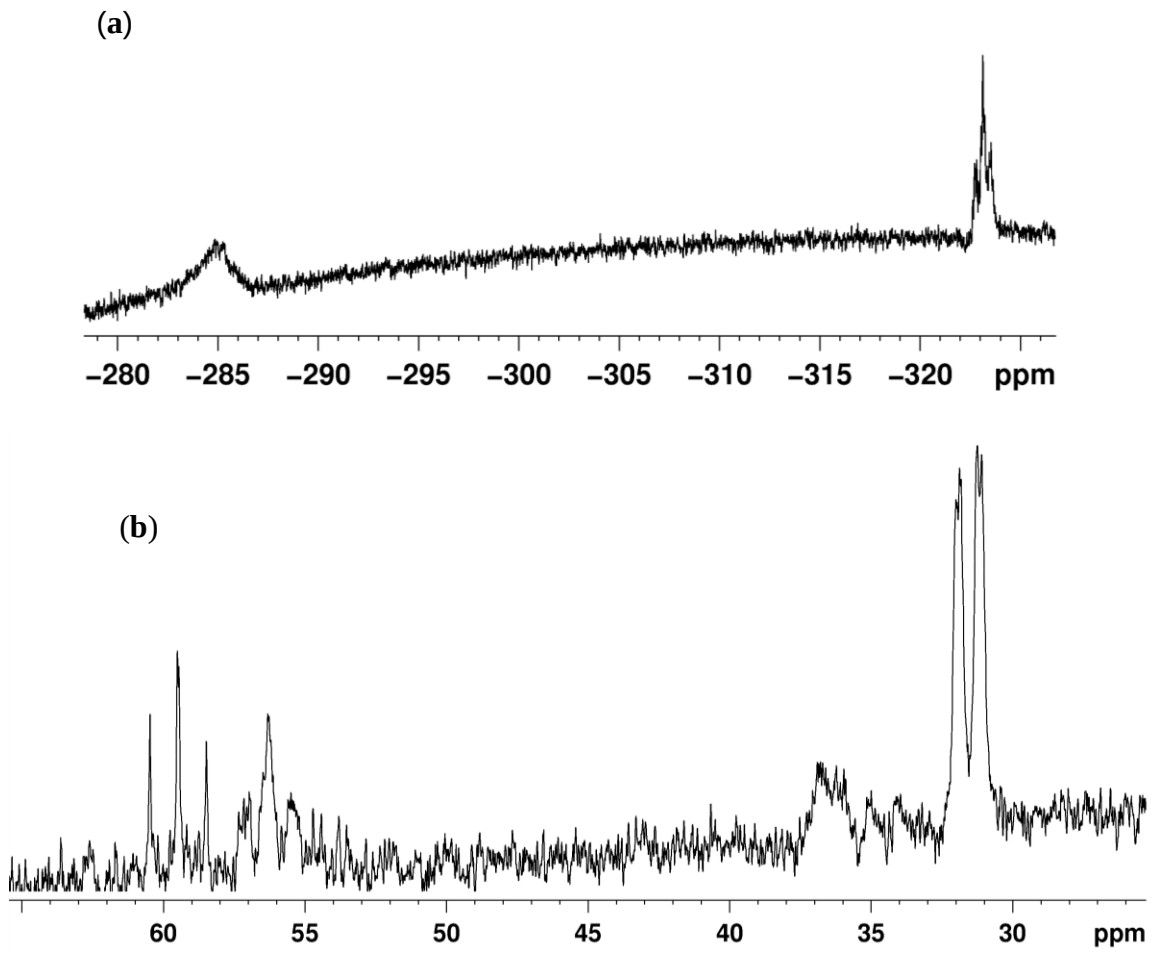

Fig 2. 14 (a) ^{19}F NMR spectrum (407.4 MHz) and (b) ^{31}P NMR spectrum (202.46 MHz) of **8** in C_6D_6 at room temperature

2.2.1.3 Complexes of platinum

Complex $Pt(PPh_3)_2FI$[10] **(10)** was prepared from the reaction of $Pt(PPh_3)_2I_2$ (**9**) and AgF in CH_2Cl_2 at 40-50^{o}C. Complex **9** is a yellow powder prepared from the reaction of $Pt(PPh_3)_4$[28] with I_2.[29] The ^{31}P NMR spectrum of **9** shows two singlets at δ 12.00 (J_{Pt-P} = 2496 Hz) and δ 11.29 (J_{Pt-P} = 3455 Hz) with platinum satellites (Fig 2. 15) assigned to the trans and cis isomers respectively.

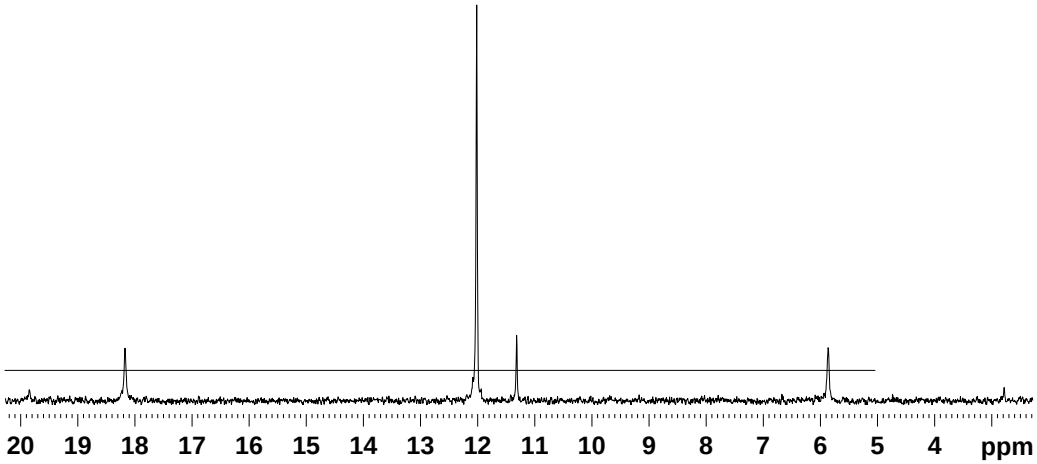

Fig 2. 15 ^{31}P NMR spectra (407.4 M Hz) of **9** in C_6D_6 at room temperature

Complex **9** was further characterized by EI and ESI mass spectrometry. The EI mass spectrum gave peaks at 846 $[M–I]^+$, 718.1 $[M–I–HI]^+$ and 262.1 $[PPh_3]^+$ showing the daughter ions (Fig 2. 16). ESI mass spectrum also gave a peak at 846 $[M–I]^+$ and another peak at 868.8 $[(M–I)+Na]^+$ corresponding to the sodiated ion (Fig 2. 17).

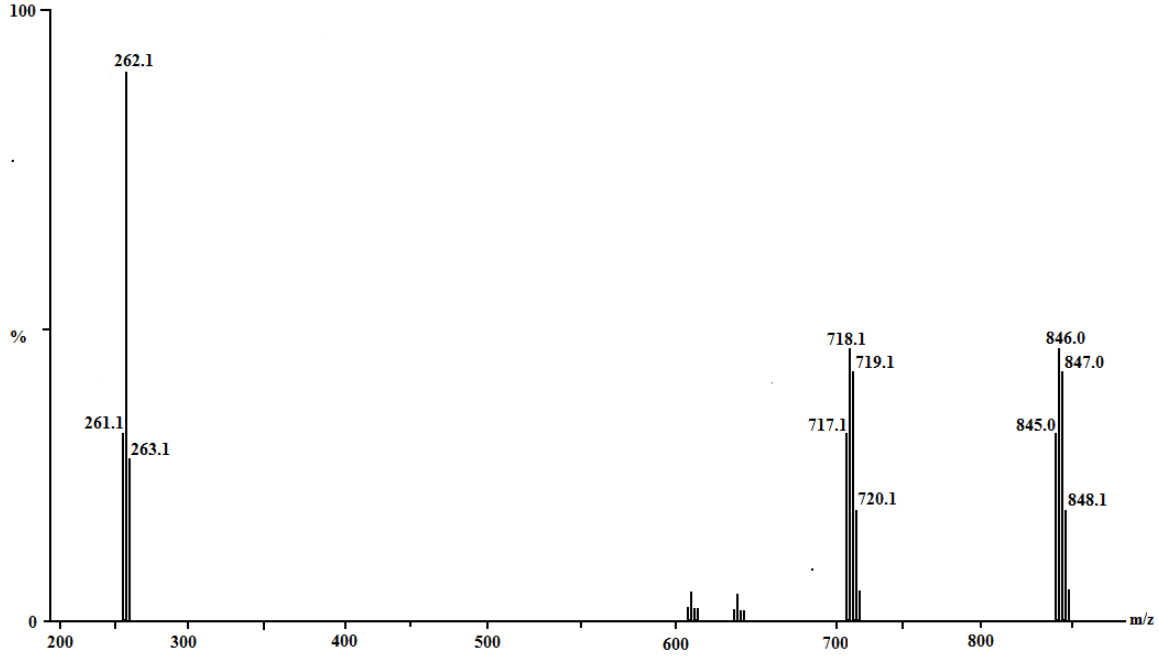

Fig 2. 16 EI mass spectrum of complex **9** in toluene

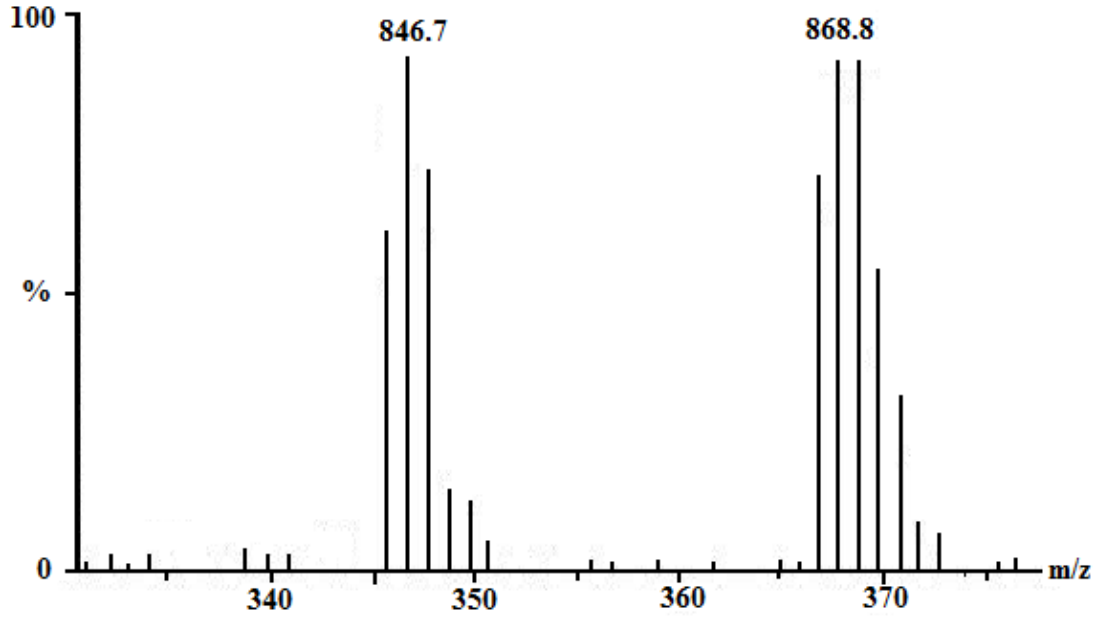

Fig 2. 17 ESI mass spectrum of $Pt(PPh_3)_2I_2$ (9) in toluene

The preparation of compound **9** was also tried by the reaction of $Pt(PPh_3)_4$ with I_2 in ethanol but it gave a mixture of $Pt(PPh_3)_2I_2$ and $Pt(PPh_3)_2IH$. Recrystallization from THF/hexane proved to be unsuccessful in separating the two compounds

The formation of **10** was confirmed by NMR and mass spectrometry. The ^{19}F NMR spectrum exhibits a triplet at δ –310.68 (J_{PtF} = 541.4 Hz, J_{PF} = 18.6 Hz) which is assigned to the metal fluoride nuclei.

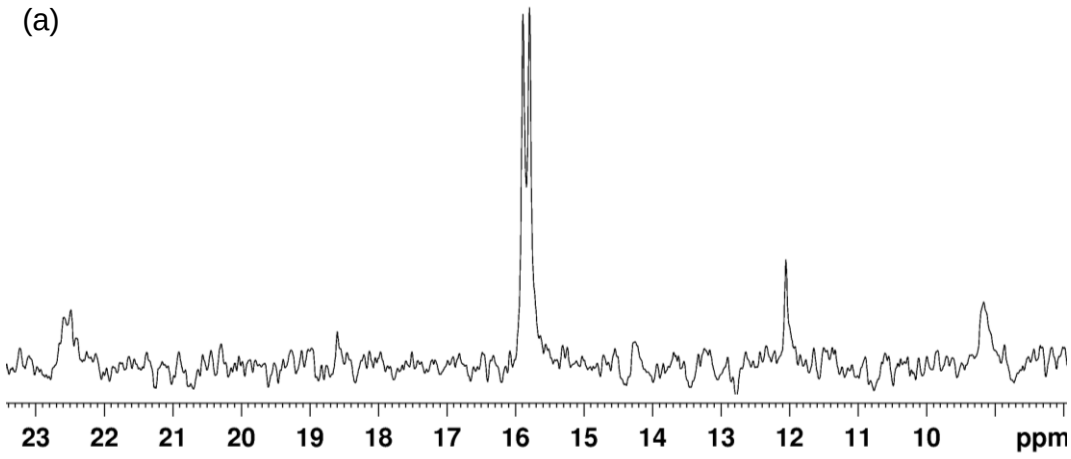

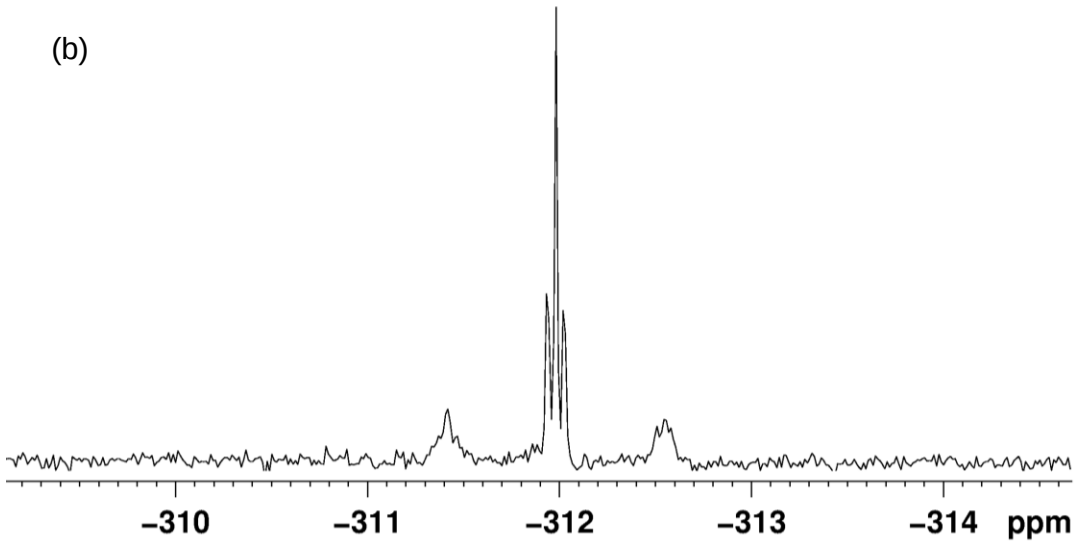

Fig 2. 18 (a) ^{31}P NMR spectra (202.46 MHz) and (b) ^{19}F NMR (407.4 MHz) of $Pt(PPh_3)_2IF$ (**10**) in C_6D_6 at room temperature

The ^{31}P NMR spectrum shows a doublet at δ 15.84 (J_{PF} = 19.2 Hz, J_{PtP} = 268.9) which is assigned to the two phosphorus nuclei. This spectrum shows that **10** have a trans configuration. These values are in close agreement with the literature values [10]. There is another resonance at δ 12.02 which is the unreacted starting material (Fig 2. 18).

The LIFDI spectrum of **10** shows the molecular ion peak $[M]^+$ at m/z = 865 and some unreacted complex **9** (starting material) ion at 972.

Purification was attempted by recrystallizing from toluene, toluene/hexane and THF/hexane but none of them was successful.

Table 2.2 ^{13}F and ^{31}P NMR data chemical shift (δ), coupling constant J/Hz, starting material is abbreviated as (**S**) and products as (**P**)

Complex		^{19}F NMR	^{19}F NMR (organic fluorine)	^{31}P NMR
3 +TMAF in THF	**S**	-373.6 (t, J_{PF} = 48.4)	-173.64 (t, J= 21.4); -151.0(m); -131.6 (t, J_{FF} = 26.7); -84.9 (m)	13.8 (d, J_{PF} = 47.7)
	P	-370.4 (t, J_{PF} = 48.0)	-172.5 (b); -160.4 (b); -164.0 (d, J_{FF} = 19.9); -130.7 (d, J_{FF} = 28.9)	13.2 (d, J_{PF} = 47.7)
	Others		-148.3 (d J_{FF} = 18.7);	45.1(s)
4 in CD_3CN	**S**	-362.4 (t, J_{PF} = 44.0)	-175.9 (dd, J_{FF} =17. 5); -152.65 (m); -134.22 (t);-88.44	13.29, (d, J_{PF}=45.9)
	P	-324.5 (d, J_{PF} = J 52.4)	-174.9 (dd) J_{FF} =17. 5; -152.6, -133.03 (t),	15.72 (s)
	Others		-97.77 (s), -148.99 (triplet 1:1:1, J 17.3) (FHF)	
3 + CsF + CD_3CN	**S**	-362.38 (t) J= 45.50	-175.83 (dd, J=15.3) ; -154.37 (m), -134.41 (t), -88.44 (dt) J= 17.05, 11.37	13.30 (d, J_{PF}= 45.9)
	P	-323.94 (d, J=57.4)	-175.64 (q), -152.69 (m), -134.22 (t, J=26.4); -89.52 (m)	15.73 (s)
	Others		-174.97 (dd, J= 15.3); -133.03 (t, J= 28.6), -88.12 (dt) J=11.54, 17.32 -97.68 (m) -148.89 (t, J=18.1) (FHF)	
3 + CsF + crown ether in CD_3CN	**S**	-362.53 (t, J=46.2) (**S**)	-175.90 (dd, J= 17.3); -160.21; -159.97,-134.37 (s), -89.50 (**S**)	13.3 (d)
	P	-359.67 (t, J= 47.1)	-175.70 (dd, J=12.5); -160.18; -154.38, -134.30(s) 88.44 (m) (**P**)	28.0 (b)
	Others	-359.16 (not clear),	-160.11, -152.70, -147.75(s) -134.21(t) J=27.1, (P) -147.49(s), -133.02 (s) (m), -147.99 (three) J=17.5,	

2.2.2 Synthesis of difluoride complexes

2.2.2.1 Complexes of titanium, zirconium and hafnium

The reaction of NaF with $(Cp^*)_2TiCl_2$ yielded $(Cp^*)_2TiF_2$ (**11**) following a literature procedure. The formation of **11** was confirmed by NMR and mass spectrometry.[30] The ^{19}F NMR spectrum exhibits a sharp resonance (C_6D_6) at d 74.69 which is assigned to the two metal fluoride nuclei.[31] Note that the ^{19}F resonance of these d^0 metal fluoride complexes appears in a completely different region from the corresponding resonance of the complexes with several d electrons.

$(Cp^*)_2ZrF_2$ (**12**) was synthesized from the reaction of $(Cp^*)_2ZrCl_2$ with NaF. The ^1H NMR spectrum shows a sharp resonance (C_6D_6) at δ 1.96, assigned to the Cp* hydrogens, while the ^{19}F NMR spectrum exhibits a sharp resonance (C_6D_6) at δ 28.72. These values are in close agreement with the literature values: the ^1H NMR spectrum (C_6D_{12}) shows a resonance at δ 1.96 and ^{19}F NMR spectrum (C_6D_{12}) at δ 34.1.[32] The LIFDI mass spectrum showed molecular ion at m/z 398 (100%) and ESI mass spectrum gave sodiated and potatiated molecular ion at m/z 421 and 437 respectively (see chapter 3).

$(Cp^*)_2HfF_2$ (**13**) synthesized from the reaction of $(Cp^*)_2HfCl_2$ with NaF. The progress of the reaction was followed by NMR spectroscopy. The ^1H NMR spectrum shows a sharp resonance (C_6D6) at δ 1.99, assigned to the Cp* hydrogens, while the ^{19}F NMR spectrum exhibits a sharp resonance (C_6D_6) at δ −17.51. These values are in close agreement with the literature values: the ^1H NMR spectrum (C_6D_6) shows a resonance at δ 1.86 (t) and ^{19}F NMR spectrum (C_6D_6) at δ −18.16. Formation of complex **13** was also confirmed by mass spectrometry.[15] The LIFDI mass spectrum gave molecular ion at m/z 488 and ESI showed sodiated molecular ion at 511 (see chapter 3).

2.2.2.2 Complexes of Ruthenium

$(PMe_3)_4RuF_2$ (**16**) was prepared by removing HF from $(PMe_3)_4Ru(FHF)_2$ (**15**). Attempts with trimethylamine were not successful but positive results were obtained with TMAF. $(PMe_3)_4Ru(FHF)_2$[33] was synthesized by a procedure developed by reaction of $(PMe_3)_4RuH_2$ with $Et_3N.3HF$ in the group previously.

The ^{19}F NMR spectrum of **16** shows a broad resonance at δ −325.4 which is assigned to the two metal fluorides. The ^{31}P NMR spectrum shows two resonances, a quintet at δ 2.98

(J_{PF} = 30.9 Hz, J_{PP} = 30.9 Hz) and two multiplets at δ 21.63 because the two mutually cis phosphorus nuclei are chemically equivalent but magnetically inequivalent (Fig 2. 19b).

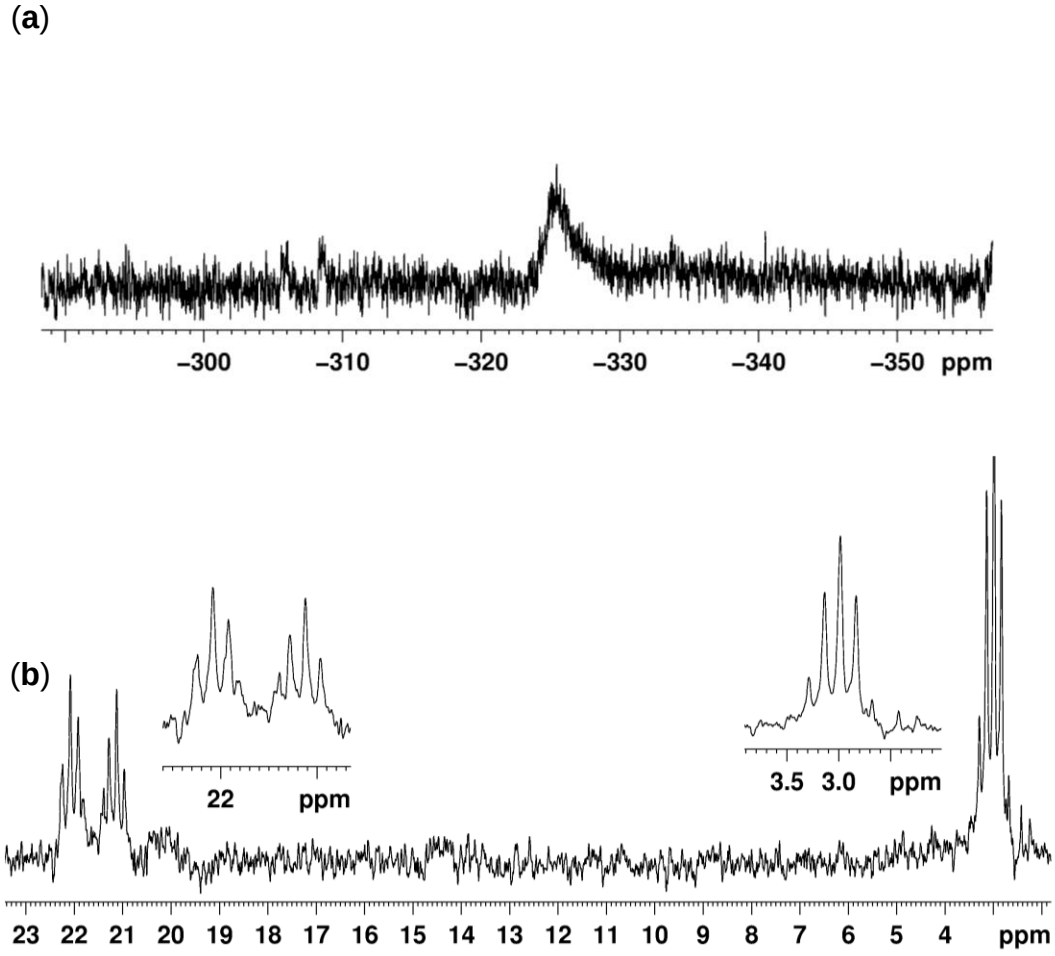

Fig 2. 19 (a) ^{19}F NMR spectrum (407.4 MHz) of the difluoride region of [trans-$Ru(PMe_3)_4F_2$ (**16**) in C_6D_6 at room temperature (b) ^{31}P spectrum (202.46 MHz)

Further evidence is provided by comparison between the spectrum of $(PMe_3)_4Ru(FHF_2)$ (**15**) and $(PMe_3)_4RuF_2$ (**16**). The ^{19}F NMR spectrum of **15** shows a broad doublet at δ -175.7 (Fig 2. 20a) which is assigned to the distal fluorine in addition to a broad resonance at δ –315.1 assigned to the proximal fluorine,[33] but the resonance of the distal fluorine is missing in the ^{19}F NMR spectrum of $(PMe_3)_4RuF_2$ which shows only a single resonance at δ –325.4. So it is concluded that HF from **15** is removed by TMAF and $(PMe_3)_4RuF_2$ is synthesized. The ^{1}H NMR spectrum of **15** also shows a doublet at δ 13.4, assigned to the acidic hydrogen [33] (Fig 2. 20b) while this resonance disappears from the ^{1}H NMR spectrum of $(PMe_3)_4RuF_2$.

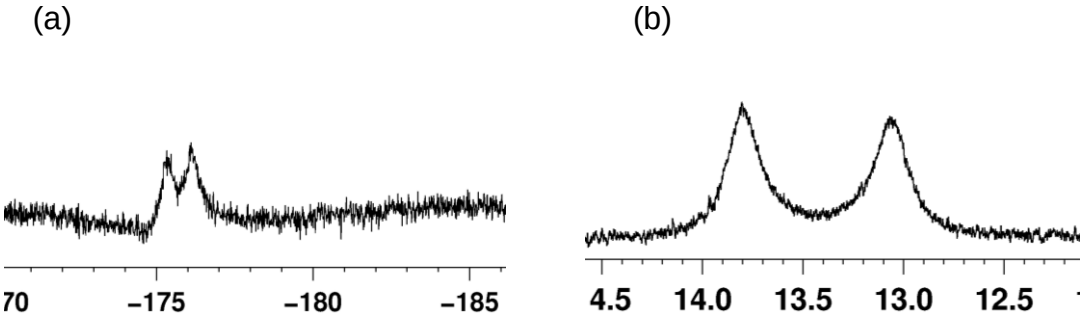

Fig 2. 20 (a) ^{19}F NMR spectra (407.4 MHz) of the distal fluorine of **15** (b) ^{1}H spectrum (500.1 MHz) of **15** showing the acidic hydrogen in C_6D_6 at room temperature .

The NMR spectrum of $(PMe_3)_4RuF_2$ was also fitted with gNMR[34] (Fig 2. 22 a & b). The calculated ^{31}P spectrum showed quite good agreement with the experimental spectrum.

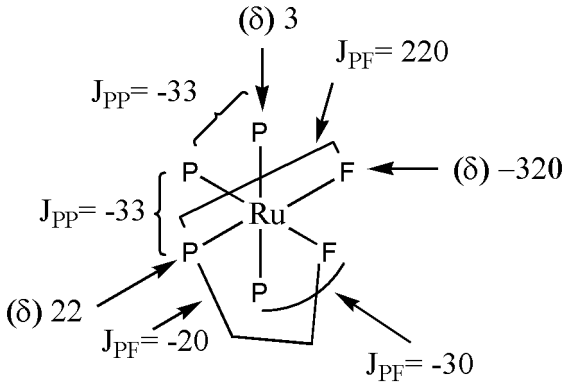

Fig 2. 21 (a) Chemical shifts and coupling constants (Hz) for cis-$(PMe_3)_4$ RuF_2 (**16**) developed by simulation of NMR spectra

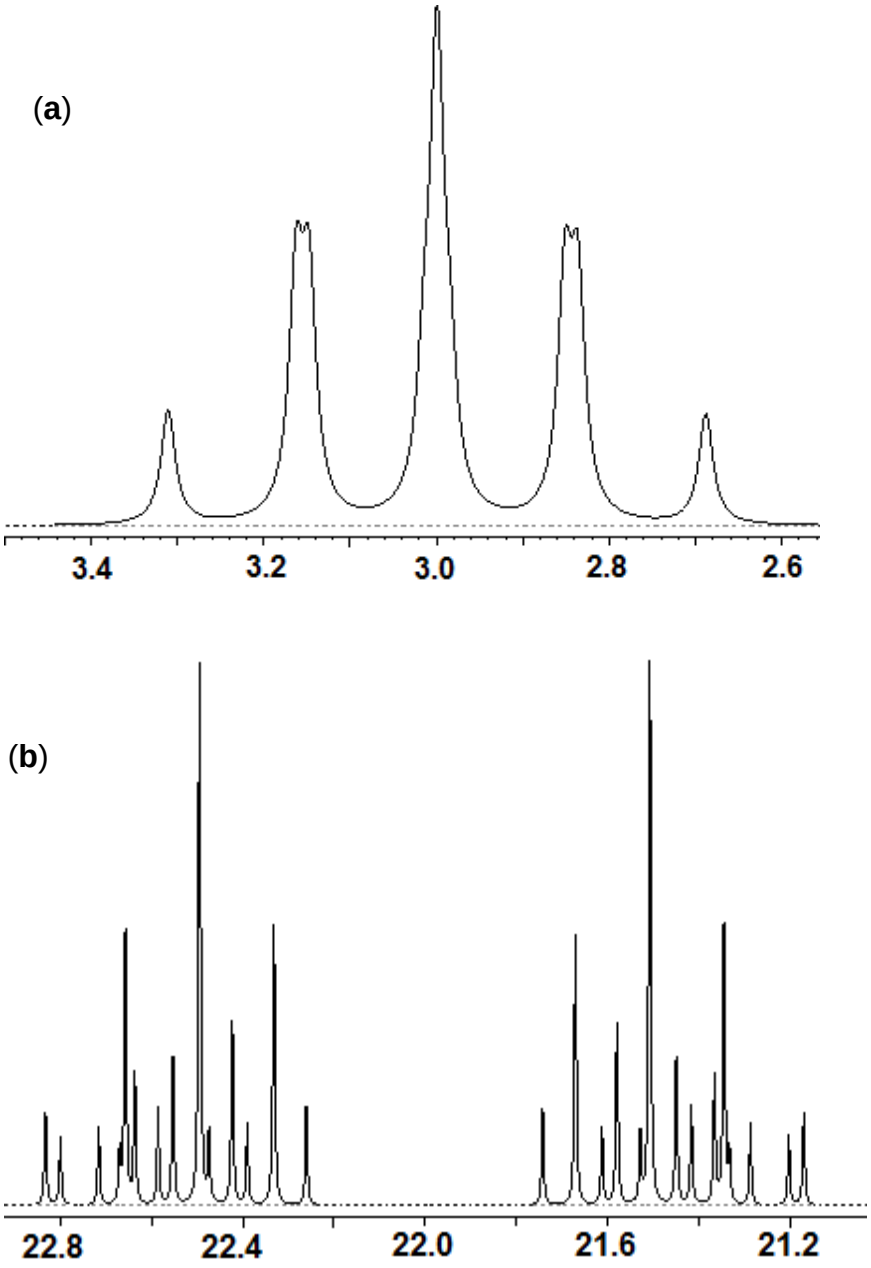

Fig 2. 22 Calculated ^{31}P NMR spectra (202.46 MHz) of **16** (b) trans phosphorus (c) cis phosphorus.

The LIFDI mass spectrum of $(PMe_3)_4RuF_2$ gave a molecular ion peak at m/z 444.

Ru(dppe) $_2$H(FHF) (**18**) and trans-Ru(dppp)$_2$H(FHF) (**20**) were prepared from the reaction of corresponding dihydride with $Et_3N.3HF$ and characterized by multinuclear NMR spectroscopy.[33]

2.2.2.3 Complexes of Platinum

cis-$Pt(PPh_3)_2F_2$ **21**[10] is a white solid prepared from the reaction of $Pt(PPh_3)_2I_2$ and AgF at room temperature. The synthesis of the compound was followed by NMR spectroscopy. The ^{19}F NMR spectrum (Fig 2. 23a) shows a resonance at δ –215.75 (AA´MXX´, $J_{P(cis)F}$ = 14.7 Hz, J_{FF} = 85.1 Hz). The ^{31}P NMR spectrum (Fig 2. 23b) shows a resonance at δ 4.45 (AA´MXX´, J_{PtF} = 3832 Hz, $J_{P(trans)F}$ = 179.4 Hz, $J_{P(cis)P}$ = 22.4 Hz). These values are in close agreement with literature.[10, 35]

The ^{19}F NMR spectrum also shows a small resonance at δ –228.04 and the ^{31}P NMR spectrum shows resonances at δ 8.1 which are assigned to the unknown impurities present in the compound. There is another resonance in ^{31}P NMR spectrum at δ 12.02 for the starting material. For purification the compound was washed with hexane and the fluorinated impurities were removed but impurities containing phosphorus are still present.

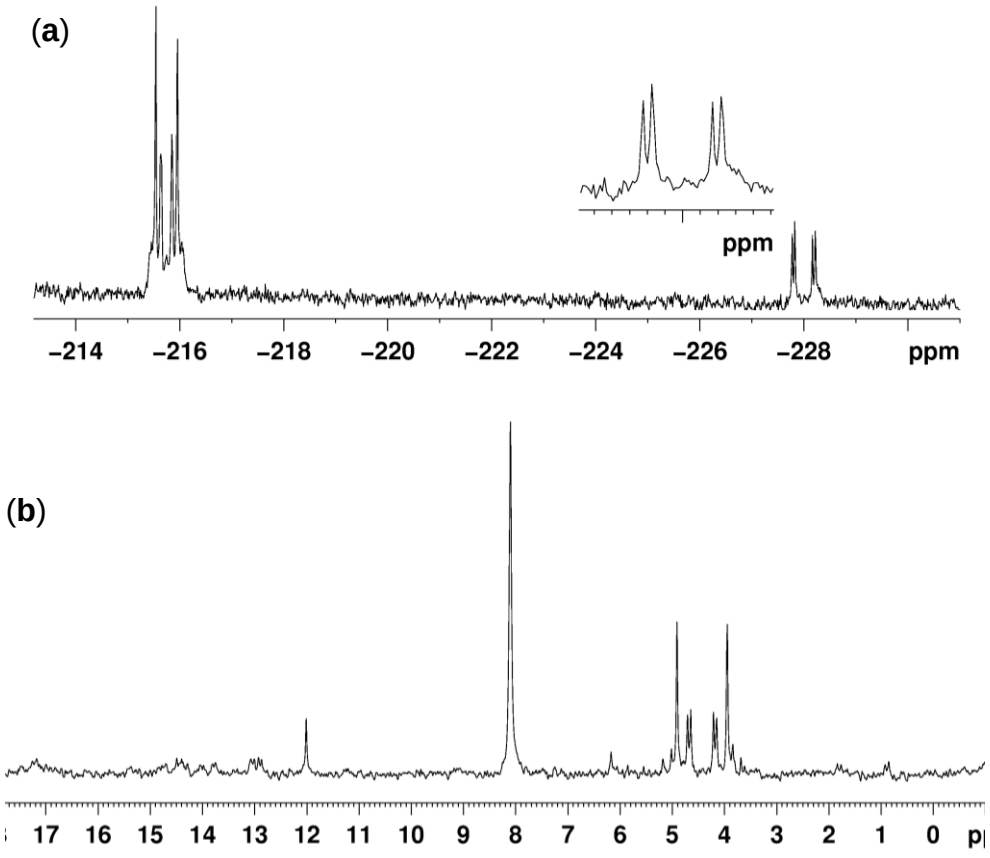

Fig 2. 23 (a) ^{19}F NMR spectra (500 MHz) of **21** in $CDCl_3$ at room temperature and (b) ^{31}P NMR

The NMR spectrum of **21** was also fitted with gNMR[34] (Fig 2. 25). The calculated ^{31}P and ^{19}F spectra showed quite good agreement with the experimental spectrum.

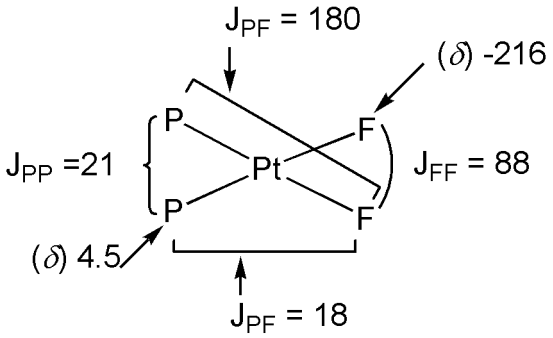

Fig 2. 24 Chemical shifts and coupling constants (Hz) for cis-$(PPh_3)_2PtF_2$ developed by simulation of NMR spectra

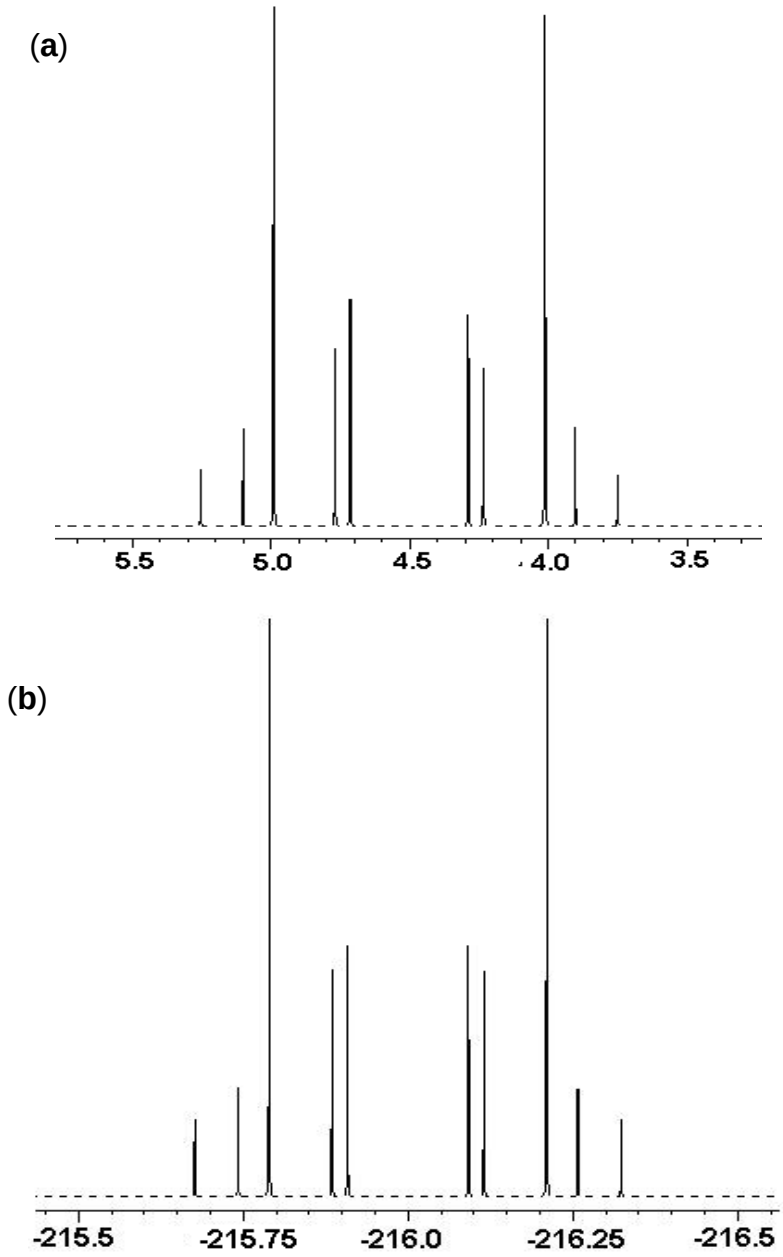

Fig 2. 25 Calculated (a) ^{31}P NMR and (b) ^{19}F NMR spectra (500 MHz) of **21**

2.2.2.4 Difluoride complexes of zinc and cobalt

$[Zn(DMEA)_2F_2]$ (**24**) and $Co(DMEA)_2F_2]$ **(25)** were prepared by reacting anhydrous ZnF_2 and CoF_2 with N,N-dimethylethylene-1,2-diamine respectively. These compounds were handled in plasticware as they react with the glassware. The compounds were partially dried under vacuum (2-3 h) and were left in the glove box to get fully dry. Complexes **24** and **25** were previously isolated by S. Nazir and the crystal structures of dihydrates was determined (Fig 2. 28, and Fig 2. 30). However Nazir's synthesis did not yield satisfactory analytical data and there was no mass spectrometric data.

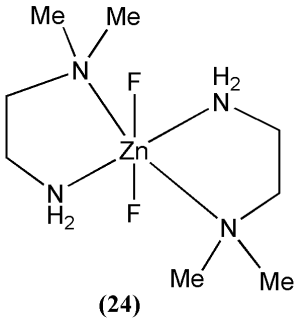

(24)

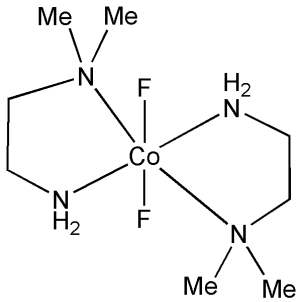

(25)

The ^1H NMR spectrum of **24** shows two triplets at δ 2.84 (J_{HH} = 5.12 Hz, 4H), 2.47 (J_{HH} = 5.77 Hz, 4H) and a singlet at δ 2.30 (12H) corresponding to the two CH_2 and CH_3 groups respectively. The ^{19}F NMR spectrum shows a singlet at δ –152 assigned to the two metal fluorides (Fig 2. 26 a & b).

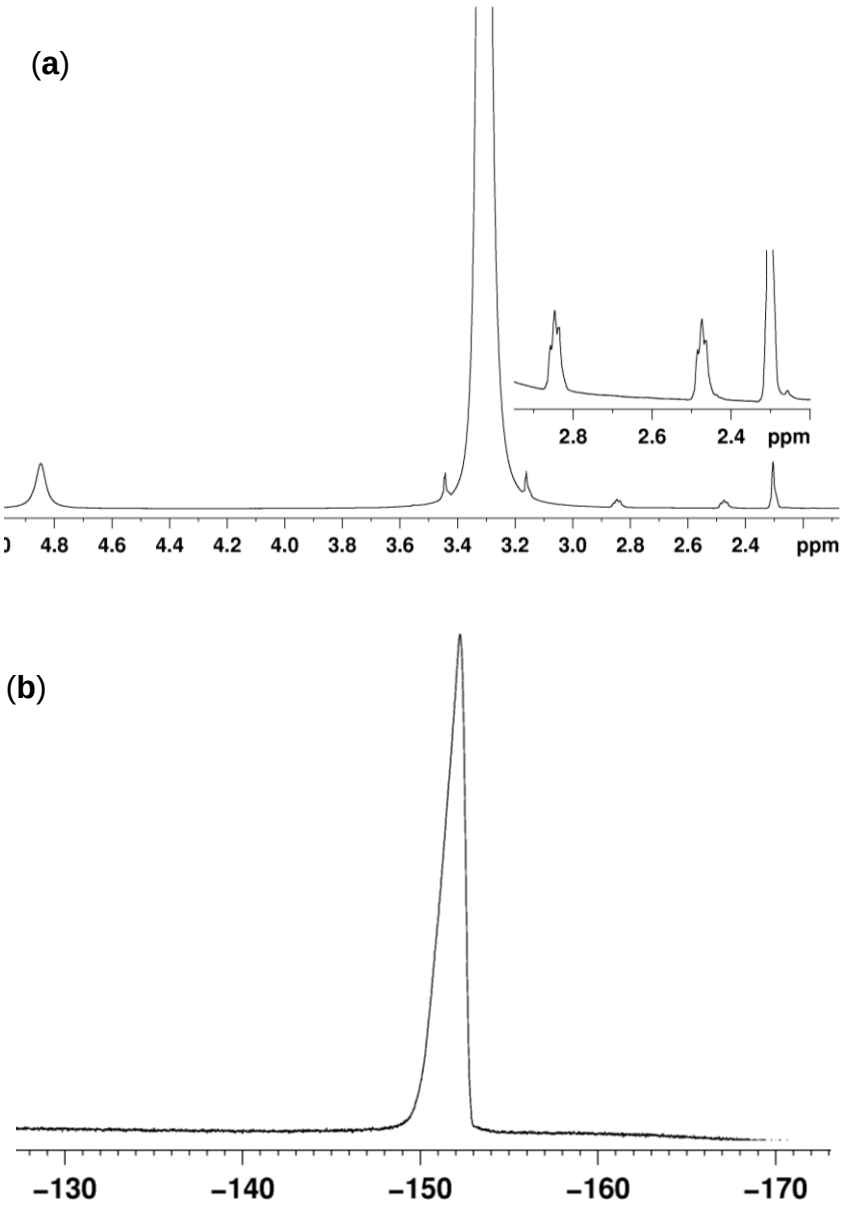

Fig 2. 26 (a) ^{1}H NMR and (b) ^{19}F NMR spectra (500 MHz) of **24** in CD_3OD at room temperature

Fig 2. 27 displays the ESI mass spectrum of complex **24**. The peak at 259.1 results from the loss of fluoride ligand from the compound $[M–F]^+$. Other peaks at 239.1 corresponds to $[(M–HF_2]^+$.

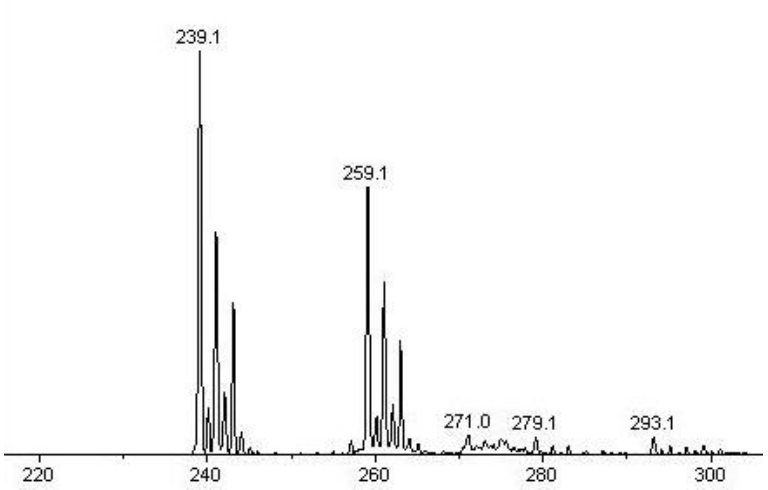

Fig 2. 27 ESI mass spectrum of **24** in CH_3OH

The formation of **24** was further by elemental analysis and the observed percentages of carbon, hydrogen and nitrogen (C, 31.58; H, 9.11; N, 18.39) are within the specified limits.

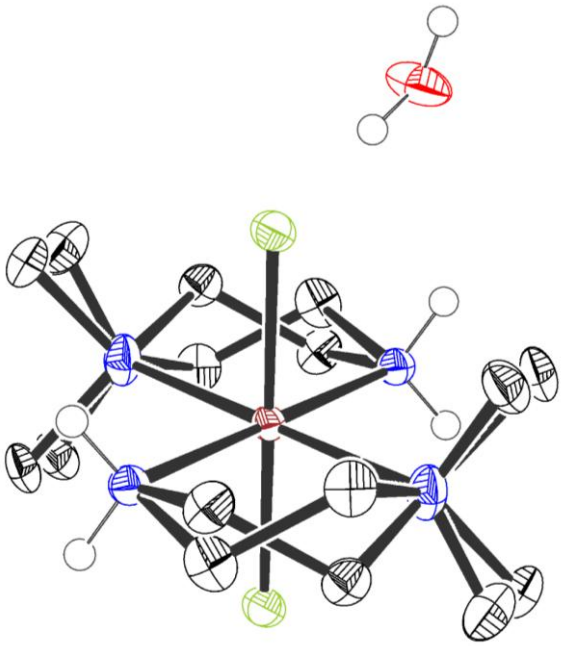

Fig 2. 28 unit cell diagram of $[Zn(DMEA)_2F_2]H_2O$ (50 % probability ellipsoids)

The ESI mass spectrum of complex **25** shows a peak for the molecular ion $[M]^+$ at m/z 273. Sodiated molecular ion peak $[M+Na-H]^+$ and molecular ion peak coordinated to ammonium ion $[M+NH_4]^+$ appears at m/z 295 and 281 respectively. Other ions at m/z 254 $[M–F]^+$ and 233 $[M–2HF]^+$ correspond to the daughter ions form by the loss of $F^–$ and HF

ligands. The exact mass was found to be 273.1294 which is in close agreement with the calculated (273.1301).

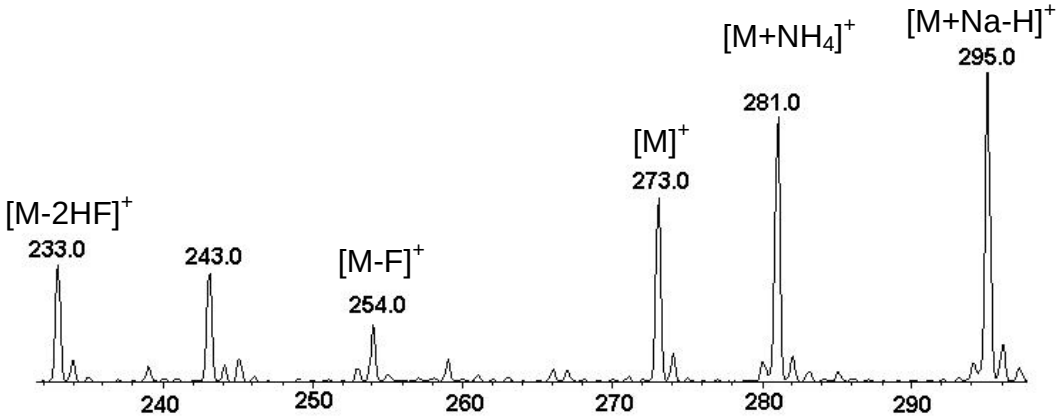

Fig 2. 29 ESI mass spectrum of **25** in CH_3OH

The formation of **25** was further by elemental analysis and the observed percentages of carbon, hydrogen and nitrogen (C, 35.80; H, 8.40; N, 19.48) are in close agreement with the calculated (C, 35.17; H, 8.85; N, 20.51).

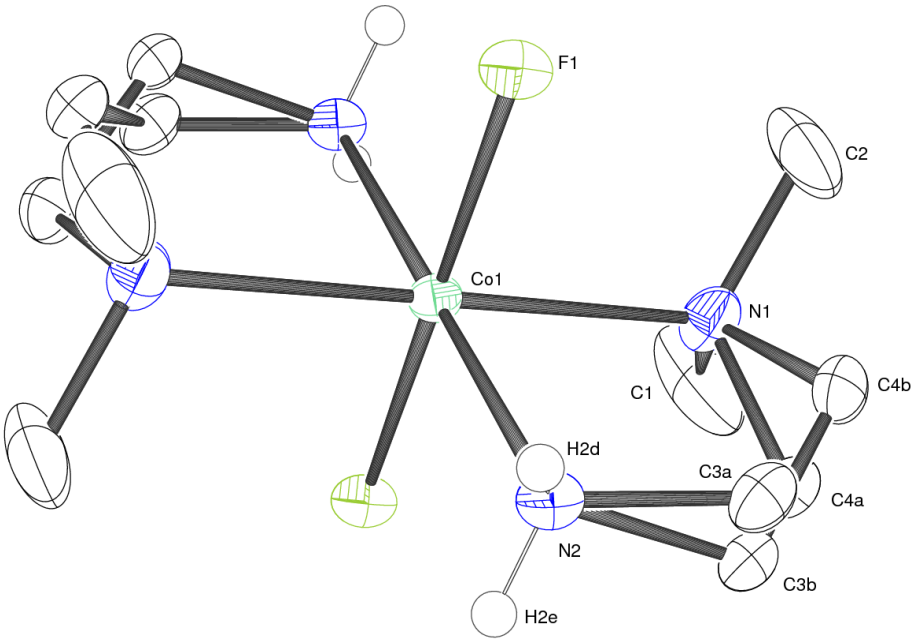

Fig 2. 30 Complete unit cell diagram of $[Co(DMEA)_2F_2]$. $2H_2O$ (50 % probability ellipsoids)

2.3 Discussion

2.3.1 NMR spectroscopy of transition metal fluoride complexes

Characterization of metal fluoride complexes is greatly assisted by the ^{19}F NMR spectroscopy. For late transition metal fluoride complexes, an upfield resonance is observed that is in a region quite distinct from that of organic fluorine. The ^{19}F NMR spectra for $Rh(PPh_3)_3F$ exhibit a resonance at $\delta -286.3$ (ddt) for Rh-F and cis– $Pt(PPh_3)_2F_2$ at $\delta -216.34$ for Pt-F. Note that the ^{19}F resonance of these d^0 metal fluoride complexes appears in a completely different region from the corresponding resonance of the d^8 complexes. For instance, the ^{19}F NMR spectrum of $(Cp^*)_2TiF_2$ exhibits a sharp resonance (C_6D_6) at $\delta 74.7$ which is assigned to the two metal fluoride nuclei.[31] The ^{19}F NMR spectrum of $(Cp^*)_2ZrF_2$ shows a sharp resonance (C_6D_6) at $\delta 28.7$.[22,32].

The ^{19}F NMR spectrum of $[NiF(2\text{-}C_5NF_4)(PEt_3)_2]$ shows a triplet at $\delta -371.35$ for the metal fluoride and four mutiplets ($\delta -173.4, -150.8, -131.3$ and -84.7) for the fluoropyridyl ligand. $[TiF(2\text{-}C_5NF_4)(Cp^*)_2$ shows an analogous pattern for the fluoropyridyl ligand while the metal fluoride resonance appears at $\delta 128.8$.[24,31]

The ^{19}F NMR spectra of bifluoride and bis-bifluoride complexes of ruthenium i-e **15**, **18** and **20** contains two resonances, the resonance for proximal fluorine appears at $\delta -290$ to -355 while for the distal fluorine at $\delta -160$ to -175.

2.4 Conclusion

Transition metal fluoride monofluoride complexes were synthesized and characterized successfully by multinuclear NMR and LIFDI mass spectrometry but with ESI the fluoride ligand was lost due to its lability. Similar behaviour was observed by Henderson with transition metal halide complexes.[36] On the other hand metallocene difluoride complexes of group 4 retained one or both of the fluorides in ESI mass spectrometry.

Table 2.3 ^{19}F and ^{31}P NMR data chemical shift (δ), coupling constant J/Hz, of transition metal fluoride complexes

Complex	$\delta(^{19}F)$	$\delta(^{31}P)$
trans-NiF{2-C_5NF_3(4-NMe_2)}$(PEt_3)_2$ [37]	–367.8 (t) J_{PF}= 47.41, –91.27 (t) J= 28.09, –121.1 (d) J= 26.76, –164.33 (d) J= 28.59	12.7 (d) J_{PF}= 48.19
trans-NiF{2-C_5NF_3(4-OMe)}$(PEt_3)_2$ [23]	–368.78 (t, 1F) J_{PF} = 45.69, -170.11 (d,1F) J_{FF} = 28.50 –128.33 (d,1F) J_{FF} = 27.99, -88.71 (t, 1F) J_{FF} = 28.52	13.05(d) $J_{PF=}$ 48.06
$Rh(PPh_3)_3F$ [37]	–285.0 (b)	31.5 δ56.3
$Pt(PPh_3)_2FI$ **(10)**	–310.68 (J_{PtF} = 541.4 Hz, J_{PF} = 18.6 Hz)	15.84 (J_{PF} = 19.2 Hz, J_{PtF} = 268.9 Hz)
$(Cp^*)_2TiF_2$ (**11**)	74.69 (s)	-
$(Cp^*)_2ZrF_2$ (**12**)	28.72 (s)	-
$(Cp^*)_2HfF_2$ (**13**)	–17.51 (s)	-
$(PMe_3)_4Ru(FHF_2$ (**15**)	–315.1 (b), –175.7 (d)	
$(PMe_3)_4RuF_2$ (**16**)	–325.4 (b)	2.98 (quintet) (J_{PF} = 30.9 Hz, J_{PF} = 30.9 Hz)21.22 (m) 2.22 (m)
cis-$Pt(PPh_3)_2F_2$ **(21)**	–215.75 (AA´MXX´, $J_{P(cis)F}$ = 14.7 Hz, J_{FF} = 85.1 Hz)	4.45 (AA´MXX´, J_{PtF} = 3832 Hz, $J_{P(trans)F}$ = 179.4 Hz, $J_{P(cis)P}$ = 22.4 Hz)
$Zn(DMEA)_2F_2$ (**24**)	–152 (s)	

LIQUID INJECTION FIELD DESORPTION/IONIZATION OF TRANSITION METAL FLUORIDE COMPLEXES

3.1 Introduction

Transition metal fluoride complexes have several characteristics that are significantly different from their analogues with heavier halides. The realization that they have special properties has led to a surge of interest in the last few years. They are prone to rearrangements involving other ligands especially phosphines,[1,2] they are highly polar and readily form complexes with hydrogen bond donors and halogen bond donors,[3,4] they are capable of C-F reductive elimination in special circumstances.[5,6] They may be formed with the aid of a wide variety of fluorinating agents such as XeF_2, $Et_3N.3HF$, AgF, etc.,[2,6-8] but a method of particular interest to us has been C-F oxidative addition.[9-21]

Characterization of metal fluoride complexes is greatly assisted by ^{19}F NMR spectroscopy. For late transition metal fluoride complexes, an upfield resonance is observed that is in a region quite distinct from that of organic fluorine. In contrast, mass spectrometric characterization has proved extremely troublesome, because of loss of fluoride or loss of HF.

Electrospray ionization (ESI), although a soft technique, cannot be used to characterize late transition metal fluorides. Most fluoride complexes are neutral molecules and require protonation or association with Na^+/K^+ to observe, but in practice as for other halide complexes, the metal fluoride bond is too labile.[22]

Electron impact ionization [23] has been used occasionally to characterize fluoride complexes but the molecular ion was very weak and the compound showed decomposition.[1] Fast atom bombardment (FAB) has also met with very limited success.

Another soft technique called field ionization (FI) was introduced by R. Gommer and M.G. Inghram which can be used with volatile compounds. The sample is introduced in the mass spectrometer in the gas phase using a micro oven where the ions are formed by electron tunneling and the positive ions are pushed towards the emitter. FI was inconvenient because of the use of very high voltage and a very delicate emitter. FI was later extended to non-volatile samples via deposition of a sample on the emitter called Field Desorption.[24-26]

Field desorption (FD) is a soft ionization technique of interest for inorganic chemists as it is capable of analysing involatile compounds of low to medium polarity,

but it was formerly considered as experimentally very demanding.[26,27] Nevertheless, it has been used successfully to analyse transition metal complexes with weakly bonded ligands.[26,28] Mass spectra produced by FD show little or no fragmentation and are dominated by molecular radical cations $M^{+\cdot}$ while protonated molecules are formed less often.[29] In the FD technique, the analyte is applied as a thin film directly to the emitter, or small crystals of solid materials are placed onto the emitter. Slow heating of the emitter then begins, and application of the electric field causes the desorption of intact molecular ions from the regions of high electric field gradient.[26]

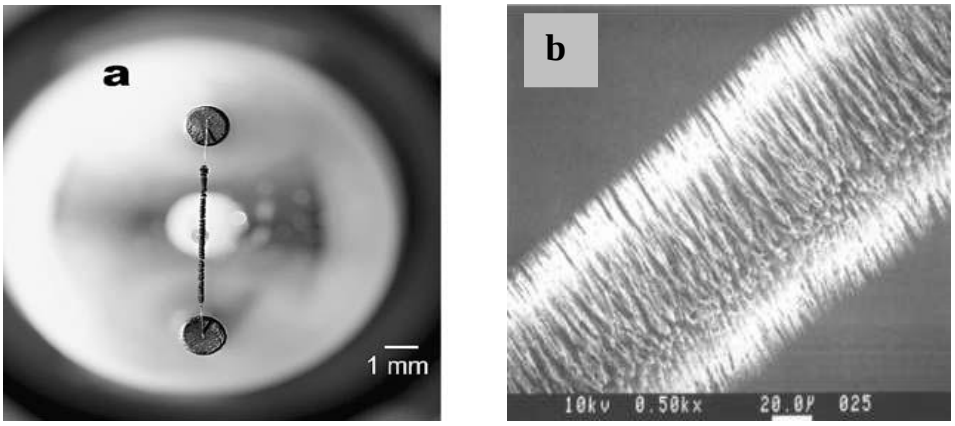

Fig 3. 1 (a) Emitter used with FD probe[30] and (b) close view of the emitter[31]

The recently developed LIFDI technique [30,32] can now be conducted much faster and more easily. Neutral transition metal complexes often ionize without fragmentation and do not undergo protonation or ion attachment. Transfer of air/moisture sensitive analyte solutions is carried out from a vial (loaded in the glove box) to the FD emitter in the ion source through a fused silica capillary under an inert atmosphere without breaking the vacuum. [29]

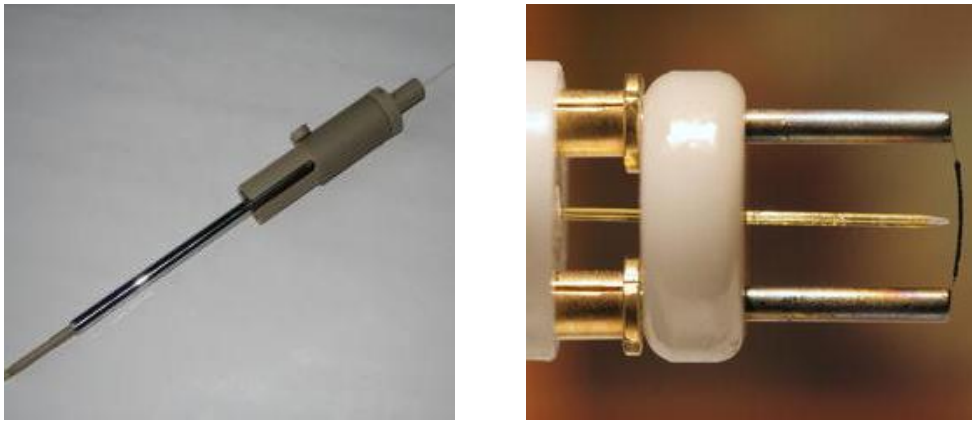

Fig 3. 2 (a) Silica capillary[31] and (b) LIFDI probe

A time-of-flight analyzer is suitable with ion sources which generate ions in a pulse. A pulse of ions is generated by the LIFDI probe and is accelerated from the FD source by application of a high voltage (about 1200 V) into the orthogonal TOF tube where the potential energy is converted to kinetic energy.

$$K.E = zeV$$

Since KE = $1/2mv^2$, the resulting velocity depends upon the inverse square root of the mass. Kinetic energy can also be expressed in terms of the Newtonian equation.

$$KE = \frac{1}{2} m(dx/dt)^2$$

Then:

$$zeV = \frac{1}{2} m(dx/dt)^2$$

By rearranging this equation, m/z for a given ion can be determined

$$m/z = 2eV\Delta t^2/\Delta x^2$$

where m is the mass, Δt is the time of flight and Δx is the path length.[26 33]

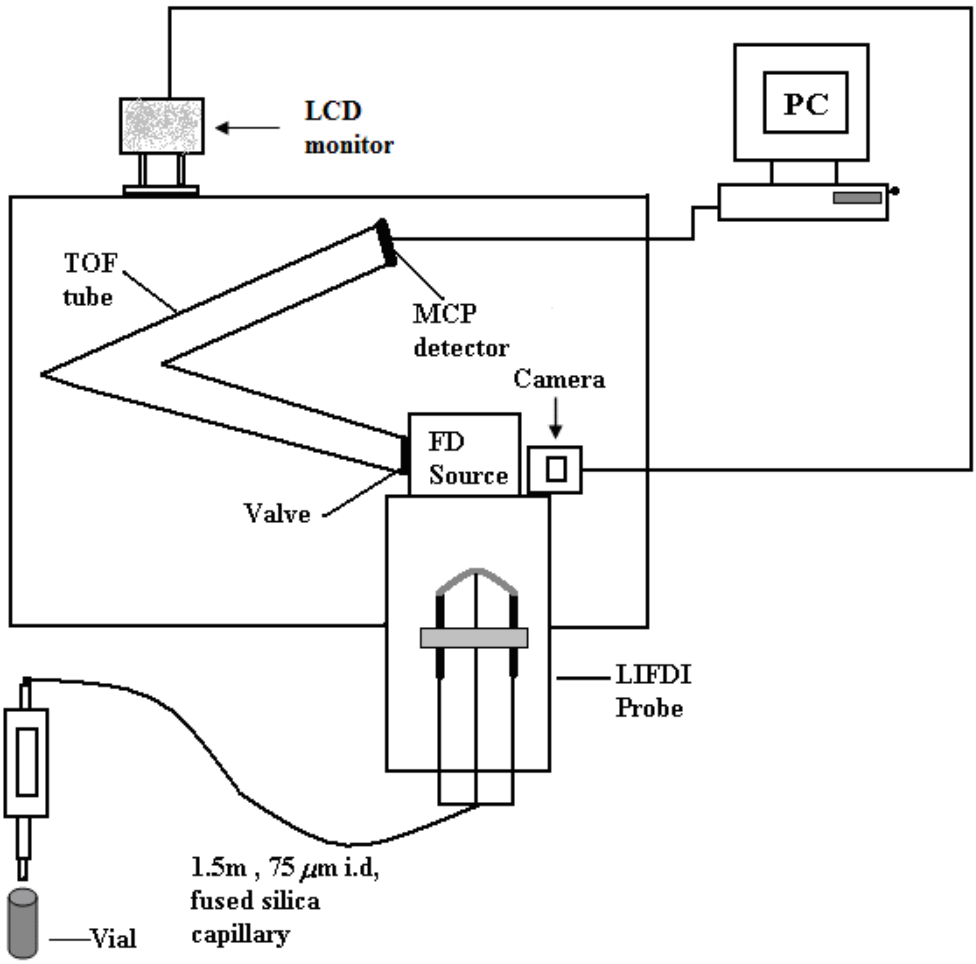

Fig 3. 3 Schematic representation of the LIFDI-TOF mass spectrometer

In order to obtain high resolution spectra, TOF analyzers are kept at low pressure to avoid collisions as the resolution is based on the time of flight of the ions.

In a time-of-flight mass spectrometer, ions are accelerated by an electric field of known strength, all of which arrive at the detector within a few microseconds and ions having close m/z values are separated by less than a nanosecond. Microchannel plate (MCP) detectors consisting of an array of small electron multipliers are used to ensure that all the ions are collected.[26]

Recently, Perutz et al found that Liquid Injection Field Desorption Ionization (LIFDI) yielded high quality mass spectra for some platinum complexes with conspicuous parent ions. With LIFDI mass spectrometry, molecular ions were observed for *cis*-[Pt(F){2-$C_5NHF_2(CF_3)$}($PiPr_3$)$_2$] and *trans*-[Pt(F){2-$C_5NHF_2(CF_3)$}(PCy_3)$_2$] at *m*/*z* 715.3 $[M]^+$ 100% and 955.4 $[M]^+$ 50% respectively.[34]

The purpose of the study was to investigate whether LIFDI in association with a time-of flight mass spectrometer is generally applicable to the characterization of air-sensitive transition metal fluoride complexes.

3.2 Results

The LIFDI measurements were performed on a Waters Micromass GCT Premier orthogonal time-of-flight instrument set to one scan per second with resolution power of 6000 FWHM and equipped with a LIFDI probe from LINDEN GmbH. The design is very similar to that described by Gross et al.[30]

Toluene was used for tuning the instrument. The polyethylene glycol probe was kept at ambient temperature with the emitter potential at 12 kV. Activated tungsten wire LIFDI emitters (13 mm tungsten from LINDEN) were ramped manually up to 100 mA for the emitter heating current during the experiment. Repeated short baking at 90 mA was used to clean up the emitter after each experiment. Solutions of the analytes (ca. 1 mg mL^{-1}) were made up in toluene or THF (a low freezing solvent is required in order to prevent freezing in the capillary) in the glove box and transferred to a small vial. Transfer from the vial to the emitter is carried out by capillary. The spectra were calibrated with polyethylene glycols.

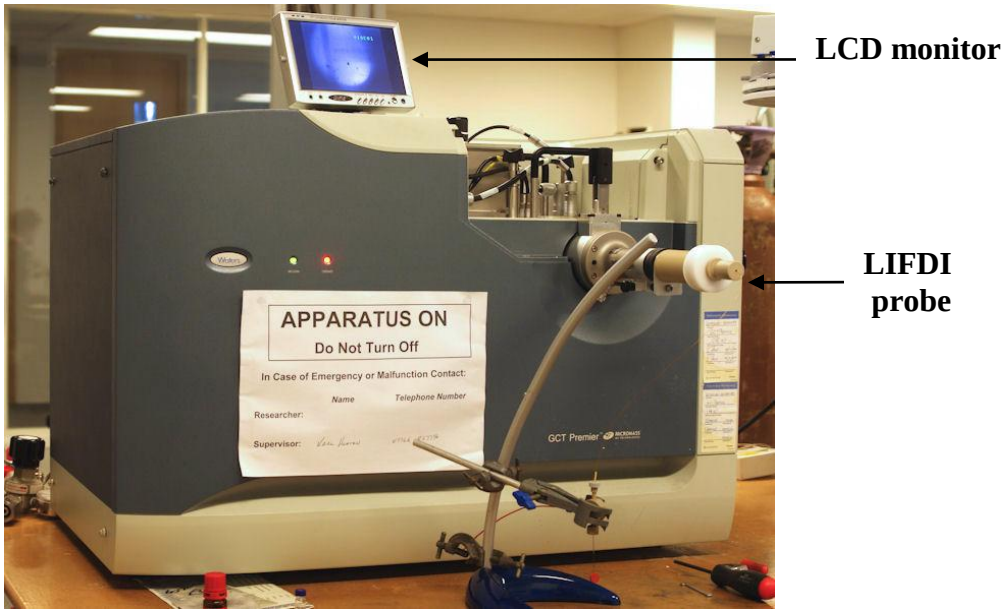

Fig 3. 4 LIFDI-TOF mass spectrometer

The ESI mass spectra were obtained using Esquire 6000 (Bruker Daltonics, Berman, Germany) mass spectrometer equipped with quadrupole 3D ion trap, having scan speed of 13000 m/z /s. The ESI source is of an orthogonal sprayer design and was operated at a spray voltage of 3-4 kV. Data were collected in standard scan mode. Nitrogen was used as bath gas (200-300˚C; 300-600 L/h) and nebulizing gas (5-10 psi). The analyte solution was introduced into the mass spectrometer by a syringe pump employing a 500 μL syringe. The sample solution was introduced at constant flow rate of 240-480 μL/h.

The theoretical isotope patterns for mass spectra were calculated using the ‘‘Fluorine chemistry mass spec simulator’’.[35] Mass peaks are quoted for ^{48}Ti, ^{58}Ni, ^{90}Zr and ^{102}Ru.

Table 3.1 List of stable isotopic masses and their natural abundance[36]

Atomic No	Element	No of isotopes	Isotopes of element and their natural abundance (%)
1	Hydrogen	3	^{1}H (99.99), ^{2}H (0.015)
6	Carbon	5	^{12}C (98.93), ^{13}C (1.07)
9	Fluorine	1	^{19}F (100)
17	Chlorine	2	^{35}Cl (75.78), ^{37}Cl (24.22)
22	Titanium	5	^{46}Ti (8.25), ^{47}Ti (7.44), ^{48}Ti (73.72), ^{49}Ti (5.41), ^{50}Ti (5.18)
27	Cobalt	1	^{59}Co (100)
28	Nickel	5	^{58}Ni (68.08), ^{60}Ni (26.22), ^{61}Ni (1.40), ^{62}Ni (3.63), ^{64}Ni (0.93)
30	Zinc	5	^{64}Zn (48.63), ^{66}Zn (27.90), ^{67}Zn (4.10), ^{68}Zn (18.75), ^{70}Zn (0.62)
40	Zarconium	5	^{90}Zr (51.45), ^{91}Zr (11.22), ^{92}Zr (17.15), ^{94}Zr (17.38), ^{96}Zr (2.80)
44	Ruthenium	7	^{96}Ru (5.54), ^{98}Ru (1.87), ^{99}Ru (12.76), ^{100}Ru (12.60), ^{101}Ru (17.06), ^{102}Ru (31.55), ^{104}Ru (18.62)
45	Rhodium	1	^{103}Rh (100)
72	Hafnium	5	^{174}Hf (0.16), ^{176}Hf (5.26), ^{177}Hf (18.60), ^{178}Hf (27.28), ^{179}Hf (13.62), ^{180}Hf (35.08)
75	Rhenium	2	^{185}Re (37.4), ^{187}Re (62.6)
78	Platinum	5	^{190}Pt (0.01), ^{192}Pt (0.78), ^{194}Pt (32.97), ^{195}Pt (33.83), ^{196}Pt (25.24), ^{198}Pt (7.16)

3.2.1. Characterization of Transition metal monofluoride complexes by LIFDI

Our initial studies centred on mass spectrometry of nickel fluoride complexes made by C-F oxidative addition of hexafluorobenzene and of fluorinated pyridines. All the compounds were characterized successfully by liquid injection field desorption ionization (LIFDI).[37] Electron Impact (EI) showed complete decomposition of these complexes. For ESI mass spectrometry, we used fluorinated pyridines with dimethylamino and methoxy groups at the 4-position in the expectation that they would be sufficiently basic for protonation or sodiation.

3.2.1.1.Complexes of nickel

Complex **1** (trans-NiF{2-C_5NF_3(4-NMe_2)}(PEt_3)$_2$) and **2** (trans-NiF{2-C_5NF_3(4-OMe)}(PEt_3)$_2$) were described in Chapter Two. They both were studied by the LIFDI and ESI techniques. LIFDI of **1** gave the molecular ion $[M]^+$ as base peak at m/z = 488 (Fig 3. 5 a) while ESI gave decomposition. Further peaks correspond to the contributions from the various Ni isotopes and ^{13}C. There is excellent agreement between the observed and calculated isotope patterns (Fig 3. 5 b & c).

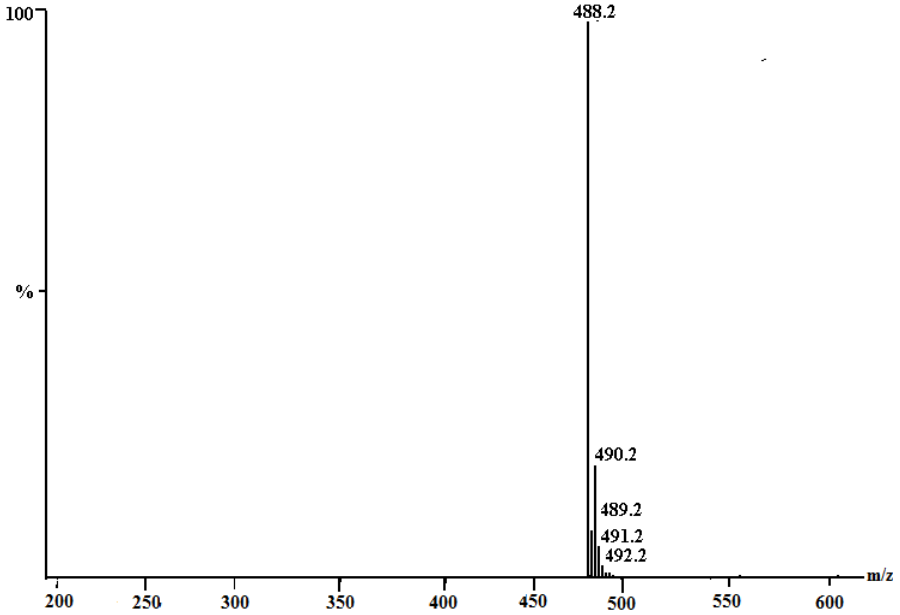

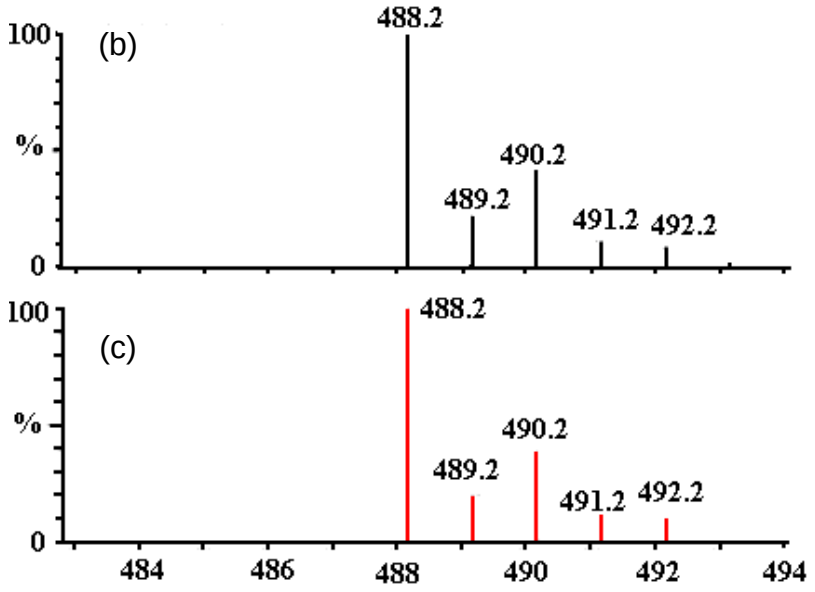

Fig 3. 5 Mass spectra (LIFDI) of **1** in toluene (a) Full scale spectrum (b) calculated and (c) expansion of the experimental spectrum

Complex **2** behaved in a similar way with the LIFDI spectrum showing the molecular ion at m/z = 475 as base peak (100%, Fig 3. 6) and other peaks at 477-479 are consistent with Ni and C isotopes. The ESI spectrum gave decomposition.

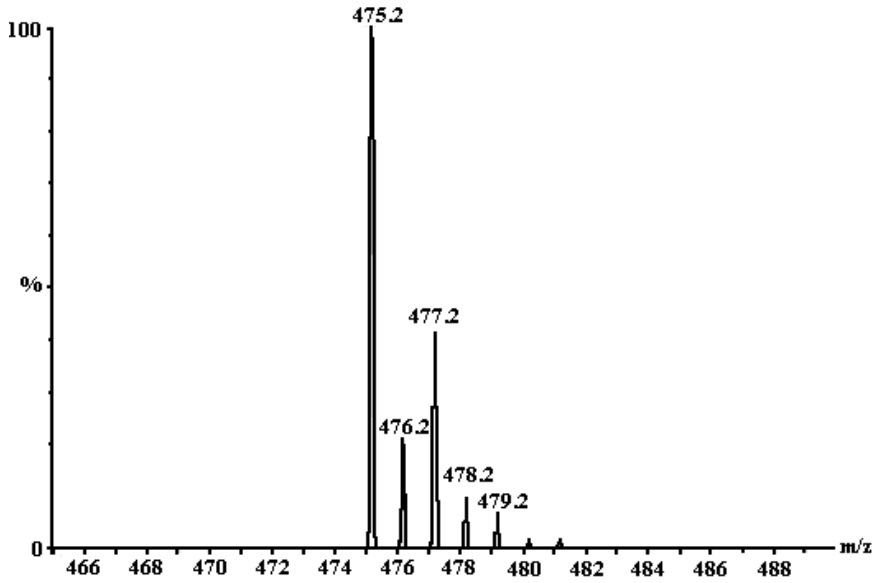

Fig 3. 6 Mass spectra (LIFDI) of **2** in toluene

Mass	Relative abundance
475.0	50.84
476.0	10.27
477.0	22.40
478.0	5.28
479.0	3.59
480.0	0.65
481.0	0.80
482.0	0.15
483.0	0.02
484.0	0.00

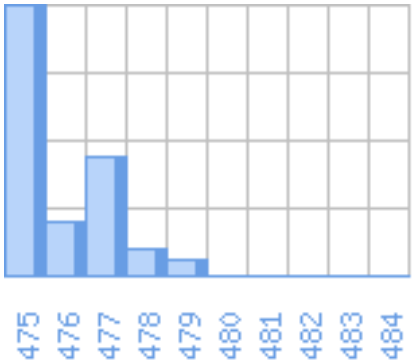

Figs 3. 7 Theoretical isotope resolution pattern calculated with the "Fluorine chemistry mass simulator[35]

Complexes **3**, **5** and **6** have been reported previously,[1] but gave mass spectra with very weak molecular ions (0.5%) by EI methods. We have now re-investigated them by mass spectrometry using LIFDI technique. LIFDI of **3**, **5** and **6** gave the molecular ion peaks $[M]^+$ as base peaks (100%) at 463, 445 and 480 respectively. With ESI, the compounds showed decomposition. The data are summarized in table 3.2.

Table 3.2 Calculated and observed isotopic signature in LIFDI mass spectrum for $Ni(PEt_3)_2(C_5F_4N)F$ **(3)**[1]; $Ni(PEt_3)_2(C_5F_3HN)F$ **(5)**[1], $Ni(PEt_3)_2(C_6F_5)F$ **(6)**[1]

Complex **3**			Complex **5**			Complex **6**		
m/z	Calcd	Obsvd	m/z	Calcd	Obsvd	m/z	Calcd	Obsvd
463.0	100		445.0	100	100	480.0	100	100
464.0	19.1	20.5	446.0	19.1	19.4	481.0	20.2	20.7
465.0	43.6	39.6	447.0	43.6	42.5	482.0	43.8	43.1
466.0	9.9	9.28	448.0	9.9	9.6	483.0	10.3	
467.0	6.8	6.2	449.0	6.8	5.5	484.0	6.9	7.2
468.0	1.2	1.3	450.0	1.2	0.9	485.0	1.3	1.2
469.0	1.6	1.9	451.0	1.6	1.37	486.0	1.6	1.8
470.0	0.3	0	452.0	0.3	0	487.0	0.3	0
471.0	0.0	0	453	0.0	0	488.0	0	0

3.2.1.2. Complexes of rhodium and ruthenium

The formation of $Ru(PPh_3)_3(CO)(H)F$ (**7**) and $Rh(PPh_3)_3F$ (8) was confirmed by comparison with literature NMR data.[2,38] The LIFDI spectrum of **7** showed $[M–HF]^+$ (m/z = 916) as base peak, and the molecular ion with intensity 27% (m/z = 936) (Fig 3. 8).

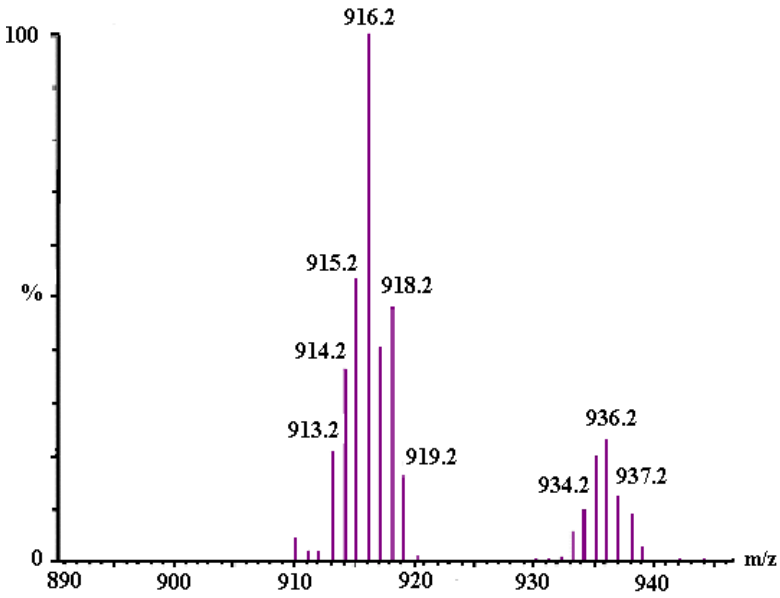

Fig 3. 8 LIFDI mass spectrum of complex 7

The LIFDI spectrum of **8** also showed $[M–HF]^+$ (m/z = 888) as base peak and the molecular ion with 10% intensity (m/z = 908) (Fig 3. 9).

In contrast, the ESI spectrum of **8** showed $[M–F]^+$ as base peak and no molecular ion. Since the NMR spectrum of **8** showed resonances of the isomer, $Rh(PPh_3)_2(PPh_2F)Ph$,[2] as a minor species, we cannot exclude the isomer as the source of the molecular ion.

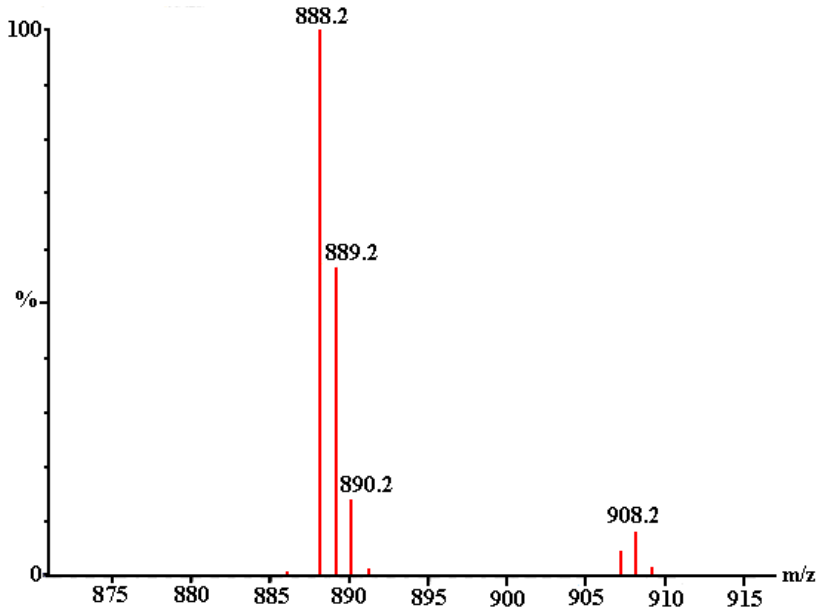

Fig 3. 9 LIFDI mass spectrum of complex **8**

3.4.1.1. Complexes of platinum

$Pt(PPh_3)_2FI$ (**10)** was also studied by mass spectrometry using LIFDI and ESI techniques. LIFDI (Fig 3. 10) gave the molecular ion peak $[M]^+$ at m/z = 865.05 as base peak. The other peaks are at m/z = 864 and 866 which are consistent with Pt isotopes (table 3.1). A major peak is at m/z = 972 which is assigned to molecular ion of $[Pt(PPh_3)_2I_2]^+$ (**9**) $[M`]^+$ present as unreacted starting material. The peak at m/z = 846 is assigned to $[Pt(PPh_3)_2I]^+$ which is the daughter ion of complex M` as $[M`–I]^+$.

Fig 3. 11 displays the ESI-MS of $Pt(PPh_3)_2IF$. The peak at m/z = 845.9 arises by the loss of fluoride ligand from the compound $[M–F]^+$. The other peak at m/z = 777.1 corresponds to $[(M–I)+K]^+$ respectively.

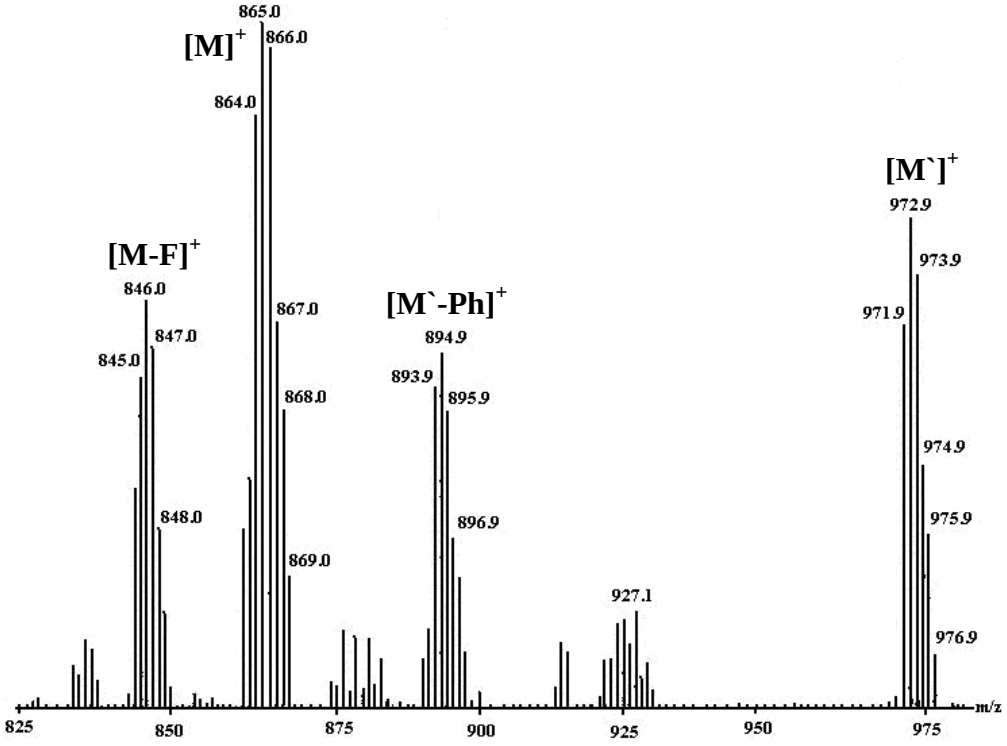

Fig 3. 10 Liquid Injection field Desorption Ionization mass spectrum of $Pt(PPh_3)_2IF$

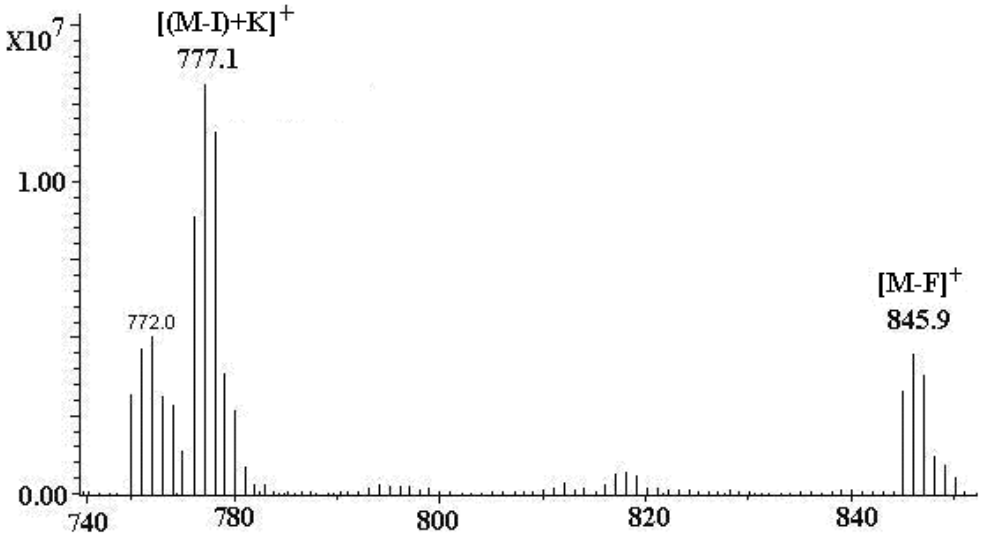

Fig 3. 11 Mass spectrum (ESI, positive ion) of $Pt(PPh_3)_2IF$

3.2.2. Characterization of Transition metal difluoride complexes by LIFDI

3.2.2.1. Difluoride complexes of Titanium, Zirconium and Hafnium

$(Cp^*)_2TiF_2$ (**11**), $(Cp^*)_2ZrF_2$ (**12**) and $(Cp)_2{}^*HfF_2$ (**13)** were also studied by mass spectrometry using LIFDI and ESI techniques. Excellent agreement between observed and

calculated isotope patterns was observed for all the major peaks. The LIFDI spectrum of **11** gave the molecular ion peaks $[M]^+$ at 356 as base peak (100%, ^{48}Ti). Other peaks at 354, 355, 357 and 358 are consistent with Ti isotopes (see table 3.1). ESI-MS of **11** gave ion peaks at 337 $[M–F]^+$, 379 $[M+Na]^+$ and 395 $[M+K]^+$ with significant intensity (from CH_3CN solution) (Fig 3. 14).

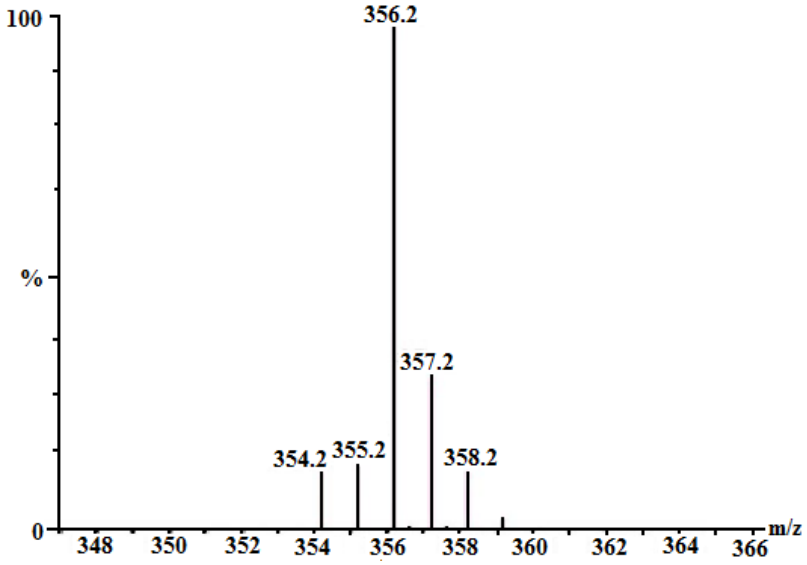

Fig 3. 12 Mass spectrum (LIFDI) of **11** in toluene.

Mass	relative abundance
354.0	6.32
355.0	7.26
356.0	60.58
357.0	17.82
358.0	6.65
359.0	1.15
360.0	0.11
361.0	0.01

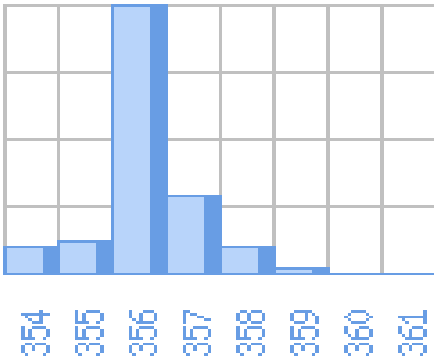

Fig 3. 13 Theoretical isotope resolution pattern of **11** calculated with Fluorine chemistry mass spec simulator [35]

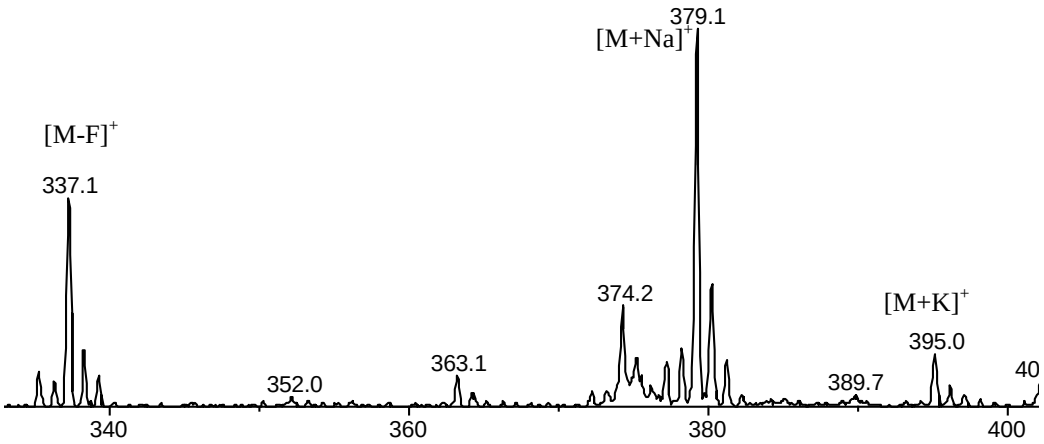

Fig 3. 14 Mass spectrum (ESI, positive ion) of $[(Cp^*)_2TiF_2]^+$ **11** (from CH_3CN solution)

For **12** LIFDI gave the molecular ion at 398 (100%, ^{90}Zr) (Fig 3. 15) while the other ions at 399, 400, 401 and 401corresponds to ^{91}Zr, ^{92}Zr, ^{93}Zr and ^{94}Zr respectively. For ESI-MS of **12** ion peaks appeared at 421 $[M+Na]^+$ and 437 $[M+K]^+$ (from CH_3CN solution) (Fig 3. 16).

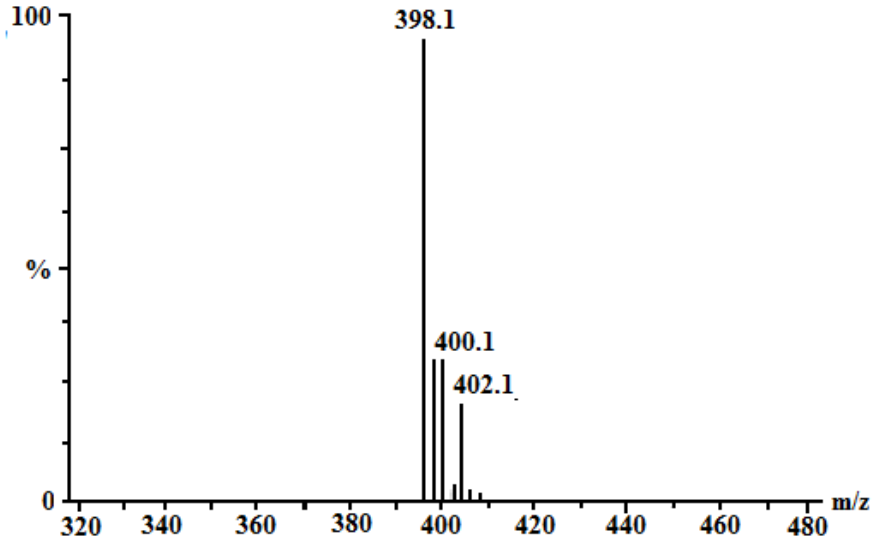

Fig 3. 15 Mass spectrum (LIFDI) of **12** in toluene.

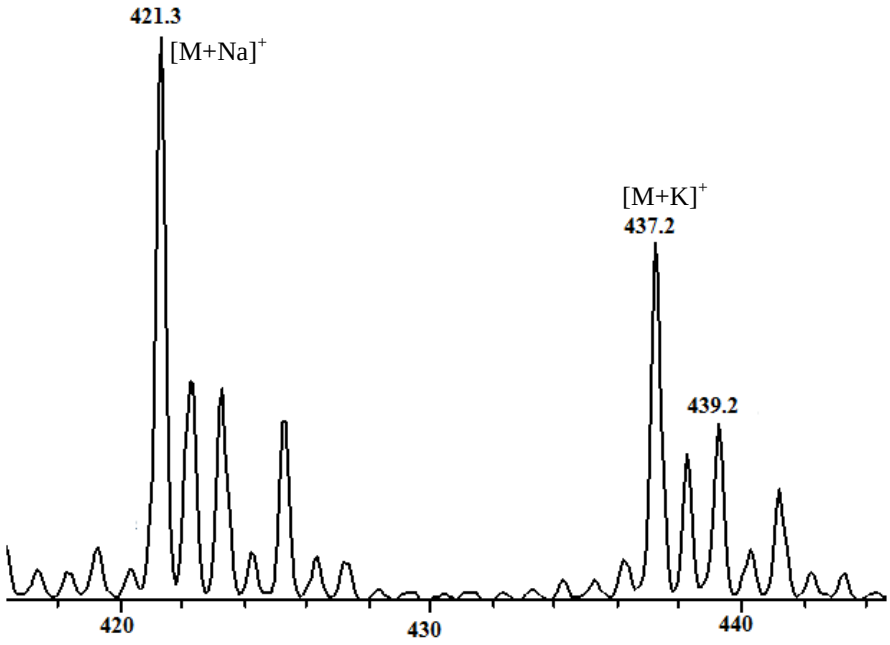

Fig 3. 16 Mass spectrum (ESI, positive ion) of **12** in CH_3CN.

Complex **13** synthesized from the reaction of (Cp)*$HfCl_2$ with NaF was also characterized by mass spectrometry. LIFDI gave the molecular ion (m/z = 488) as base peak and the ion distribution was in close agreement with the isotopic pattern of hafnium. The ESI spectrum showed the sodiated molecular ion.

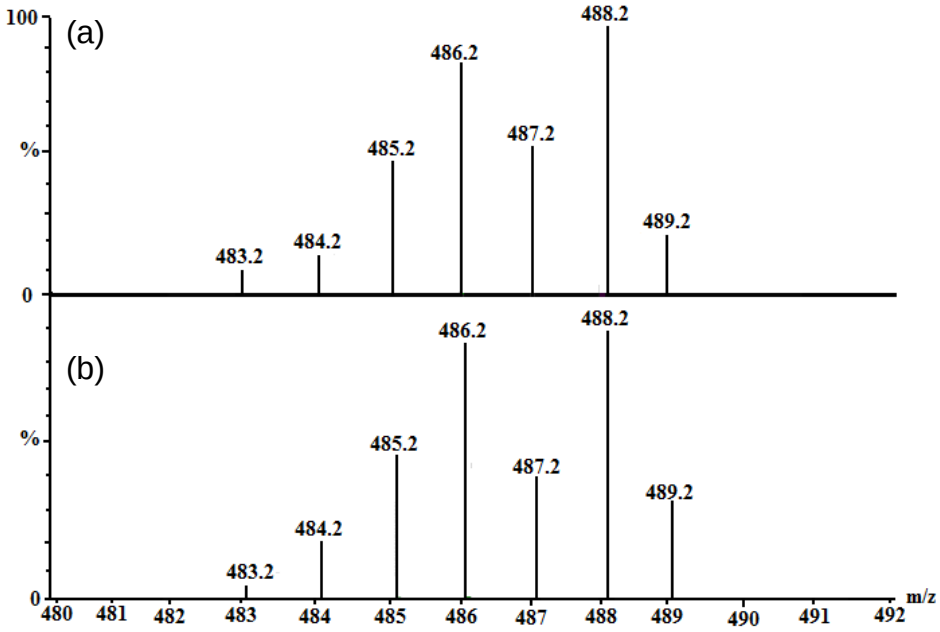

Fig 3. 17 Mass spectrum (LIFDI) of **13** in toluene (a) calculated and (b) observed.

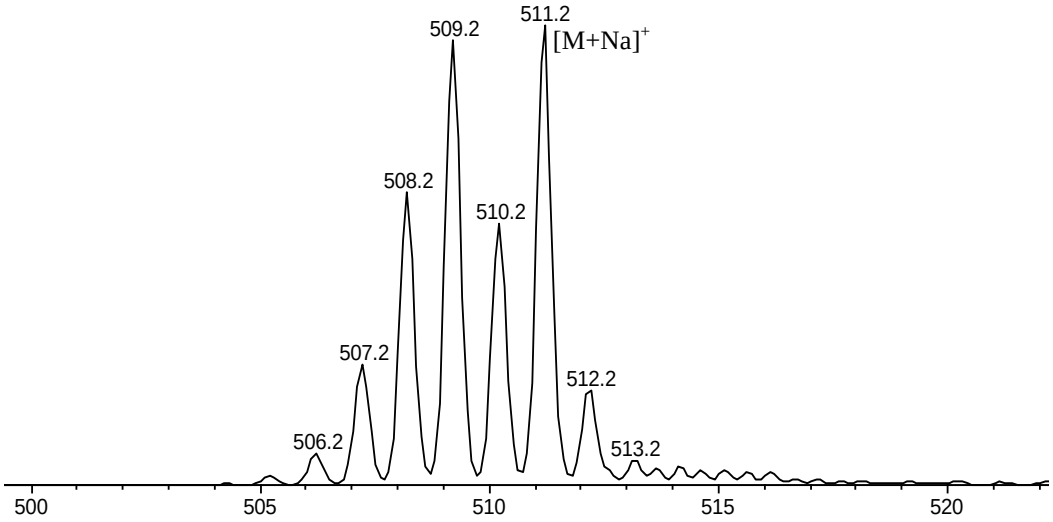

Fig 3. 18 Mass spectrum (ESI, positive ion) of **13** in CH_3CN.

3.2.2.2. Ruthenium difluoride , bifluoride and bis bifluoride complexes

$Ru(PMe_3)_4(F)_2$ **16** was also characterized by mass spectrometry. LIFDI gave the molecular ion at m/z 444 as base peak and $Ru(PMe_3)_4(Cl)F$ at 460.

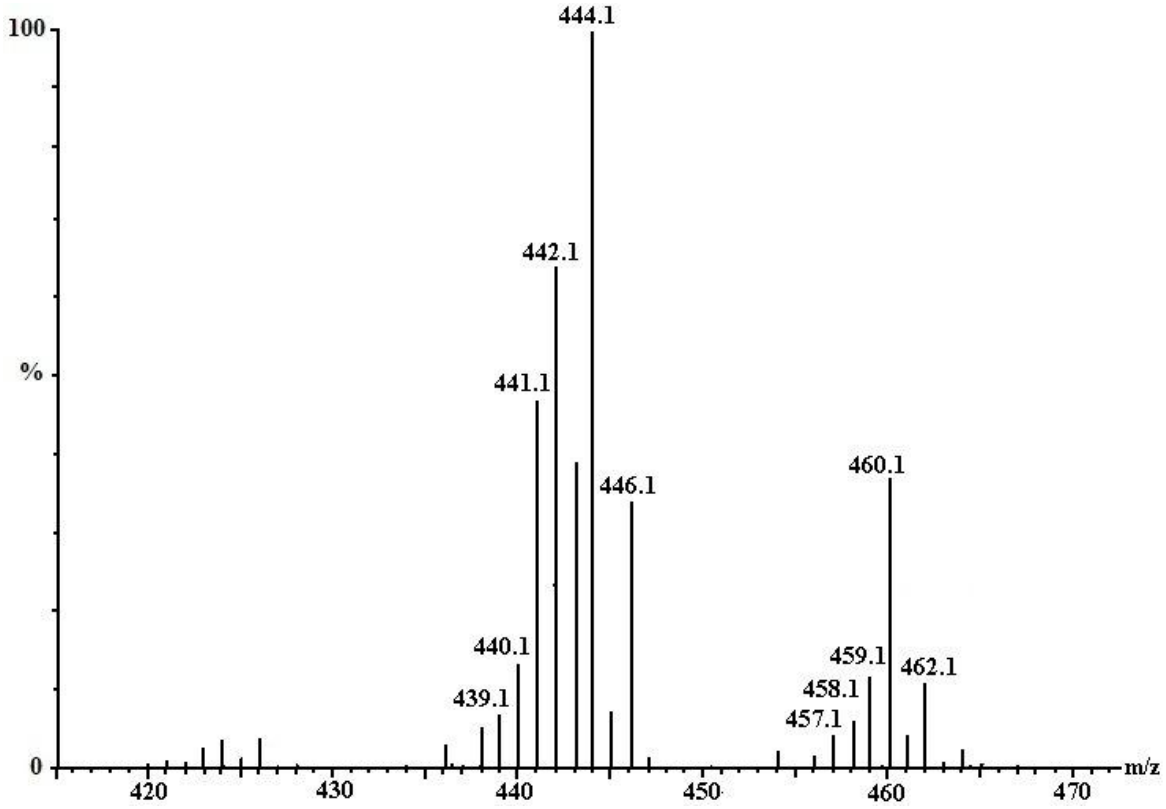

Fig 3. 19 Liquid Injection field Desorption Ionization mass spectrum of **16**

The LIFDI mass spectrum of $(PMe_3)_4Ru(FHF)_2$ (**15**) shows a peak at m/z = 444.1 and 716.1 corresponding to $[(PMe_3)_4RuF_2]^+$ and $[(Me_3P)_3Ru(\mu\text{–}F)_3Ru(PMe_3)_3]^+$. The peak at m/z = 476 may be from $[(PMe_3)_4RuClF]^+$ and 732 may be assigned to a bridged complex having one fluoride ligand replaced by chloride ligand $[(Me_3P)_3Ru(\mu\text{–}F)_2(\mu\text{–}Cl)Ru(PMe_3)_3]^+$ (Fig 3. 20). The calculated spectra for the above mentioned ions agree very closely with the observed spectra. Peaks can also be observed for $[(Me_3P)_3Ru(\mu\text{–}F)(\mu\text{–}Cl)_2Ru(PMe_3)_3$ and $[(Me_3P)_3Ru(\mu\text{–}Cl)_3Ru(PMe_3)_3$ at m/z 748 and 764 respectively.[39] The source of the chloride appears to be the $[RuCl_2(COD)]_x$ used as a starting material for the synthesis of $(PMe_3)_4RuH_2$ (**14**) from which $(PMe_3)_4Ru(FHF)_2$ was synthesized.

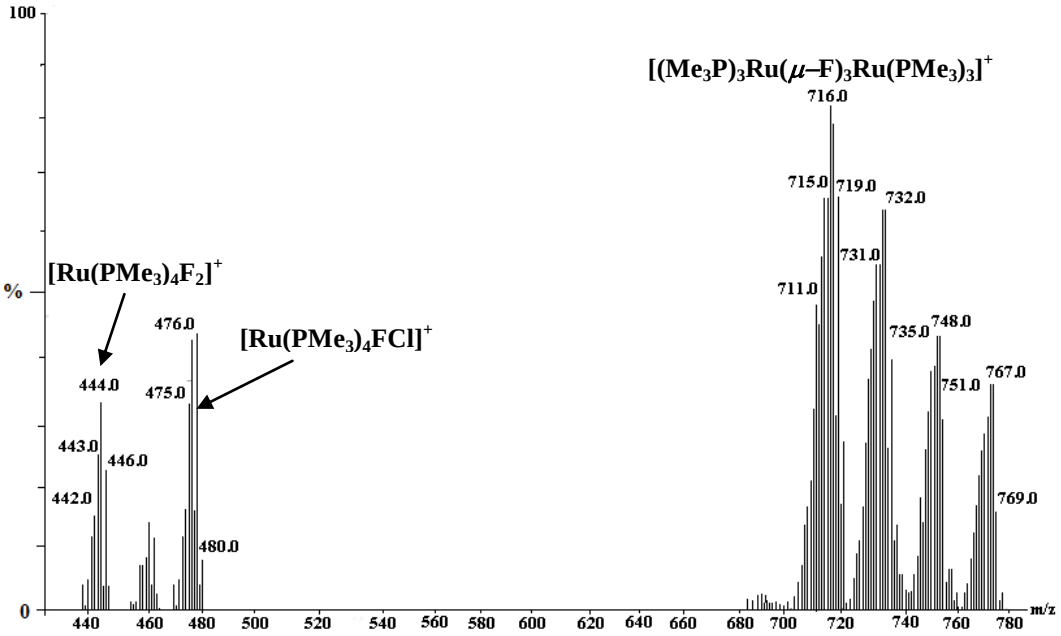

Fig 3. 20 Liquid Injection field Desorption Ionization mass spectrum of **15**

From the comparison of the spectra of complexes **15** and **16** it is concluded that bifluoride complexes are thermally not very stable.

The LIFDI spectrum of $Ru(dppe_2)_2H(FHF)$ (**18**) gave ions at m/z 936, 918 and 899 corresponding to the loss of H_2, HF and FHF respectively. As ions at m/z 899 and 918 appears with quite strong intensity, it further strengthens the conclusion that bifluoride complexes are thermally not very stable.

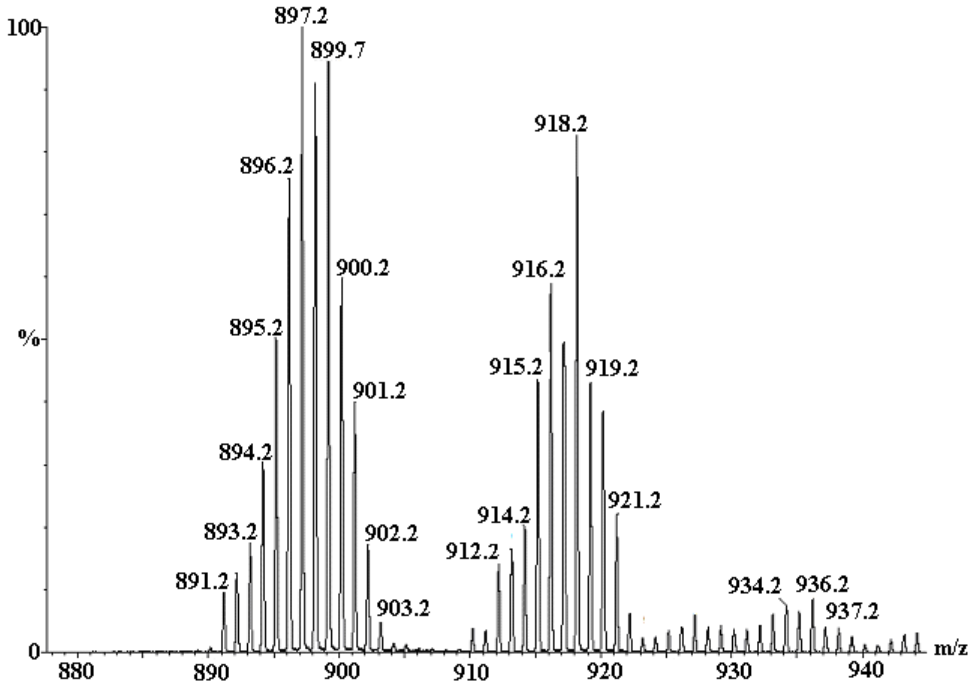

Fig 3. 21 Liquid Injection field Desorption Ionization mass spectrum of **18** in toluene.

3.3 Discussion

Nickel monofluoride complexes **1**, **2**, **3, 5** and **6** synthesized by C-F oxidative addition of hexafluorobenzene and of fluorinated pyridines were studied by mass spectrometry. All the compounds were characterized successfully by LIFDI[37] while they showed decomposition with EI and ESI. Since this work was performed, Perutz et al. reported nickel fluoride complexes characterized by LIFDI mass spectrometry including trans-[Ni(F)(2-C_5NF_4)(PCy_3)$_2$] trans-[Ni(F){2-$C_5NF_2H(CF_3)$}(PCy_3)$_2$] and trans-[Ni(F){2-$C_5NF_2H(CF_3)$}($PCyp_3$)$_2$] showing 100% of the molecular ion.[40] Complexes of rhodium were recently reported to be characterized by LIFDI in the group. Examples are Tp`RhF($C_5NF_4$) and Tp`Rh(CNR)F (R = neopentyl) which showed the molecular ion with high intensity.

Goldman characterized iridium complexes (PCP)Ir(CH_3)F (PCP = κ_3-C_6H_3-2,6-[CH_2P(t-Bu)$_2$]$_2$) by LIFDI observing the molecular ion peak as a base peak.[41]

The reason that fluoride complexes are not stable in ESI (although a soft technique) is the lability of fluoride ion. Henderson studied transition metal monohalide complexes by ESI-MS and general ionization via loss of halide ion was observed due to the lability of

halide ion. In some cases the loss of the halide ion was followed by coordination of the solvent molecule such as CH_3CN.[22]

Certain dihalide complexes like cis$[PtCl_2(PPh_3)_2]$, cis$[PtCl_2(dppe)]$, cis $[Cp^*IrCl_2(PPh_3)]$ and $[(p\text{-cymene})RuCl_2]_2$ were analysed by ESI-MS in positive ion mode. The ionization pathway observed at high voltage was the loss of one halide ligand from the molecule and the spectra were dominated by $[M\text{-halide}]^+$.[22] Similar behaviour was observed with the difluoride complexes. In the ESI-MS spectra, complexes **11**, **12** and **13** showed $[M\text{-}F]^+$ ions as well as sodiated and potassiated molecular ions. Sodium and potassium ions are present in the mass spectrometer.[26] On the other hand LIFDI spectra of the above mentioned complexes gave the molecular ion at 100% intensity. It is important to note that LIFDI is very good for Ni complexes, but is not needed for the difluoride complexes of Ti, Zr and Hf.

LIFDI is not very good for high molecular mass compounds because more heat is required for molecules to evaporate from the emitter which can lead to decomposition. The ruthenium complex, $Ru(PPh_3)_3(CO)(H)F$ showed a molecular ion of 27%, while the fluorine analogue of Wilkinson's complex, $Rh(PPh_3)_3F$, showed a much weaker molecular ion. Both of these molecules showed loss of HF as the base peaks.

LIFDI is not very suitable for the bifluoride complexes as they have lost HF and converted to difluoride and bridged complexes.

3.4 Conclusions

The LIFDI method has proved very successful for the mass spectrometric characterisation of a range of metal fluoride complexes. The nickel complexes had been very difficult to identify mass spectrometrically by conventional ionisation methods but gave the molecular ions as base peaks by LIFDI. We have also observed the molecular ions as base peaks for platinum complexes.[34] Nevertheless, there are other examples of higher molecular mass than the complexes reported here that were less successful. We have also analyzed bifluoride and bis-bisfluoride complexes of ruthenium by LIFDI but the spectra are dominated by ions formed by loss of HF from the molecule. They also underwent other

complicated reactions leading to dinuclear complexes. These observations further strengthen the conclusion that bifluoride complexes are thermally not very stable.

COLLISION INDUCED DISSOCIATION OF TRANSITION METAL COMPLEXES AND MULTILY CHARGED ANIONS

4.1 Introduction

Electrospray mass spectrometry is a soft ionization technique[1,2] and of great interest for inorganic and organometallic chemists.[3,4] The development of this technique started from the work of Dole and co-workers in 1960's. Much current importance of this technique derives from the work of Fenn who in 1984 coupled electrospray source with a quadrupole mass analyzer.[1,5] It is especially useful in producing gas phase ions from macromolecules by spraying a solution from the tip of an electrically charged capillary. The development of electrospray ionization for the analysis of biological macromolecules was rewarded with the Nobel Prize in Chemistry to Fenn in 2002. [6]

The combination[7] of electrospray (ESI) ionisation with quadrupole ion trap (QIT),[8,9] has brought a revolution in mass spectrometry. The quadrupole ion trap (QIT) was invented by Wolfgang Paul, for which he was awarded nobel prize in 1989[10]. A QIT provides multi-stage mass spectrometry capabilities to manipulate ions and examine structure and reactivity by collision induced dissociation (CID) and gas phase ion molecule reactions.[4,11]

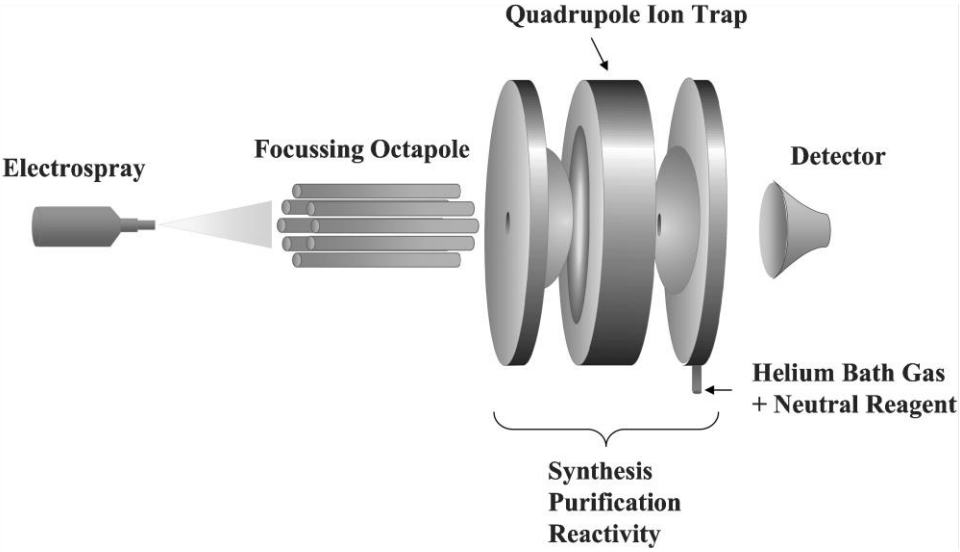

Fig 4. 1 "Simplified schematic diagram of ESI-QIT mass spectrometer. Ions are generated and passed into the QIT through focusing octapoles. CID takes place in the QIT where ions can be synthesized, purified by mass selection and subjected to reactivity using either CID or ion–molecule reactions."[11]

Collision induced dissociation (CID) is a process during which ions are excited by increasing their internal energy upon collision with neutral gas molecules (noble gases such as helium or nitrogen etc), these excited ions undergo decomposition/fragmentation. CID is also referred as collision activated decomposition (CAD).

The CID process consists of two steps, (i) collision of fast ions with neutral gas atom (helium) when translational energy is converted to internal energy and (ii) the fragmentation of the collisionally excited ion. The ion in its activated form redistributes its energy among its vibrational modes (3N−6 for an ion with N atoms in a non-linear molecule). The first step should be longer than the second (quasi equilibrium). [12]

The CID method acquired much importance with the advent of soft ionization techniques like electrospray and chemical ionization because these methods provide information about the molecular ion. CID is very useful in providing structural information through the fragmentation pattern of molecules. [13]

In a tandem mass spectrometer the mass analyser can be separated either in space (triple quadrupole and quadrupole time–of–flight), or in time (ion trap, Fourier Transform ion cyclotron). In the triple quadrupole, the first quadrupole (MS1) is set so that it passes only ions of a certain m/z value. Fragmentation occurs in the collision cell which is occupied by inert gas (typically argon) to assist in fragmentation. The third quadrupole (MS2) scans the mass range of interest and generates the daughter ion spectrum.

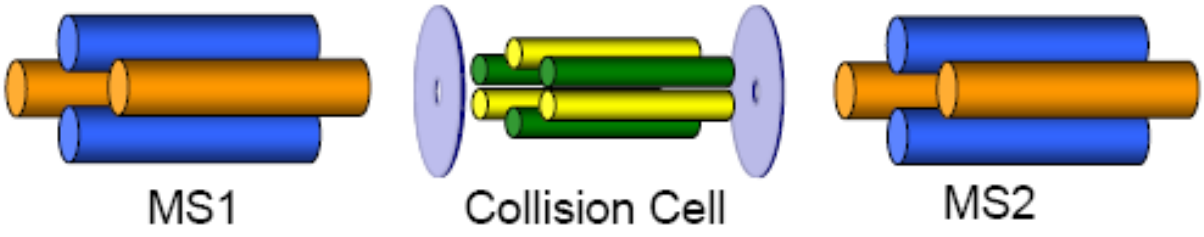

Fig 4. 2 Schematic diagram of a triple quadrupole mass spectrometer

In a MS/MS in time instrument, all the steps of MS with ions trapped occurs in the same place, with multiple separation steps taking place over time. A quadrupole ion-trap has constant background pressure of 10^{-3} mbar, so the instrument does not need to be evacuated and refilled between different steps. A trapping instrument can perform multiple steps of analysis, which is sometimes referred to as MS^n (n = 1 to 10).[4,12]

High energy CID is only suitable with the sector and TOF mass spectrometer because they analyze ions with high energies (keV). A collision cell is useless with these conditions. Just a region having collision gas is sufficient but in this method the loss of ions is high which makes CID less efficient. Triple quadrupole, ion trap and ion cyclotron mass spectrometers are suitable for measuring low energy CID.

Dimethylaurate has been investigated for its synthesis and gas phase reactivity by O'Hair et al using negative ion electrospray ionization source coupled with an ion trap mass spectrometer.[14] Dimethylaurate was synthesized from gold(III) tetraacetate $[(CH_3CO_2)_4Au]^-$ through multisteps of low energy CID. In the first two steps (i-e MS^1 and MS^2) $[(CH_3CO_2)_4Au]^-$ loses acetyl peroxide $(CH_3CO_2)_2$ and yields the gold(I) acetate anion $[CH_3CO_2AuO_2CCH_3]^-$.

The MS^3 spectrum of $[CH_3CO_2AuO_2CCH_3]^-$ shows that CID proceeded through decarboxylation yielding $[CH_3CO_2AuCH_3]^-$.

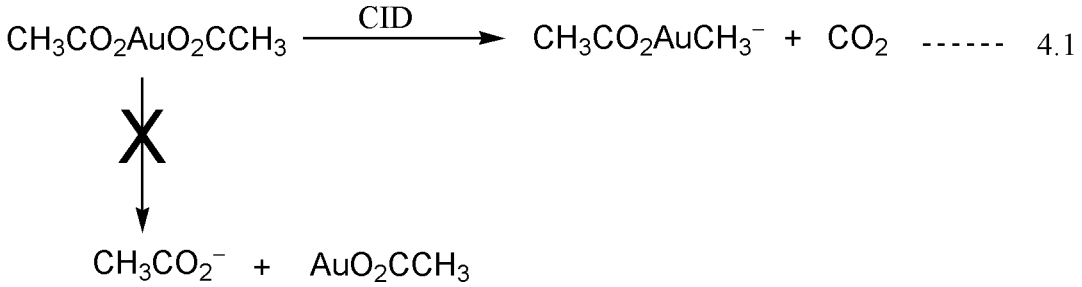

The examination of the CID MS^4 spectrum of $[CH_3CO_2AuCH_3]^-$ shows the loss of CO_2 and yields $[CH_3AuCH_3]^-$ which is the desired product. Formation of $CH_3CO_2^-$ is observed as a minor product.

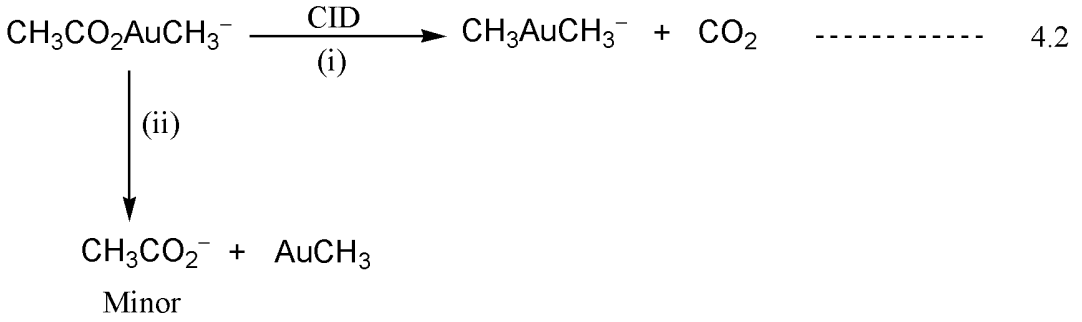

It was realized that it is easy to study formation, synthesis and reactivity of organometallic complexes in gas phase so that the solvent effects can be avoided. The ions of interest can be synthesized from the precursor ions through ESI followed by CID. The fragmentation pathway of diethylcuprate was also observed through a low energy CID

experiment and it was shown that the dominant fragmentation product is hydride $[CH_3CH_3CuH]^-$ formed through β–hydride transfer and this was further confirmed by using the deuterium labeled analogue (Fig 4. 3). A small amount of $[HCuH]^-$ is formed as a result of the secondary loss of ethene and confirmed by an additional stage of CID on $[CH_3CH_2CuH]^-$. CID of the perfluorinated analogues (complexes of Cu, Ag and Au) have shown several fragmentation pathways and can occur through loss of CO_2, CF_2, CF_2CO_2 and $CF_2CO_2^-$.[15]

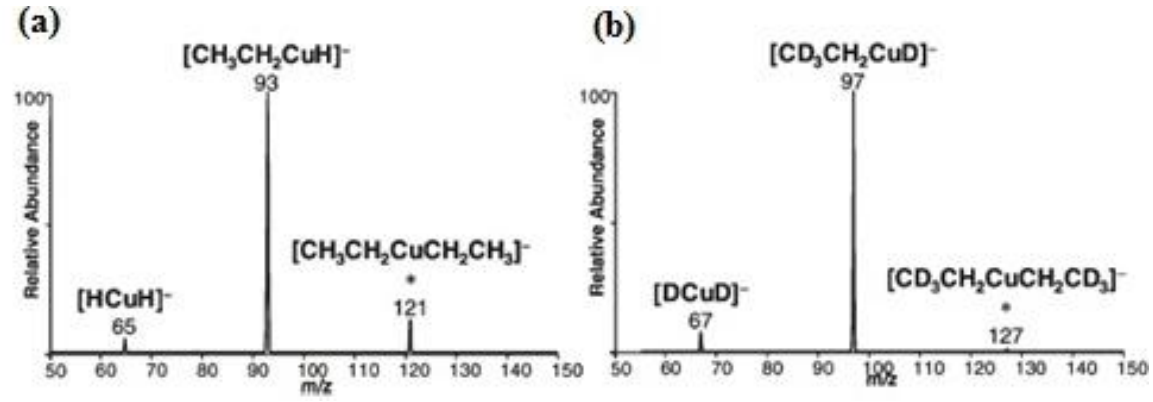

Fig 4. 3 Collision-induced dissociation (CID) mass spectra showing the diethylcuprates: (a) $[CH_3CH_2{}^{63}CuCH_2CH_3]$-, m/z 121; (b) $[CD_3CH_2{}^{63}CuCH_2CD_3]^-$, m/z 127.[15]

The fragmentation pathway of cyclam macrocycles tetrasubstituted with amino-, thiourea, and sugar-terminated side chains and their complexes with transition metals were investigated through collision induced dissociation (CID) using Fourier transform ion cyclotron mass spectrometer equipped with electrospray. It was observed that fragmentation of both cyclam and their complexes with transition metal ions (Zn^{2+}, Co^{2+} and Ni^{2+}) occurs within the side chains through 1-2 elimination. [16]

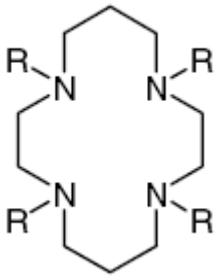

Structure of cyclam, R= different substituents[16]

A mechanistic study was conducted on group 10 metal complexes (Ni, Pt and Pd) for cyclometalation in the gas phase via low energy CID using a mass spectrometer of QHQ configuration (Q: quadrupole, H: hexapole) equipped with an ESI source.[17]

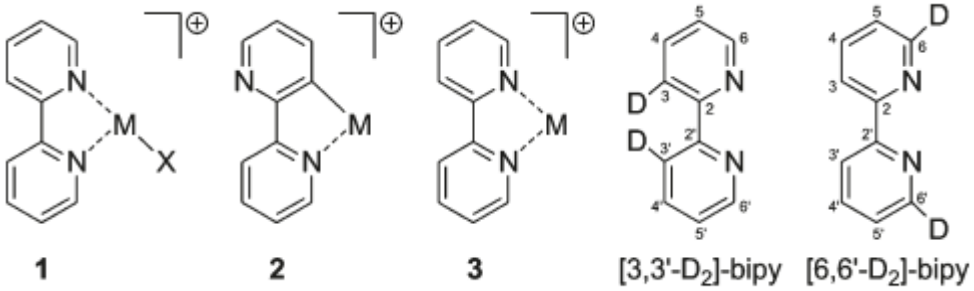

Fig 4. 4 Group 10 metal complexes of **(**M = Ni, Pd, Pt), (X = CH_3, F, Cl, Br, I, OAc), (deuterated 2,2′–Bipyridine Ligands = [3,3′–D_2]-bipy and [6,6′–D_2]-bipy)[17]

Upon CID [PtX(bipy)] (X= CH_3, Cl) loses HX (CH_4, HCl) and "rollover" cyclometalation was observed as a dominant process

$$[Pt(CH_3)(bipy)] \xrightarrow{CID} [Pt(bipy\text{-}H)] + CH_4 \quad \text{----------} \quad 4.3$$

The experiments were conducted using [3,3′–D_2] –bipy (see Fig 4. 4) to make it clear whether the hydrogen for M–X is abstructed from the 3 and 3′ position. [M(CH_3)(bipy)] (M= Ni, Pd) underwent homolytic cleavage of M-CH_3 bond and C–H bond is not activated. In contrast both processes were observed side by side from the analogous chloride complexes i-e elimination of HCl followed by C-H activation and homolytic cleavage of M–Cl bond was observed. With increasing in the collision energy, the ratio of HCl to Cl is decreases (Fig 4. 5). It was concluded that the branching pattern depends on metal ions as well as the nature of the ligands.

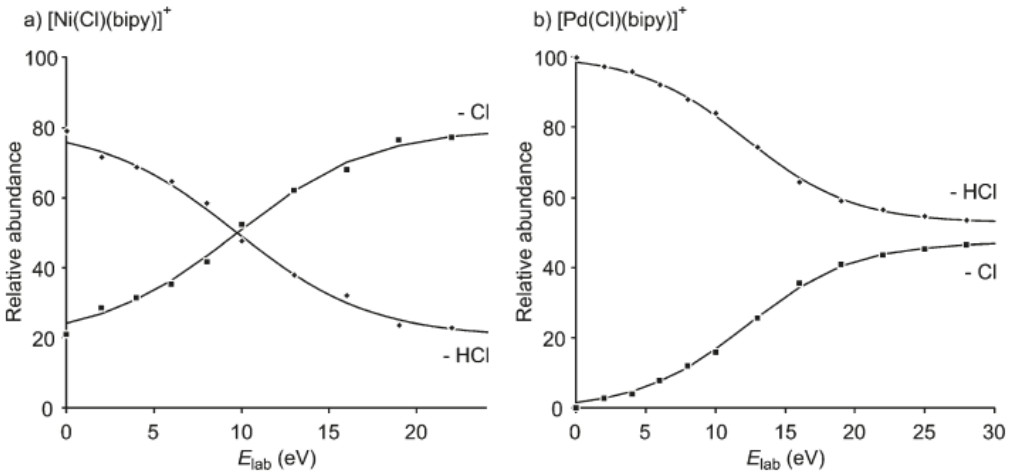

Fig 4. 5 Relative intensities for the losses of HCl and Cl in the CIDs of mass-selected (a) $[NiCl(bipy)]^+$ and (b) $[PdCl(bipy)]^+$ at variable collision energies

Metal ion-ligand binding is one of the noncovalent bonding interactions which has been investigated to provide bond dissociation energies by Rodgers and Armentrount. Collision-induced dissociation (CID) has been used for the measurement of metal ligand bond dissociation energies.[18-20]

Very little has been done on the analysis of neutral transition metal halide complexes using ESI-MS. Upon analysis of these complexes by ESI-MS the general ionization via loss of halide ion was observed due to lability of this ligand, though alternative pathways were also observed in some cases like loss of halide ligand and coordination of solvent molecule such CH_3CN, depending upon the cone voltage employed. [3]

4.1.1 Multiply Charged Anions (MCAs)

MCAs are of considerable importance because they represent highly energetic molecules in the gas phase due to columbic repulsion that exists between the excess charges. Examples of MCAs are $IrCl_6^{-2}$, $ReCl_6^{-2}$, $IrBr_6^{-2}$, $PtBr_6^{-2}$. MCAs are common in solids and solutions form. In solution they are stable because in solution the excess charges are stabilized by solvent or counter ions. They are difficult to study in the gas phase due to the strong columbic forces which make them highly susceptible to decay either by electron detachment or ionic fragmentation. Electrospray ionization (ESI) has made it possible to transfer MCAs from solution directly to the gas phase in amounts sufficient for spectroscopic studies.[21,22]

The potential energy surfaces exhibited by MCAs are strongly influenced by the repulsive coulombic barrier (RCB) which arises from the superimposition of long range coulombic repulsive interaction between the anion and outgoing electron and short range binding forces of this electron.[21,22]

The decay pathway of transition metal dianion ($IrCl_6^{-2}$, $ReCl_6^{-2}$, $IrBr_6^{-2}$, $PtBr_6^{-2}$) was investigated by Dessent et al. using electrospray ionization coupled with quadrupole ion trap. The dianions were isolated and subjected to fragmentation via low energy CID. These transition metal dianions decayed through ionic fragmentation rather than spontaneous electron detachment because the repulsive coulombic barrier for ionic fragmentation (RCB_{if}) is lower than the repulsive columbic barrier for electron detachment (RCB_{ed}), as represented graphically in Fig 4. 6.

MCAs are subject to decay by either electron detachment or ionic fragmentation.

$$X^- + MX_5^- \xleftarrow[(ii)]{\text{ionic fragmentation}} MX_6^{2-} \xrightarrow[(i)]{\text{electron detachment}} MX_6^- + e^- \text{ ------ } 4.4$$

MX_6^{2-} represents a multiply charged dianion, which can decay either through electron detachment (i) or Ionic fragmentation.[23]

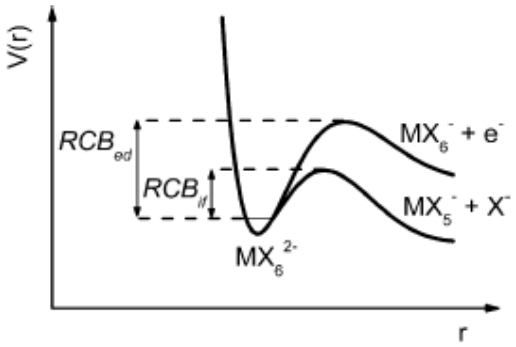

Fig 4. 6 Schematic diagram of the potential energy surfaces for decay of an MX_6^{2-} dianion via ionic fragmentation and electron detachment. The RCBs (inner) for electron detachment (RCB_{ed}) and ionic fragmentation (RCB_{if}) are illustrated[23]

In contrast to the above mentioned MCAs, $Cr_2O_7^{2-}$ decays with electron loss upon resonance excitation. Smaller molecular systems decay by electron detachment because the repulsive coulombic barrier for electron detachment is lower than repulsive coulombic barrier for ionic fragmentation. The negative ion electrospray ionization mass spectrum (ESI-MS) of $Cr_2O_7^{2-}$ shows $CrO_4^-/HCrO_4^-$ as a major peak. The $NaCr_2O_7^{2-}$ and $Cr_2O_7^{2-}$ ions are also peaks with significant intensity. Upon isolation and subsequent resonance

excitation $Cr_2O_7^{2-}$ decays primarily into $Cr_2O_7^-$ with CrO_4^- can also be seen as a minor fragment. this shows that $Cr_2O_7^{2-}$ decays mainly through electron detachment into $Cr_2O_7^-$.

$$Cr_2O_7^{2-} \longrightarrow Cr_2O_7^- + e^- \quad \text{4.5}$$

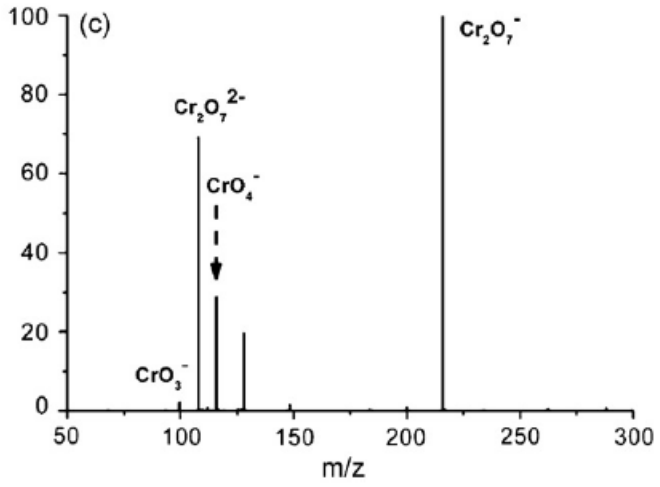

Fig 4. 7 CID mass spectrum $Cr_2O_7^{2-}$ (9% collision energy) showing $Cr_2O_7^{2-}$ is fragmented into $Cr_2O_7^-$ (considerable amount of $CrO_4^-$and CrO_3^- is also formed).[24]

The presence of CrO_4^- indicates that $Cr_2O_7^{2-}$ also decays to a lesser extent through ionic fragmentation into CrO_4^- and CrO_3^-.[24] It can be concluded that ionic fragmentation will be the dominant decay mechanism for medium and large size MCAs rather than spontaneous electron detachment.[21]

Low energy collision induced dissociation of cation-anion complexes like M^+PtCl6^{2-}, $M^+PtCl_4^{2-}$, $M^+PtCN_6^{2-}$, and $M+PdCN_4^{2-}$, where $M^+ = Na^+, K^+, Rb^+$ decay by the same fragmentation pattern as the multiply charged anion alone. This shows that in such types of complexes the electronic structure of the MCA is not considerably affected by the counter ion.[25]

In this chapter the electrospray ionization and fragmentation upon low energy CID of transition metal fluoride complexes, multiply charged anions and transiton metal cation complexes will be discussed.

4.2 Results

The CID mass spectra were obtained using an Esquire 6000 ion trap mass spectrometer (discussed in chapter 3) fitted with an ESI source. The ESI source is of an orthogonal

sprayer design and was operated at a spray voltage of 3-4 kV. Data were collected in standard scan mode. Nitrogen was used as bath gas (200-300˚C; 300-600 L/h) and nebulizing gas (5-10 psi). The analyte solution was introduced into the mass spectrometer by a syringe pump employing a 500 μL syringe. The sample solution was introduced at a constant flow rate of 240-480 μL/h. The collision gas used for the CID was He.

The millimolar solutions of various ions were prepared in methanol, water, and acetonitrile mentioned separately with different compounds. The precursor ions of interest were optimized where needed. The desired ions were isolated in the ion trap and collisionally excited by probing at different collision energies between 0-25 V. The ions were mass selected with a window of 4-10 Da in order to see the isotopic signature of the ions. The diamond sign on the top of the peaks indicates the parent ions which undergoes CID. The resolution of the mass spectrometer was set at standard.

The theoretical isotope patterns for the mass spectra were calculated using ''Fluorine chemistry mass spec simulator'' [26] and ChemDraw. Mass peaks are quoted for ^{58}Ni, ^{48}Ti, ^{90}Zr, ^{180}Hf, ^{64}Zn, ^{59}Co, ^{187}Re and ^{93}Nb.

4.2.1 CID of transition metal monofluoride complexes

4.2.1.1 Complexes of Nickel

$Ni(PEt_3)_2(C_5F_3HN)F$ (**5**) was investigated by negative ion ESI in the presence of CsF as ionizing agent. Fig 4. 8 shows that the molecular ion is not observed in the mass spectrum and the base peak represents the ion formed by the replacement of one of the PEt_3 ligands by acetonitrile. The peak at 368 was isolated in the ion trap and subjected to multistep CID in order to see the fragmentation pattern.

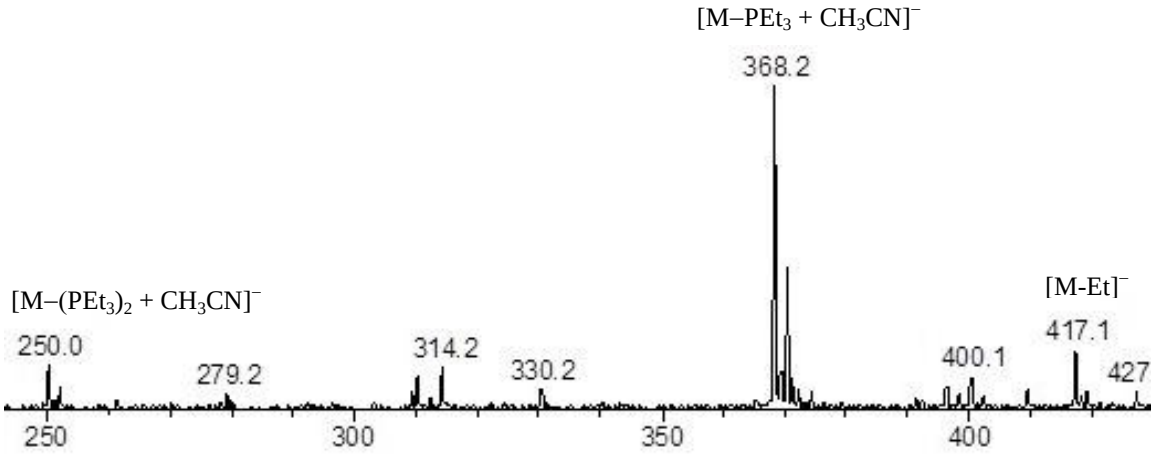

Fig 4. 8 Negative ion ESI mass spectrum of **5** (in CH_3CN) in the presence of CsF

It was observed that during MS^2 phosphine was lost instead of the halide ion (which is usually very labile).[3] During MS^3 two products are observed, one daughter ion is formed by Ni–F bond dissociation while the other daughter ion is formed by the loss CN^- from the coordinated acetonitrile (scheme 4.1) see Fig 4. 9. In contrast the positive ion mode the spectrum is dominated by [M–F] ion.

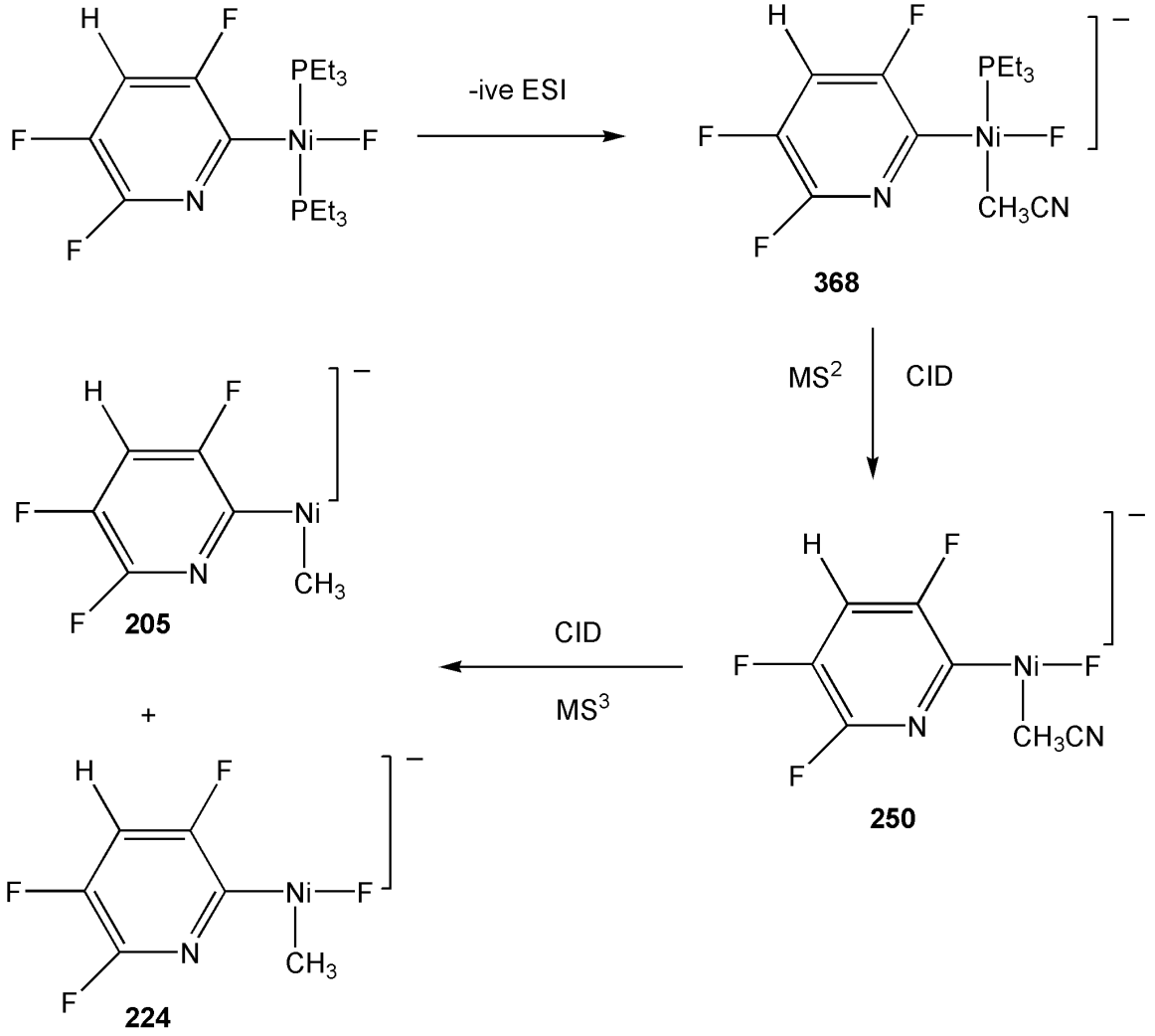

Scheme 4. 1 Multi stages of CID on $Ni(PEt_3)(CH_3CN)(C_5F_3HN)F$

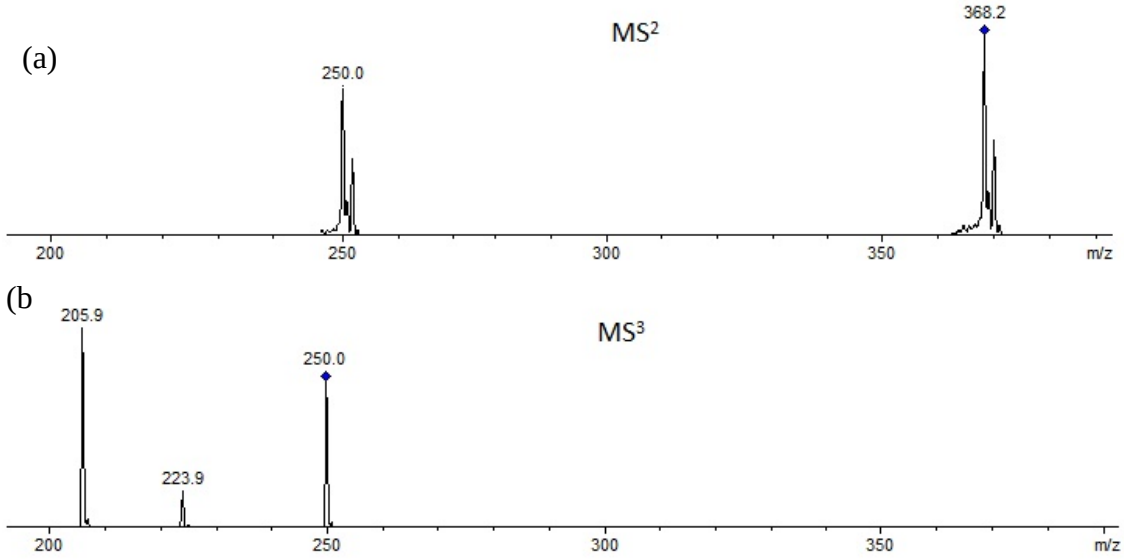

Fig 4. 9 CID of $[Ni(PEt_3)(C_5F_3HN)(CH_3CN)F]^+$ m/z 368. (a) MS^2 and the bottom is MS^3

4.2.2 CID of transition metal difluorides complexes

4.2.2.1 Difluoride complexes of titanium, zirconium and hafnium

The positive ion ESI-mass spectrum of $(Cp^*)_2TiF_2$ (**11**) gave ion peaks at m/z = 337 $[M–F]^+$, 379 $[M+Na]^+$ and 395 $[M+K]^+$ with significant intensity (from CH_3CN solution) see Fig 4. 10.

$$\underset{m/z356}{(Cp^*)_2TiF_2} \xrightarrow{ESI} \underset{m/z337}{[(Cp^*)_2TiF]^+} + \underset{m/z379}{[(Cp^*)_2TiF_2{+}Na]^+} + \underset{m/z395}{[(Cp^*)_2TiF_2{+}K]^+} \quad \text{----} \quad 4.6$$

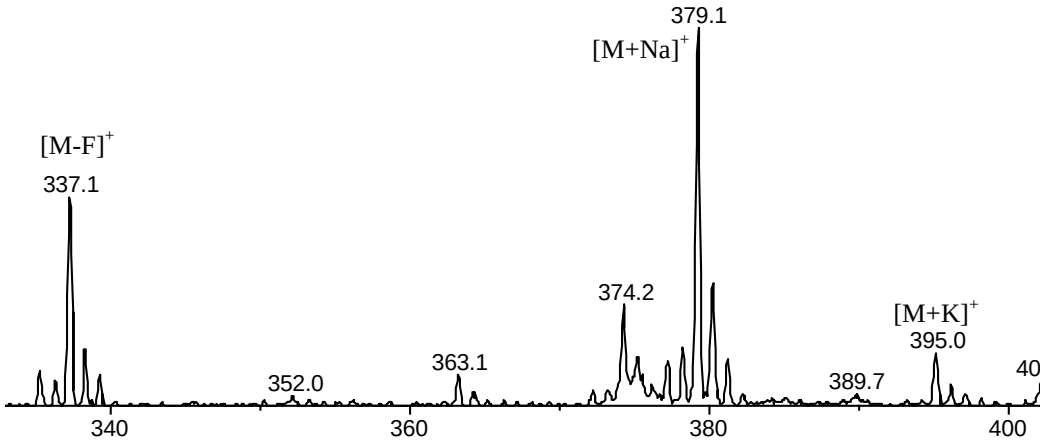

Fig 4. 10 Mass spectrum (ESI, positive ion) of $[(Cp^*)_2TiF_2]^+$ **11** (from CH_3CN solution)

The daughter ions were isolated in the ion trap one by one and fragmentation was investigated as a function of the collision energy.

i. Resonance excitation of the $[(Cp^*)_2TiF]^+$ cation (m/z 337)

To investigate the decay pathway of $[(Cp^*)_2TiF]^+$, the cation was isolated in the quadrupole ion trap (QIT) and activated using resonance excitation. At 0% (V is converted to % energy by assuming 25V as 100%) collision energy there is no production of daughter ions . Fig 4. 11 displays the resulting ionic fragments at 1.4 % collision energy, illustrating that $[(Cp^*)_2TiF]^+$ decays by losing HF resulting in the formation of $Cp^*(C_5Me_4CH_2)Ti^+$ (**11`**).

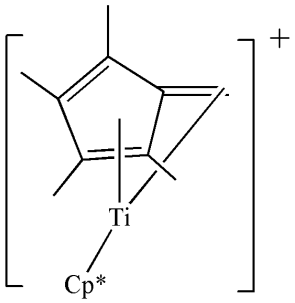

11`

This reaction could occur by conversion of one C_5Me_5 ligand into the tetramethylfulvene ($C_5Me_4CH_2$).

$$[(Cp^*)_2TiF]^+ \longrightarrow [Cp^*(C_5Me_4CH_2)Ti\text{-}H]^+ + HF \qquad 4.7$$

m/z337 m/z317

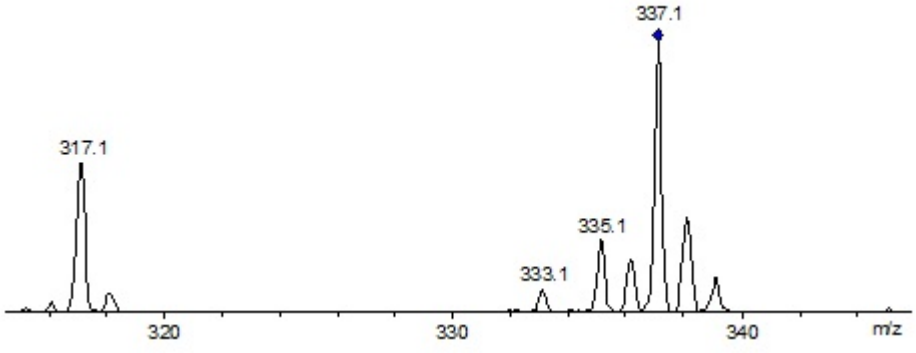

Fig 4. 11 CID mass spectrum of $[(Cp^*)_2TiF]^+$ at 1.4% collision energy illustrating fragmentation by elimination of HF. The diamond sign at the top of the peak represents the ion which underwent CID

Fig 4. 12 displays % fragmentation curves (i-e., plot of ion counts divided by total ion counts versus collision energy) for decay of parent ion $[(Cp^*)_2TiF]^+$ into daughter ions $Cp^*(C_5Me_4CH_2)Ti^+$ (**11`**).

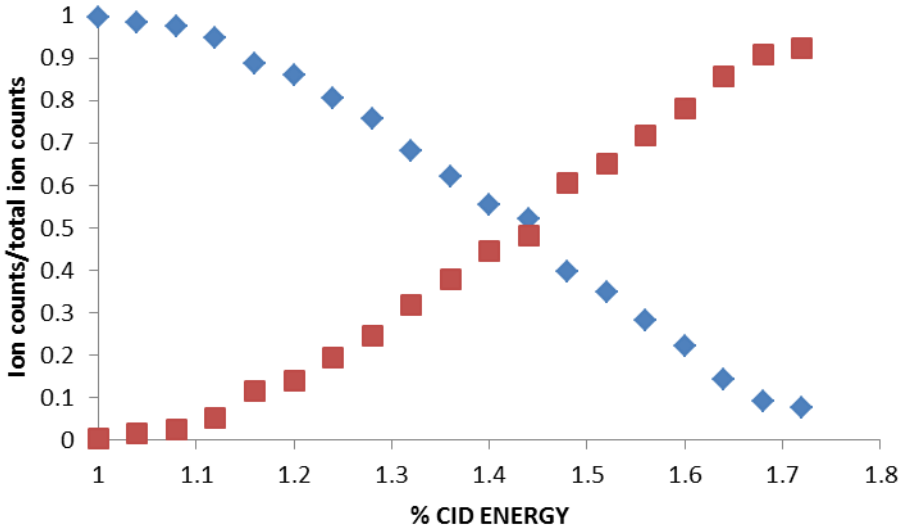

Fig 4. 12 Fragmentation curves for the decay of parent ion $[(Cp^*)_2TiF]^+$ into daughter ions $[Cp^*(C_5Me_4CH_2)Ti]^+$. The blue squares shows the parent ion decaying and the red squares shows the daughter ion growing. The error can be ±3.[21-23]

ii. Resonance excitation of $[(Cp^*)_2TiF_2+Na]^+$ (m/z 379)

$[(Cp^*)_2TiF_2+Na]^+$ (m/z 379) is the other significant resonance in ESI-MS spectra of $[(Cp^*)_2TiF_2]$. This was also isolated and subjected to resonance excitation CID in quadrupole ion trap. Upon resonance excitation $[(Cp^*)_2TiF_2+Na]^+$ can be seen to decay with the production of $[(Cp^*)TiF_2]^+$ and $[C_5Me_4CH_2]^+$ at 1.28% collision energy (see Fig 4. 13).

$$\underset{\text{m/z 379}}{[(Cp^*)_2TiF_2+Na]^+} \longrightarrow \underset{\text{m/z 243.9}}{[(Cp^*)TiF_2+Na]^+} + \underset{\text{m/z134}}{[C_5Me_4CH_2]^+} \quad \text{---------- 4.8}$$

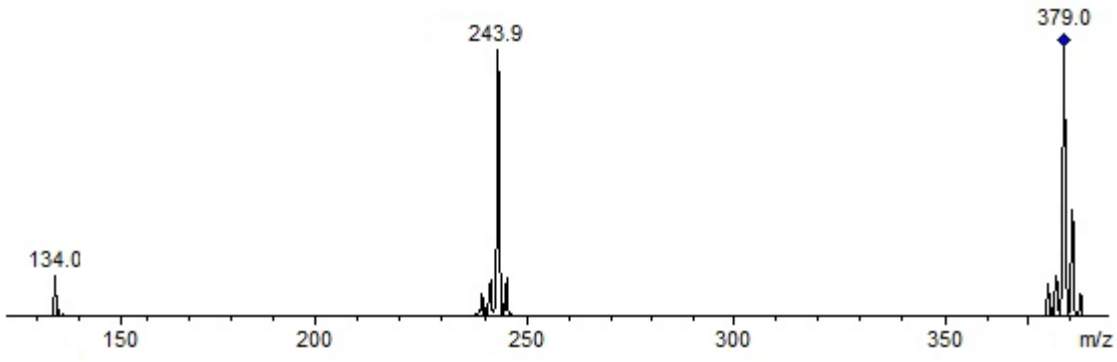

Fig 4. 13 CID mass spectrum of $[(Cp^*)_2TiF_2Na]^+$ at 1.52% collision energy illustrating fragmentation of $[(Cp^*)_2TiF_2+Na]^+$ into $[(Cp^*)_2TiF]^+$ and $[C_5Me_4CH_2]^+$

Fig 4. 14 displays the % fragmentation curves for the decay ion $[(Cp^*)_2TiF_2+Na]^+$ into daughter ions $[(Cp^*)TiF_2]^+$ and $[C_5Me_4CH_2]^+$. The onset of the fragmentation for $[(Cp^*)_2TiF_2+Na]^+$ occurs at 1.24% CID energy and conversion is completed at 2% of the CID energy.

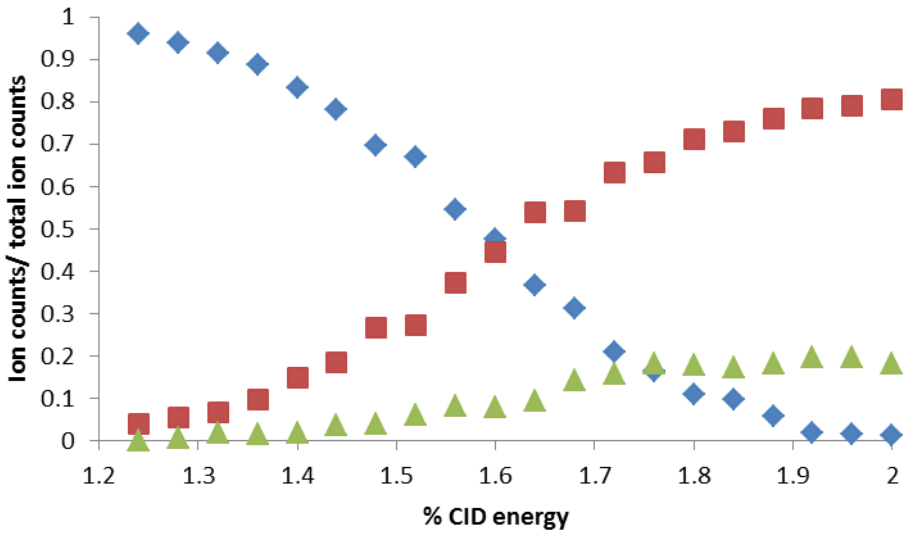

Fig 4. 14 Fragmentation curves for the decay of parent ion $[(Cp^*)_2TiF_2+Na]^+$ (blue squares) into daughter ions $[(Cp^*)TiF_2]^+$ (red squares) and $[C_5Me_4CH_2]^+$ (green triangles). The error can be ±3.[21-23]

iii. Resonance excitation of $[(Cp^*)_2TiF_2+K]^+$ (m/z 395)

To investigate the reaction further the potassiated molecular ion peak at m/z 395 was isolated in the quadrupole ion trap, and subjected to resonance excitation CID. This cation decayed into daughter ions at m/z = 337 and 391. The fragment at 337 is the loss of

potassium fluoride ion from the molecular ion while the other peaks at m/z 391 cannot be identified as the ion intensity become very low when trying to isolate in MS^3.

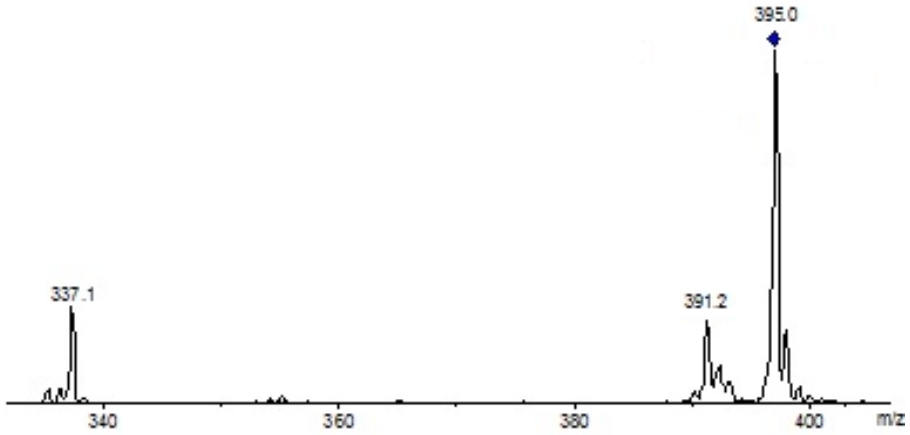

Fig 4. 15 CID mass spectrum of $[(Cp^*)_2TiF_2+K]^+$ showing fragmentation into daughters ions at m/z 379 and 391.

iv. Negative Ion ESI-MS spectra $[(Cp^*)_2TiF_2]$

The negative ion electrospray ionization ESI-MS of **11** in CH_3CN (solvent) showed very low ion intensity and the molecular ion peak at 356 was missing. In the presence of CsF as ionizing agent, the molecular ion was observed at m/z 356 as a major peak. The other signals at 375 and 394 are proposed to be the adduct ions $[M+F]^-$ and $[M+2F]^-$ (Fig 4. 16).[27]

$$(Cp^*)_2TiF_2 \xrightarrow[\text{-ive ESI}]{CsF} \underset{m/z356}{[(Cp^*)_2TiF_2]^-} + \underset{m/z375}{[(Cp^*)_2TiF_2+F]^-} + \underset{m/z394}{[(Cp^*)_2TiF_2+2F]^-} \quad \text{------} \quad 4.9$$

The intensity of the ions is low, due to which the peaks are broad and not well resolved for the isotopic pattern.

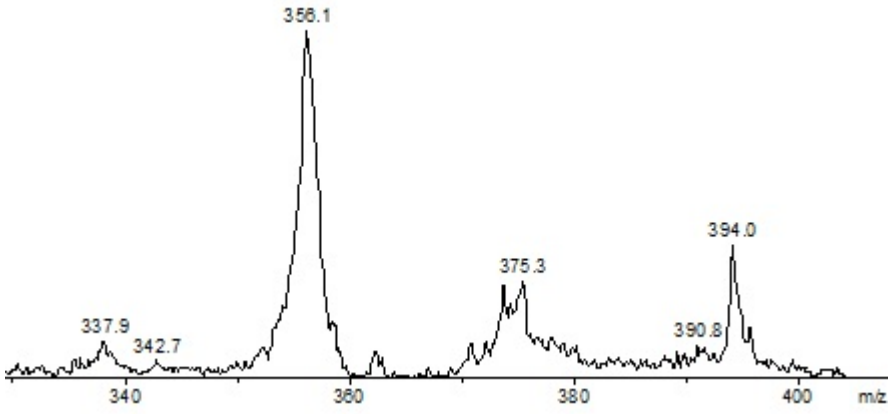

Fig 4. 16 Negative ion electrospray ionization ESI-MS of $[(Cp^*)_2TiF_2]^-$ in MeCN with CsF added to the solution.

v. Positive ion ESI-MS of $(Cp^*)_2ZrF_2$

The positive ion ESI mass spectrum of $(Cp^*)_2ZrF_2$ (**12**) shows sodiated and potassiated molecular ions at m/z 421 and 437 respectively as well ion the formed by elimination of one fluoride ion at m/z 379. The peak at m/z 397 is considered to be formed by loss of a hydride ion and resulted in the formation of $[Cp^*(C_5Me_4CH_2)ZrF_2]^+$ abbreviated as $[M–H]^+$.

$$\underset{398}{(Cp^*)_2ZrF_2} \xrightarrow{+ive\ ESI} \underset{379}{[(Cp^*)_2ZrF]^+} + \underset{397}{[Cp^*(C_5Me_4CH_2)ZrF_2]^+} + \underset{421}{[(Cp^*)_2ZrF_2Na]^+} + \underset{437}{[(Cp^*)_2ZrF_2K]^+} \quad 4.10$$

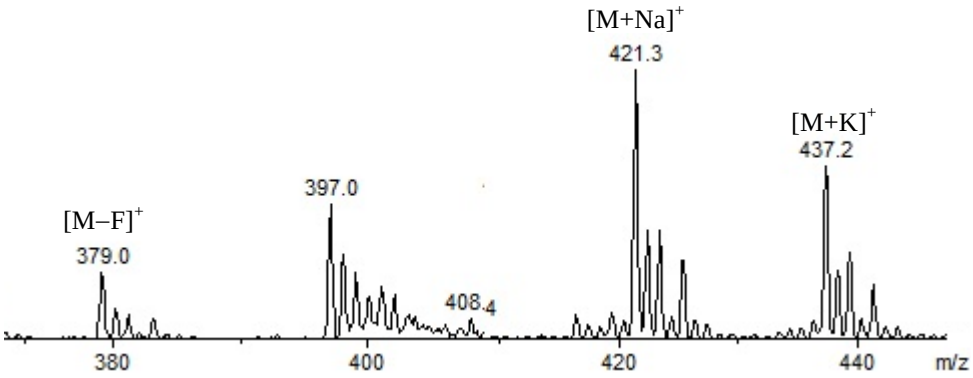

Fig 4. 17 positive ion ESI mass spectrum of $(Cp^*)_2ZrF_2$ in CH_3CN

The fragmentation pathways of these daughter ions were further investigated by isolating the ions one–by–one in the trap and subjecting to the low energy CID. CID MS^2 spectrum of the sodiated molecular ion shows the loss of sodium hydride and sodium fluoride ligand resulting in the formation of daughter ions at m/z 397 $[M–H]^+$ and 379 $[M–F]^+$ respectively

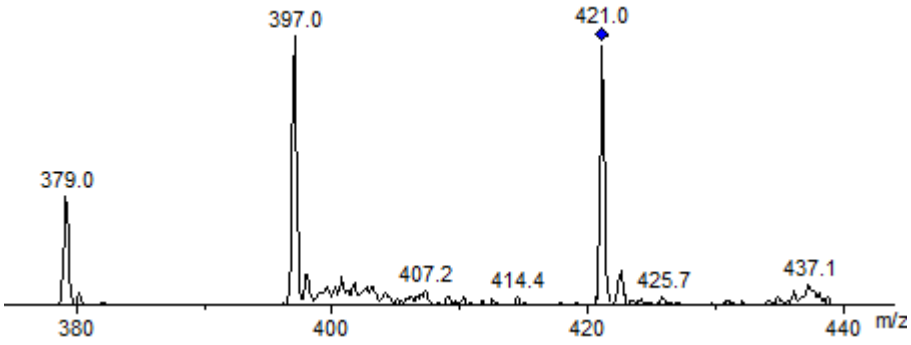

Fig 4. 18 CID on $[(Cp^*)_2ZrF_2Na]^+$ having m/z 421 from $(Cp^*)_2ZrF_2$

The potassiated molecular ion showed a similar fragmentation pattern upon low energy CID with helium (Fig 4. 19). The $[M+K]^+$ was also isolated in the ion trap and subjected to CID which fragmenting by loss of KH and KF and resulting in the formation daughter ions m/z 397 $[M–H]^+$ and 379 $[M–F]^+$ respectively (Fig 4. 20).

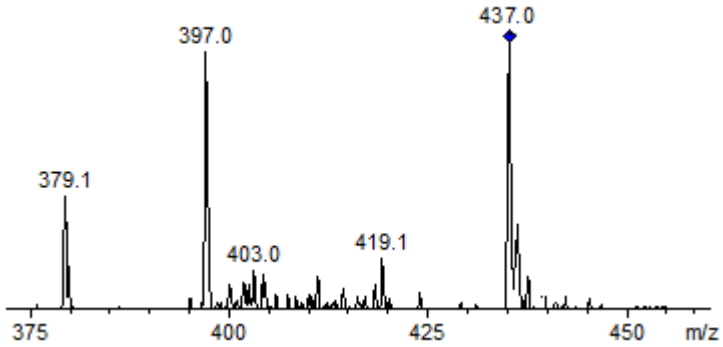

Fig 4. 19 CID on potassiated molecular ion $[(Cp^*)_2ZrF_2K]^+$ from $[(Cp^*)_2ZrF_2]^+$

The $[Cp^*(C_5Me_4CH_2)ZrF_2]^+$ was isolated in the ion trap and subjected to CID (MS^3) which loses the fluoride ion and daughter ions at m/z 379 appears in the spectrum. Loss of 18 is not consistent with experiments, suggesting that m/z 379 is the daughter ion of either 437 or 421 formed by loss of either KF or NaF respectively.

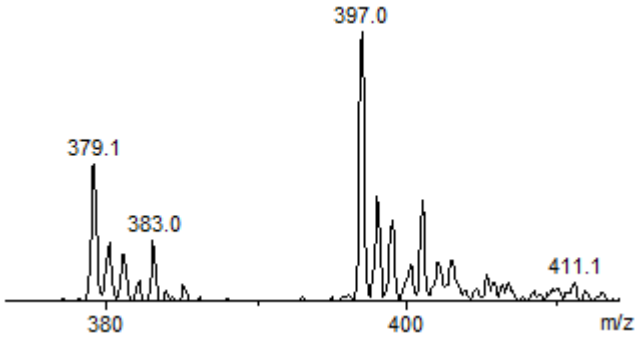

Fig 4. 20 CID on $[Cp^{*}(C_5Me_4CH_2)ZrF_2]^+$ (m/z 397) from $[(Cp^*)_2ZrF_2]^+$

vi. Positive ion electrospray ionization of $(Cp^*)_2HfF_2$

The electrospray ionization of $(Cp^*)_2HfF_2$ (**13**) in positive mode behaves in a similar way to **12** and results in the formation of sodiated molecular ion at m/z 501, the ion formed by the loss of fluoride ion $[M–F]^+$ at m/z 469 and another ion formed by the loss of hydrogen $[M–H]^+$ (see Fig 4. 21).

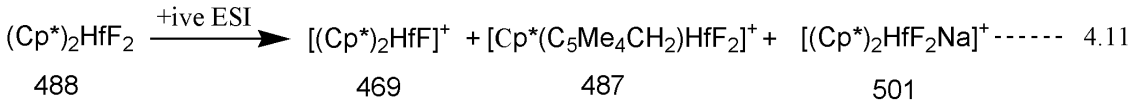

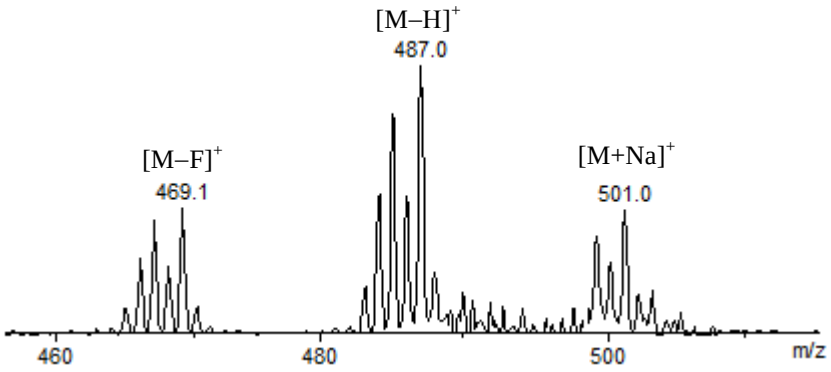

Fig 4. 21 Positive ion ESI mass spectrum of $(Cp^*)_2HfF_2$ in CH_3CN

The CID MS^2 spectrum of $[M–H]^+$ highlights the loss of fluoride ion which is consistent with the low energy CID on $[M–H]^+$ from **12**.

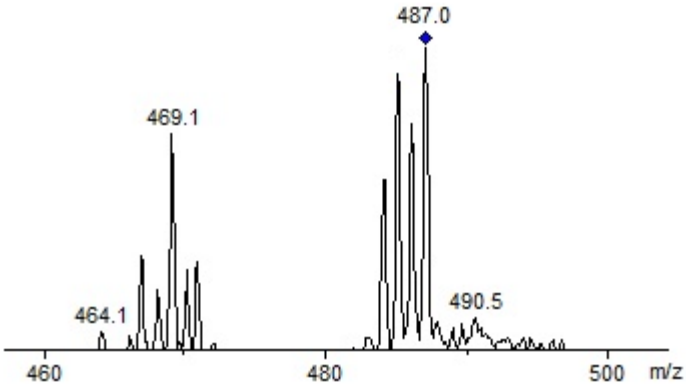

Fig 4. 22 Low energy CID on $[M\text{-}H]^+$ from $(Cp^*)_2HfF_2$

4.2.2.2 Ruthenium difluoride and bis bifluoride complexes

The positive ion ESI mass spectrum of $Ru(PMe_3)_4(F)_2$ **16** gave peaks at m/z 406 and 425 assigned to $[(PMe_3)_4Ru–H]^+$ and $[(PMe_3)_4RuF]^+$ respectively, while the peak at 441 is assigned to $[Ru(PMe_3)_4Cl]^–$.

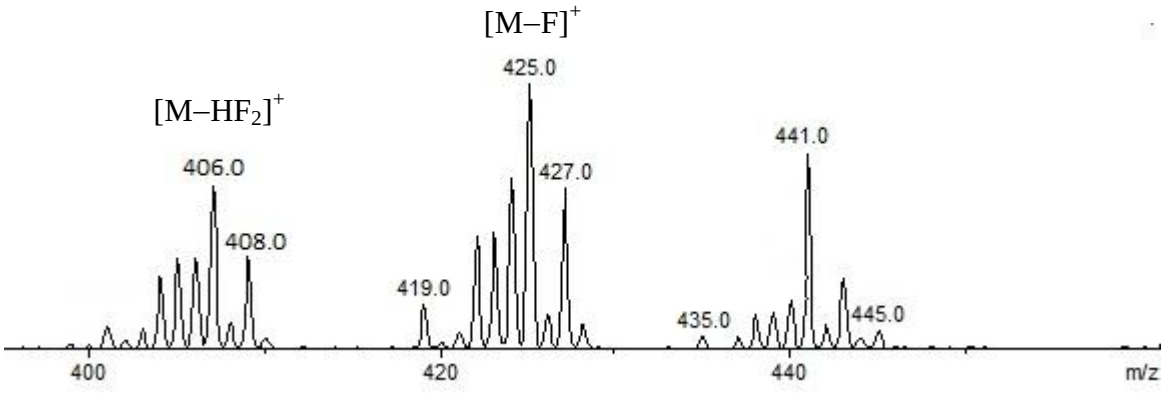

Fig 4. 23 ESI mass spectrum (positive ion) of **16** in THF

The positive ion ESI mass spectrum of $(PMe_3)_4Ru(FHF)_2$ (**15**) shows peaks at m/z = 407.0, 425.1, 441 and 716.1 corresponding to $[(PMe_3)_4Ru]^+$, $[(PMe_3)_4RuF]^+$ $[(PMe_3)_4RuCl]^+$ and $[(Me_3P)_3Ru(\mu–F)_3Ru(PMe_3)_3]^+$. These peaks are also observed in the ESI spectrum of **16** which shows that F–HF is also not stable with respect to electrospray ionization. The peak at m/z = 686 may be from $[(Me_2PH)(Me_3P)_2Ru(\mu–F)_2Ru(PMe_3)_3]^+$ may be assigned to a bridged complex having two fluorines and a CH_3 group from the PMe_3 ligand is replaced by hydrogen.[28] As discussed in chapter 3 the source of chloride ions appears to come from the

starting material used in the synthesis of complex **15** and **16**. There are still some other peaks in the spectra which are unassigned.

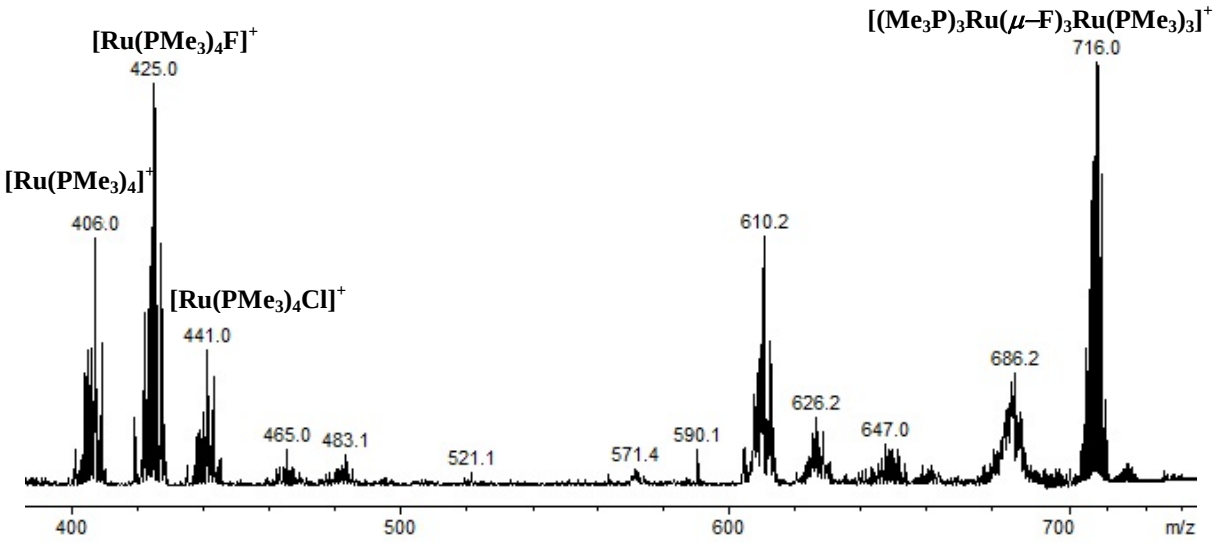

Fig 4. 24 ESI mass spectrum (positive ion) of **15** in THF

CID on the $[M\text{-}F]^+$ from both complexes **15** and **16** showed similar behaviour. Fragmentation occurred by the loss of PMe_3 ligand instead of fluoride ligand which would considered to be very labile (Eq 4.12). Similar behaviour was showed by the chloride analogue (Eq 4.13).

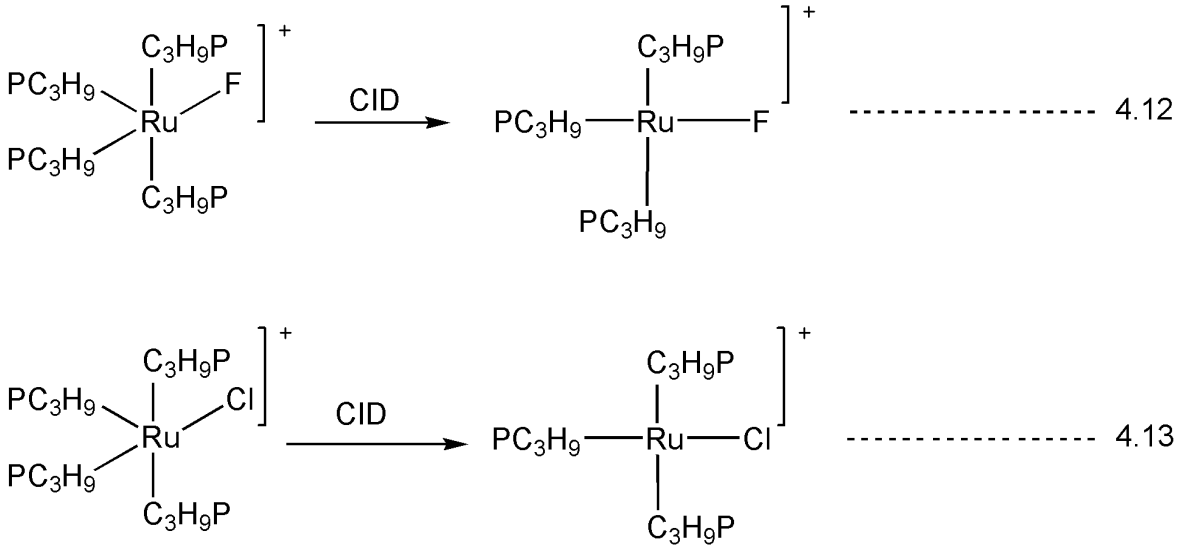

CID studies on the bridged ion having m/z = 716 shows that the daughter ion at m/z 624 is formed by the loss of one of the fluoride ligand and trimethylphosphine ligand while the

other daughter ions are formed either by the loss of the PMe_3 ligand or methyl groups from PMe_3 (scheme 4.2).

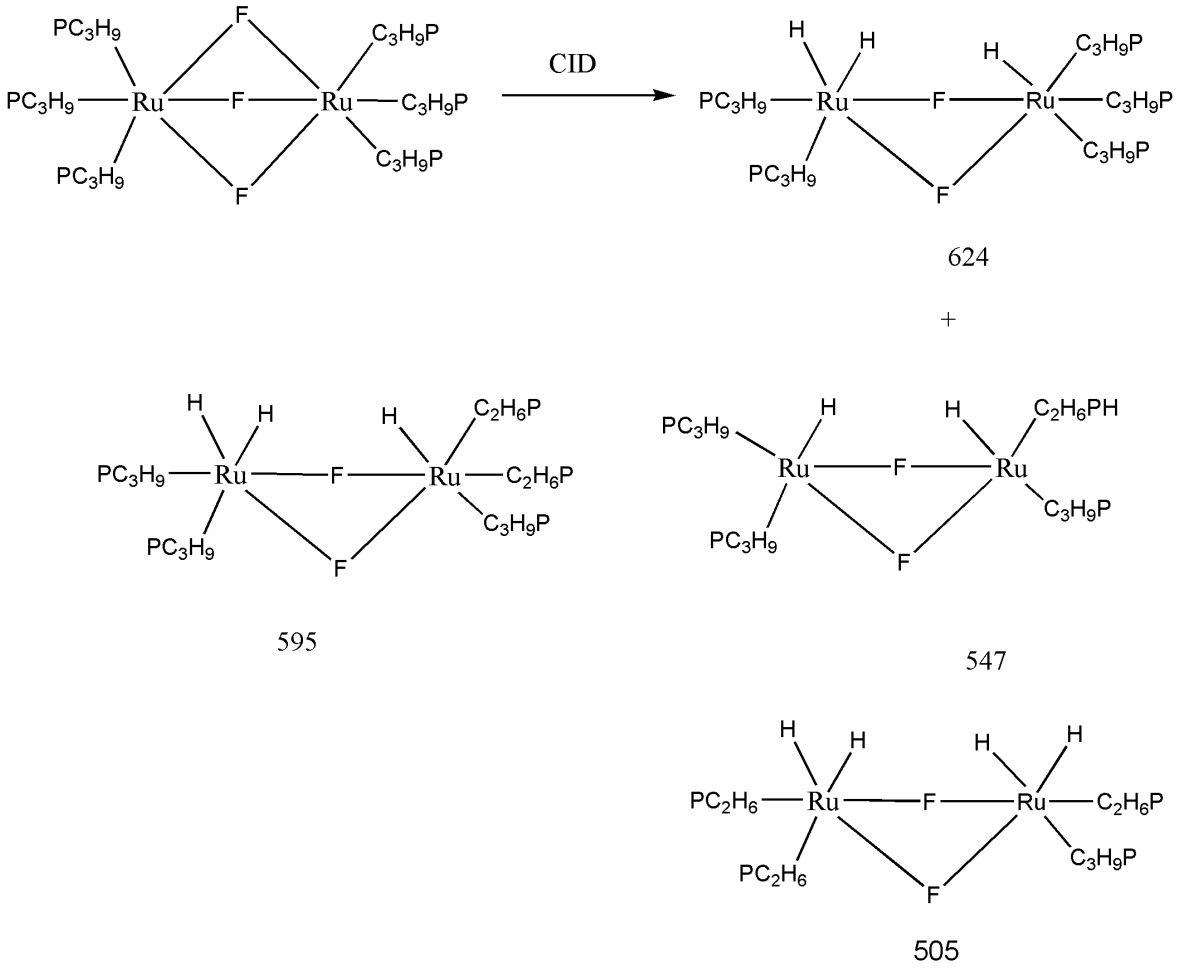

Scheme 4.2 CID on $[(Me_3P)_3Ru(\mu\text{–}F)_3Ru(PMe_3)_3]^+$ from **15** and **16**

It seems that difluoride compounds having phosphine ligands will lose the first fluoride ligand upon ionization in ESI and the second ligand to be lost will either by the phosphine itself or methyl groups from the phosphine.

4.2.2.3 CID on zinc, cobalt and nickel difluoride complexes

The positive ion ESI mass spectrum of $Zn(DMEA)_2F_2$ (**24**) shows a peak at m/z = 259.1 results from the loss of fluoride ligand from the compound $[M–F]^+$. Other peaks at 239.1 correspond to $[(M–HF_2]^+$ (see figure 2.25). The CID MS^2 spectrum of $[M–F]^+$ highlights the loss of HF.

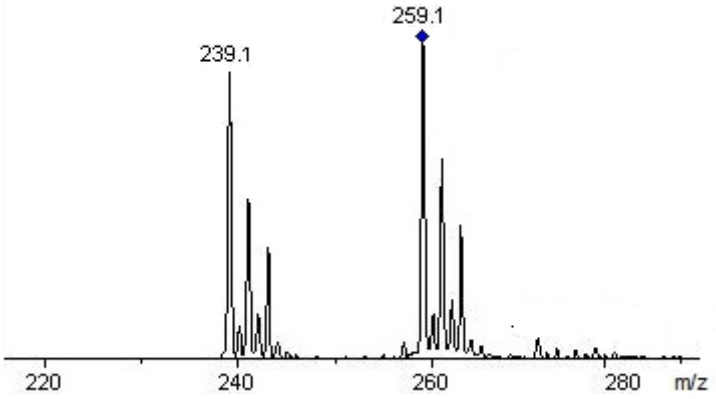

Fig 4. 25 CID mass spectrum of $[M\text{-}F]^+$ (m/z = 259) from $Zn(DMEA)_2F_2$

The CID MS^3 spectrum of m/z 239 showed the loss of the dimethyl ethylenediamine (DMEA) ligand giving the daughter ion having m/z 153.

The positive ion ESI mass spectrum of complex $Co(DMEA)_2F_2$ (**25**) shows a peak for the molecular ion $[M]^+$ at m/z 273.0 and sodiated ion $[M+Na\text{-}H]^+$ at m/z 295.0. The other ions at m/z 254.0 $[M–F]^+$ and 233.0 $[M–2HF]^+$ correspond to the daughter ions formed by the loss of $F^–$ and HF ligands (see fig 2.27).

The fragmentation of the molecular ion upon low energy CID, fragmentation occurs through loss of HF molecules in two steps (Fig 4. 26). Upon isolation of the $[M\text{-}HF]^+$ in the ion trap and subjecting to CID showed the loss of second HF molecule (Fig 4. 27).

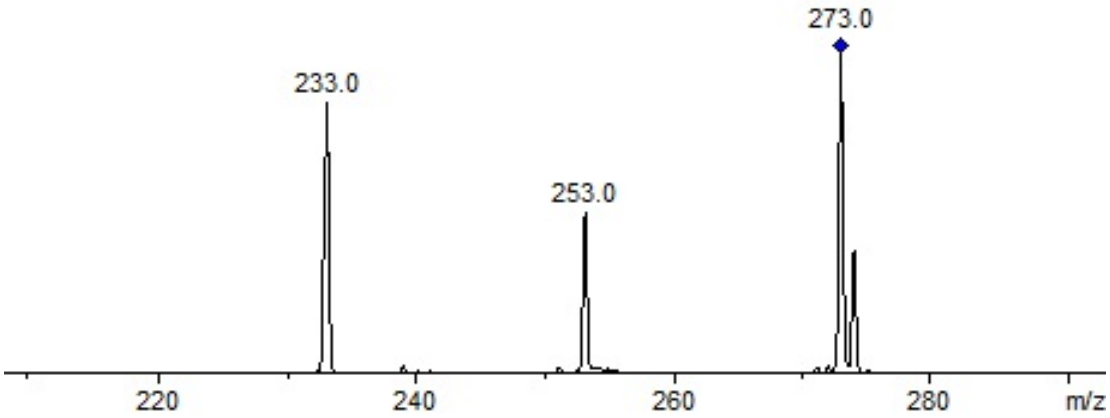

Fig 4. 26 CID was performed at m/z 273 on $Co(DMEA)_2F_2$

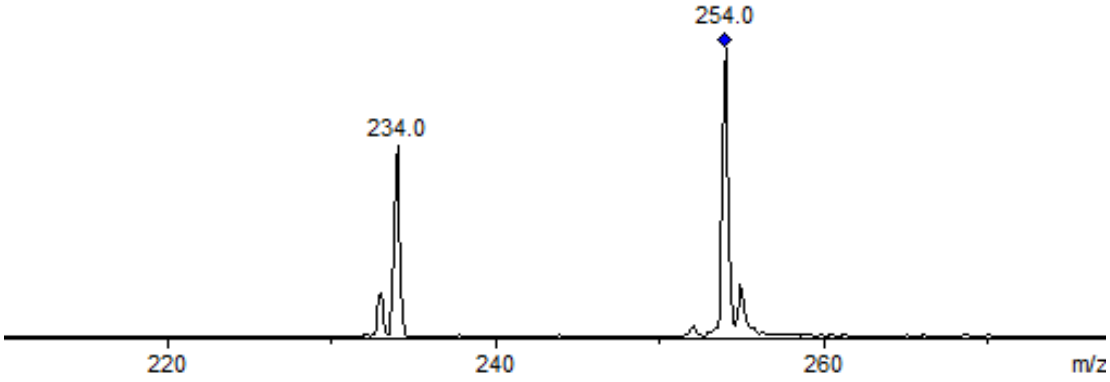

Fig 4. 27 CID was performed at 254 on $[Co(DMEA)_2F_2]^+$

The positive ion ESI mass spectrum of $Ni(DMEA)F_2$ shows the quasimolecular ion at m/z 273, other ions formed by loss of fluoride ion and HF_2 at 253 and 233 respectively (Fig 4. 28).

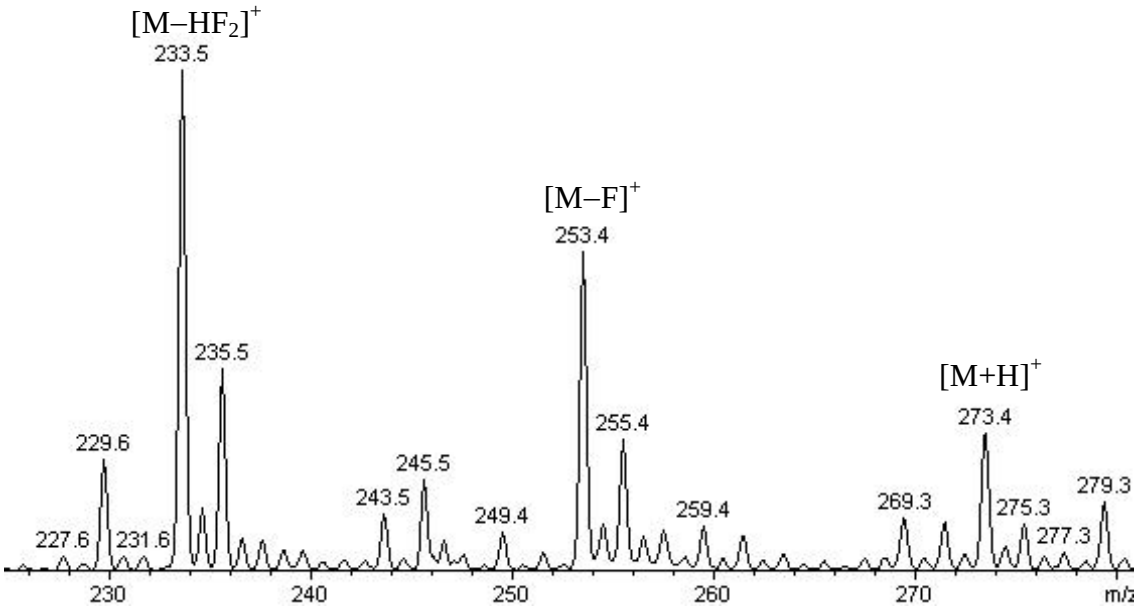

Fig 4. 28 Positive ion ESI spectrum of $[Ni(DMEA)_2F_2]^+$ in CH_3OH

The CID spectrum on the quasimolecular ion is consistent with the CID on the molecular ion of **25**, showing the loss of two HF molecules in two steps giving daughter ions at m/z 253 and 233 respectively (Fig 4. 29).

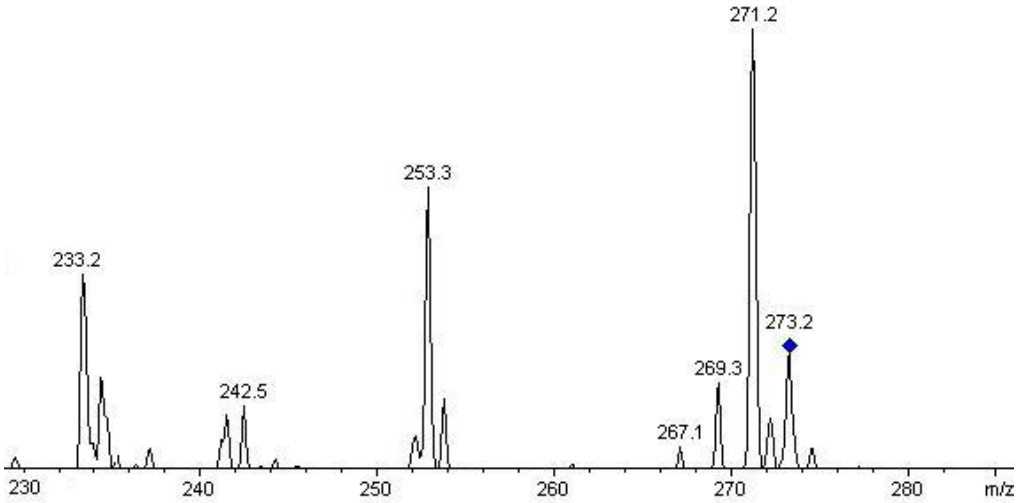

Fig 4. 29 CID mass spectrum of m/z 273 of $[Ni(DMEA)_2F_2]^+$

Similarly the low energy CID on m/z 253 showed elimination of a HF molecule giving a daughter ion at 233 (Fig 4. 30).

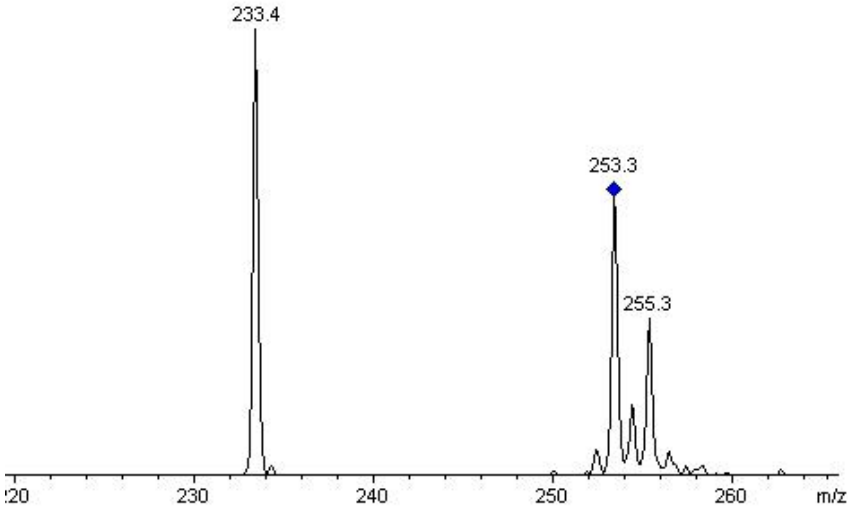

Fig 4. 30 CID mass spectrum of m/z 253 of $Ni(DMEA)F_2$

4.2.3 CID of multiply charged anions (MCAs)

4.2.3.1 Potassium hexafluorozirconate (K_2ZrF_6) and Potassium hexafluorotitanate (K_2TiF_6)

Fig 4. 31 displays the negative ion electrospray ionization spectrum (ESI–MS) of K_2ZrF_6 (**36**). ZrF_5^- (m/z 184.8, 100%) appears to be the dominant peak in the mass spectrum, The parent dianion ZrF_6^{2-} (m/z 101.9, 35%) also appears at significant intensity. $KZrF_6^-$ (m/z

242.8, 10%) is the other significant resonance. $KZrF_6^-$ and ZrF_5^- are singly charged ions, the isotopic peaks differ by 1 mass unit while ZrF_6^{2-} is a doubly charged ion and the isotopic peaks differ by 0.5 mass units and so on. From the separation of the isotopic peaks the charge state of a peak can be deduced and thus the mass (Fig 4. 31).

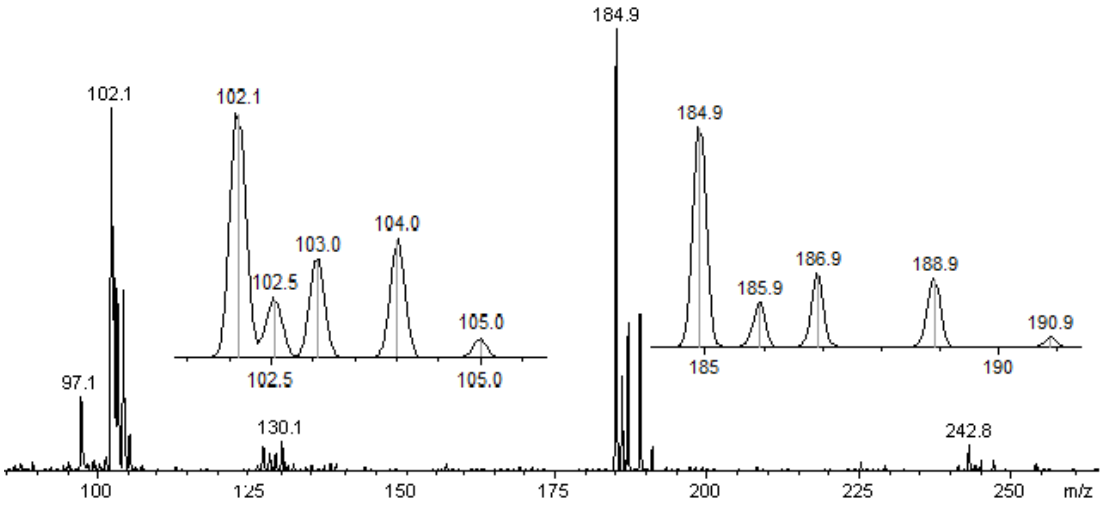

Fig 4. 31 (a) Negative ion Electrospray ionization ESI-MS of $[K_2ZrF_6]^-$ in H_2O

Upon CID the parent dianion decayed through ionic fragmentation and lost fluoride ion which could not be seen in the spectrum as it lies outside the mass spectrometer window (see Fig 4. 32).

$$ZrF_6^{2-} \longrightarrow ZrF_5^- + F^- \qquad 4.14$$

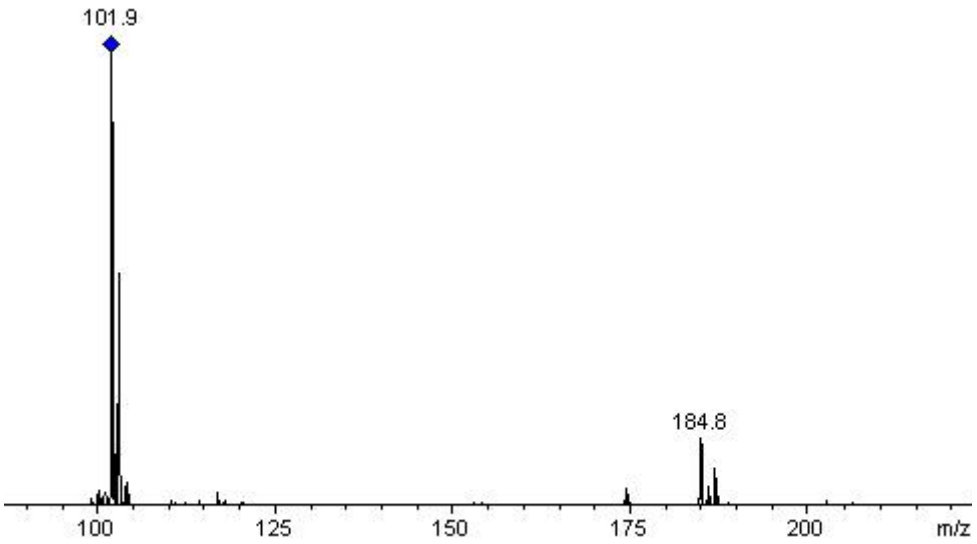

Fig 4. 32 CID mass spectrum of ZrF_6^{2-} (m/z = 102)

Fig 4. 33 shows the negative ion electrospray ionization spectrum (ESI-MS) of potassium hexafluorotitanate (K_2TiF_6) (**37**). TiF_6^{2-} (81, 100%) appears to be the dominant resonance in this case and the other peak TiF_5^- (m/z 142.8) appears at reasonable intensity. TiF_6^{2-} is a a doubly charged ions and the isotopic peaks are separated by a half mass unit. TiF_5^- is singly charged so the isotopic peaks differ by 1 mass unit.

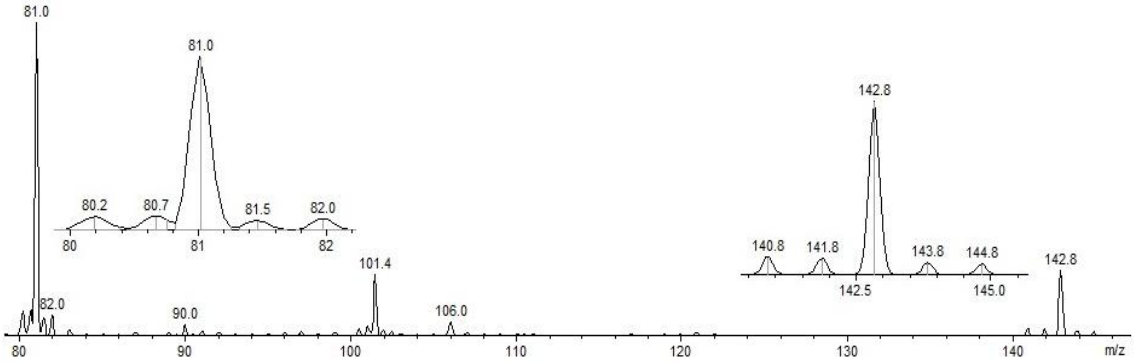

Fig 4. 33 Negative ion electrospray ionization ESI-MS of K_2TiF_6 in H_2O+CH_3CN

The CID MS^2 spectrum of the parent dianion (TiF_6^{2-}) shows the elimination of F^- and the daughter ion TiF_5^- appears at m/z = 143.8 (Fig 4. 34).

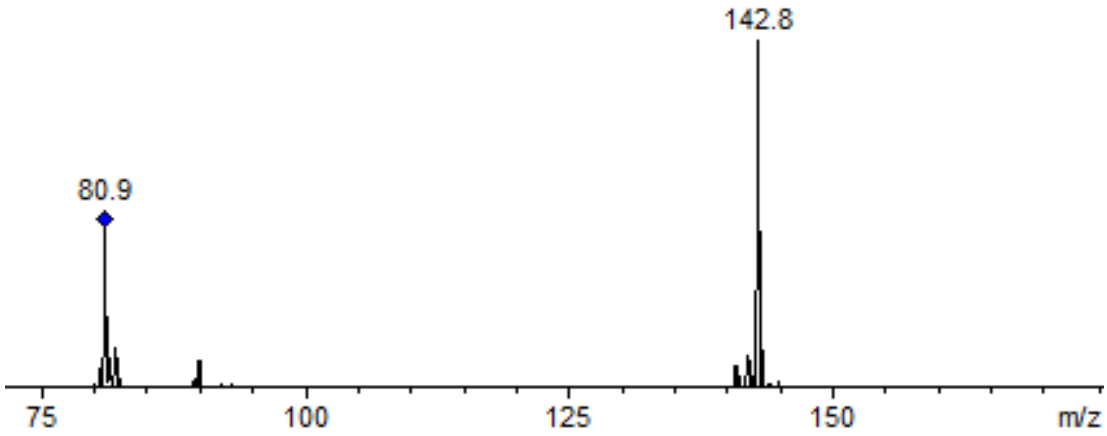

Fig 4. 34 CID mass spectrum of TiF_6^{2-} (m/z = 142.8)

The decay mechanism of TiF_5^- was further investigated by subjecting to low energy CID. Upon increasing the resonance excitation energy TiF_5^- starts to decrease in intensity and finally vanishes. It is concluded that it decays by ionic fragmentation into TiF_4 and F^-.

As TiF_4 is neutral and F^- lies outside the mass range of the ion trap spectral window, so no resonance is observed.

$$TiF_5^- \xrightarrow{\text{Increasing energy}} \text{Vanishes} \longrightarrow TiF_4 + F^- \quad \text{4.15}$$

m/z 142.8

4.2.3.2 Potassium heptafluoroniobate (K_2NbF_7) Potassium heptafluorotantalate (K_2TaF_7) and Potassium hexafluoronickelate (K_2NiF_6)

Potassium heptafluoroniobate (K_2NbF_7) **38** represents an example of a transition metal compound with the metal atom in a heptacoordinate environment; the arrangement of fluorine atoms around the metal forms a capped trigonal prism.[29] The crystal structure of K_2NbF_7 has been determined by X-ray and neutron diffraction.[30]

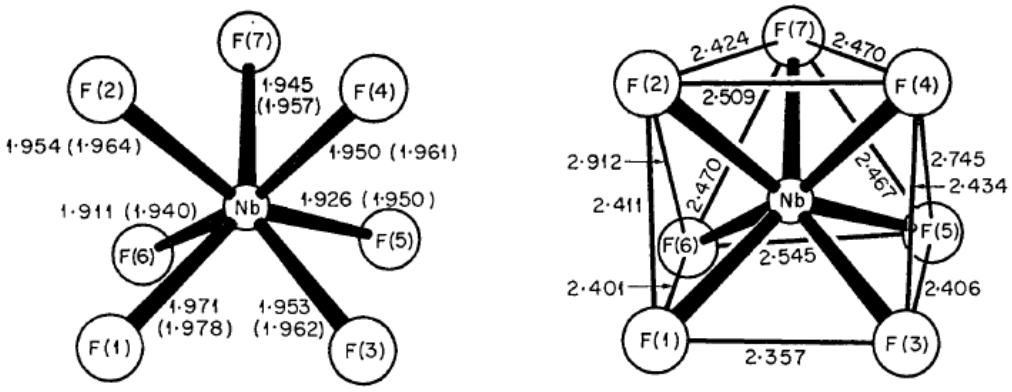

Fig 4. 35 Crystal structure of K_2NbF_7. Interatomic distances Å in the NbF_7^- ion.[30]

Potassium heptafluoroniobate (K_2NbF_7) was investigated by negative ion electrospray ionization spectrum (ESI-MS). The K_2NbF_7 solution in CH_3CN gave a dominant resonance at m/z = 113 which is assigned to the parent dianion $[NbF_7]^{2-}$ and the K_2NbF_7 solution in methanol gave resonances at m/z = 206 and 265 which are assigned to $[NbF_6]^-$ $[KNbF_7]^-$ respectively. For this complex it is not possible to demonstrate 2^- charge in the same ways because Niobium is mono-isotopic.

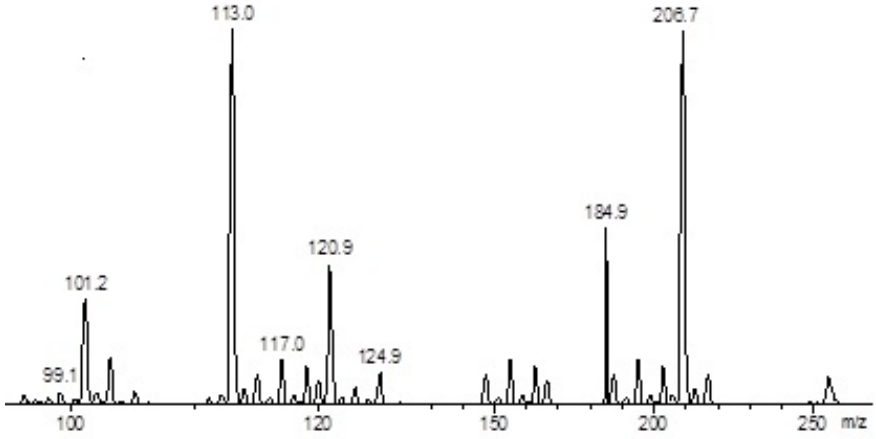

Fig 4. 36 Negative ion ESI-MS of K_2NbF_7 CH_3CN/MeOH solution

Potassium heptafluorotantalate (**39**) and Potassium hexafluoronickelate (**40**) were also tried to study by negative ion mass spectrometry but no sensible results were obtained.

4.2.4 CID on Re tricarbonyl complexes

The positive ion ESI spectrum of $[Re(CO)_3(bpy)(pic)]^+PF_6^-$ (**26**) shows the cationic molecular ion $[M]^+$ at m/z 520 and another peak appears at 427 corresponding to $[Re(CO)_3(bpy]^+$. The cationic molecular ion was isolated in the ion trap and subject to CID with helium resulting in the formation of daughter ions at m/z 427 and 445 corresponding to $[Re(CO)_3(bpy]^+$ and $[Re(CO)_3(bpy)(H_2O)]^+$ respectively.

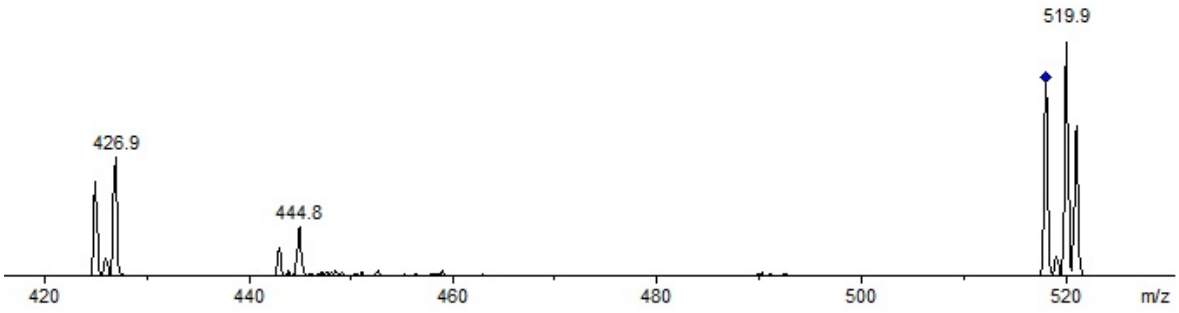

Fig 4. 37 CID mass spectrum of cationic molecular ion (m/z 520)

$[Re(CO)_3(bpy]^+$ (m/z 427) could not be isolated separately from $[Re(CO)_3(bpy)(H_2O)]^+$ (m/z 445) in the ion trap. It was observed that $[Re(CO)_3(bpy)(H_2O)]^+$ (m/z 445) cannot exist isolated in the ion trap. It was concluded that $[Re(CO)_3(bpy]^+$ (m/z 427) is very reactive towards water and with increasing the collisional excitation energy the intensity of the peak at m/z 445 increases until an equilibrium is

established between them. Upon low energy CID, a CO ligand eliminates from the peak at m/z 445. Another peak appears at m/z 275 which cannot be assigned.

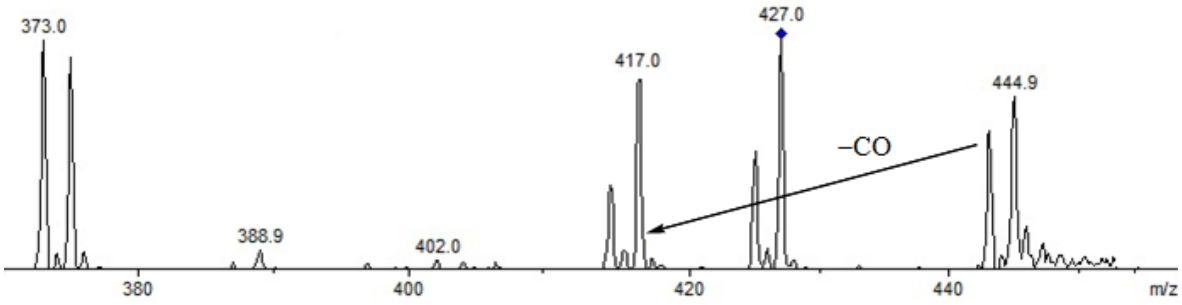

Fig 4. 38 CID on $[Re(CO)_3(bpy]^+$ (m/z 427)

The positive ESI mass spectrum of $[Re(CO)_3(bpy)(P(OEt)_3]^+PF_6^-$ **(27)** gave a peak at m/z 593 that is the cationic molecular ion peak $[M^+]$. Another peak at 565 results from loss of one of carbonyl ligand from the molecular ion $[M\text{-}CO]^+$.

The CID MS^2 spectrum of the cationic molecular ion (m/z = 593) shows that the loss of the carbonyl ligand is the major, while the loss of the triethylphosphite is the minor fragmentation pathway.

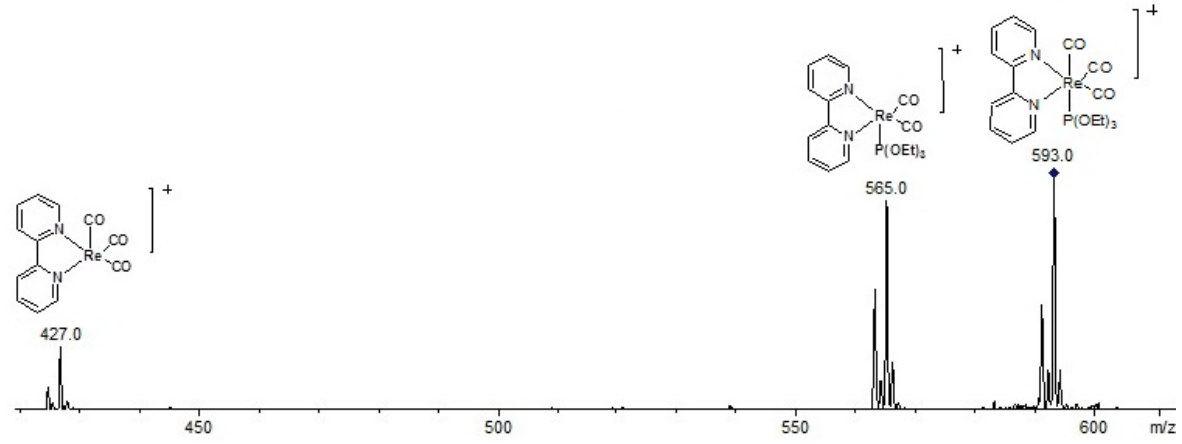

Fig 4. 39 CID mas spectrum of $[Re(CO)_3(bpy)(P(OEt)_3]^+$ (m/z 593)

The fragmentation of $[Re(bpy)(P(OEt)_3)(CO)_2]^+$ m/z 565 was also investigated through low energy CID studies. It seems that the $[M\text{-}CO]^+$ can lose an ethoxy molecule giving a daughter ion at m/z 521 which can further lose carbonyl ligands. Other significant ions observed are the $[Re(bpy)(CO)_3]^+$ and $[Re(bpy)(CO)_2]^+$at m/z 426.9 and 399 respectively.

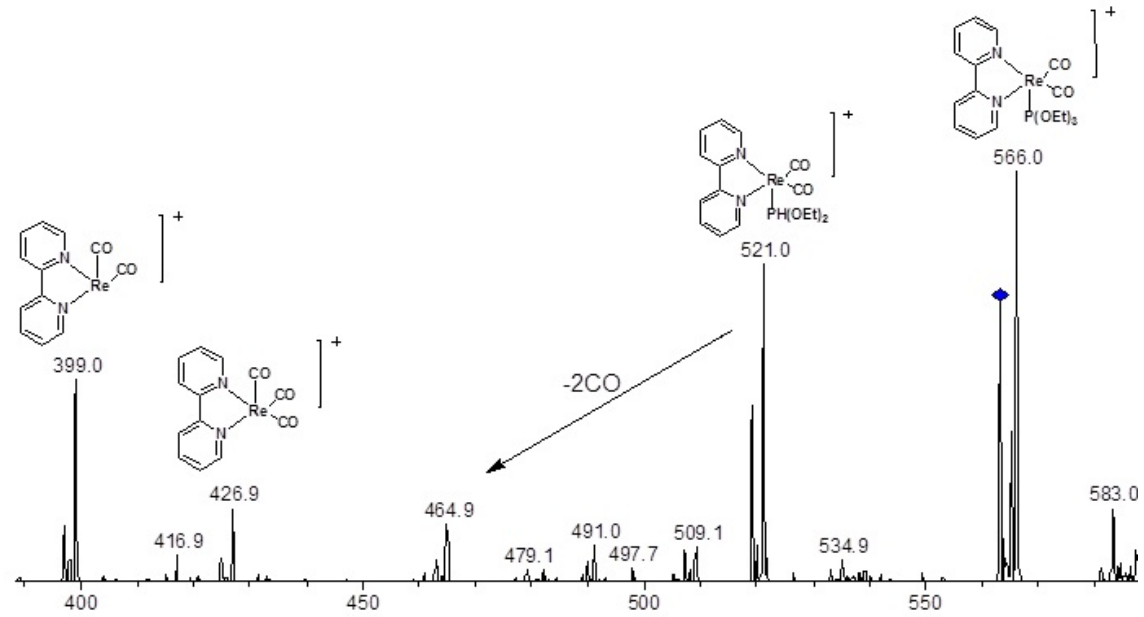

Fig 4. 40 CID on $Re(bpy)(P(OEt)_3)(CO)_2]^+$ m/z 565 giving daughter ions by loss of various ligands

4.2.5 CID of Mn tricarbonyl complexes

The positive ion ESI mass spectrum of $[Mn(bpy)(pic)CO)_3]^+$ shows the cationic molecular ion at m/z. the other ions are formed by the loss of either the picoline ligand or the carbonyl liagand (see 5.17). Upon subjecting to low energy CID of the cationic molecular ion fragmented through the loss of picoline ligand and as well the carbony ligands Fig 4. 41.

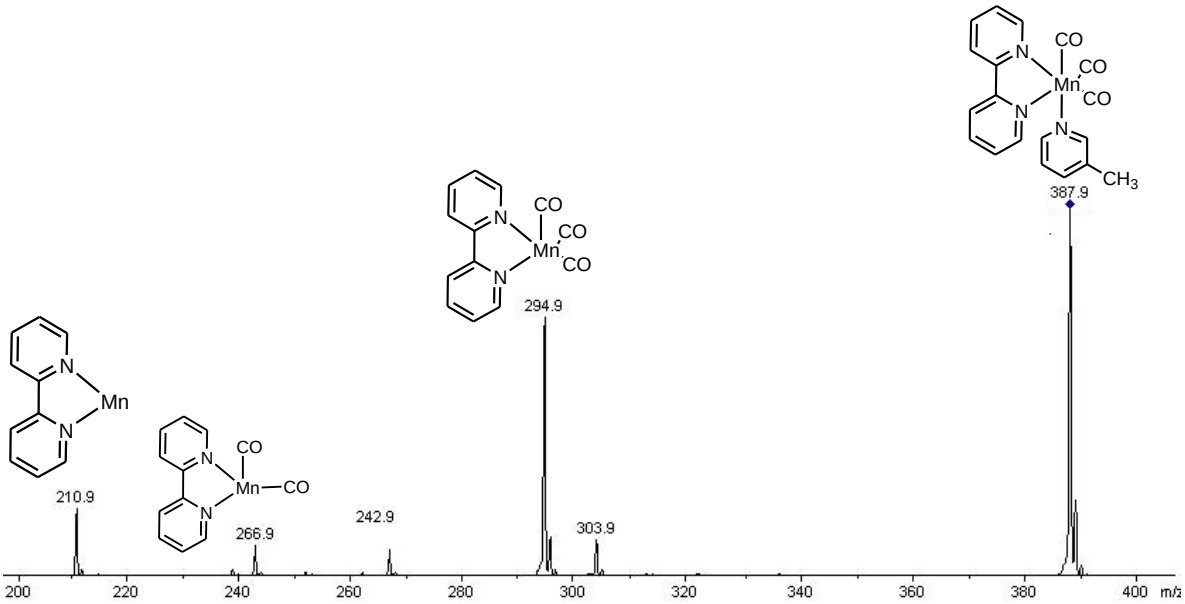

Fig 4. 41CID of $[Mn(bpy)(pic)CO)_3]^+$ m/z 388

The ion at $[Mn(bpy)(CO)_3]^+$ ion at m/z 294.9 was isolated again in MS^2 and fragmented through low energy CID. It was observed that the carbony ligand is lost sequentially. The peak at 242.9 could not be identified.

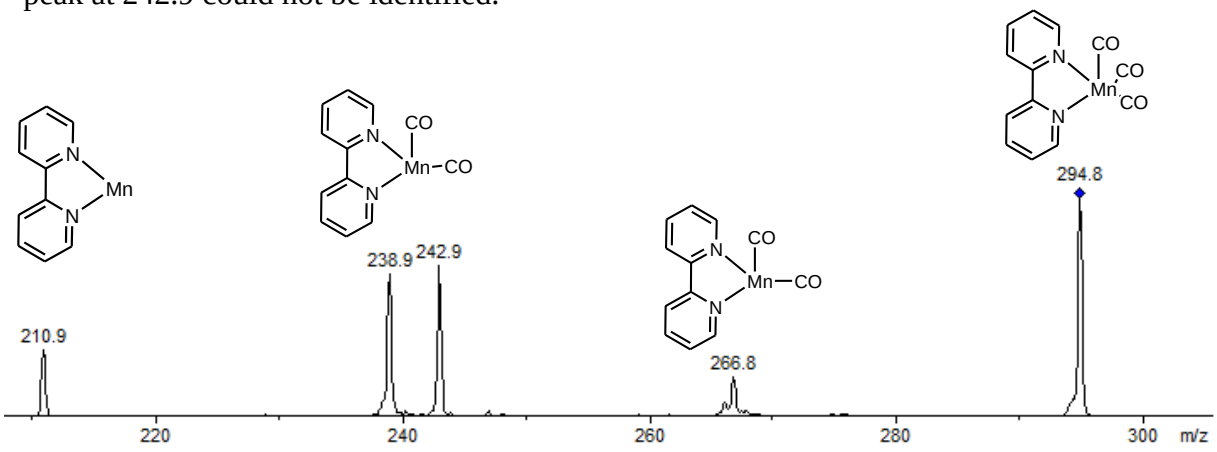

Fig 4. 42 CID on $[Mn(bpy)(CO)_3]^+$ m/z 295 from $[Mn(bpy)(CO)_3]^+$

4.3 Discussion

The molecular ion is not observed for transition metal monofluoride complexes in either positive or negative ion modes of ESI. In positive ion ESI the nickel monofluoride complex **5** loses the fluoride ligand but in the negative ion ESI, in the presence of CsF, the phosphine ligand eliminates first, followed by coordination with acetonitrile. On subjecting to low energy CID, the loss of a second phosphine ligand is observed (scheme 4.1).

The Cp^*MF_2 complexes (M = Ti, Zr, Hf) **11**, **12** and **13** gave sodiated and potassiated molecular ions as well as ions formed by the loss of a fluoride ion. Complexes **12** and **13** showed $[M–H]^+$ which cannot be seen in the spectrum of **11**. Upon low energy CID, the $[M–F]^+$ ion (for all three) fragmented through the loss of HF. The sodiated ion of **11** decayed through the loss of a Cp^* ligand while the potassiated ion decayed into $[M–F]^+$. The fragmentation of sodiated and potassiated ions of **12** and **13** occurred through loss of H and F. The CID of $[M–H]^+$ of **12** and **13** also gave $[M–F]^+$.

The positive ion ESI mass spectrum of $Ru(PMe_3)_4(FHF)_2$ (**15**) showed similar peaks to $Ru(PMe_3)_4F_2$ (**16**). It is concluded that FHF complexes are not stable in electrospray. Upon low energy CID, the $[M–F]^+$ and its chloride analogue fragmented via loss of phosphine. The bridged complex $[(Me_3P)_3Ru(\mu–F)_3Ru(PMe_3)_3]^+$ fragmented by loss of one of the bridged fluorines which further decayed through elimination of either the phosphine

or methyl groups from the phosphines. The same is the case with **5** where the metal-phosphine bond become less stable than the metal fluorine bond.

The positive ion ESI mass spectrum of $Zn(DMEA)_2F_2$ (**24**) does not show the molecular ion, while molecular ion and quasimolecular ions are observed with cobalt and nickel analogues **25** and **26**, respectively. Another ion observed in the mass spectrum of all three compounds is $[M–F]^+$. The molecular ion and quasimolecular ions from **25** and **26** fragmented through the loss of HF. Similar behavior was shown by $[M–F]^+$ for all three compounds.

The negative ion ESI mass spectra of K_2MF_6 (M= Zr, Ti) **36** and **37** show that the parent dianion $[MX_6]^{2–}$ and $[MX_5]^–$ (loss of $F^–$ from the parent dianion) appears as the major ions. Another ion present at significant intensity is $KMX_6^–$ while $MX_6^–$ is missing from the spectra. Upon low energy CID the parent dianion $[MX_6]^{2–}$ of **36** and **37** decayed through ionic fragmentation. The results are very similar to the work done by Dessent et al..[21,24] The negative ion electrospray ionization of the parent dianion of K_2NbF_7 **38** could not be isolated due to low ion intensity.

The positive ion ESI of metal rhenium tricarbonyl complexes **26** and **27** gave the cationic molecular ion as the major peak. Another dominant peak in the mass spectrum of **26** is $[M–picoline]^+$ and for **27** is $[M–CO]^+$. CID fragmentation of the cationic molecular ion of **26** resulted in the formation of $[M–picoline]^+$ while fragmentation of **27** occurred to a major extent by loss of carbonyl ligand and loss of triethylphosphite ligand is the minor pathway.

4.4 Conclusions

Studies of transition metal difluoride complexes by ESI mass spectrometry and CID show that gaseous ions decay through the loss of fluoride ion while in the presence of an acidic hydrogen, HF is eliminated twice in sequential steps. $(Cp^*)_2MF_2$ complexes gave $[M+K]^+$ and $[M+Na]^+$ ion which decay through loss of KF or KH and NaF or NaH respectively. The stability of the metal fluoride bond also depends upon the ancillary ligands. It is observed that in the presence of phosphine, the first fluoride ligand is lost upon ionization while further fragmentation occurs through elimination of phosphines or alkyl groups from the phosphines.

The decay pathway of the MCAs notably TiF_6^{2-} and ZrF_6^{2-} is concluded to be ionic fragmentation rather that electron detachment.

Re and Mn tricarbonyl complexes give good positive ion electrospray ionization spectra and the cationic molecular ion decay through either loss of CO or picoline and triethylphosphite.

Table 4.1 ESI-MS data of transition metal complexes.

Transition metal complexes	Molecualr weight	ESl mode	solvent	Ion present in ESI-MS
$(Cp^*)_2TiF_2$	356	+ive	CH_3CN	$[(Cp^*)_2TiF]^+$ (m/z 337), $[(Cp^*)_2TiF_2+Na]^+$ (m/z 379), $[(Cp^*)_2TiF_2+K]^+$ (m/z 395),
$(Cp^*)_2TiF_2$	356	-ive	CH_3CN	$[(Cp^*)_2TiF_2]^-$ (m/z356.1), $[(Cp^*)_2TiF_2+F]^-$ (m/z 375.3), $[(Cp^*)_2TiF_2+2F]^-$ (m/z 394.0)
$(Cp^*)_2ZrF_2$	398	+ive	CH_3CN	$[(Cp^*)_2ZrF]^+$ (m/z 379), $[(Cp^*)_2ZrF_2–H]^+$ (m/z 397), $[(Cp^*)_2TiF_2+Na]^+$ (m/z 421)
$(Cp^*)_2HfF_2$	488	+ive	CH_3CN	$[(Cp^*)_2HfF]^+$ (m/z 469), $[(Cp^*)_2HfF_2–H]^+$ (m/z 487), $[(Cp^*)_2TiF_2+Na]^+$ (m/z 501)
$Zn(DMEA)_2F_2$	278	+ive	CH_3OH	$[Zn(DMEA)_2F]^+$ (m/z 259), $[Zn(DMEA)_2–H]^+$ (m/z 239)
$Co(DMEA)_2F_2$	273	+ive	CH_3OH	$[Co(DMEA)_2F_2]^+$ (m/z 273), $[Co(DMEA)_2F]^+$ (m/z 254), $[Co(DMEA)_2–H]^+$ (m/z 233)
$Ni(DMEA)_2F_2$	272	+ive	CH_3OH	$[Ni(DMEA)_2F_2+H]^+$ (m/z 273), $[Ni(DMEA)_2F]^+$ (m/z 253), $[Ni(DMEA)_2–H]^+$ (m/z 233)
$Ru(PMe_3)_4F_2$	444	+ive	THF	$[Ru(PMe_3)_4Cl]^+$ (m/z 441), $[Ru(PMe_3)_4F]^+$ (m/z 425), $[Ru(PMe_3)_4–H]^+$ (m/z 406)

$Ru(PMe_3)_4(FHF)_2$	464	+ive	THF	$[Ru(PMe_3)_4Cl]^+$ (m/z 441), $[Ru(PMe_3)_4F]^+$ (m/z 425), $[Ru(PMe_3)_4–H]^+$ (m/z 406) $[(Me_3P)_3Ru(\mu–F)_3Ru(PMe_3)_3]^+$ (m/z 716)
K_2TiF_6	240	-ive	H_2O/ CH_3OH	$KTiF_6^-$(m/z 201), TiF_5^- (m/z 143), TiF_6^{2-} (m/z 81)
K_2ZrF_6	281.8	-ive	CH_3OH	ZrF_5^-(m/z 185), $KZrF_6^-$(m/z 242), ZrF_6^{2-}(m/z 102)
K_2NbF_7		-ive	K_2ZrF_6	

GAS PHASE ION MOLECULE REACTIONS

5.1 Introduction

Gas phase chemistry is of much interest for inorganic chemists. It has been realized over the last two decades that knowledge about fundamental properties of bare or ligated transition metal ions can provide useful information on the mechanism of reactions operative in solution, their efficiencies of stoichiometric or catalytic processes.[1,2] Gas phase ion-molecule reactions are useful for understanding the intrinsic properties and chemicals reactions of charged particles because in the gas phase they are not affected by solvent effects and other factors common in the solution chemistry. [3,4,5]

Electrospray ionization in combination with ion trap mass spectrometer provides a well adopted environment for studying gas phase reactions. Ion molecule (I-M) reactions are important as they are highly selective, efficient and fast. O'Hair et al studied gas phase reactions of chloro(diethylenetriamine)platinum chloride abbreviated as [Pt(dien)Cl]Cl with small neutral molecules using a modified LCQ mass spectrometer.[6]

Ion molecule reactions (I-M) may be potentially useful for providing limited structural information about the coordination sphere of transition metal complexes. The gas phase reactivity of transition metal complexes depends upon the metal's electronic structure, ligand field around the metal, the complex geometry and the degree of coordinative unsaturation.[7-9] Combariza and Vachet using the modified Bruker Esquire quadrupole ion trap, conducted I-M reactions of Co and Cu complexes with acetonitrile. It was found that acetonitrile can be used as a titrant to determine the coordination number of the complexes with donor groups other than nitrogen. The ion-molecule reactions of pentacoordinate complexes of 1,9-bis(2-pyridyl)-2,5,8-triazanonane (DIEN-(pyr)2) and 1,9-bis(2-imidazolyl)-2,5,8-triazanonane (DIEN-(imi)2] with transition metals showed the addition of one acetonitrile molecule to complete the coordination sphere (Fig 5. 1 a&b) while the coordination of a second acetonitrile molecule is less than 5% (Fig 5. 2). The rate of the reaction can be determined by fitting the kinetic data for the following reactions. [8]

$$ML^{2+} + CH_3CN \underset{k_2}{\overset{k_1}{\rightleftharpoons}} (ML + CH_3CN)^{2+}$$

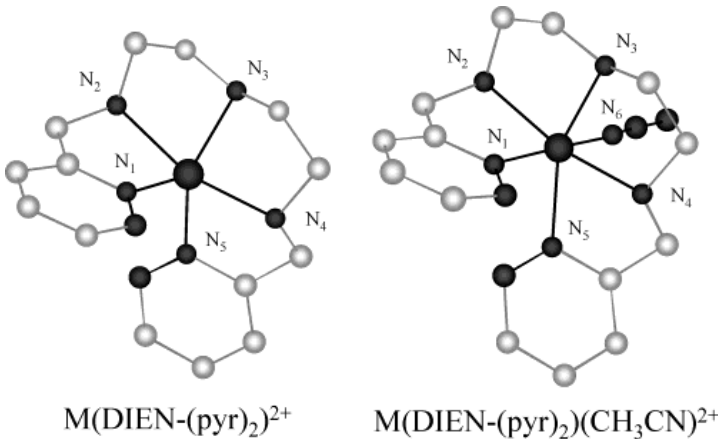

Fig 5. 1 Compound of 1,9-bis(2-pyridyl)-2,5,8-triazanonane (DIEN-$(pyr)_2$) with metal (M) and coordination of one acetonitrile $M(DIEN\text{-}(pyr)_2)(CH_3CN)^+$.[8]

It was concluded from the kinetic and electronic data that the reactivity of the complexes for a given ligand depends upon the electronic structure of the metal and follow the trend mentioned below.

Ni > Mn > Fe > Co > Cu ≈Zn

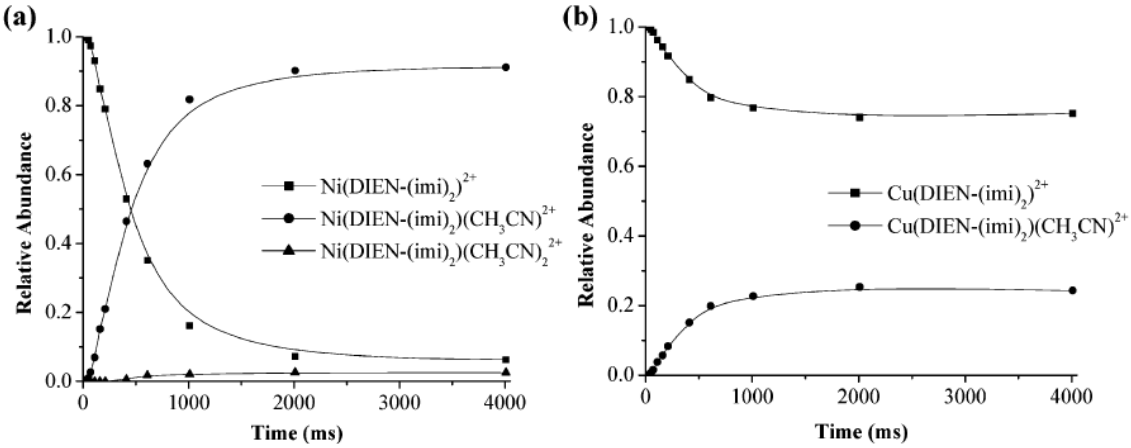

Fig 5. 2 Typical kinetic plots obtained from the reactions of acetonitrile with (a) Ni(DIEN-$(imi)_2)^{2+}$ and (b) Cu(DIEN-$(imi)_2)^{2+}$.[8]

Gas phase I-M reactions of Ni (II) complex ions with acetonitrile also revealed that both inductive and steric effects are responsible for complex reactivity. The goal of these ion-molecule reactions was to provide information about the coordination sphere of Ni. A series of nickel complexes were prepared by reacting $NiCl_2$ with pentadentate polyamine ligands (e.g ligand I &II), varying from each other by attachment of various methyl and methylene groups. Ni complexe ions were reacted with acetonitrile and experimental

kinetic plots were obtained (Fig 5. 3). These graphs show that equilibrium of the reactions is achieved at 2000 ms and one acetonitrile molecule is added to the complex.[10]

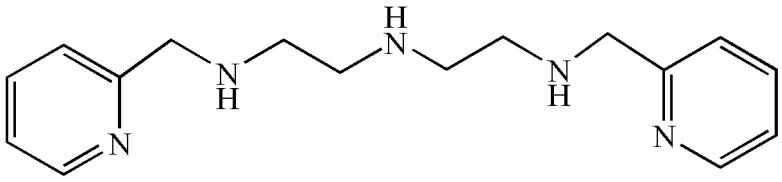

I, DIEN-$(py)_2$

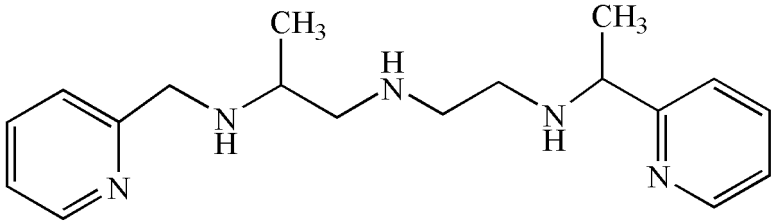

II, DI-iPN-$(py)_2$

The equilibrium constant and rate constant of the reaction were determined from fitting the kinetic data. The equilibrium constant decreases with increasing chelate ring size. It was further concluded that the ligand with more strongly donating groups strengthens the metal ligand bond and reduces its reactivity towards acetonitrile.[10]

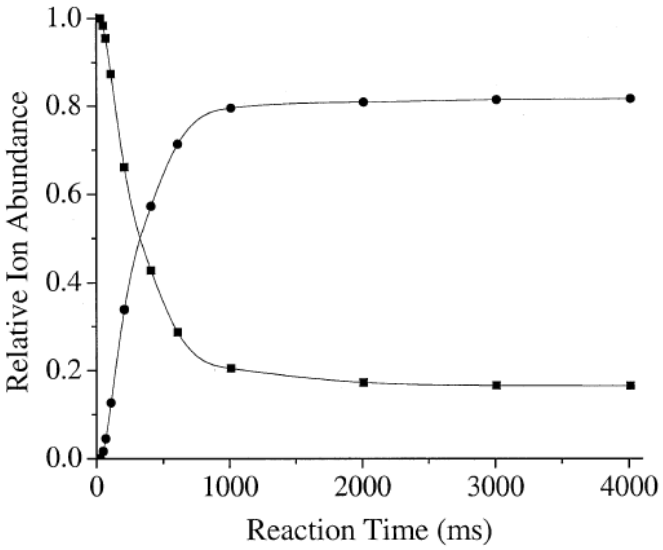

Fig 5. 3 Reaction of Ni complexes with CH_3CN showing an experimental kinetic plot,of ion abundance vs time. Squares represents parent ion and circles product ions.[10]

Ligand-exchange ion molecule reactions of transition metal cluster fragments have been studied over 20 years before using a two-section ion cell and a Fourier transform ion cyclotron resonance mass spectrometer.[11]

Reactions of small cations and anion with alkanes and fluoroalkanes in the gas phase have also investigated using a selected ion flow tube (SIFT) (see Fig 5. 1) and their reaction rates were determined.[12]

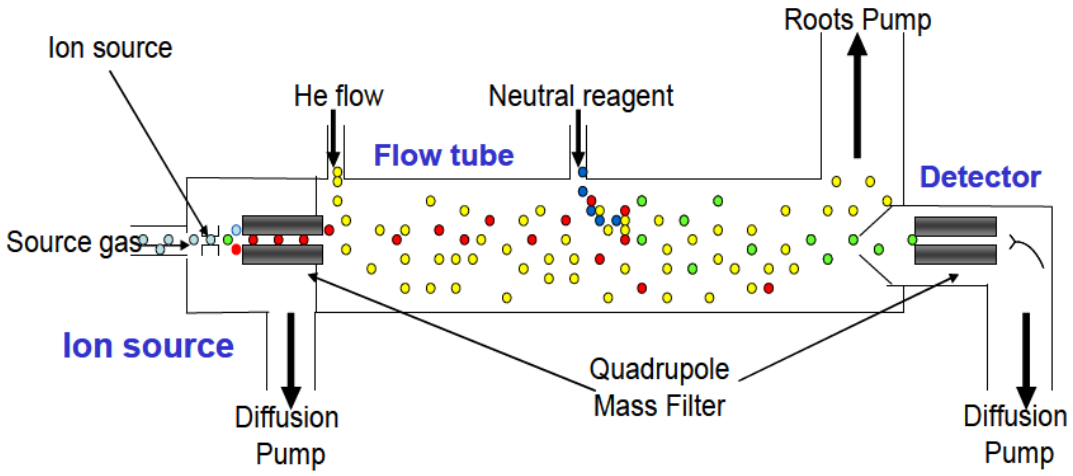

Fig 5. 4 "A basic schematic of the Selected Ion Flow Tube apparatus. The red circles represent the ions generated in the ion source, the yellow circles represent the helium buffer gas, the blue circles represent the neutral reactant gas, and the green circles represent the product species."[12]

Quadrupole ion traps have been available for several decades but their ability to separate the ions of a specific charge to mass ratio and complete MS^n experiments has revolutionized the field. They have become powerful tools for studying ion molecule reactions.[13]

O'Hair et al investigated the gas phase ion molecule reactions of coinage metal (Cu, Ag and Au) dimethylmetallate with methyl iodide using a quadruple ion trap mass spectrometer. It was observed that only dimethylcuprate is reactive towards CH_3I. The nonreactivity of dimethylargentate and dimethylaurate was further supported by DFT calculations showing significant endothermic barriers.[14,15]

The purpose of the studies reported here was to investigate gas phase ion molecule reactions of transition metal complexes and MCAs with small neutral molecules (volatile

liquid and gases) such as CH_3CN, C_2H_2 and CO. The rate of these ion molecule reactions was also investigated.

5.2 Results

All the experiments were performed using a quadrupole ion trap mass spectrometer (Esquire Bruker) equipped with electrospray ionization (ESI) and modified to allow the introduction of a neutral reagent via the helium background gas inlet line. Two T-pieces were inserted into the helium line was removed and replaced. One arm of the T-split **1** allows the introduction of the neutral reagent into the helium gas flow and the second arm connects it with the second T-split **2**. One arm of the split **2** goes to the fused silica capillary which continues into the ion trap and the other is open to the waste (Fig 5. 5 & Fig 5. 6). 10% of this mixture goes into the trap while the remaining 90% is wasted. The waste is connected through pipes with the roof where they are removed through exhaust system.

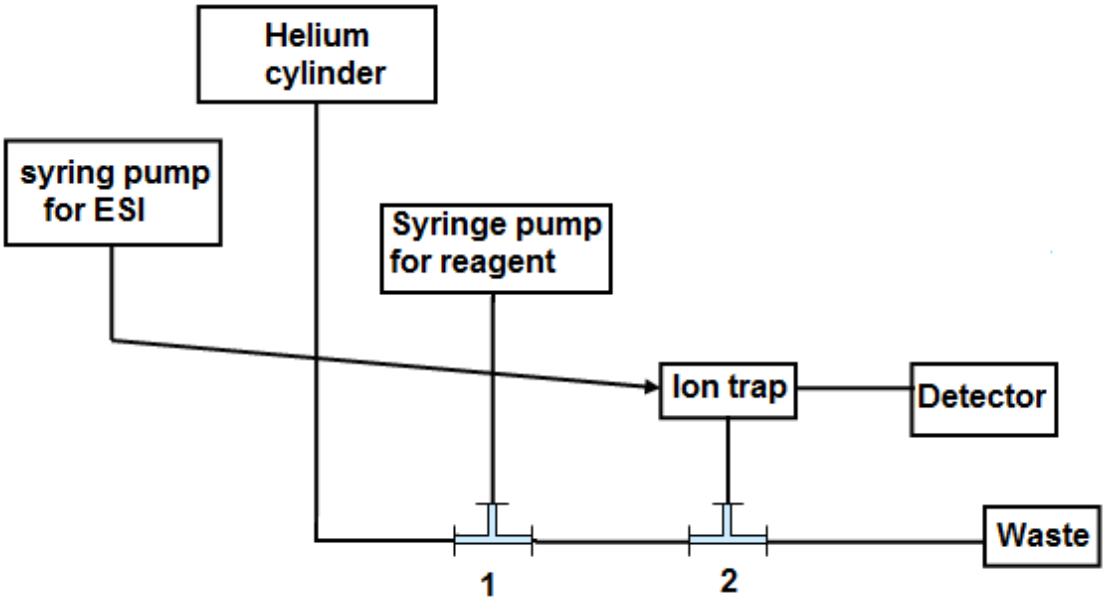

Fig 5. 5 Schematic representation of the modified mass spectrometer for gas phase reactions

The helium pressure is maintained at about 2.5 atm. The neutral liquid reagents used in these experiments, D_2O, CH_3CN, CD_3CN, CH_3OH, Et_3N, C_5H_5N, $C_6F_2H_2(NH_2)_2$ $C_6H_4F_2$, C_6F_5H, 1-hexene and pentyne were introduced into the gas stream via a syringe pump at 10 μL/h. The gaseous reagents (CO_2**,** D_2) were used directly from small cylinders provided with regulators.

The platinum complexes were dissolved in a 1:1 mixture of CH_3OH/H_2O while the rhenium, tungsten and molybdenum complexes were dissolved in CH_3CN. The samples were introduced via electrospray ionization (spray voltage 3.8-4.5 kV) at flow rate of 4 μL/min. The time for the mass selected ion to undergo ion molecule reaction was varied from 100 ms to 4 s.

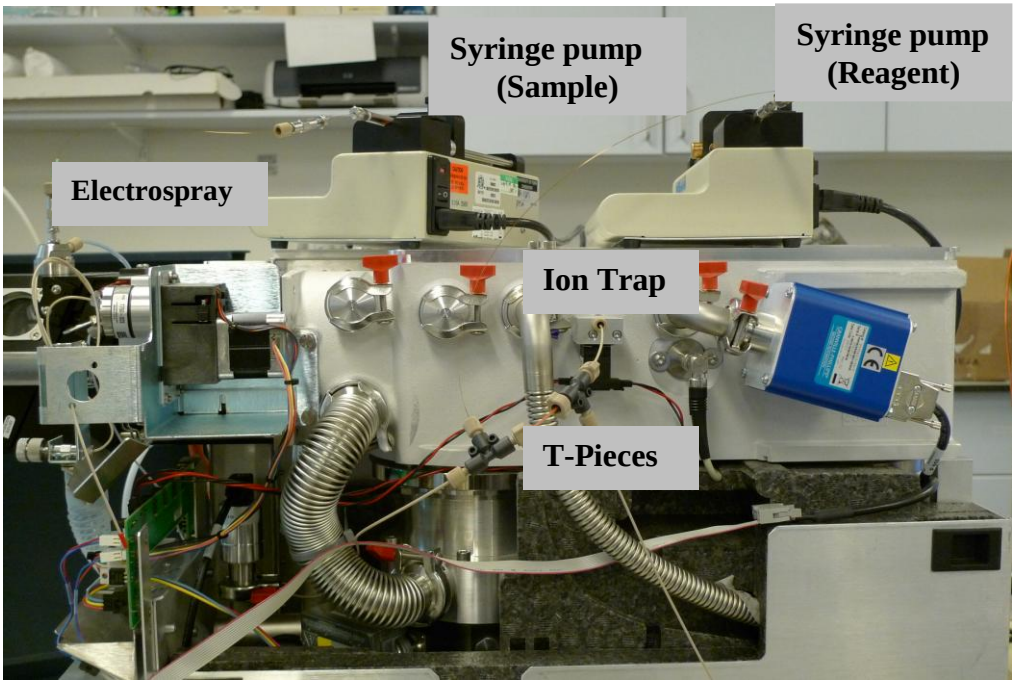

Fig 5. 6 Modified ion trap mass spectrometer for gas phase ion molecule (I-M) reactions

The peaks of the metal complexes ions were optimized (by changing parameters at the capillary, skimmer, lenses, trap drive and octopoles) if the ion intensity was low. The diamond signs on the top of the peaks in the mass spectra represent the parent ion which underwent either CID or reacted with a neutral molecule.

5.2.1 Ion-molecule reactions of platinum complexes with small neutral molecules

[Pt(dien)Cl]Cl[16] **(23)** was investigated to compare with the literature data. It was synthesized from the reaction of $Pt(DMSO)_2Cl_2$[17] with diethylenetriamine.[16] The complex **23** was characterized by ESI-MS showing an ion cluster of $[Pt(dien)Cl]^+$ at m/z = 334 and another peak is at m/z = 297 corresponding to loss of HCl giving the coordinatively unsaturated platinum ion $[Pt(dien-H)]^+$. This is in agreement with the literature.[6]

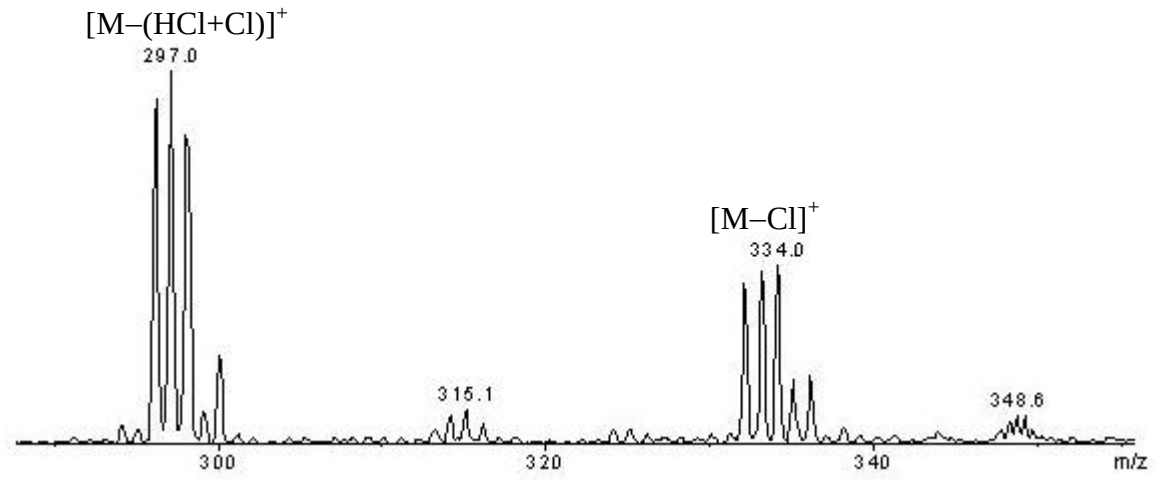

Fig 5. 7 Positive ion ESI-MS spectrum of **23** in 50:50 water:methanol mixture.

Ion-molecule reactions of coordinately unsaturated platinum complexes

In order to test our system we repeated already reported reactions of coordinatively unsaturated platinum ion $[^{196}Pt(H_2NCH_2CH_2)NH(CH_2CH_2NH_2)]^+$ with simple neutral molecules i.e. D_2O, CH_3CN, CH_3OH and C_5H_5N.[6] In addition, we investigated gas-phase reactions of $[^{196}Pt(H_2NCH_2CH_2)NH(CH_2CH_2NH_2)]^+$ with 1-hexene, triethylamine and CD_3CN. The peak at m/z 382.1 in Fig 5. 8 is the product with hexene.

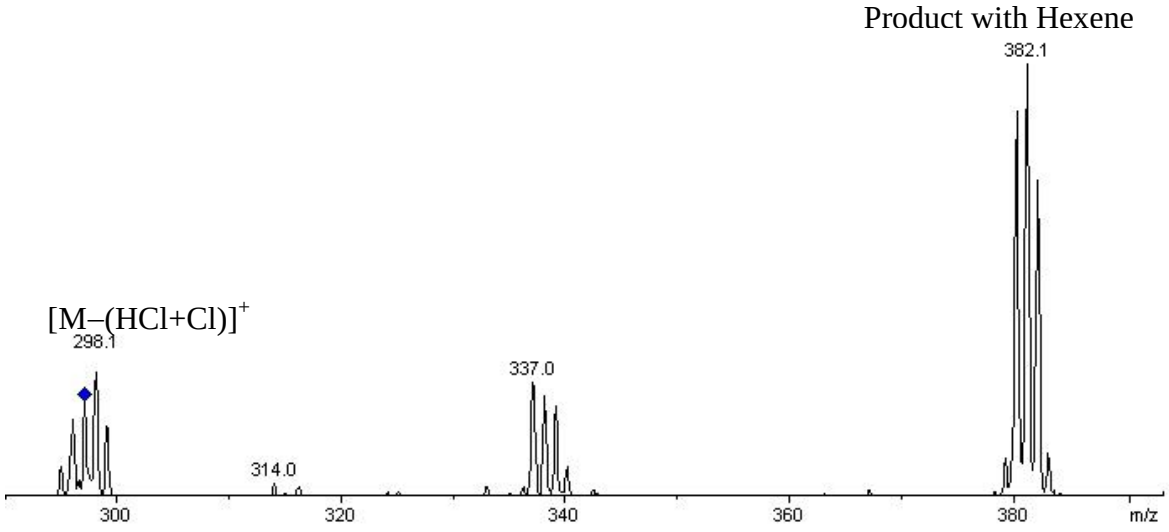

Fig 5. 8 Isolation of m/z 298 corresponding to $[^{196}Pt(H_2NCH_2CH_2)NH(CH_2CH_2NH_2)]^+$ and reaction with hexene.

Similarly, peaks at m/z 341and 397 in Fig 5. 9 (a) and (b) are the products with CD_3CN and Et_3N respectively.

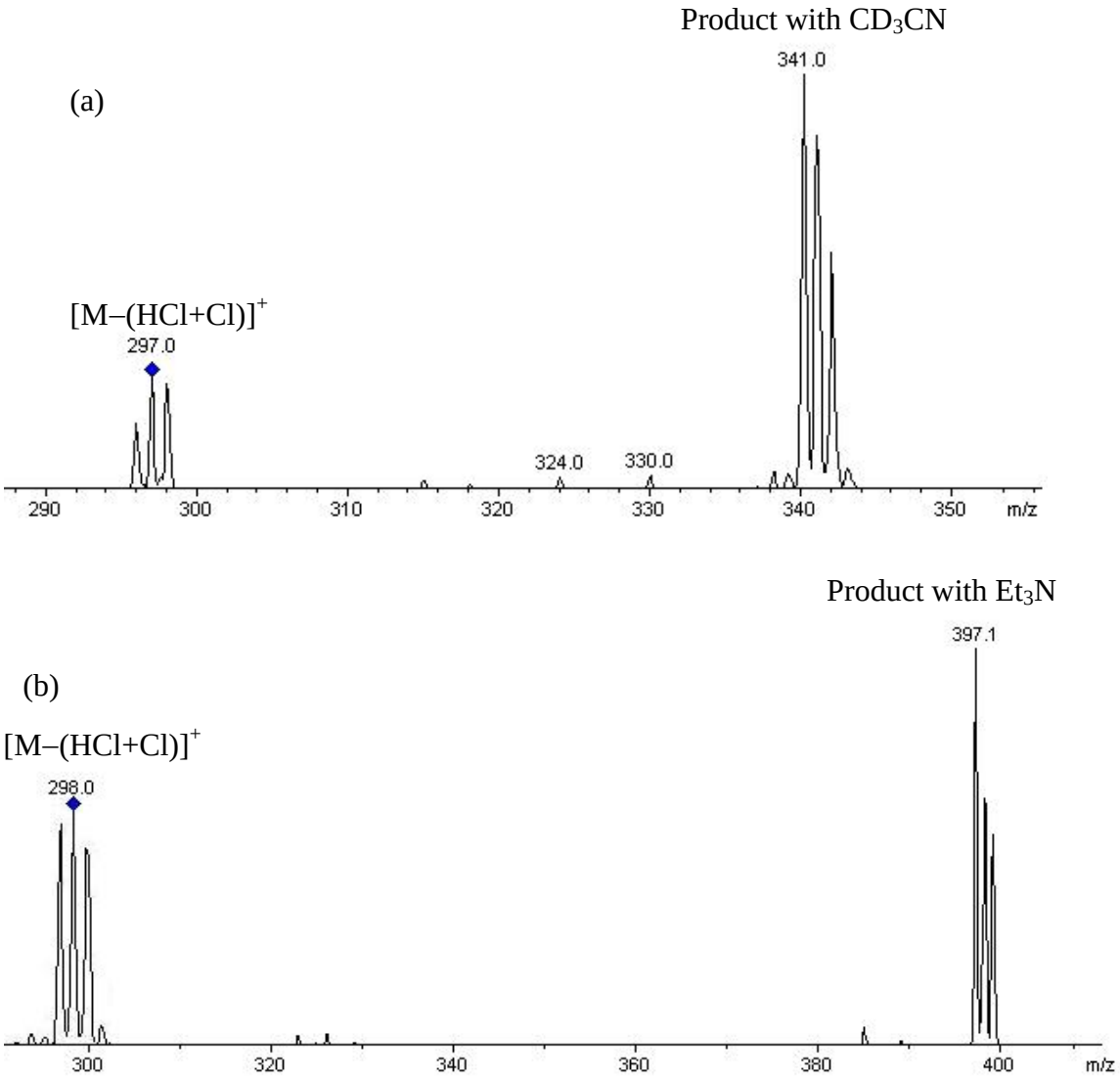

Fig 5. 9 Isolation of m/z 298 corresponding to $[^{196}Pt(HNCH_2CH_2)NH(CH_2CH_2NH_2)]$ and reaction with (a) CD_3CN (b) triethylamine

5.2.2 Ion-molecule reactions of transition metal cations with small neutral molecules

It should be possible to investigate gas phase reactions of trapped transition metal ions with other neutral molecules. Although not yet successful with transition metal fluoride complexes, these experiments succeeded with $[Re(CO)_3(bpy)]^+$ derivatives. $[Re(CO)_3(bpy)]^+$ derivatives were donated by Jacob Schneider.

5.2.2.1 Reactions of Re tricarbonyl cations with small neutral molecules

$[Re(CO)_3(bpy)(pic)]^+PF_6^-$ (**27**) was studied by positive ion ESI mass spectrum (Fig 5. 10).

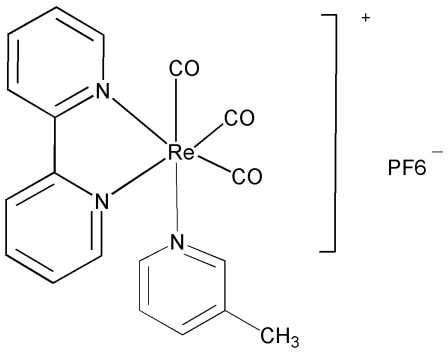

The peak at m/z 520 is the cationic molecular ion peak $[M]^+$. Another peak at m/z = 427 arises from the loss of picoline from the molecular ion peak $[M\text{-}X]^+$. This peak is very reactive towards water giving a sharp peak at m/z 444.9 showing the addition of one water molecule $[M\text{-}X+H_2O]^+$.

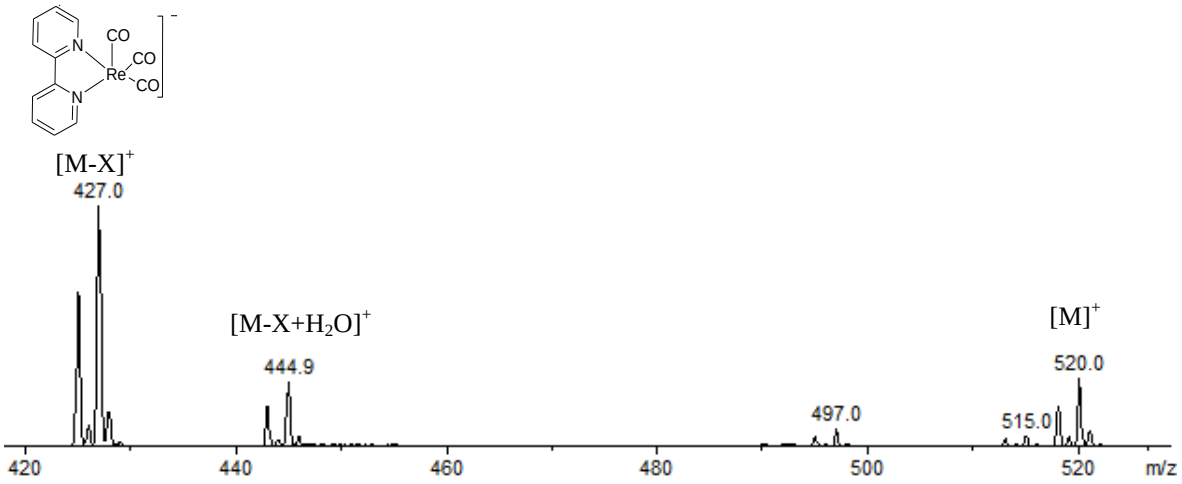

Fig 5. 10 Positive ion ESI mass spectrum of $[Re(pic)(bpy)(CO)_3]^+$ in CH_3CN

$[Re(pic)(bpy)(CO)_3]^+$ (m/z 520) did not react with neutral reagents while $[Re(bpy)(CO)_3]^+$ (m/z 427) reacted with Et_3N, CD_3CN, pyridine, 1-hexene, pentyne, SO_2, NO and isobutene and showed complete conversion to the product. In some cases the product peak was isolated which converted back to $[Re(bpy)(CO)_3]^+$ (m/z 427) upon increasing the CID energy. No reaction was observed with methanol, $C_6F_2H_2(NH_2)_2$, $C_6H_4F_2$, C_6F_5H, CO_2 and D_2. Fig 5. 11 (a) & (b) shows a peak at 445 corresponding to the reaction of $[M\text{-}X]^+$ with residual water in addition to the peaks at m/z 511 and 495 corresponding to products with 1-hexene and pentyne respectively.

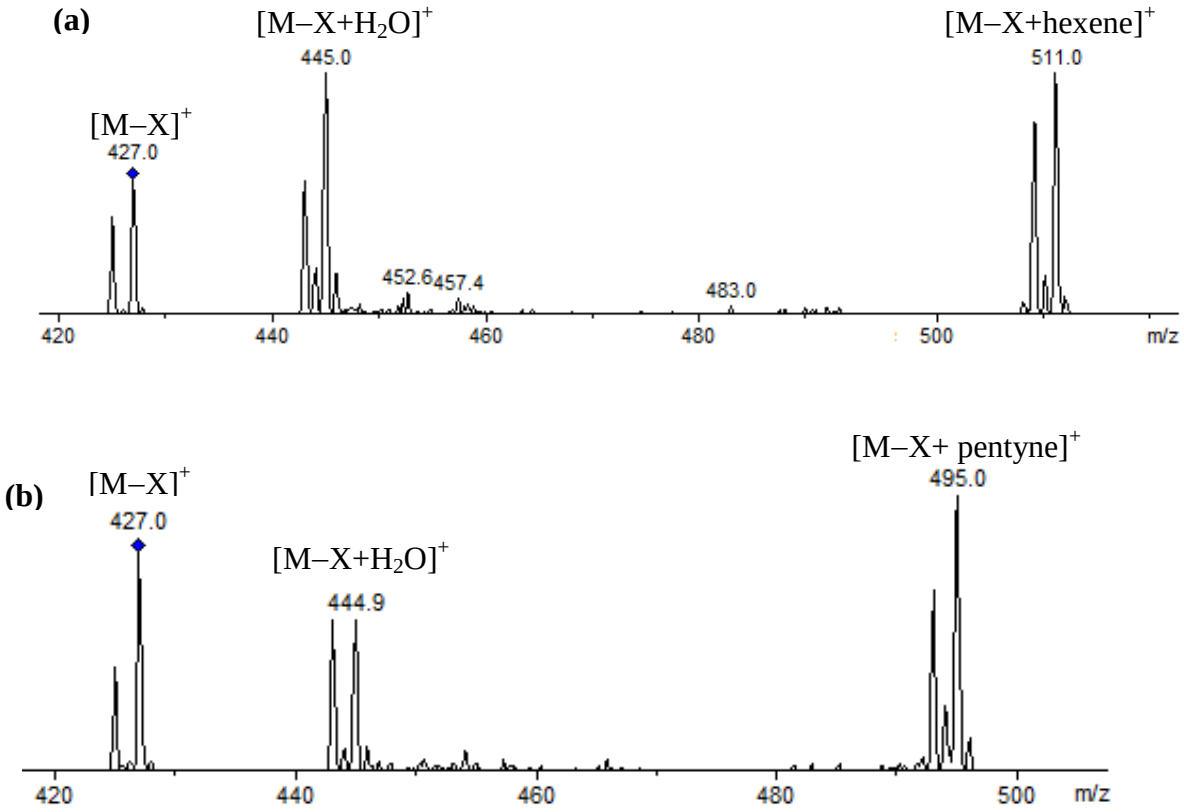

Fig 5. 11 Positive ion ESI mass spectrum showing reaction of $[Re(bpy)(CO)_3]^+$ with (a) 1-hexene and (b) pentyne in CH_3CN

The positive ESI mass spectrum of $[Re(CO)_3(bpy)(P(OEt)_3]^+PF_6^-$ (**28**) gave a peak at m/z 593 which is the cationic molecular ion peak $[M^+]$ (Fig 5. 12). Another peak at m/z = 565 results from loss of one carbonyl ligands from the molecular ion $[M\text{-}CO]^+$.

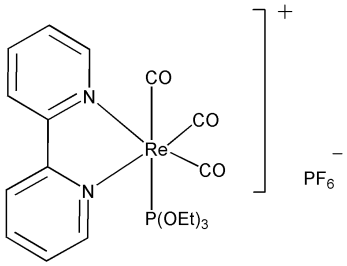

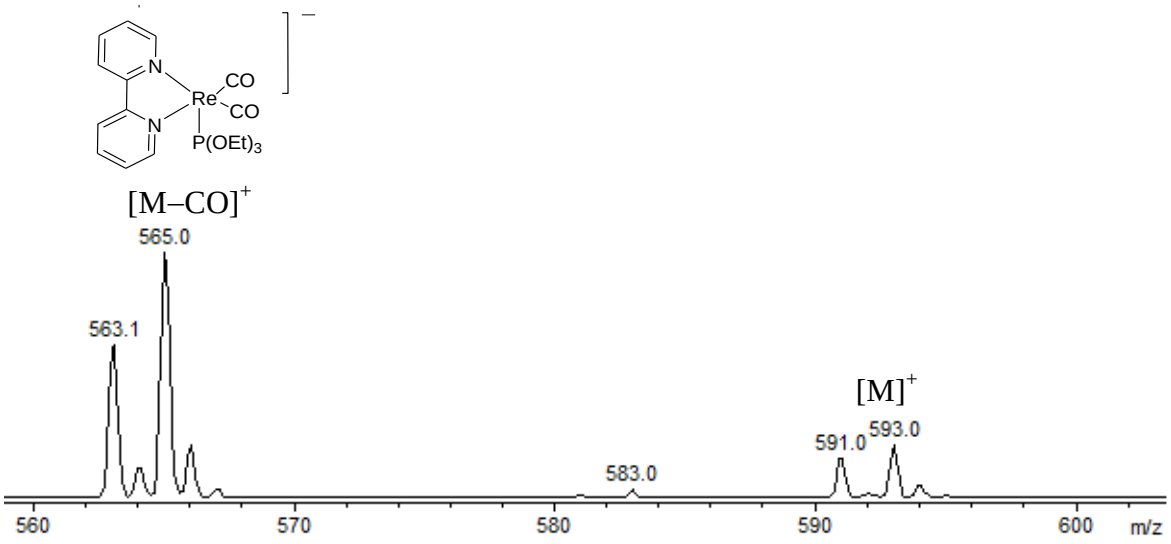

Fig 5. 12 Positive ion ESI mass spectrum of $Re(bpy)(P(OEt)_3)(CO)_3]^+$ in CH_3CN

$[Re(bpy)(P(OEt)_3)(CO)_3]^+$ (m/z 593) did not react with neutral reagents while $Re(bpy)(P(OEt)_3)(CO)_2]^+$ (m/z 565) reacted with Et_3N, CD_3CN, pyridine, 1-hexene, pentyne, SO_2, NO and isobutene and showed complete conversion but did not react with methanol, $C_6F_2H_2(NH_2)_2$ $C_6H_4F_2$, C_6F_5H, D_2 and CO_2. The successful reactions were characterized by the comparison of peaks with m/z corresponding to $[Re(bpy)(P(OEt)_3)(CO)_2L]^+$.

The positive mode electrospray ionization of $[Re(CO)_3(H_2O)_3]Br$ **29** is dependent upon than solvent used for making the solution. The water molecule in **29** is replaced by the solvent molecule so the cationic molecular ion peak $[M^+]$ at m/z 324.9 is only observed when water is used as a solvent (Fig 5. 13) but cannot be isolated in the ion trap to perform low energy CID. Other peaks at m/z 306.9 and 288.9 are formed by loss of one water molecule $[M\text{-}H_2O]^+$ and two water molecules $[M\text{-}2H_2O]^+$ respectively. The peak at m/z 288.9 was isolated and reacted with water which resulted in the addition of one and two water molecules giving peaks at at m/z 306.9 and 324.9, respectively.

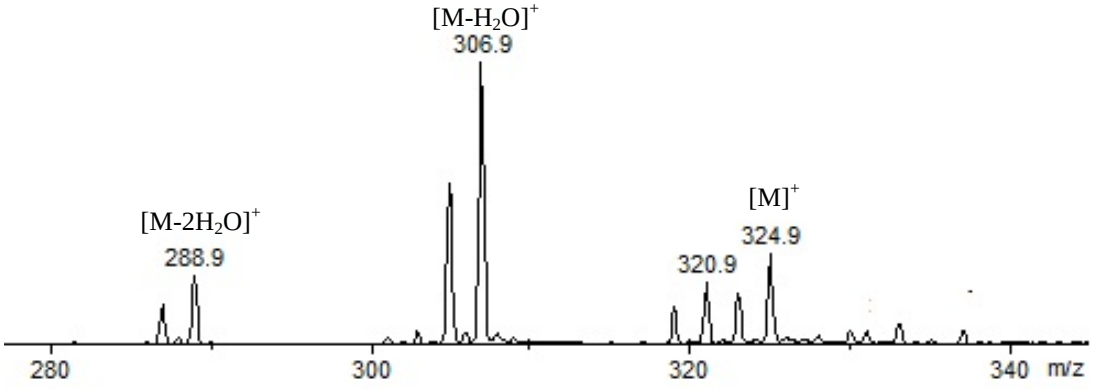

Fig 5. 13 Positive ion ESI mass spectrum of $[Re(H_2O)_3(CO)_3]Br$ in H_2O

The positive ion ESI spectrum of **29** in methanol shows peaks at m/z 338.9 assigned to the replacement of one water molecule by methanol. Other peaks at m/z 352.9, 334.9, 321 and 302 correspond to $[Re(CO)_3(H_2O)(CH_3OH)_2]^+$, $[Re(CO)_3(CH_3OH)_2]^+$, $[Re(CO)_3(H_2O)(CH_3OH)]^+$ and $[Re(CO)_3(CH_3OH)]^+$ respectively (Fig 5. 14).

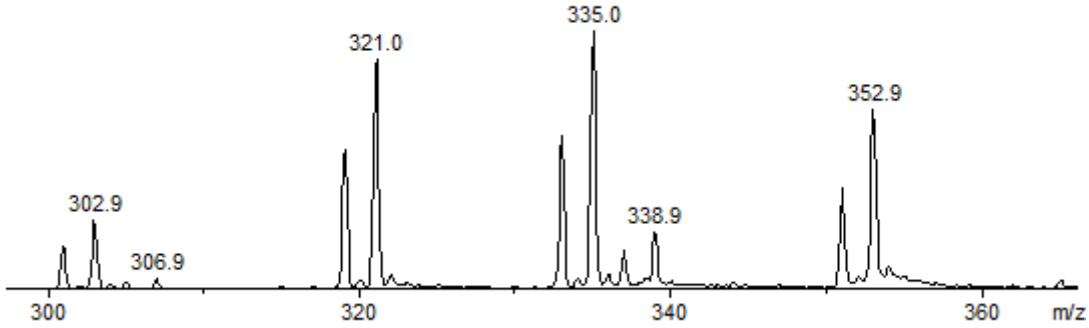

Fig 5. 14 Positive ion ESI mass spectrum of $[Re(H_2O)_3(CO)_3]Br$ in CH_3OH

The acetonitrile solution of **29** showed similar behavior in positive ion mode electrospray ionization. The water molecules are replaced by acetonitrile which is a good coordinating solvent (Fig 5. 15). In the mass spectrum peaks are observed at m/z 302, 312.0, 330.0, 353.0 and 371.0 corresponding to $[Re(CO)_2(H_2O)(CH_3CN)]^+$, $[Re(CO)_3(CH_3CN)]^+$, $[Re(CO)_3(H_2O)(CH_3CN)]^+$, $[Re(CO)_3(CH_3CN)_2]^+$ and $[Re(CO)_3(H_2O)(CH_3CN)_2]^+$.

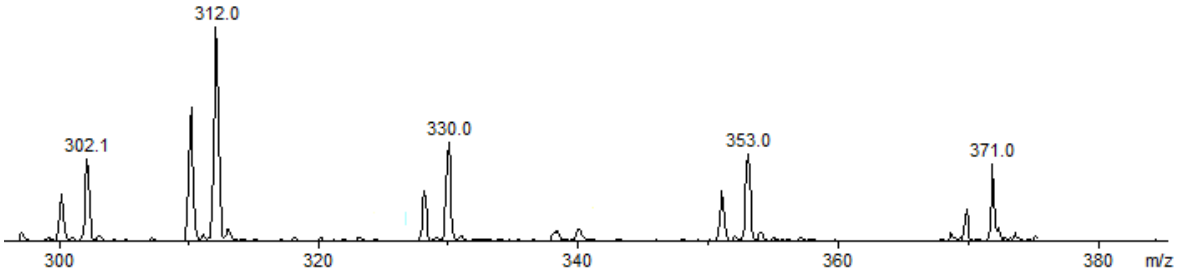

Fig 5. 15 Positive ion ESI mass spectrum of $Re(H_2O)_3(CO)_3]Br$ in CH_3CN

Ions at m/z 353, 312 (from CH_3CN) and 288.9 (solution in water) of **29** underwent successful ion-molecule reactions with Et_3N, CD_3CN, pyridine, 1-hexene, pentyne, SO_2, NO and isobutene but did not react with methanol, $C_6F_2H_2(NH_2)_2$ $C_6H_4F_2$, C_6F_5H, D_2 and CO_2. The ions mentioned above showed similar behaviour as **27** and **28**.

5.2.2.2 Ion-molecule reactions of Mn cations (**30**)

$[Mn(CO)_3(bpy)(pic)]^+PF_6^-$ was prepared as a yellow powder from the reaction of $Mn(CO)_3(bpy)Br$ with picoline and $AgPF_6$ in THF.

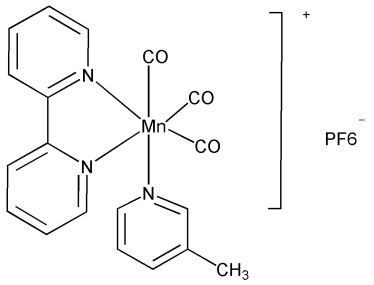

The formation of **30** was confirmed by mass spectrometry and multinuclear NMR spectroscopy. The ^{31}P NMR spectrum shows a septet at δ −130.84 (J_{PF} = 707.6 Hz) and the ^{19}F NMR shows a doublet at δ −73.91 (J_{PF} = 707.5 Hz). The ^{1}H NMR spectrum is broad probably due to the quadrupole of ^{55}Mn or due to the presence of paramagnetic impurities.

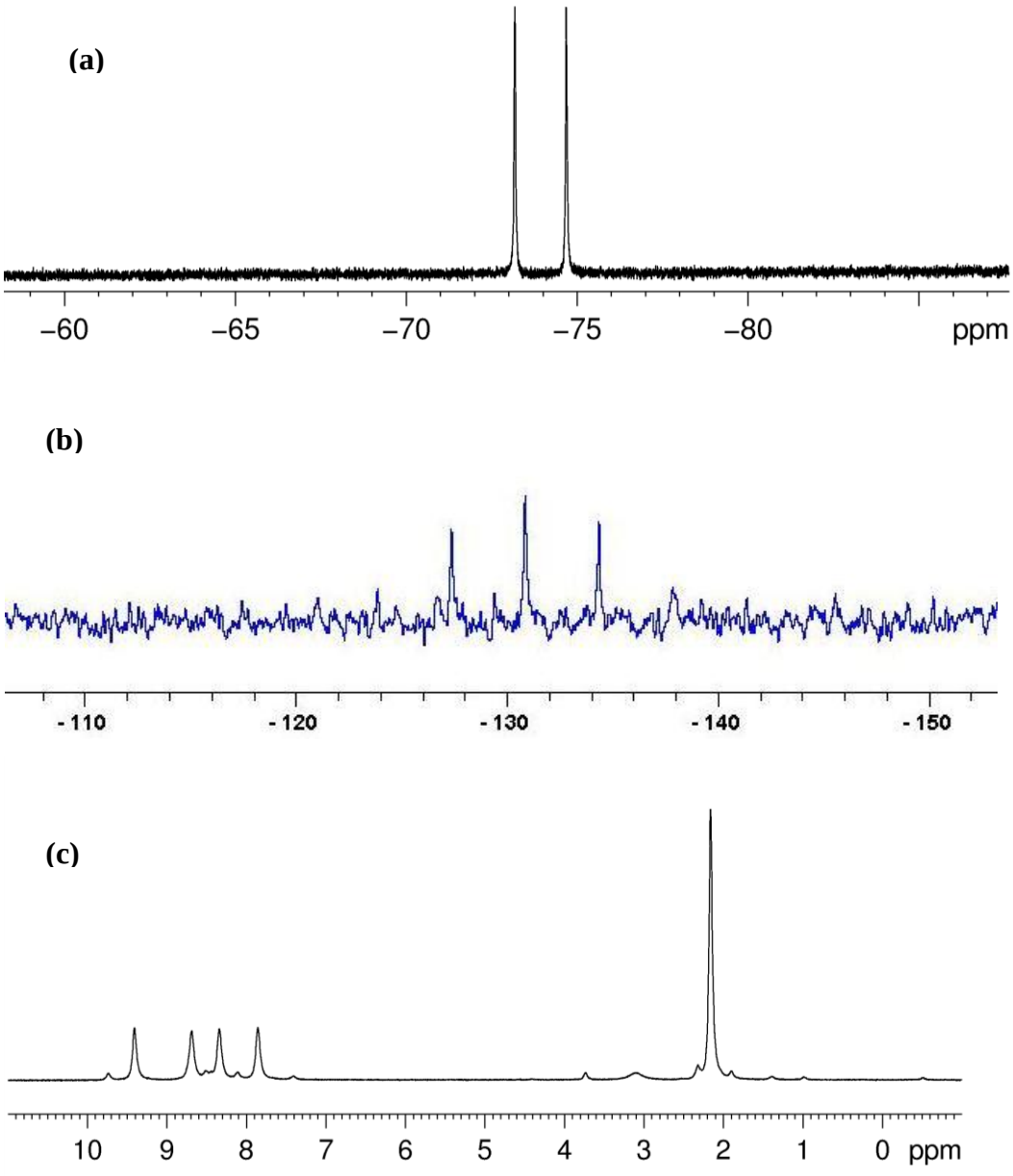

Fig 5. 16 (a) ^{19}F NMR spectrum of $[Mn(CO)_3(bpy)(pic)]^+PF_6^-$ in $(CD_3)_2CO$ at room temperature (407.4 MHz) (b) ^{31}P NMR spectrum (202.46 MHz) and (c) ^{1}H NMR spectrum (500.13 MHz)

The positive ion ESI mass spectrum shows the cationic molecular ion peak $[M^+]$ at m/z 387.9. Other ions at 303.0, 294.9 (major) and 210.9 corresponding to $[M–3CO]^+$, $[M–(pic)]^+$ and $[M–(pic+3CO)]^+$ (Fig 5. 17).

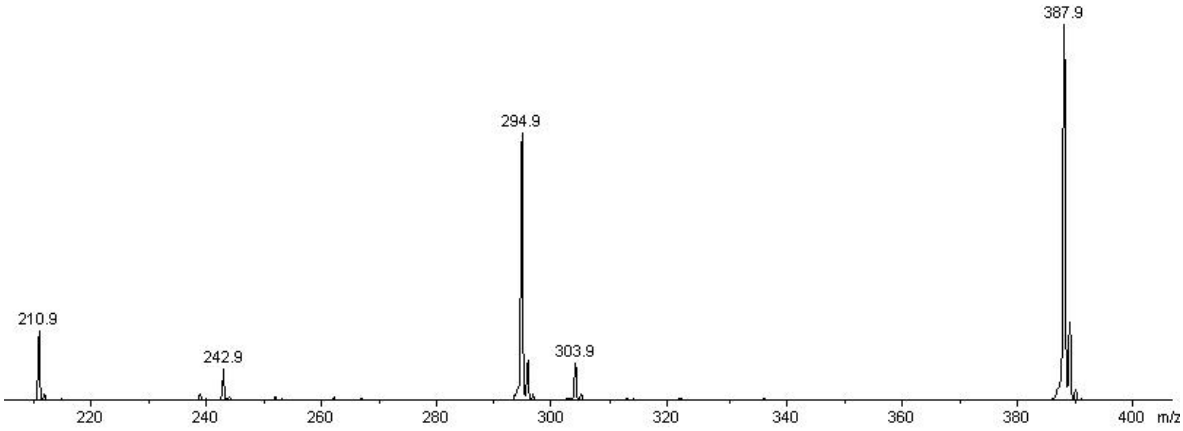

Fig 5. 17 Positive ion ESI mass spectrum of $Mn(pic)(bpy)(CO)_3]^+$ in CH_3CN

$[Mn(bpy)(pic)(CO)_3]^+$ (m/z 387.9) did not react with the neutral reagents while $[Mn(bpy)(CO)_3]^+$ (m/z 294.9) reacted with Et_3N, CD_3CN, pyridine, 1-hexene, pentyne, SO_2, NO and isobutene and showed complete conversion but did not react with $C_6F_2H_2(NH_2)_2$ $C_6H_4F_2$, C_6F_5H, D_2 and CO_2. It also reacted with methanol but the conversion to product was about 50% (Fig 5. 18).

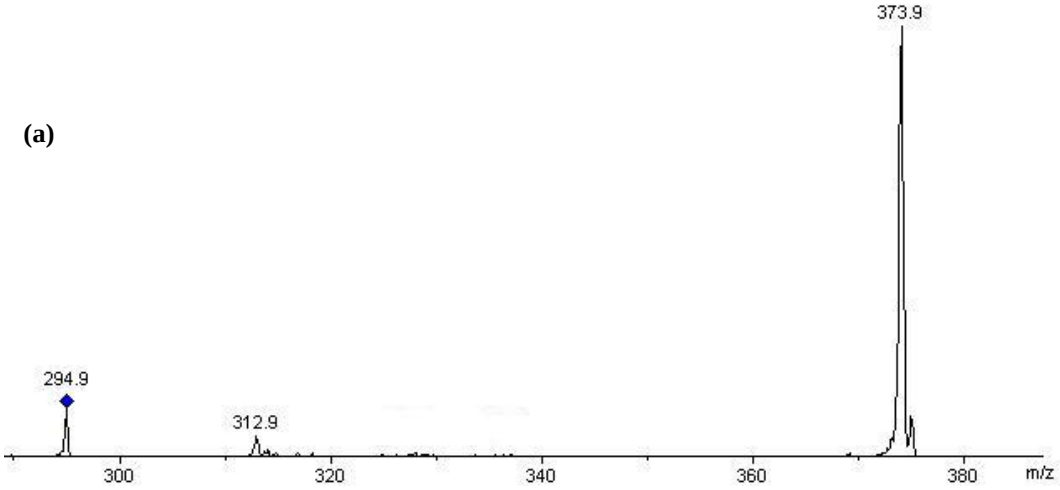

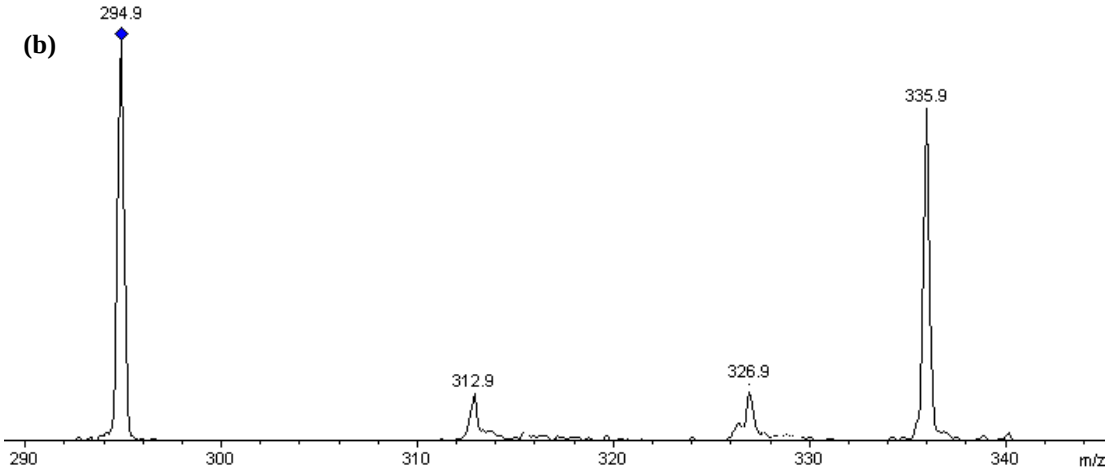

Fig 5. 18 Positive ion ESI mass spectrum showing reaction of $[Mn(bpy)(CO)_3]^+$ with (a) pentyne and (b) methanol in CH_3CN

5.2.3 Ion molecule reactions of transition metal anions with small neutral molecules

I-M reactions were also tried with transition metal anions. Good negative ion spectra were obtained for the compounds $[Et_4N][W(CO)_5Br]$ (**31**), $[Et_4N][W(CO)_5I]$ (**32**), $[Et_4N][W(CO)_4I_3]$ (**33**) and $[Et_4N][Mo(CO)_5Br]$ (**34**) but $[Et_4N][Cr(CO)_5Br]$ (**35**) could not be characterized due to solubility problems. All these transition metal anion salts were donated by Dr Jason Lynam.

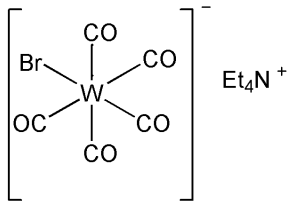

31

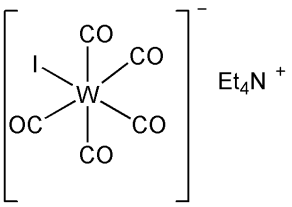

32

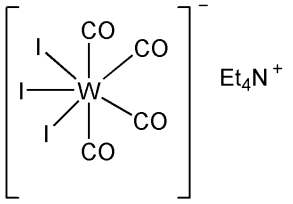

33

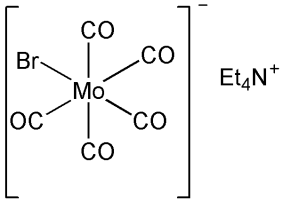

34

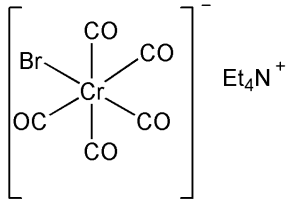

35

The negative ion spectrum of **31** shows the anionic molecular ion $[M]^-$ at m/z 404.9 and the daughter ions at m/z 375.0 and 349.1, formed by the loss of one carbonyl ion $[M–CO]^-$ and two carbonyl ions $[M–2CO]^-$, respectively (Fig 5. 19).

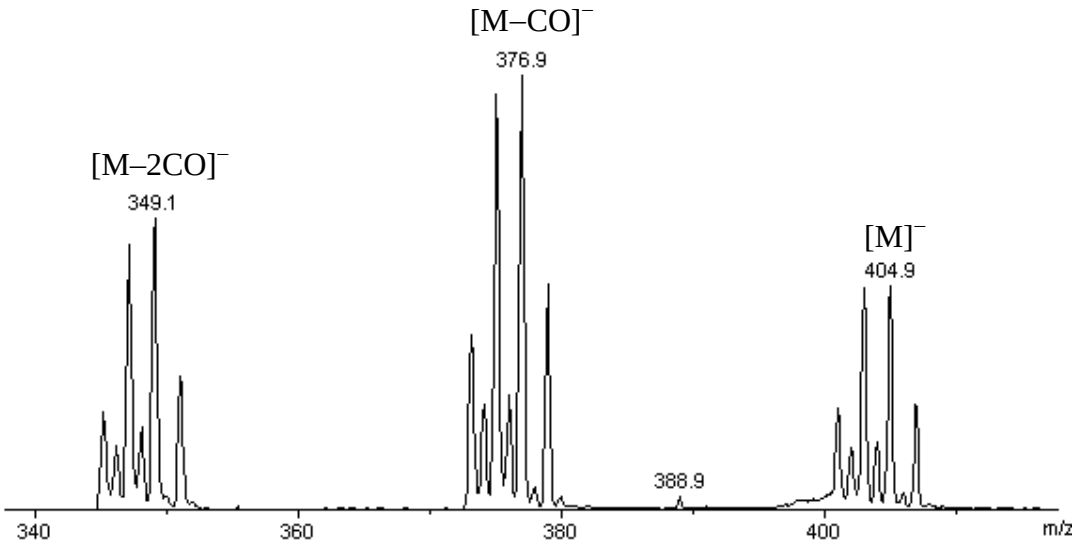

Fig 5. 19 Negative ion ESI mass spectrum of $[Et_4N][W(CO)_5Br]$

Tungsten has four stable isotopes ^{182}W, ^{183}W, ^{184}W, and ^{186}W. The calculated spectrum of $W(CO)_5Br$ is having peaks at 404.8 (100.0%), 402.8 (96.5%), 406.8 (47.0%), 400.8 (44.6%), 403.8 (28.9%), 401.8 (26.5%) which is in close agreement with observed spectrum.

The anionic molecular ion $[M]^-$ and the two daughter ions $[M–CO]^-$, $[M–2CO]^-$ were isolated and reaction were tried with methanol, pyridine, 1–hexene, pentyne, CO_2, SO_2, NO, isobutene and D_2 but no product peaks were observed.

Compound **32** also behaved in a similar manner. The negative ion spectrum of **32** shows molecular ion $[M]^-$ at m/z 450.8 and the daughter ions at m/z 421.2 $[M–CO]^-$ and 395.2 $[W(CO)_4]^-$.

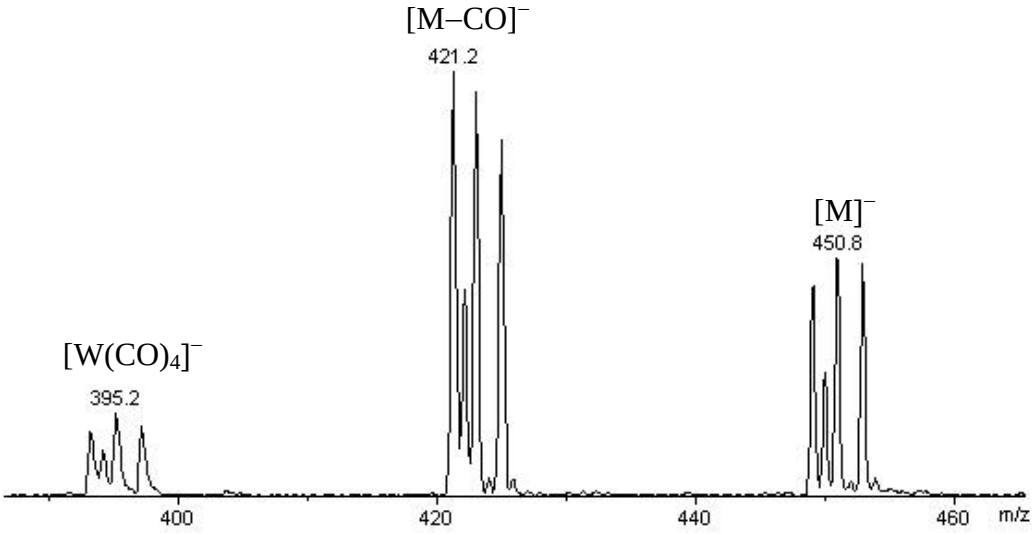

Fig 5. 20 Negative ion ESI mass spectrum of $[Et_4N][W(CO)_5I]$ **32**

The molecular ion $[M]^-$ and the two daughter ions $[M–CO]^-$, $[W(CO)_4]^-$ were isolated and tried to react with methanol, pyridine, 1-hexene, pentyne, phenylsilanes, CO_2, SO_2, NO, isobutene and D_2 but no product peaks were observed.

The negative ion spectrum of **33** shows the anionic molecular ion $[M]^-$ at m/z 674.9 and the daughter ions at m/z 648.9 and 621.3 formed by the loss of one ion carbonyl $[M–CO]^-$ and two carbonyl ions $[M–2CO]^-$, respectively.

The molecular ion $[M]^-$ and the two daughter ions $[M–CO]^-$ and $[M–2CO]^-$ were isolated and investigated for reaction with methanol, pyridine, 1-hexene, pentyne, CO_2, SO_2, NO, isobutene and D_2 but no product peaks were observed.

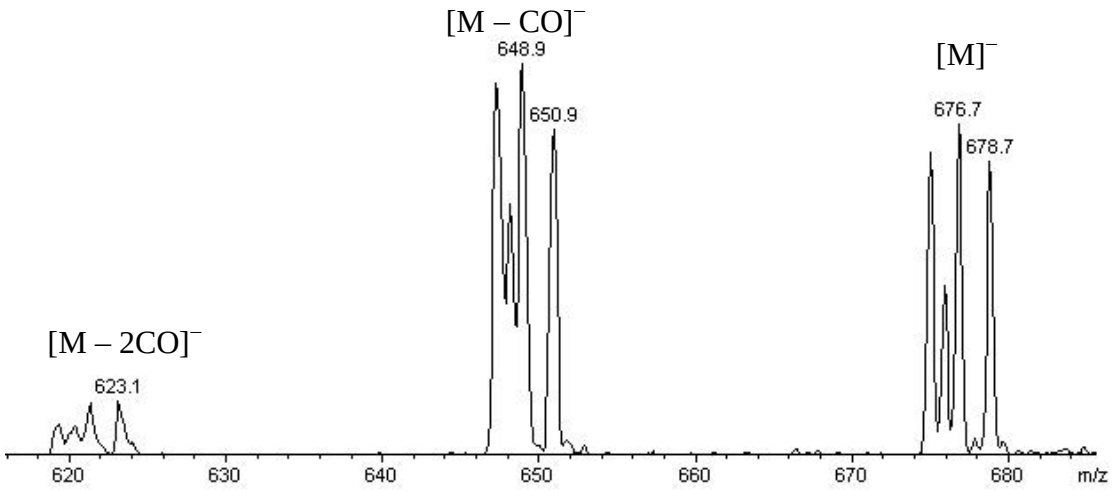

Fig 5. 21 Negative ion ESI mass spectrum of $[Et_4N][W(CO)_4I_3]$, **33**

The negative ion spectra of **34** shows the molecular ion $[M]^-$ at m/z 316.7 and the daughter ions at m/z 289 $[M–CO]^-$ and 360.2 $[M–2CO]^-$. Molybdenum (Mo) has seven stable isotopes 97.9 (100.0%), 95.9 (69.1%), 94.9 (66.0%), 91.9 (61.5%), 99.9 (39.9%), 96.9 (39.6%), 93.9 (38.3%). The calculated spectrum of $Mo(CO)_5Br$ has peaks at m/z 316.8 (100.0%), 318.8 (81.1%), 314.8 (63.8%), 315.8 (63.4%), 312.8 (56.7%), 313.8 (41.0%), 310.8 (35.3%), 317.8 (28.2%), 320.8 (23.2%), 319.8 (4.7%) which are in close agreement with the experimental peaks.

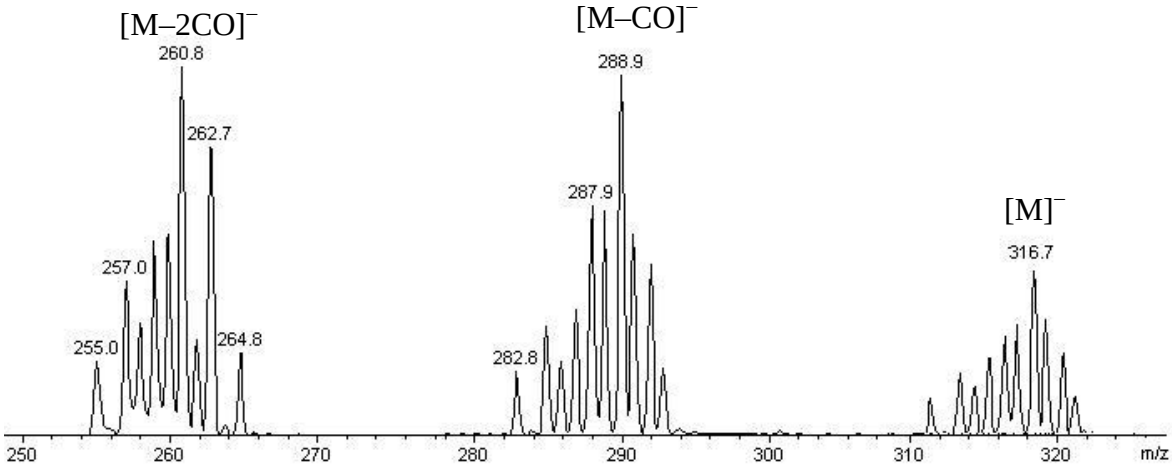

Fig 5. 22 Negative ion ESI mass spectrum of $[Et_4N][Mo(CO)_5Br]$, **34**

The molecular ion $[M]^-$ and the two daughter ions, $[M–CO]^-$ and $[M–2CO]^-$, were isolated and reactions were tried with methanol, pyridine, 1–hexene, pentyne, CO_2, SO_2, NO, isobutene and D_2 but no product peaks were observed.

5.2.4 Reaction of transition metal fluoride with small neutral molecule

The $[M–F]^+$ ions of the transition metal difluoride and diodide complexes $(DMEA)_2ZnF_2$, $(DMEA)_2CoF_2$, $Cp^*_2TiF_2$, $Cp^*_2ZrF_2$, $Ru(PMe_3)_4F_2$, $(PPh_3)_2PtI_2$ were isolated in the ion trap and subjected to reactions with CO_2, SO_2, NO, isobutene and D_2. No reaction was observed except for a $[M–F]^+$ peak of $Ru(PMe_3)_4F_2$ and $(PPh_3)_2PtI_2$ showed 30% conversion to the product with CD_3CN only

5.3 Discussion

The Bruker Esquire mass spectrometer has been successfully modified for gas-phase ion molecule reactions and the setup was checked by repeating already known reactions of complex **2** with small liquid molecules. Reactions were also successful with small gaseous molecules.

The positive ion electrospray ionization of Re and Mn tricarbonyls gave the molecular ions as well as the daughter ions formed by the loss of either a carbonyl ligand or the other ligand X (X = picoline, $POEt_3$) depending upon the ligand attached. The molecular ions of **27**, **28** and **30** with saturated coordination spheres did not react with neutral molecules while the daughter ions reacted with both liquid and gaseous small molecules (Et_3N, CD_3CN, pyridine, 1-hexene, pentyne, SO_2, NO and isobutene). Similar behaviour was shown by the platinum diiodide complexes.[6]

The negative ion electrospray ionization of transition metal anions gave the anionic molecular ion $[M^-]$ as a base peak and further fragmentation occurs via loss of carbonyl ligands. Neither the molecular ion nor any of the other ions (formed by the loss of CO ligand) reacted with the neutral molecules in the gas phase.

The gas phase ion molecule reactions of small neutral molecules with the transition metal fluoride complexes were not successful.

5.4 Conclusions

Ion molecule reactions of $Re(CO)_3$ cations are quite successful with liquid reagent and we have observed 100% conversion of these cations to product but still did not obtain any positive results with transition metal anions. Transition metal fluoride complexes also have failed to show any I-M reactions.

HYDROGEN BONDING OF $(Cp^*)_2MF_2$ COMPLEXES

6.1 Introduction

6.1.1 Hydrogen bonding

Hydrogen bonding (HB) is an attractive interaction (10-65 kJ mol^{-1}) between a weak acid like O-H or N-H with a weak base. HB has good chemical specificity and directionality. The hydrogen bond is generally stronger than Van der Waals forces but weaker than covalent bonding. These properties make it very important in supramolecular chemistry[1-3] and crystal engineering.[4-7] Hydrogen bonds are also of great importance in biological structures,[8,9] coordination and organometallic chemistry[10] and materials chemistry[11]. There are three categories of hydrogen bonding, weak, moderate and strong having stabilization energies of 16 kJ mol^{-1}, 60 kJ mol^{-1} and 120 kJ mol^{-1} respectively.[12] Hydrogen bonding can be intramolecular or intermolecular. The intramolecular interaction introduced by Sidgwick and Callow, does not have much effect on the physical properties as no association is involved here.[13,14]

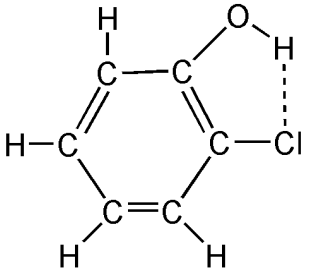

o- chlorophenol

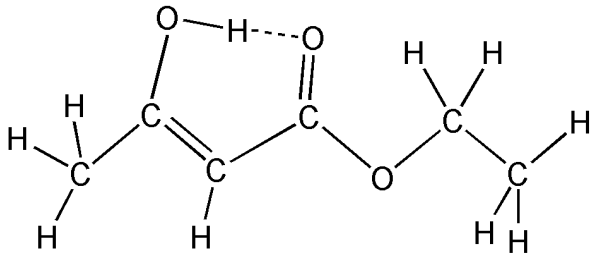

ethyl acetoacetate

Intermolecular hydrogen bonding exists between two or more molecules and changes many physical properties like mass, shape, melting point, boiling point, density and electronic structure etc. A dynamic equilibrium exists between the bonded and monomeric molecules. The equilibrium constant can be used to determine the thermodynamic parameters.[13,14]

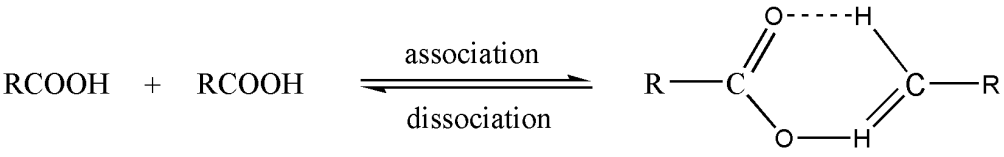

Hydrogen bonding has been reported in metal fluoride complexes. The crystal structure of $[Cu(na)_2F_2(H_2O)_2].4H_2O$ (na = nicotinamide) has been determined by X-ray

crystallography (Fig 6. 1) which shows that there is hydrogen bonding between the fluoride ligand attached to copper and the water lattice (CuF···HOH).[9]

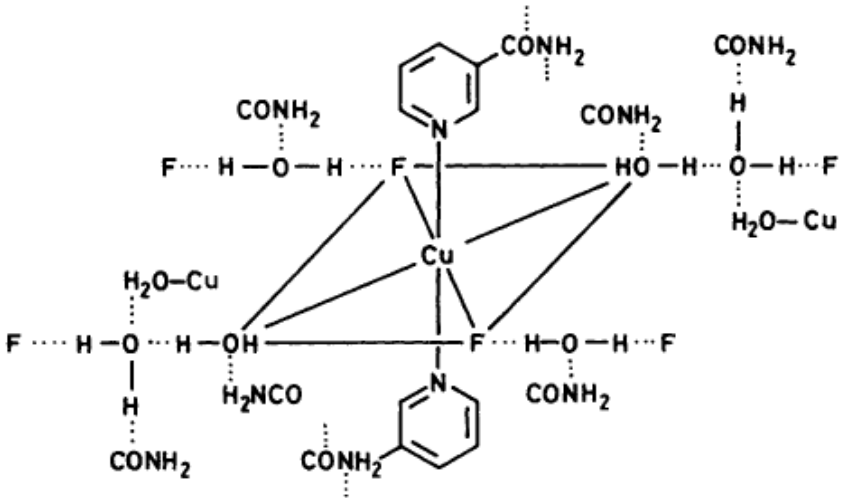

Fig 6. 1 Hydrogen bonding of ligated fluorine with water lattice in $[Cu(na)_2F_2(H_2O)_2].4H_2O$[9]

The hydrogen bond acceptor capability of halogens is of key importance in the discussion of hydrogen bonding interactions. The greater the negative charge around the halogen, the greater will be the ability to form a hydrogen bond (HB), giving a trend F > Cl > Br > I. Four main types of HB acceptor have been discussed by Kovacs and Varga, anionic acceptor (X^-), M–X (M= transition metal halide), C–X (carbon halide) and H–X (hydrogen halide) acceptors.[15-17] Studies have been performed on the similarities and differences of M–X and C–X as potential hydrogen bond acceptors. It was also found that M–F···H (having the ability to form strong directional hydrogen bonds) is of great importance in crystal engineering while M–X···H (forming weak hydrogen bonds) is important for solid state rearrangements.[18]

Hydrogen bond donors

Indole has been studied for the strength of hydrogen bond formation. Hydrogen bonding of indole with different systems like indole–water, indole–alcohol, and indole–dioxane complexes have been studied by fluorescence excitation spectroscopy where hydrogen bonded complexes have been observed. Indole is a good hydrogen bond donor, even stronger than water. The nitrogen has a lone pair of electrons which is part of the aromatic

ring. This makes the indole a poor base and it does not undergo hydrogen bonding with itself.[19-22]

Isopropanol was investigated for its hydrogen bond donor abilities by infra-red spectroscopy. The complexes used as a proton acceptor are di-isopropyl ether, liquid poly(propylene oxide), and poly(n-butyl methacrylate) and the enthalpies calculated are –9 ± 2, –16 ± 3, and –10 ± 2 kJ mol^{-1}.[23]

1,1,1,3,3,3 Hexafluoroisopropanol is a good hydrogen bond donor and was studied by IR spectroscopy for its hydrogen bonding capabilities by investigating the change in the hydrogen OH bond stretch.[24] Hexafluoroisopropanol is also a Lewis acid with a pKa of 9.3 in H_2O.[25,26]

6.1.2 Halogen bonding

Halogen bonding refers to the noncovalent interaction involving a halogen as an electron acceptor (Lewis acid).[27,28] This kind of bonding can be represented by a general scheme "D···X-Y" where D is the Lewis base or electron density donor, X represents halogen/electron density acceptor or Lewis acid and Y is the carbon, transition metal, nitrogen etc. Halogen bonding has an important role in crystal engineering. An important type of these interactions occur between metal halide complexes and organic halides (M–X···X`–C), and has studied by Brammer and Perutz.[29,30]

Halogen bond donors

Iodopentafluorobenzene is a strong halogen bond donor and is of great importance in supramolecular chemistry.[30-32] Iodopentafluorobenzene is electron deficient at the iodine atom due to the high degree of fluorination of the benzene ring.[33-35] Brammer and Perutz investigated metal fluoride complexes for hydrogen and halogen bonding using multinuclear NMR spectroscopy. $Ni(PEt_3)_2(C_5F_4N)F$ (**3**) forms adducts with indole (hydrogen bonding) and pentafluoroiodobenzene (halogen bonding). The metal fluoride shows a considerable ^{19}F NMR chemical shift with the adduct formation. Titration curves were plotted at different temperature between the ^{19}F chemical shift and the ratio of molar concentration of nickel fluoride and the titrant (indole) see Fig 6. 2. Similar plots were also obtained for the titration of NiF with C_6F_5I. The enthalpy and the entropy of the reaction

were obtained using the Van't Hoff plot. It was found that these complexes form halogen bonds of equivalent strength to hydrogen bonds.[34]

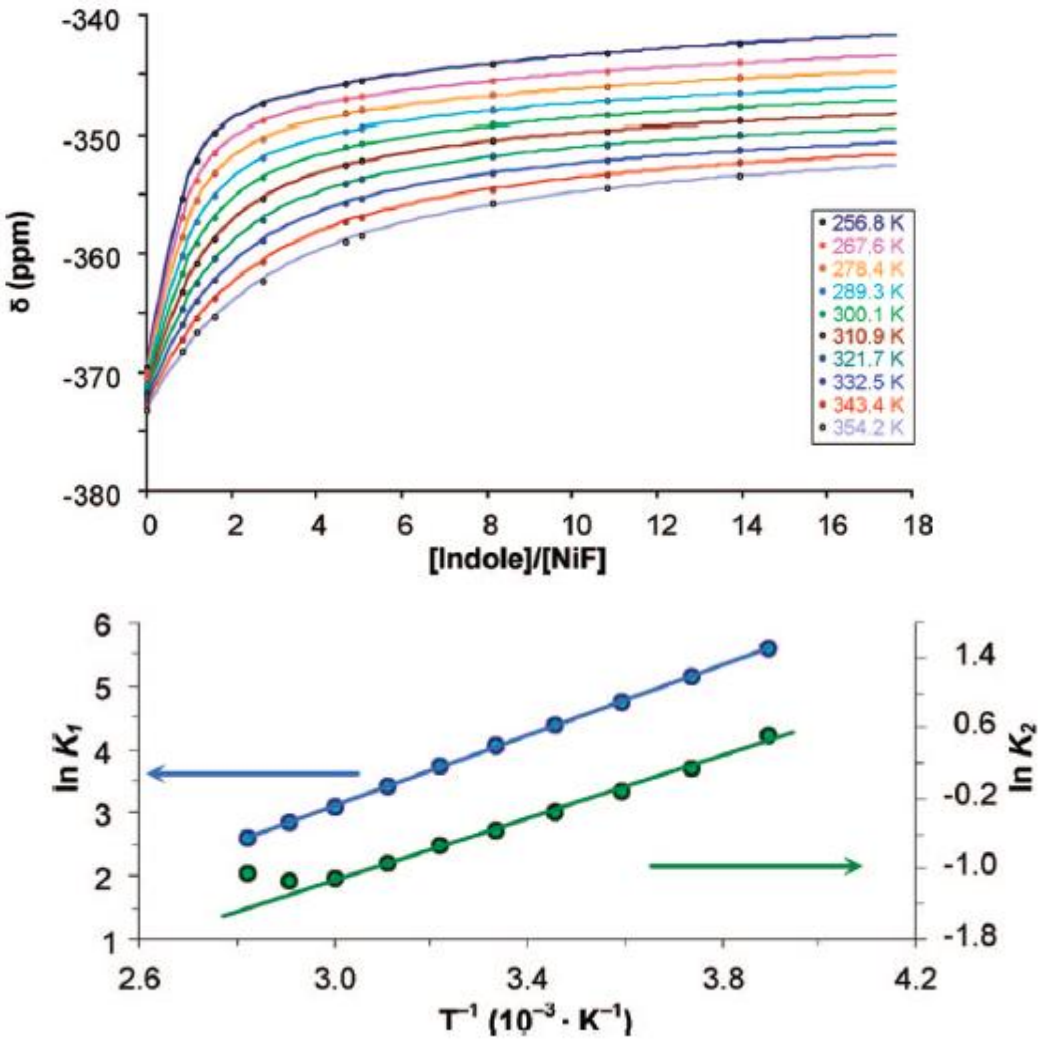

Fig 6. 2 (a) Fit of the titration curves at different temperatures, showing observed δ_F versus ratio of molar concentrations of indole and NiF in toluene-d_8; (b) Van't Hoff plot.[34]

Recently, the thermodynamics of halogen bonding of group 10 transition metal fluoride complexes with iodopentafluorobenzene (Fig 6. 3) has been studied. C_6F_5I is a good halogen bond donor due to the highly fluorinated aromatic which increases the electrophilicity of the iodine. The ^{19}F NMR signal of the metal fluoride moves downfield upon the addition of C_6F_5I. The equilibrium constants K were determined from the plot fitted between the between the ^{19}F NMR chemical shift and the ratio of the concentration of the metal fluoride and C_6F_5I. The enthalpy (ΔH) and entropy (ΔS) were determined from

the Van't Hoff plot and it was found that the enthalpies of the halogen bond increases on moving down the column in the Periodic Table. The formation of 1:1 adducts was confirmed by a Job plot.[30]

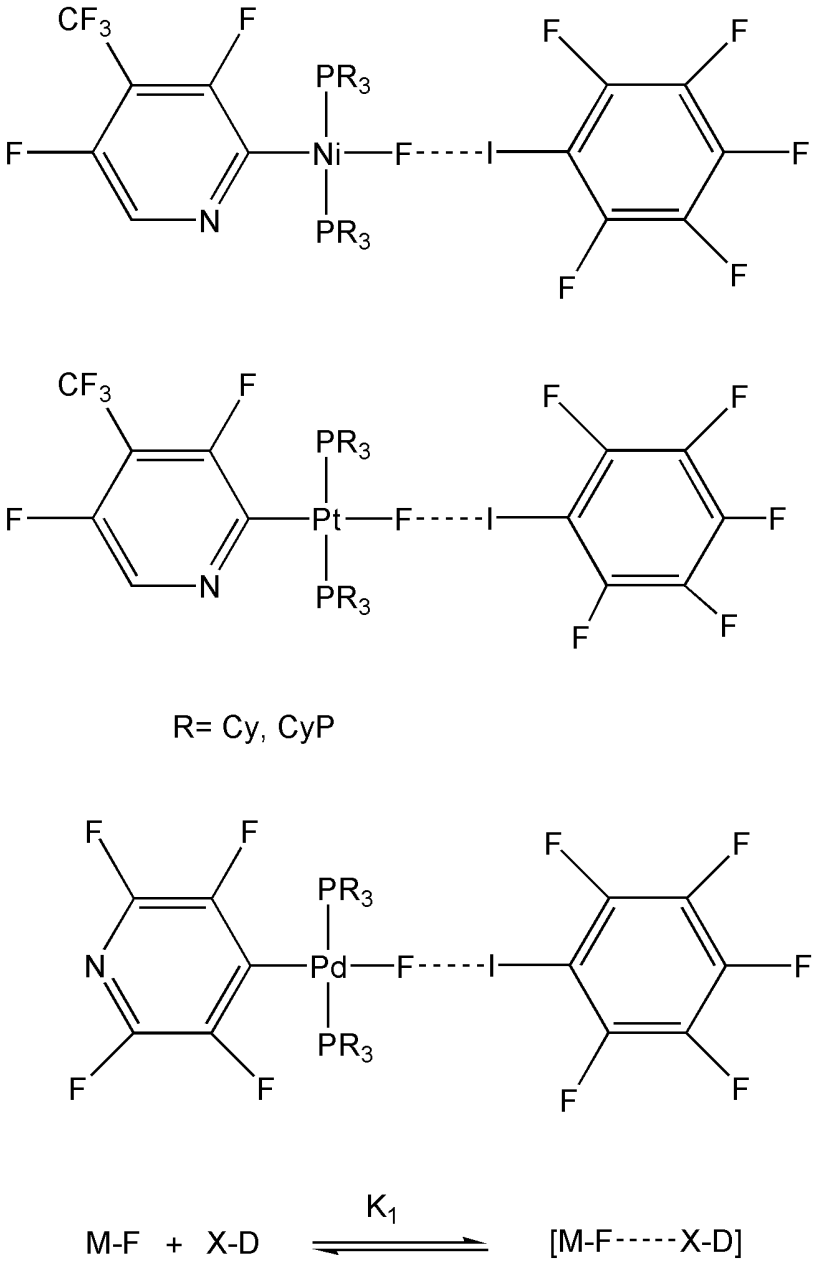

Fig 6. 3 Halogen bonding of transition metal fluoride complexes with iodopentafluorobenzene.

This chapter will be focused on establishing the strength of hydrogen and halogen bonds formed by group 4 transition metal difluoride complexes and determination of the effect of the metal on the thermodynamic parameters as we move down the series in the Periodic Table.

6.2 Results

The strategy for this work was to synthesize closely related d^0 transition metal difluoride complexes so that the periodic trends in the thermodynamics of hydrogen bonding and halogen bonding can be observed. For this purpose isostructural complexes of Ti, Zr and Hf were prepared. All these compounds can be easily handled spectroscopically and show sharp signals in the NMR spectra. Protio toluene was used as a solvent for carrying out the titration experiments.

Indole and hexafluoroisopropanol (HFIP) were used as hydrogen bond donors. Indole was kept under vacuum for 1 hour and stored in the glove box. Iodopentafluorobenzene was dried using molecular sieves (3Å) and also stored in the glove box.

Titration of d^0 transition metal difluorides against hydrogen bond donors and halogen bond donors was investigated by ^{19}F NMR spectroscopy. The change in the chemical shift of the fluoride ligand coordinated to the metal was recorded. The equilibrium constants were obtained by plotting the data of the NMR titration at constant or variable temperatures. For calculating the densities of the solutions, it was assumed that the sum of the volumes of the component of the solutions is equal to the volumes of the solutions. Microsoft Excel®, using a macro program developed by Professor C. A. Hunter of the University of Sheffield was used to carry out the calculations for determining the equilibrium constants. Van't Hoff plots, developed from the equilibrium constants, and were used to calculate the enthalpy (ΔH^0) and entropy ΔS^0 of the reaction. Sometimes some restraints were put in order to get an acceptable fit of the parameters.

Temperature calibration of the NMR probe

All the NMR spectra were collected on a Bruker AMX 500 spectrometer. The temperature of the probe was calibrated using methanol in a capillary which was put inside toluene d_8. The $\Delta\delta$ separation of the signals of hydrogen atoms on the methyl and hydroxyl groups of methanol provides the basis for the determination. The following equation was used to connect temperature with $\Delta\delta$.[36]

$$T(K)\ (methanol) = 409.0 - 36.54\ \Delta\delta - 21.85\ (\Delta\delta)^2$$

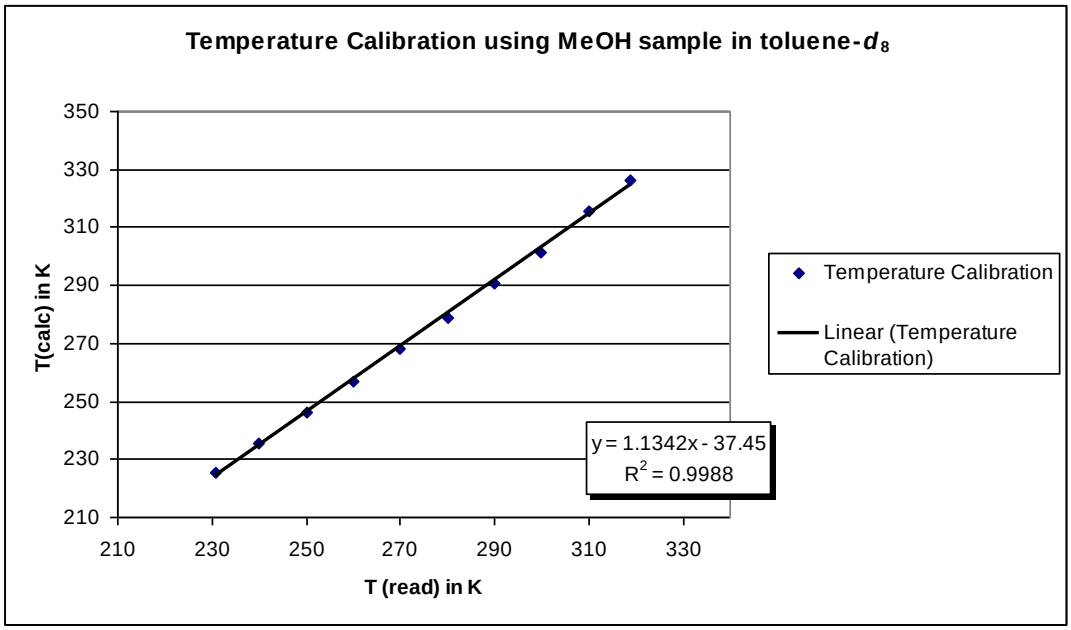

The following table shows that the nominal temperature and corrected temperature of the probe.

Table 6.1 Corrected values of temperature

T(nominal)/K	T(corrected)/K
250.0	246.0
260.0	256.8
270.0	267.6
280.0	278.4
290.0	289.3
300.0	300.1

Calculation of the thermodynamic parameters (ΔH^o and ΔS^o) from the Van't Hoff plots for variable temperature experiments

Measurement of the equilibrium constants connects to the Gibbs free energy [37] via the relationship

$\Delta G^o = - RTInK_{eq}$

R = gas constant = 8.314 J/mol·K

T = temperature (kelvin)

K_{eq} = equilibrium constant

Equilibrium constants can be used to evaluate standard enthalpy-entropy using the Van 't Hoff equation which correlates change in temperature (T) to the change in the equilibrium constant (K).

From the van 't Hoff equation[38]

$$\ln(K) = -\frac{\Delta H^o}{RT} + \frac{\Delta S^o}{R} \qquad 6.1$$

The plot of In(K) vs 1/T will result in a straight line. ΔH can be calculated from the slope and ΔS from the intercept.

ΔH^o = –Slope x R

And

ΔS^o = intercept x R

6.2.1 Hydrogen bonding of $(Cp^*)_2TiF_2$ (11) with indole

Compound **11** shows a sharp signal for both the fluorides in the NMR spectrum and is soluble in a range of organic solvents. ^{19}F NMR spectroscopy was used to study the formation of the hydrogen bonding between the indole and **11**. An upfield shift of about 32.5 ppm was observed in the ^{19}F spectrum upon addition of excess of indole at 300 K (Fig 6. 4).

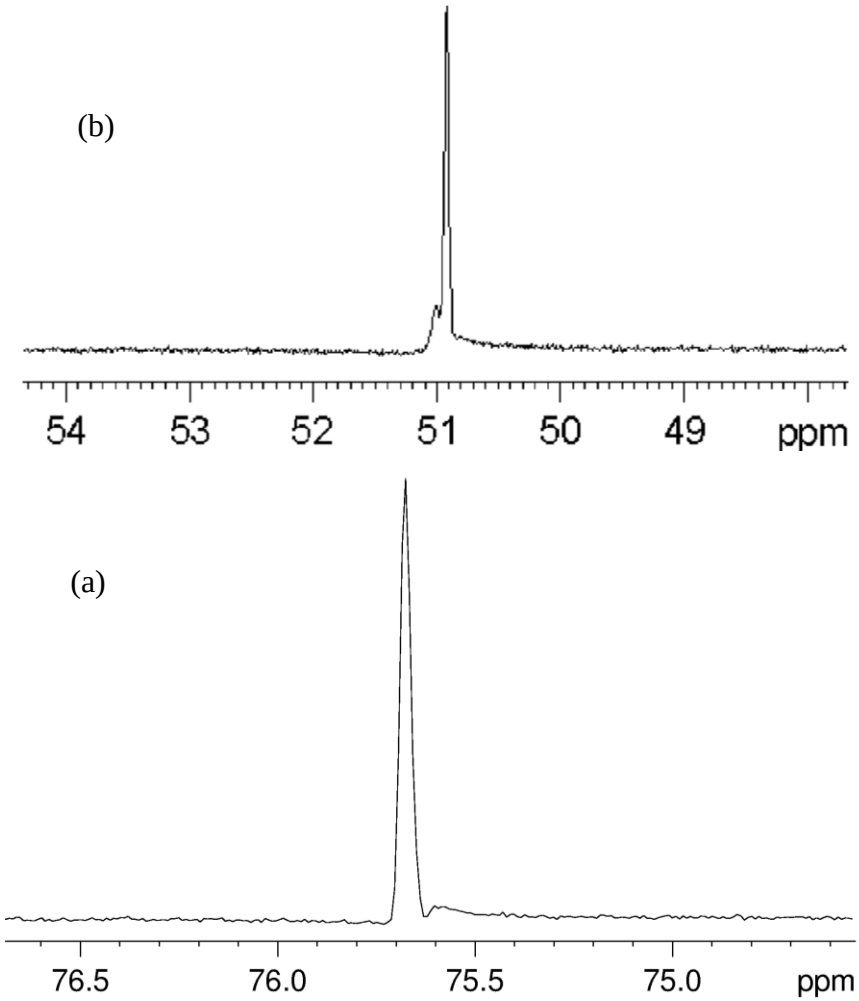

Fig 6. 4 ^{19}F NMR spectrum of (a) **11** in toluene (b) hydrogen bonded adduct formed from the mixture of **11** and indole

NMR spectra were recorded at six different temperatures ranging from 246.0 to 300.1 K. Titration curves were fitted between changes in the ^{19}F chemical shift vs the ratio of the concentration of metal fluoride and indole at different temperature using the model shown in equation 6.2 (Fig 6. 5). Equilibrium constants for the formation of adducts, K were obtained from the plots. The 2nd equilibrium constant is very small compared to the first equilibrium constant (in the range of 1-2, compared to 15-150 for K_1) and can be neglected. Parameters used for fitting the curves are shown in the Table 6.2.

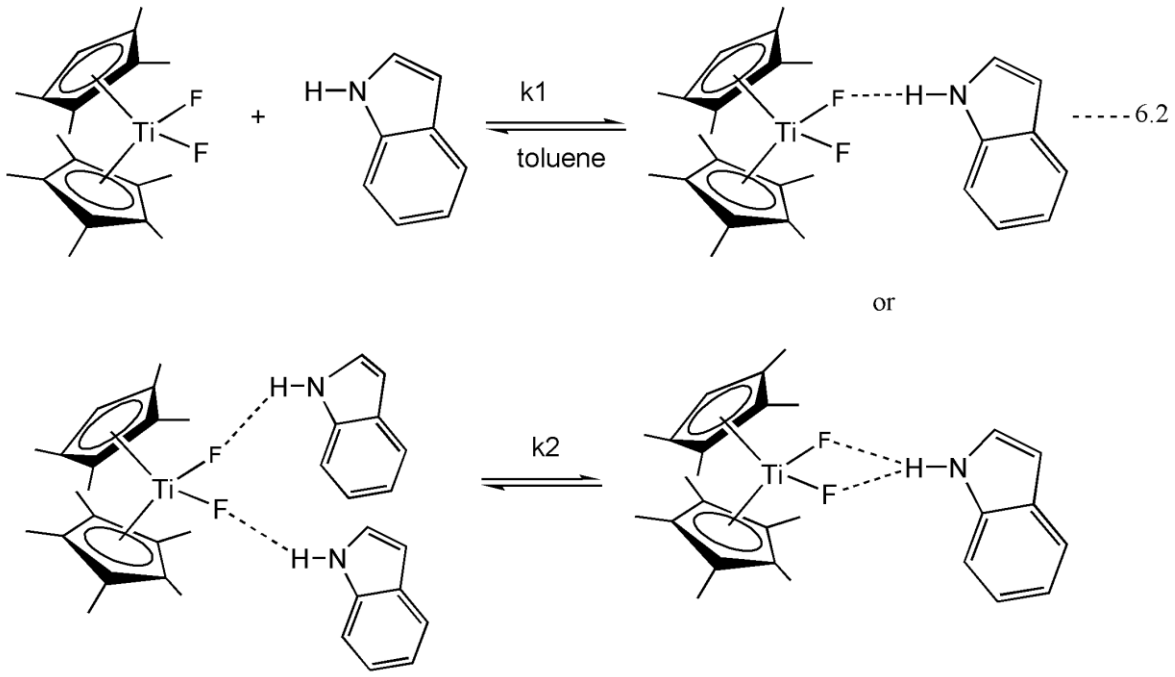

The thermodynamic parameters ΔS^o and ΔH^o can be calculated by plotting In K vs T^{-1} (Van't Hoff plot). The values of ΔS^o and ΔH^o are determined as -67 ± 8 J K^{-1} mol^{-1} and -27 ± 2 kJ mol^{-1} respectively.

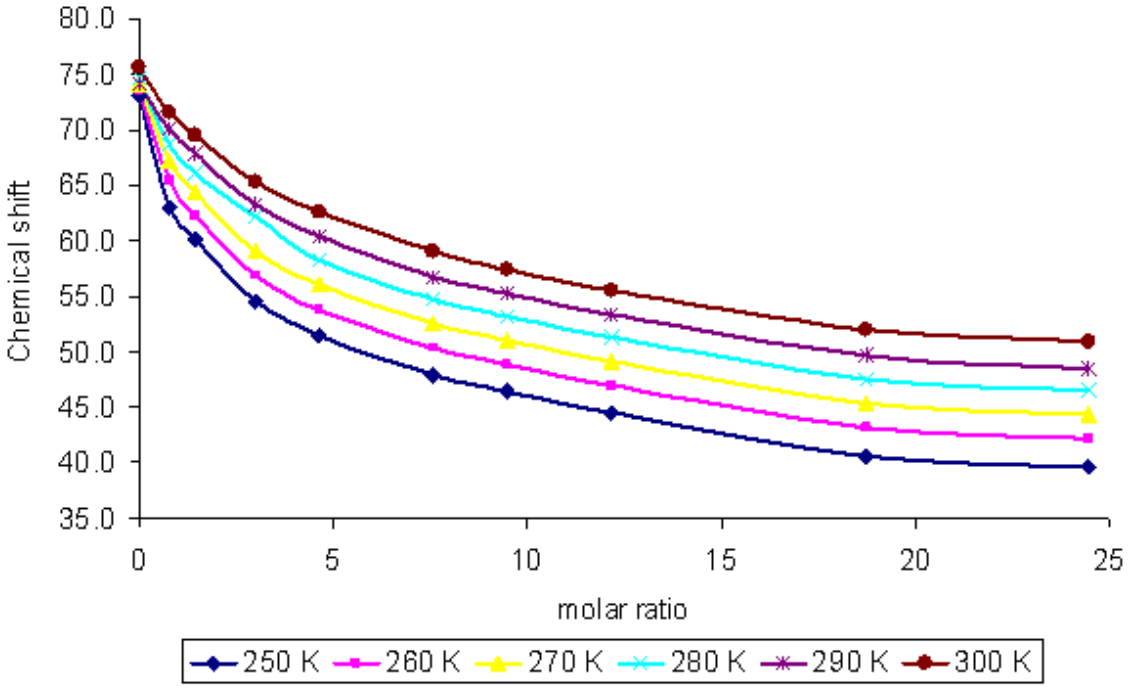

Fig 6. 5 Fitting curves for the titration of **11** vs indole for a range of temperature. The best fit of the points on the curves was in a range of ± 0.2 as seen from the residual graph on microsoft Excel®, macro program.

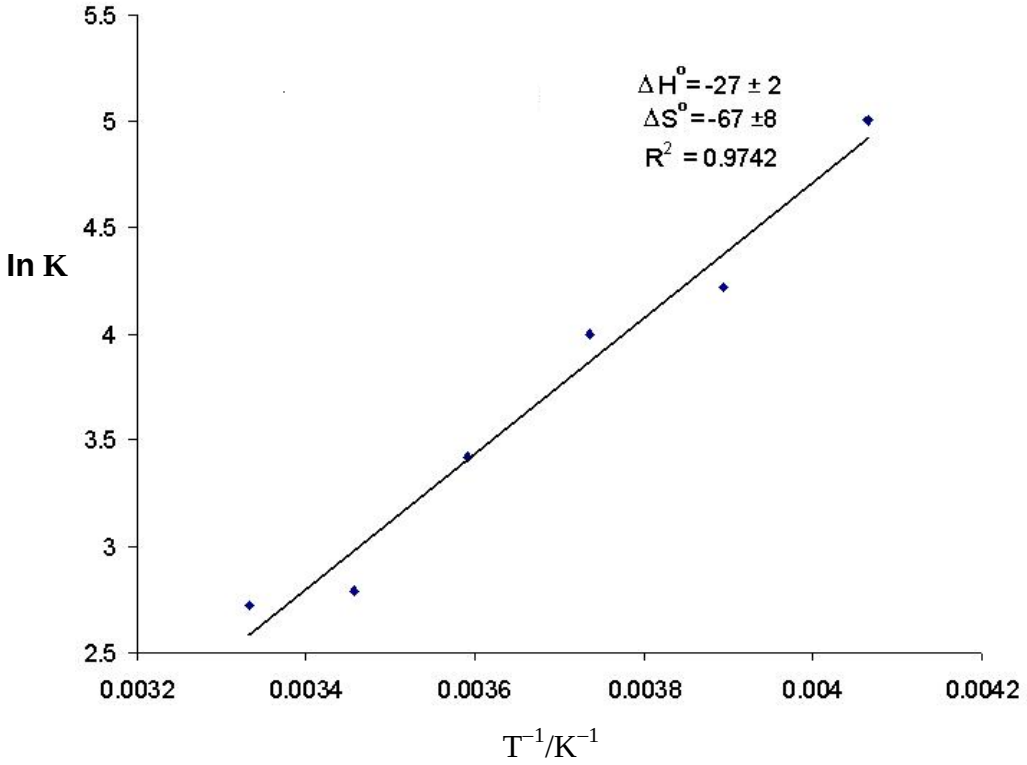

Fig 6. 6 Van't Hoff plot for K_1 for indole/TiF_2 adducts in toluene.

Table 6.2 Experimental data used for fitting the curves. Concentration of stock solution of **11** were 0.044 M and the concentration of the indole stock solution was 3.524M

$V_{MF}/\mu L$	$V_{indole}/\mu L$	**^{19}F NMR shift of the TiF_2 (11)**					
		250 K	**260 K**	**270 K**	**280 K**	**290 K**	**300 K**
500	0	73.05	73.63	74.19	74.70	74.14	75.68
513	5	63.04	65.48	67.19	68.69	70.08	71.54
515	9	60.19	62.37	64.34	66.16	67.85	69.53
514	20	54.56	56.90	59.07	62.20	63.25	65.31
526	31	51.46	53.78	56.04	58.22	60.36	62.6
528	50	47.96	50.34	52.53	54.69	56.80	59.08
526	63	46.40	48.80	51.03	53.16	55.27	57.47
530	81	44.57	46.97	49.20	51.34	53.34	55.54
514	121	40.57	43.10	45.31	47.54	49.68	52.03
514	158	39.58	42.14	44.4	46.57	48.5	50.90
	K1	149	68	54.3	30.5	16.3	15.2
	K2	1.85	1.61	1.59	1.33	1.01	0.9

6.2.2 Hydrogen bonding of $(Cp^*)_2TiF_2$ with HFIP

A similar procedure to that in 6.2.1 was adopted for this experiment. The formation of the hydrogen bond adduct was also studied by NMR spectroscopy. The ^{19}F NMR chemical shift moves by 80.13 ppm upfield upon addition of excess HFIP. NMR spectra were recorded at six different temperatures ranging from 246.0 to 300.1K.

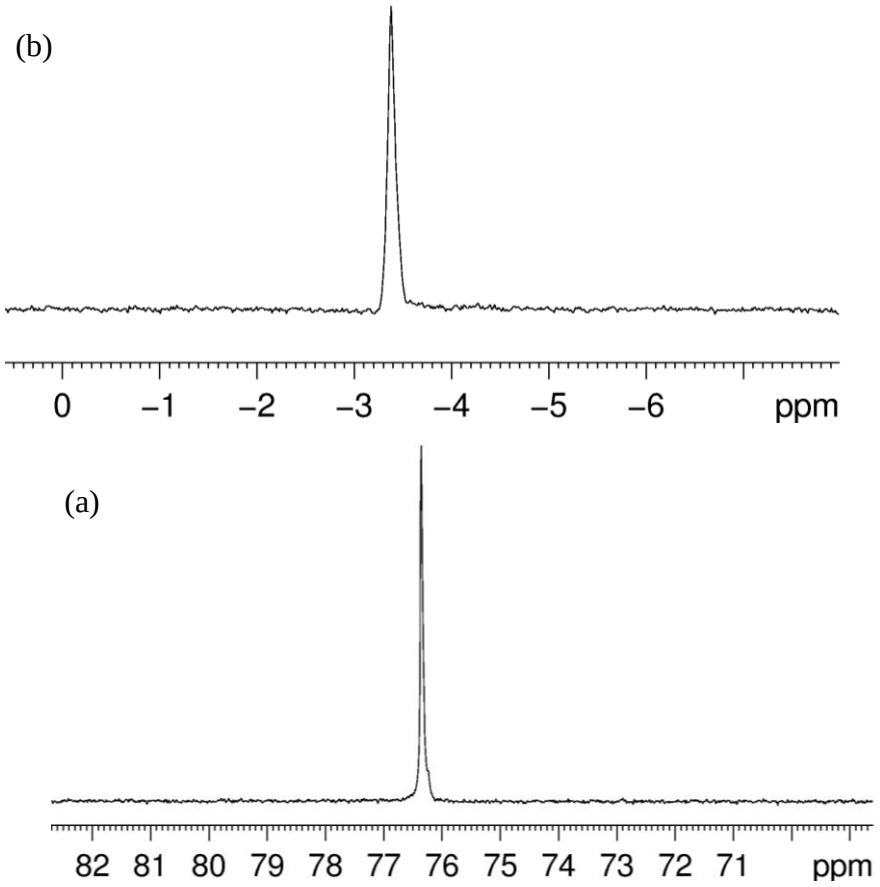

Fig 6. 7 ^{19}F NMR spectrum of (a) **11** in toluene (b) hydrogen bonded adduct formed from the mixture of **11** and HFIP

The titration curves were fitted according to the model shown by equation 6.3. The adduct is formed in a ratio of 1:2 (metal fluoride and the HFIP) (Fig 6. 8). The parameters used for fitting the plots are given in Table 6.3.

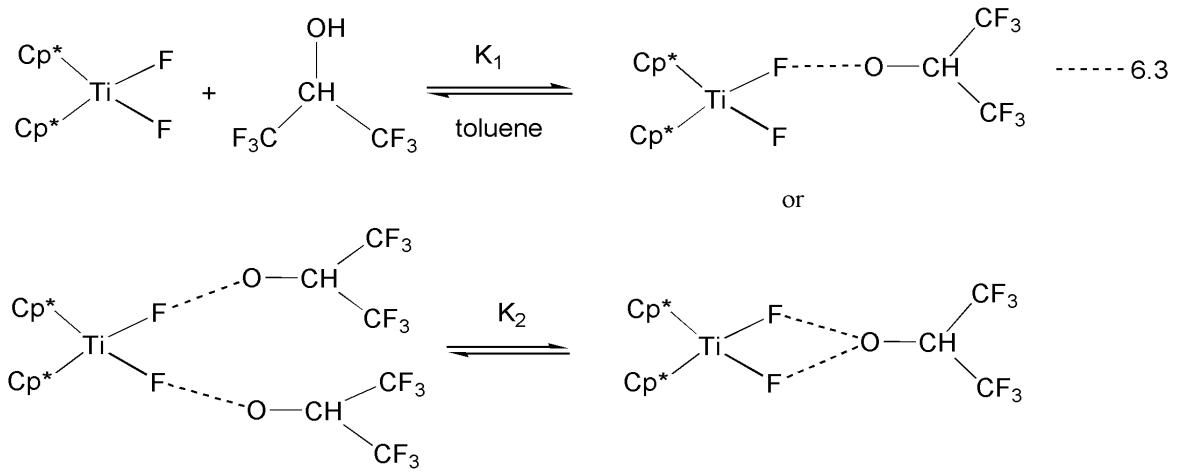

The equilibrium constant K for the formation of the hydrogen bond adduct was determined by plotting ^{19}F chemical shift vs the ratio of concentration of **11** and HFIP. It was observed that the value of the 2nd equilibrium constant is negligibly small as compared to the 1st equilibrium constant.

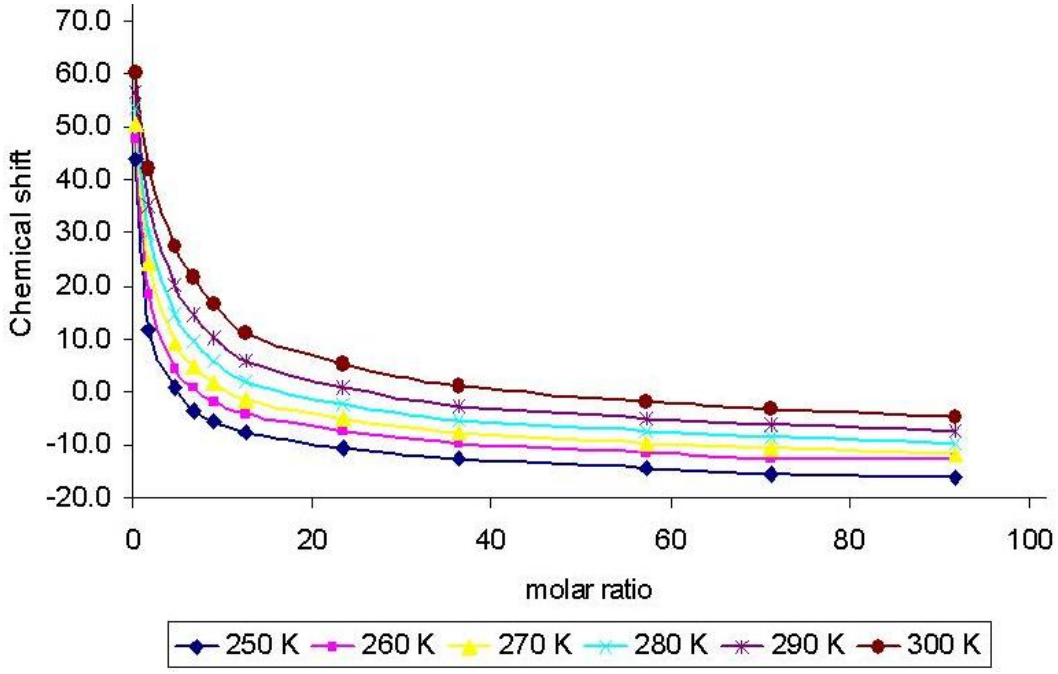

Fig 6. 8 Fitting curves for the the titration of **11** vs HFIP indole for the whole range of temperature. The best fit of the points on the curves was in a range of ± 0.4 as seen from the residual graph on microsoft Excel®, macro program.

The thermodynamic parameters ΔS^o and ΔH^o can be calculated by plotting ln K vs T^{-1} (Van't Hoff plot). The values of ΔS^o and ΔH^o being determined as -35 ± 3 J K^{-1} mol^{-1} and -19.2 ± 0.7 kJ mol^{-1}, respectively.

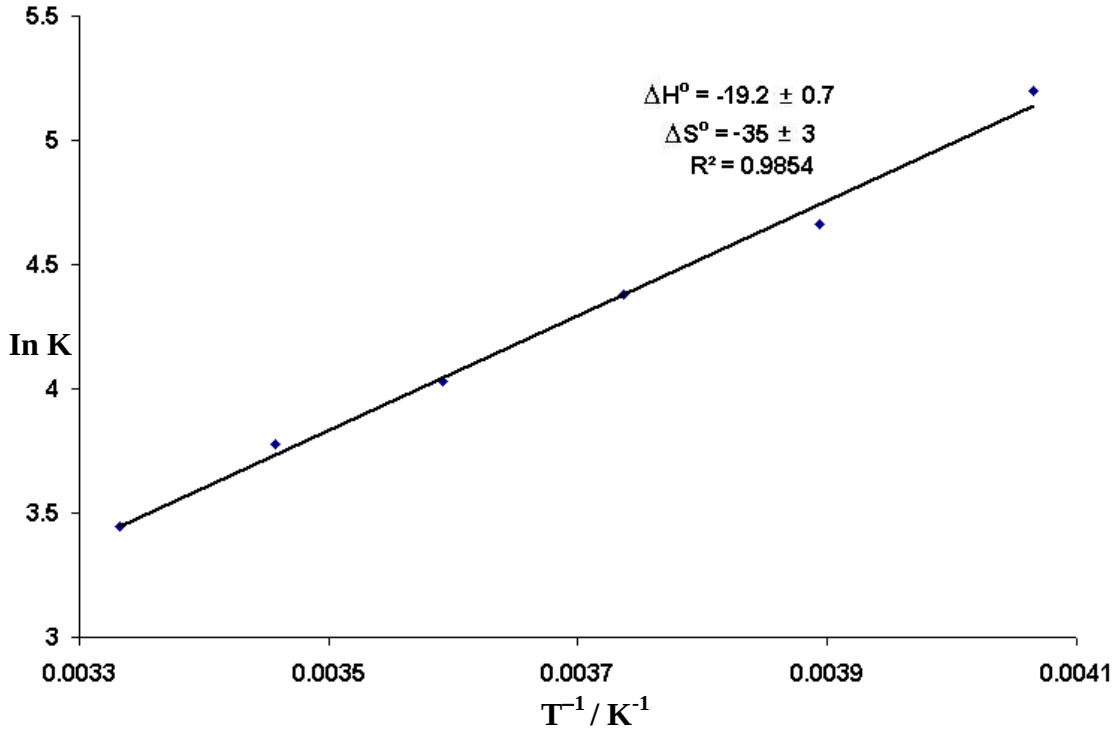

Fig 6. 9 Van't Hoff plot for K_1 for HFIP/TiF_2 adducts in toluene.

Table 6.3 Experimental data used for fitting the curves (Fig 6.8). Concentrations: 0.02 M of stock solutions of **11** and 4.87 M of HFIP

$V_{MF}/\mu L$	$V_{HFIP}/\mu L$	^{19}F NMR shift of the TiF_2 (11)					
		250 K	**260 K**	**270 K**	**280 K**	**290 K**	**300 K**
500	0	64.25	65.98	67.05	69.89	72.98	76.75
520	4	43.95	47.60	50.53	53.49	56.43	60.20
577	11	11.74	18.53	24.16	29.81	35.21	42.10
536	15	0.91	4.39	9.21	14.62	20.21	27.56
526	20	-3.72	0.83	4.88	9.63	14.68	21.62
531	28	-5.72	-1.76	1.65	5.69	10.21	16.53
534	53	-7.82	-4.29	-1.44	1.94	5.80	11.20
528	81	-10.59	-7.37	-5.02	-2.31	0.80	5.10
531	129	-12.80	-9.74	-7.66	-5.29	-2.61	0.98
534	161	-14.54	-11.62	-9.62	-7.44	-5.01	-1.85
518	202	-15.48	-12.60	-10.69	-8.63	-6.28	-3.38
	K_1	181	106	79.6	56.3	43.7	31.3
	K_2	3.37	2.53	2.35	2.39	2.60	2.77

6.2.3 Hydrogen bonding of $(Cp^*)_2ZrF_2$ + indole

The formation of the hydrogen bonded adduct formed between $(Cp^*)_2ZrF_2$ and indole was also studied by NMR spectroscopy. The ^{19}F NMR chemical shift moves upfield by 14.58 ppm upon addition of excess of indole at 300 K (Fig 6. 10). NMR spectra were recorded at six different temperatures ranging from 246.0 to 300.1K.

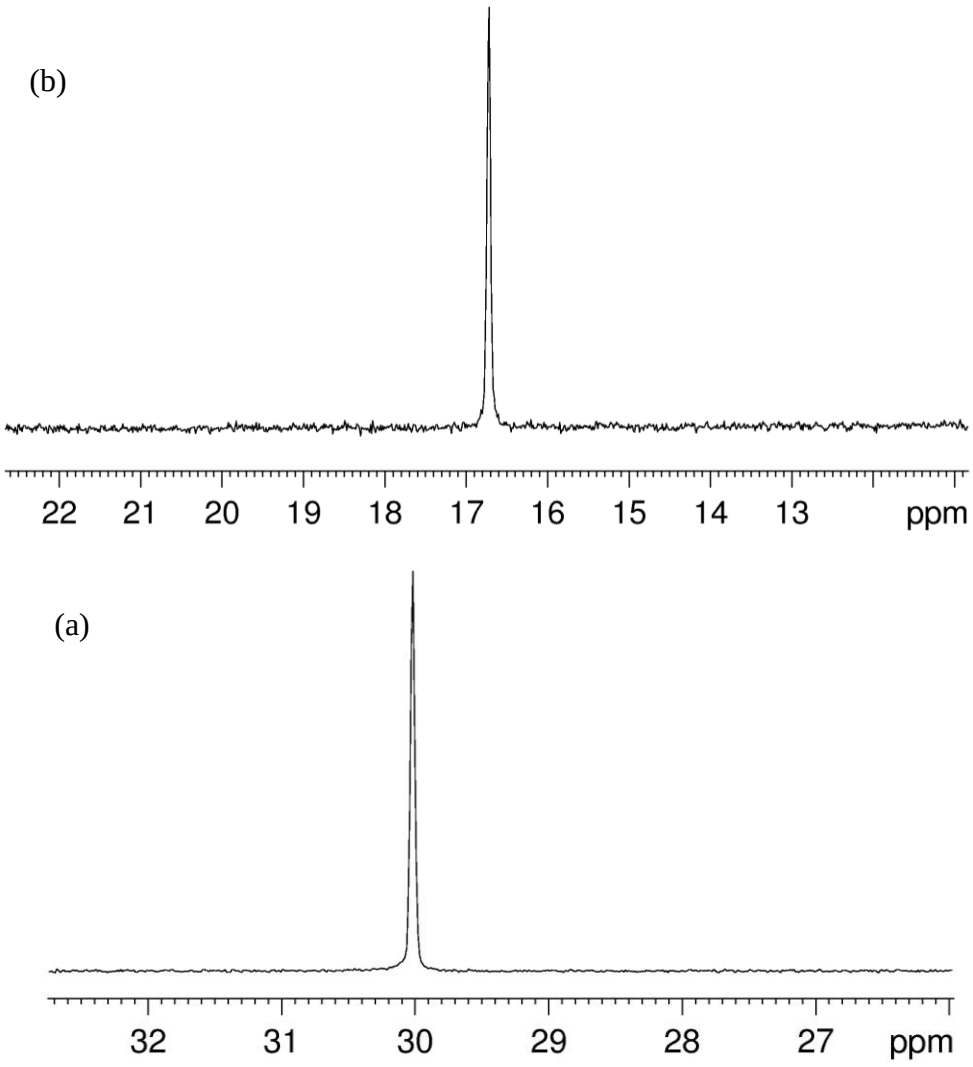

Fig 6. 10 ^{19}F NMR spectrum of (a) **12** alone (b) adduct with indole

The titration curves were fitted (1:1 ratio of metal fluoride and the indole) according to the model shown by equation 6.4. The parameters used for fitting the plots is given in Table 6.4.

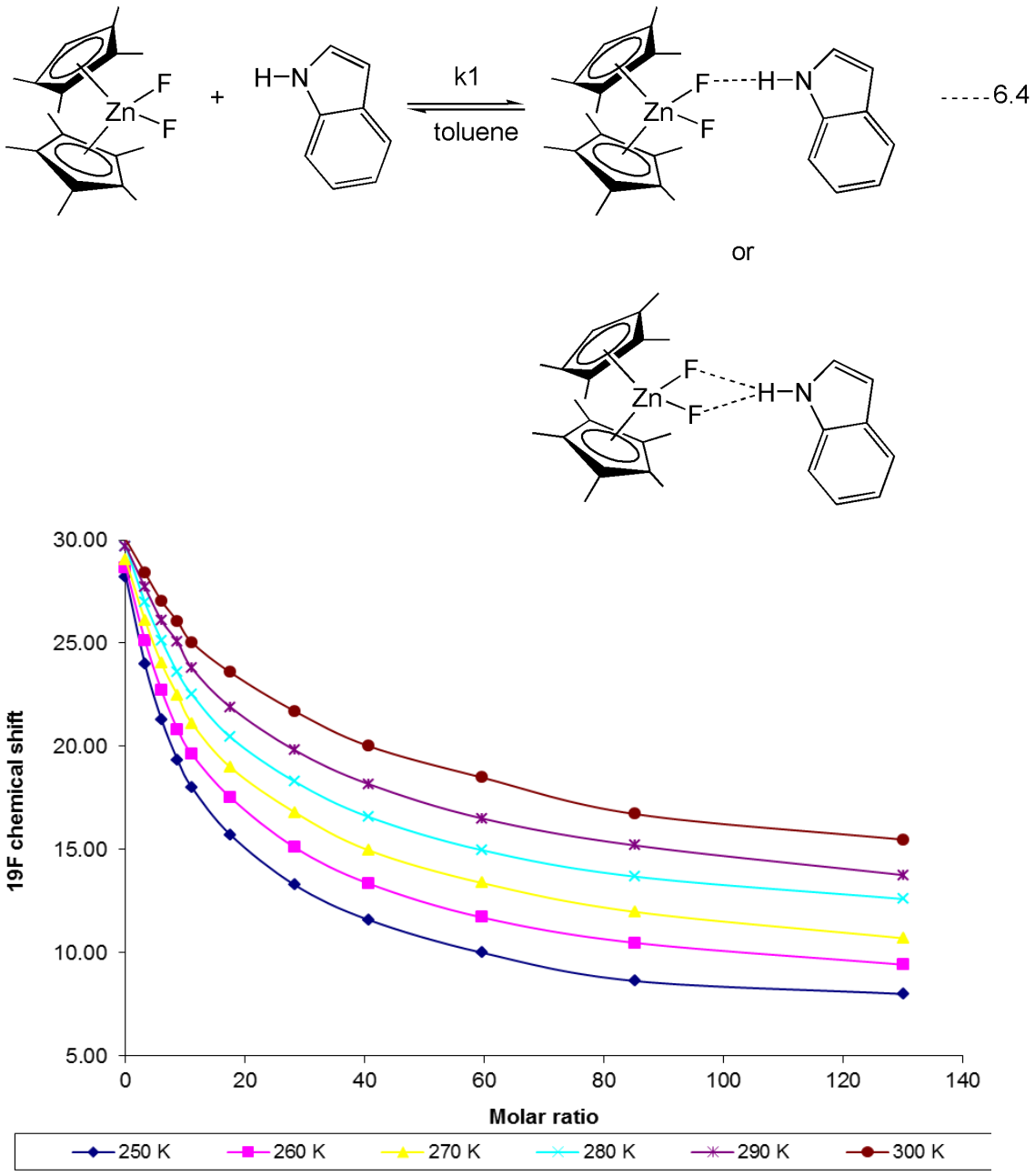

Fig 6. 11 Fitting curves for the titration of 12 vs indole for the whole range of temperature. The best fit of the points on the curves was in a range of ± 0.5 as seen from the residual graph on microsoft Excel®, macro program.

The equilibrium constant K for the formation of the hydrogen bonded adduct was determined by plotting the ^{19}F chemical shift vs ratio of concentration of **12** and indole. The thermodynamic parameters ΔS^o and ΔH^o can be calculated by plotting the titration curves at different temperatures and plotting In K vs T^{-1}, (Van't Hoff plot). The values of ΔS^o and ΔH^o determined as -36 ± 4 J K^{-1} mol^{-1} and -11 ± 1 kJmol^{-1} respectively.

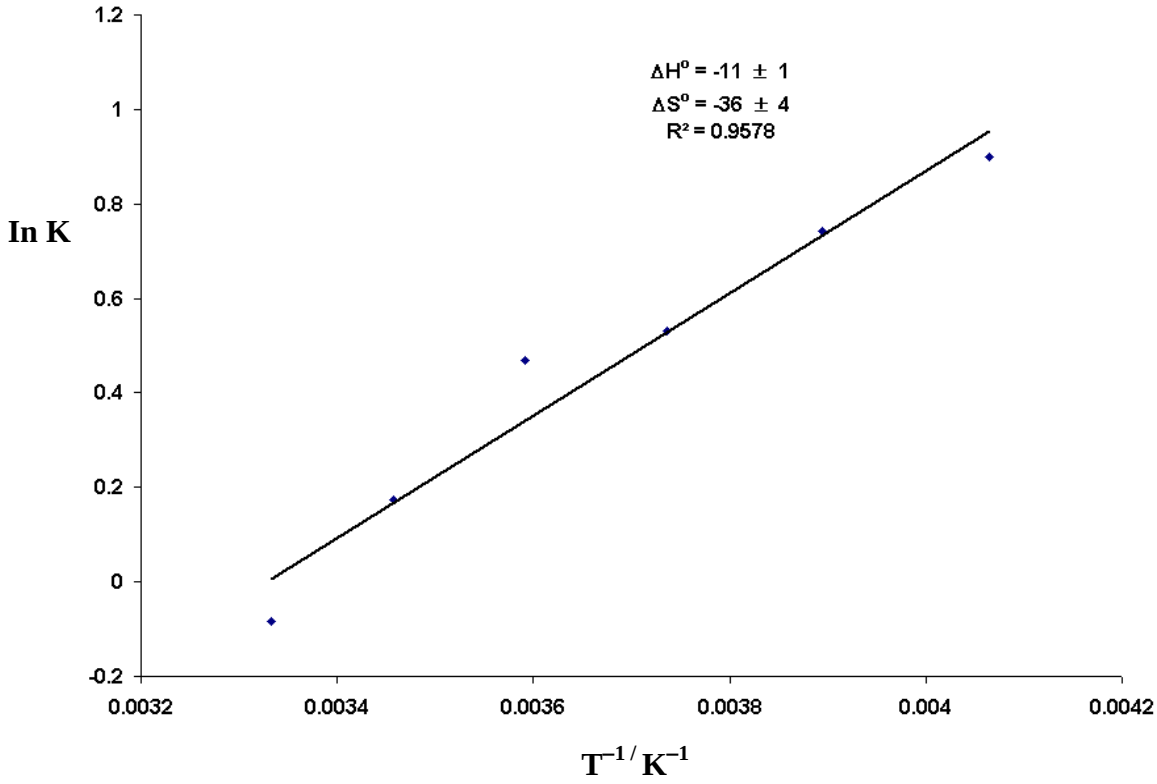

Fig 6. 12 Van't Hoff plot for K_1 for indole/ZrF_2 adduct in toluene.

Table 6.4 Experimental data used for fitting the curves (Fig 6.11). Concentration of stock solution of **12** was 0.028 M and the concentration of the indole stock solution was 3.582 M

$V_{MF}/\mu L$	$V_{indole}/\mu L$	**^{19}F NMR shift of the ZrF_2 (12)**					
		250 K	**260 K**	**270 K**	**280 K**	**290 K**	**300 K**
500	0	28.23	28.67	29.03	29.70	29.70	30.02
482	12	23.97	25.12	26.10	26.97	27.70	28.40
476	23	21.30	22.71	24.02	25.14	26.10	27.05
463	32	19.35	20.83	22.47	23.58	25.06	26.05
455	40	18.00	19.61	21.11	22.51	23.78	25.03
436	61	15.71	17.52	18.98	20.44	21.90	23.58
407	91	13.28	15.10	16.80	18.29	19.81	21.70
377	121	11.60	13.36	14.97	16.59	18.18	20.02
337	159	10.00	11.71	13.38	14.97	16.51	18.49
298	201	8.63	10.48	11.98	13.69	15.20	16.72
	K	2.46	2.1	1.7	1.6	1.2	0.92

6.2.4 Hydrogen bonding of $(Cp^*)_2ZrF_2$ with HFIP

A similar procedure was adopted in order to study the formation of hydrogen bond adducts between $Cp^*)_2ZrF_2$ (**12**) and HFIP. NMR spectra were recorded at six different temperatures ranging from 246.0 to 300.1.

The ^{19}F NMR spectrum of the **12** alone and with the hydrogen bond adduct [$(Cp^*)_2ZrF_2\cdots$ HFIP] shows that there is a chemical shift of 39.06 ppm upon addition of excess of HFIP at 300 K (Fig 6. 13).

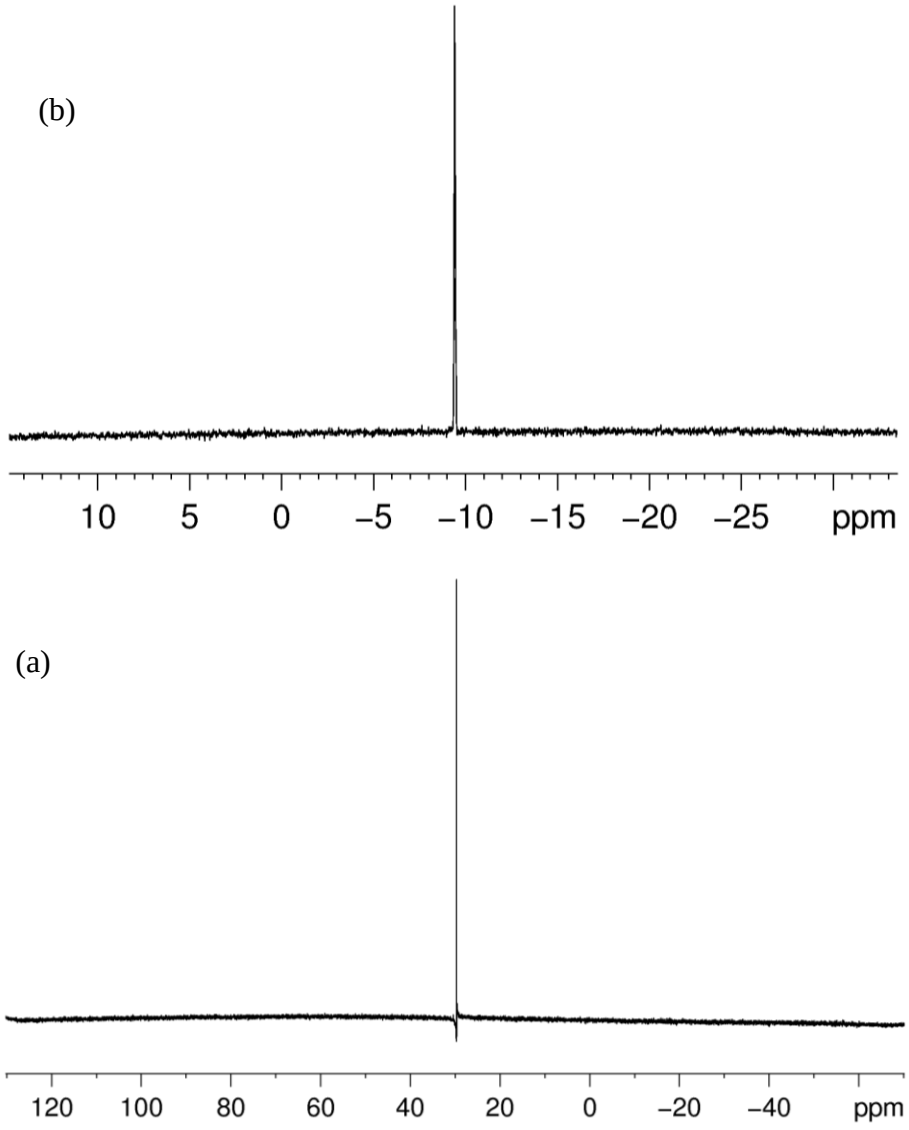

Fig 6. 13 [19] FNMR spectrum of (a) **11** alone (b) adduct formed by adding excess of HFIP

The titration plot was fitted according to the model (equation 6.5) which shows that there is ratio of 1:2 between the metal complex and HFIP.

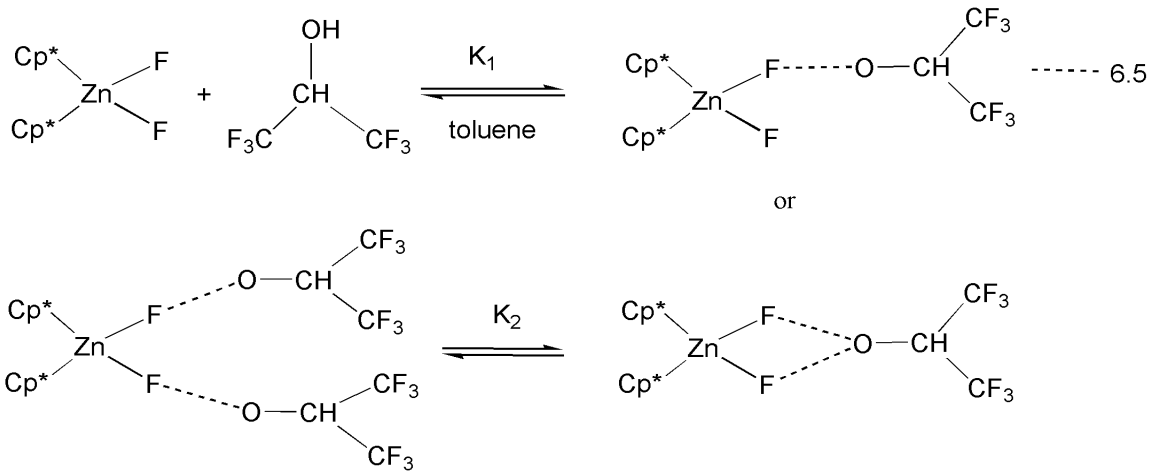

The equilibrium constants K_1 and K_2 for the formation of hydrogen bond adducts were determined by plotting the ^{19}F chemical shift vs ratio of concentration of **12**. The thermodynamic parameters ΔS^o_1, ΔS^o_2 and ΔH^o_1 and ΔH^o_2 have been calculated by plotting the titration curves at different temperatures and plotting In K vs T^{-1} (Van't Hoff plot). The values of ΔS^o_1, ΔS^o_2 and ΔH^o_1 and ΔH^o_2 determined are -68 ± 3, -49 ± 3 J K^{-1} mol^{-1} and -28.5 ± 0.8, -15.7 ± 0.7 kJ mol^{-1} respectively.

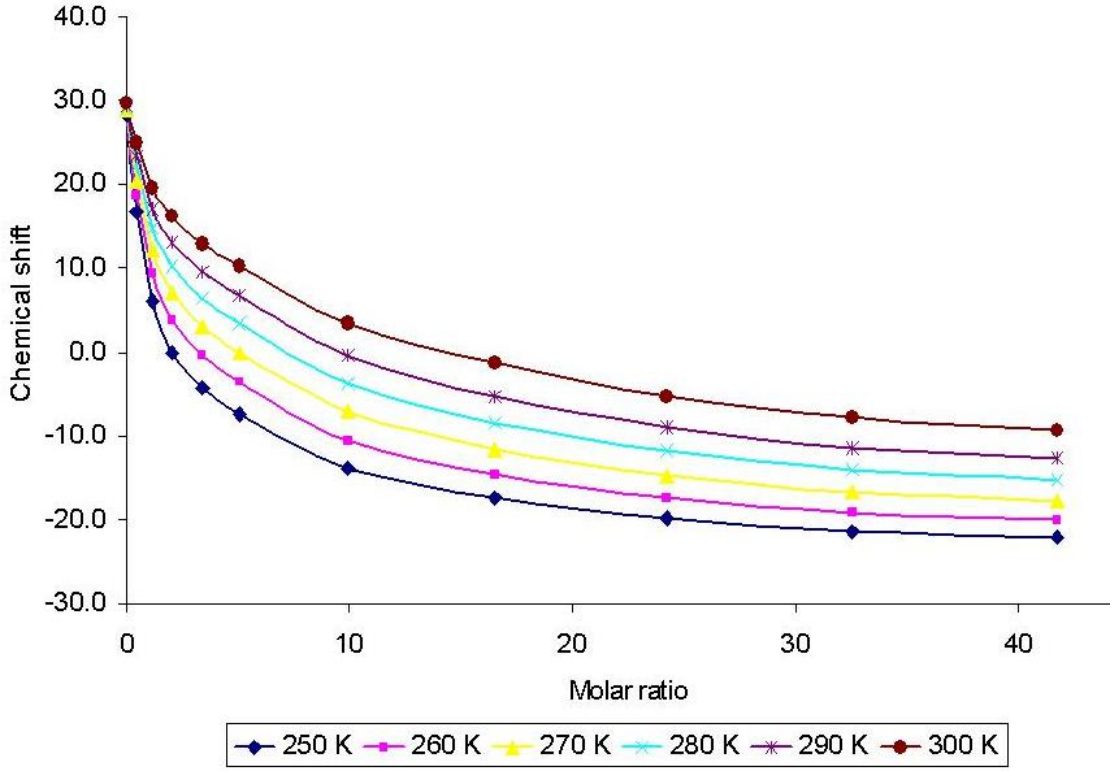

Fig 6. 14 Fitting curves for the titration of 12 vs HFIP for the whole range of temperature. The best fit of the points on the curves was in a range of ± 0.5 as seen from the residual graph on microsoft Excel®, macro program.

Experimental data used for fitting the curves. Concentration of the stock solution of **12** was 0.044 M and the concentration of indole stock solution was: 3.524M

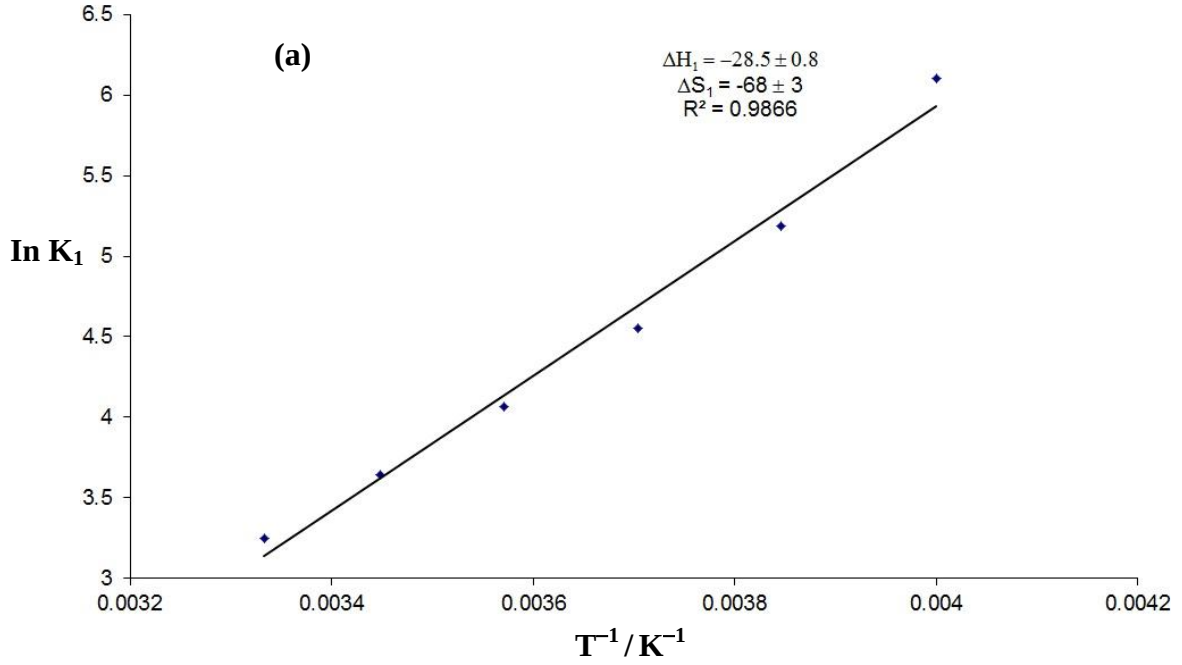

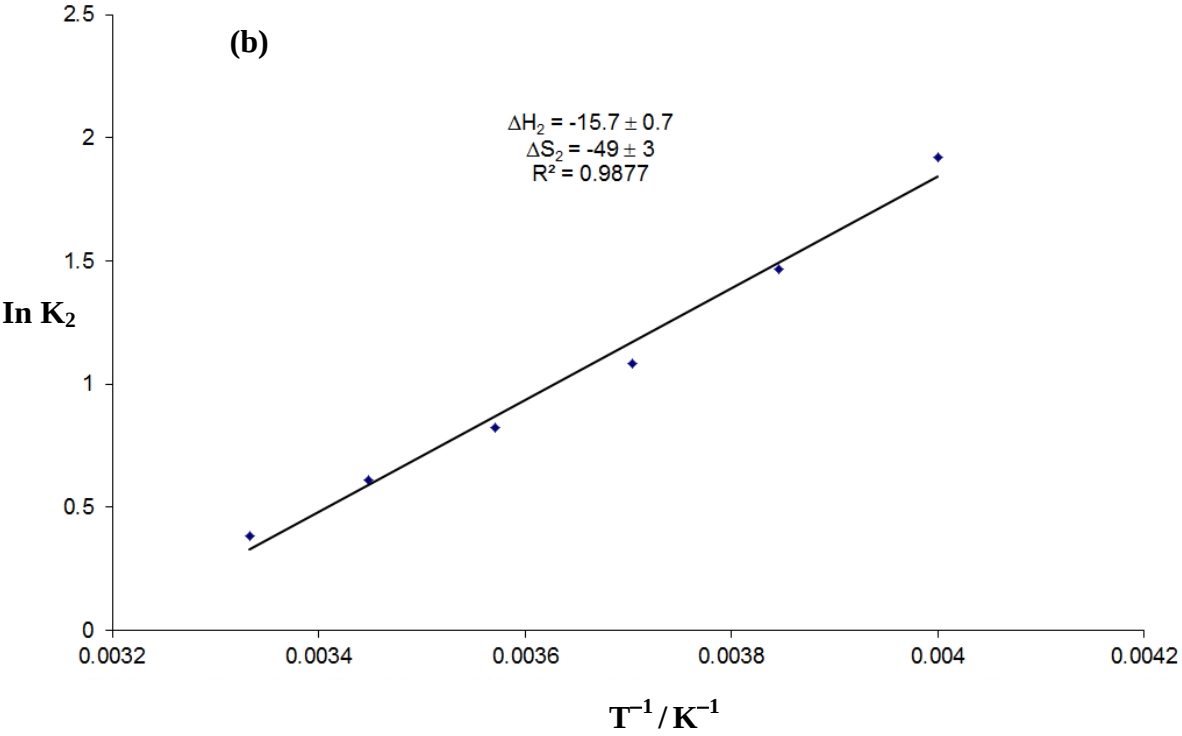

Fig 6. 15 Van't Hoff plot (a) for K_1 for HFIP/ZrF_2 adducts in toluene and (b) for K_2 for HFIP/ZrF_2 adduct in toluene.

Table 6.5 Experimental data used for fitting the curves (Fig 6.14). Concentration of the stock solution of **12** was 0.044 M and the concentration of HFIP stock solution were: 3.524M

$V_{MF}/\mu L$	$V_{HFIP}/\mu L$	**^{19}F NMR shift of the Zr-F_2**					
		250 K	**260 K**	**270 K**	**280 K**	**290 K**	**300 K**
522	0	28.27	28.62	28.90	29.19	29.33	29.66
536	6	6.06	9.30	12.10	14.76	17.11	19.55
533	10	-0.01	3.81	7.09	10.21	13.04	16.15
533	17	-4.31	-0.43	3.08	6.45	9.55	12.94
531	24	-7.41	-3.60	-0.01	3.46	6.73	10.24
527	48	-13.89	-10.53	-7.14	-3.73	-0.40	3.48
531	80	-17.48	-14.67	-11.63	-8.48	-5.34	-1.34
529	117	-19.87	-17.37	-14.72	-11.86	-8.98	-5.33
522	155	-21.37	-19.15	-16.71	-14.10	-11.39	-7.83
516	196	-22.2	-20	-17.77	-15.24	-12.67	-9.40
	K1	446	179	95.1	58.3	38.3	25.7
	K2	6.84	4.33	2.96	2.28	1.84	1.47

6.2.5 Halogen bonding of $(Cp^*)_2TiF_2$ and $(Cp^*)_2ZrF_2$ with C_6F_5I and $C_6F_4I_2$

The formation of a halogen bond adduct between $(Cp^*)_2TiF_2$ with C_6F_5I and $C_6F_4I_2$ and $(Cp^*)_2ZrF_2$ with C_6F_5I and $C_6F_4I_2$ was investigated by ^{19}F NMR spectroscopy but the change in the chemical shift was very small.

6.2.6 Test reactions of $(Cp^*)_2HfF_2$ (**13**) with Indole

Compound **13** also showed good solubility in toluene and a test experiment was performed on it. **13** has an the ^{19}F NMR resonance at δ –17.51 and upon addition of an excess amount of indole, it shifts by δ –4.45 ppm.

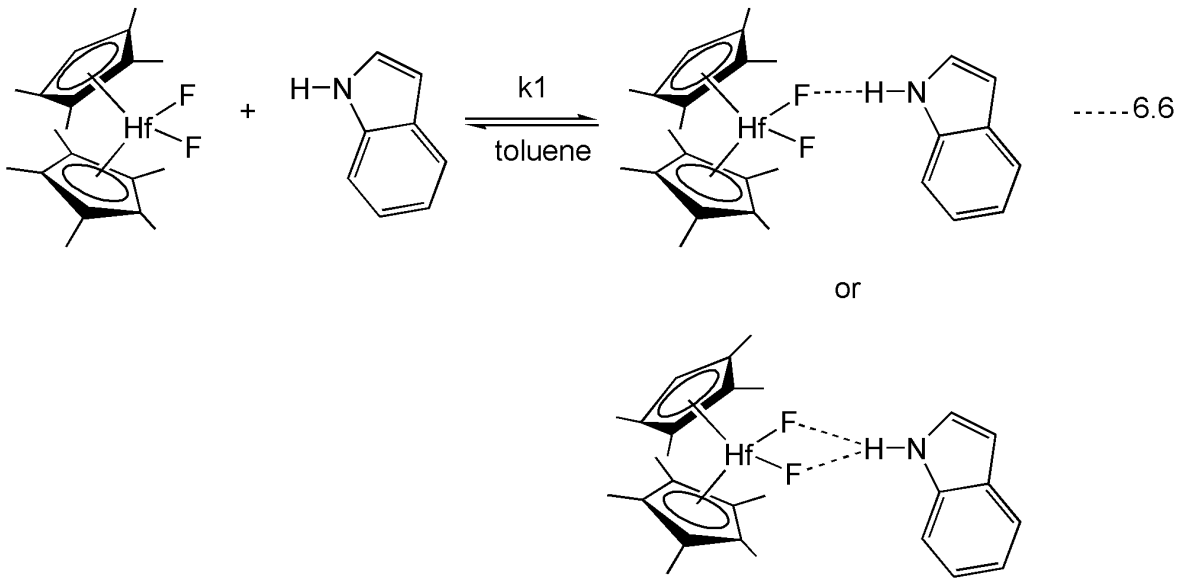

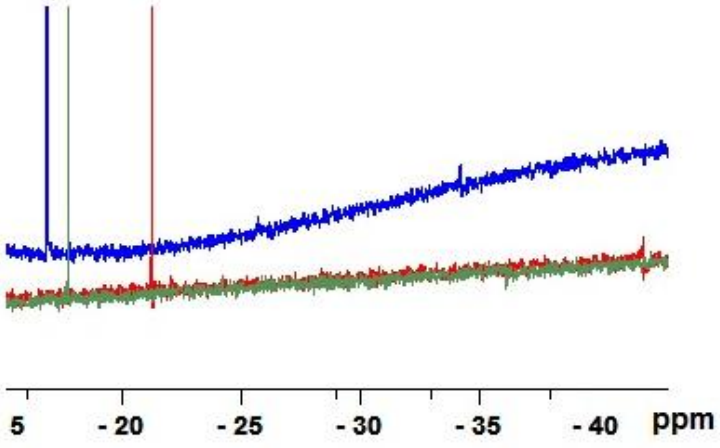

Fig 6. 16 [19] F NMR spectrum of (a) alone blue line, (b) adduct formed by adding 3 equivalents of indole green line and (c) adduct formed by adding excess of indole red line

6.2.7 Test reations of $(Cp^*)_2HfF_2$ with HFIP

Test experiment was also performed on the formation of adduct with HFIP. Upon addition of an excess amount of HFIP, ^{19}F NMR showed a shift of δ 17.34 ppm.

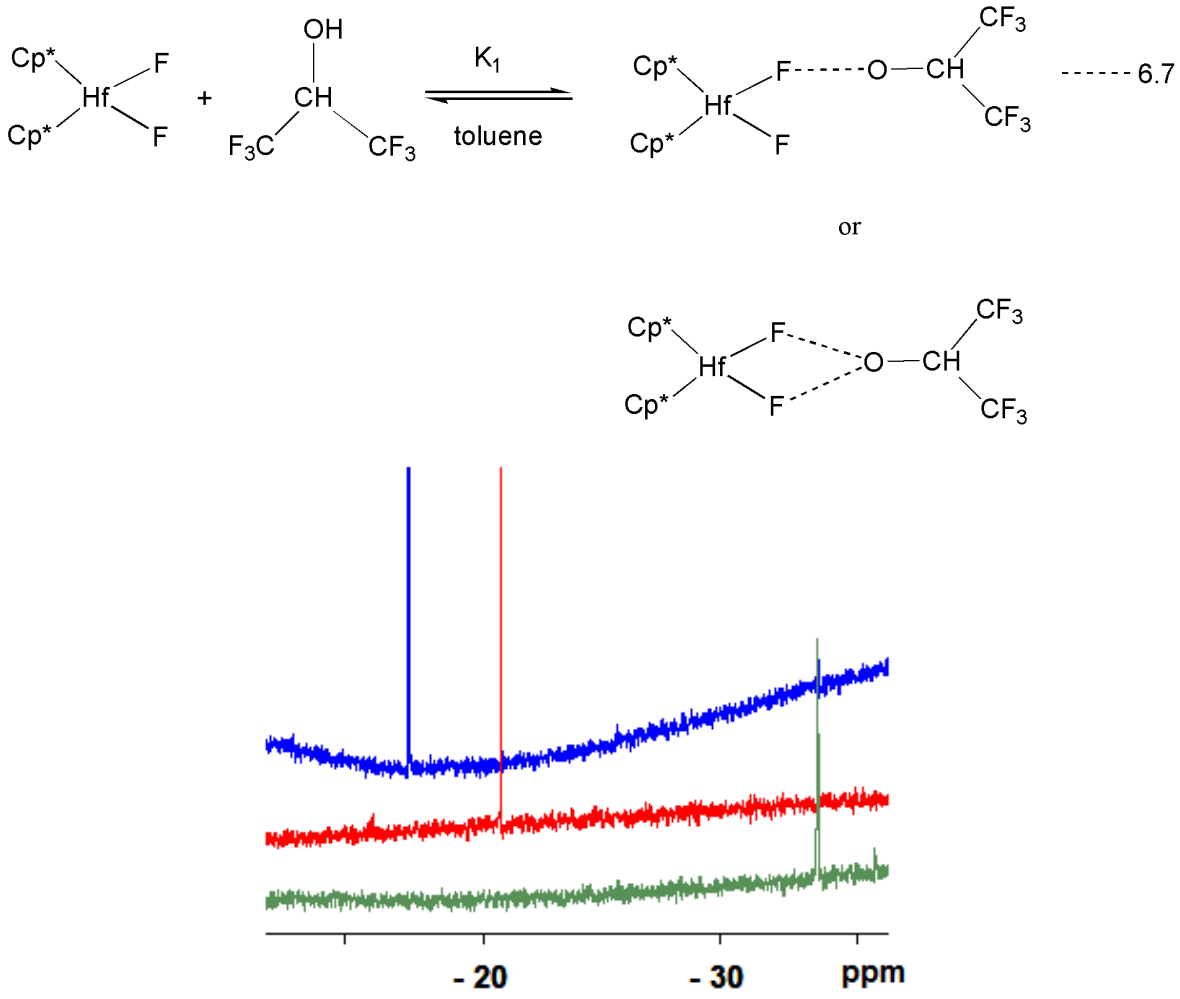

Fig 6. 17 ^{19}F NMR spectrum of (a) **13** alone blue line, (b) adduct formed by adding 3 equivalents of indole green line and (c) adduct formed by adding excess of indole red line

Table 6.6 Comparison of thermodynamic parameters of the hydrogen bonding of metal fluoride complexes with different hydrogen bond donors

Metal Complex	Hydrogen bond donor	ΔS^o_1 J K^{-1} mol^{-1}	ΔS^o_2 J K^{-1} mol^{-1}	ΔH^o_1 kJ mol^{-1}	ΔH^o_2 kJ mol^{-1}
$(Cp^*)_2TiF_2$	Indole	–67 ± 8	-	–27 ± 2	-
$(Cp^*)_2ZrF_2$	Indole	–36 ± 4	-	–11 ± 1	-
$(Cp^*)_2TiF_2$	HFIP	–35 ± 3	-	–19.2 ± 0.7	-
$(Cp^*)_2ZrF_2$	HFIP	–68 ± 3	–49 ±3	–28.5 ± 0.8	–15.7 ± 0.7

6.3 Discussion

Titration curves showed a dependence on the temperature and there is a significant change in the chemical shift caused by hydrogen–bond donors. This effect is more prominent at high concentrations of hydrogen–bond donors and reduced at low concentration. The equilibrium constants K_1 and K_2 have been calculated from plotting the molar ratio of the metal fluoride and hydrogen–bond donor vs ^{19}F chemical shifts. The value of K_2 is very small in comparison with K_1, so that sometimes it can be neglected. At the lowest temperature, K_1/K_2 ranges from 54 to 81 for the three determinations. The Van't Hoff plot obtained from equilibrium constants values and showed a good fit giving the correlation coefficient (R^2) greater than 0.97.

Values of $-\Delta S^o$ and $-\Delta H^o$ for hydrogen bond adduct of metal fluoride with indole decrease while moving from titanium to zirconium, while with HFIP the trend is the opposite way. The $-\Delta H$ values of the hydrogen bond adduct of $(Cp^*)_2TiF_2$ with indole is greater than that with HFIP, but for $(Cp^*)_2ZrF_2$ behaves in the opposite way. Hafnium difluoride will be discussed later. There are clearly some strange features in these data that require further investigation.

6.4 Conclusions

A series of d^0 transition metal difluoride complexes have been synthesized successfully and thermodynamic parameters of hydrogen–bonded adduct were studied. It was observed that ^{19}F NMR resonance is shifted more for the adduct hexafluoroisopropanol than adducts of indole. Trends in the increase or decrease of the thermodynamic parameters in the series will be established after completing the experiments of $(Cp^*)_2HfF_2$. There is a strong difference in the behavior of K_1 and K_2 although a second interaction is possible in difluoride complexes. K_2 is very small in comparison to K_1 and even second interaction cannot be observed for the hydrogen–bonded adducts of **12** with indole. The previously published measurements were for monofluorides.[22, 30] These are the first difluoride. The presence of two M–F bonds creates the opportunity for a second H-bonding interaction.

Halogen bond donors have very little effect on the d^0 transition metal difluoride complexes and there is a slight change in the chemical shift.

CONCLUSIONS AND FUTURE WORK

7.1. Conclusions

The aim of this work was to synthesize transition metal fluoride complexes and characterize them by mass spectrometry. For this purpose a series of NiF{2-C_5NF_3R)}$(PEt_3)_2$ complexes where R= H, F, NMe_2, CH_3O were synthesized by C-F activation and characterized by multinuclear NMR spectroscopy. All these complexes were successfully characterized by LIFDI mass spectrometry. EI mass spectrometry gave complete decomposition. Introduction of these complexes into positive ESI resulted in the loss of the fluoride ligand because the metal fluoride bond is very labile and it will decompose first to give positively charged ions.

$[(Cp^*)_2MF_2]$ where M = Ti, Zr, Hf were synthesized by reacting the respective dichloride with NaF. The ^{19}F chemical shifts of these of d^0 complexes appear in a completely different region from the d^8 complexes. $(Cp^*)_2TiF_2$, $(Cp^*)_2ZrF_2$ and $(Cp^*)_2HfF_2$ exhibits sharp resonances at δ 74.69, 28.72 and −17.51 respectively. These metallocene difluoride complexes were successfully characterized by LIFDI mass spectrometry and gave the molecular ion as base peak. The positive ion ESI mass spectra of these compounds showed the sodiated and potassited molecular ion as well as the ion formed by loss of one fluoride ligand while the other fluoride was retained i.e. $[M–F]^+$. The negative ion ESI showed the molecular ion but the ion intensity was low.

Upon subjecting to low energy CID the sodiated molecular ion of $[(Cp^*)_2MF_2]$ fragmented by the loss of NaF and NaH and potasstiated molecular ion by loss of KF and KH. The $[M–F]^+$ dissociated through the loss of HF resulting in the formation of $Cp^*(C_5Me_4CH_2)M^+$.

$M(DMEA)F_2$ (M = Zn, Co, Ni) are hygroscopic complexes and were synthesized in plastic ware. These complexes can be partially dried under vacuum but were completely dried in the glove box. The positive ion ESI spectrum of $Zn(DMEA)F_2$ and $Ni(DMEA)F_2$ gave the $[M–F]^+$ as a base peak while $Co(DMEA)F_2$ gave the molecular ion as base peak. The CID of these complexes occurs through the loss of two HF in molecular sequential steps.

The LIFDI mass spectra of ruthenium difluoride and bis bifluoride showed that these compounds F---HF bond is not very stable in the LIFDI as the samples are thermally

desorbed from the emitter. This can lead to the formation of $[LMF_2]^+$ (L= PMe_3, dppe and M = Ru) complexes as well as bridged complexes. The positive ion ESI of difluoride and bis bifluoride complexes led to the formation of $[LMF]^+$ (L= PMe_3, dppe and M=Ru) as well bridged complexes. The CID of $[M\text{-}F]^+$ resulted in the loss of PMe_3 instead of losing the second fluoride. The chloride analogue also behaved in a same way. Similar behavior was observed with the CID of $[Ni(PEt_3)(C_5F_3HN)(CH_3CN)F$ m/z 368 obtained from negative ion ESI. Upon isolating this ion in the ion trap and subjecting to multistage CID, fragmentation occurred with the loss of phosphine instead of losing fluoride. From these examples it is concluded that the presence of phosphine strengthens the metal fluoride bond in the mass spectrometry.

Platinium fluoride iodide complexes behaved in a similar way as the other transition metal difluoride complexes. LIFDI mass spectrometry showed the molecular ion while positive ion ESI is dominated by the ion formed by loss of fluoride ligand $[M–F]^+$. The positive ion ESI spectra of a series of platinum diiodide complexes were dominated by $[M–I]^+$. It is suggested that in competation of fluoride and iodide ion, fluoride is more labile and will be lost first.

The CID of $M(bpy)(X)CO)_3$ cations (M = Re, Mn and X= picoline, $POEt_3$) gave ions formed by loss of either CO or X depending upon the ancillary ligand X. In the multistage CID carbonyl ligands were lost sequentially.

We have successfully modified the Esquire Bruker ion trap for gas phase ion molecule reaction. The $M(bpy)X(CO)_2$ and $M(bpy)(CO)_3$ cations (M = Re, Mn and X = picoline, $POEt_3$) reacted successfully with those liquid and gaseous reagents which either have a double or triple bond or atom have lone pair of electron available for coordination at the empty site. The M^+ ion did not reacted with any neutral reagent probably due to the saturated coordination sphere. Ion molecule reactions were also not successful with the $[M–F]^+$ ions of transition metal difluoride.

We studied the formation of hydrogen bond adducts with a series of structurally similar difluoride complexes of group 4 transition metals. Indole and hexafluoroisopropanol were used as hydrogen bond donors. The chemical shift is very sensitive to the adduct formation and this effect is much greater in case of HFIP. $(Cp^*)_2TiF_2$ (**11**) forms 1:2 adducts with both indole and HFIP but the 2nd equilibrium constant is negligible while $(Cp^*)_2ZrF_2$ (**12**) forms 1:1 adduct with indole and 1:2 adducts with HFIP.

The ^{19}F chemical shift was determined between -250 and 300K and the thermodynamic parameters were calculated from this data. The values of ΔS^o_1 and ΔH^o_1 seem to be dependent on hydrogen bond donor. Both these values decreases from $(Cp^*)_2TiF_2$ to $(Cp^*)_2ZrF_2$ with the MF_2----indole adduct while behaves in opposite way with MF_2----HFIP adducts, where M = Ti, Zr.

7.2. Future work

It will be interesting to investigate the kinetics of the gas phase ion molecule reactions by reacting different concentrations of the neutral reagent with the rhenium and manganese tricarbonyls.

Secondly the gas phase ion molecule reactions are not very successful with the transition metal difluoride complexes although we managed to do similar reactions with platinum dichloride. We will try to investigate the reason for the failure and will try to overcome the difficulties.

Finally $(Cp^*)_2HfF_2$ has already been synthesized and purified, will be studied for hydrogen bonding. The thermodynamic parameters will be calculated so that comparison can be made in the column in the periodic table.

EXPERIMENTAL

8.1 General Methods

All the compounds were synthesized under inert conditions using glove box and schlenk lines (10^{-2} mbar). Analytical grade solvents were used for the synthesis and were dried by reflex under argon using drying agents. THF, toluene and methanol were dried over sodium. Ethanol was dried over magnesium turning (5 g) and iodine (0.5g). CH_2Cl_2, $CHCl_3$ was dried over CaH_2. All the solvent were distilled under argon.

8.1.1 Chemicals

The following compounds were purchased and used without any further purification; triphenylphosphine (PPh_3), bis(diethylphosphino)ethane (dppe), trimethylphosphine (PMe_3) and 1,3-bis-(diphenylphosphino)propane (dppp) (Sigma Aldrich). C_6F_6, C_5F_5N and C_5F_4HN (Aldrich) were dried over molecular sieves and stored in ampule provided with Young's taps. 1, 1 N,N-dimethylethylene-1,2-diamine (DMEA) (Aldrich) bis-pentamethylcyclopentadienyl titantium dichloride $(Cp^*)_2TiCl_2$, bis-pentamethylcyclopentadienyl zirconium dichloride $(Cp^*)_2ZrCl_2$ and bis-pentamethylcyclopentadienyl hafnium dichloride $(Cp^*)_2HfCl_2$ (Strem) zinc difluoride, cobalt difluoride, nickel difluoride (Strem). Potassium tetrachloroplatinate (K_2PtCl_4) (Aldrich). Tetramethylammonium fluoride (NMe_4F) tetrabutylammonium fluoride (NBu_4F), sodium fluoride, cesium fluoride triethylaminetrishydrofluoride ($NEt_3 \cdot 3(HF)$ and iodine (I_2) were purchased from Aldrich.

Gases; CO_2, D_2, SO_2, NO and isobutene (BOC) were already available in the lab.

8.1.2 Spectroscopic techniques

A Mattson research series FTIR spectrometer fitted with a KBr beam splitter was used to record infrared spectra. The sample chamber was purged with dry, CO_2-free air. Samples of compounds were run on the spectrometer as ITR, KBr pellets and nujol mulls held between KBr windows.

Elemental analyses for $NiF\{2\text{-}C_5NF_3(4\text{-}NMe_2)\}(PEt_3)_2$ and $NiF\{2\text{-}C_5NF_3(4\text{-}OMe)\}(PEt_3)_2$ were performed by Elemental Microanalysis Ltd, Devon, UK while for $[Zn(DMEA)_2F_2]$, $[Co(DMEA)_2F_2]$ and $[Ni(DMEA)_2F_2]$ were performed on elemental analyser (CE-440) from Exeter Analytical Inc. with a Sartorius (SE2) analytical balance .

8.1.3 NMR spectroscopy

NMR spectra were recorded on a Bruker AMX 500 (^{1}H 500.13 MHz; ^{31}P 202.46 MHz; ^{19}F at 407.4 MHz, ^{13}C 125.78 MHz) spectrometer. Protio-solvents such as benzene (δ 7.15), chloroform (δ 7.30), dichloromethane (δ 5.30), tetrahydrofuran (δ 1.73, δ 3.85) and toluene (δ 2.10) were used as reference for recording the ^{1}H NMR spectra while external H_3PO_4 (85%) was used as reference for ^{31}P {^{1}H} spectra. ^{19}F NMR spectra were referenced to external $CFCl_3$ at δ = 0.0 or internal C_6F_6 at δ = -162.9. All NMR deuterated solvents, d_6-benzene, d_2-dichoromethane, d_8-tetrahydrofuran, d_3-acetonitrile and d_8-toluene (Goss Scientific), were dried over sodium or potassium and distilled on high vacuum line. Chlorinated solvents were dried over molecular sieves. All NMR tubes (Wilmad 528-PP) were provided with a Young's tap to allow sealing under argon atmosphere. Samples were run from 250–300K. NMR spectra were simulated using *g-NMR*.[1]

8.1.4 Mass spectrometry

The LIFDI measurements were performed on a Waters Micromass GCT Premier orthogonal time-of-flight instrument set to one scan per second with resolution power of 6000 FWHM and equipped with a LIFDI probe from LINDEN GmbH.

Toluene was used for tuning the instrument. The polyethylene glycol probe was kept at ambient temperature with the emitter potential at 12 kV. Activated tungsten wire LIFDI emitters (13 mm tungsten from LINDEN) were ramped manually up to 100 mA for the emitter heating current during the experiment. Repeated short baking at 90 mA was used to clean up the emitter after each experiment. Solutions of the analytes (ca. 1 mg mL^{-1}) were made up in toluene or THF (a low freezing solvent is required in order to

prevent freezing in the capillary) in the glove box and transferred to a small vial. Transfer from the vial to the emitter is carried out by capillary. The spectra were calibrated with polyethylene glycols.

The ESI mass spectra and CID experiments were performed using Esquire 6000 (Bruker Daltonics, Berman, Germany) mass spectrometer equipped with quadrupole 3D ion trap, having a scan speed of 13000 m/z /s. The ESI source is of an orthogonal sprayer design and was operated at a spray voltage of 3-4 kV. Data were collected in standard scan mode. Nitrogen was used as bath gas (200-300˚C; 300-600 L/h) and nebulizing gas (5-10 psi). The analyte solution was introduced into the mass spectrometer by a syringe pump employing a 500 μL syringe. The sample solution was introduced at constant flow rate of 240-480 μL/h.

The millimolar solutions of various ions were prepared in methanol, water, and acetonitrile and are specified separately with different compounds. The precursor ions of interest were optimized (by changing parameters at capillary, skimmer, lenses, trap drive and octopoles) if needed. The desired ions were isolated in the ion trap and collisionally excited by probing at different collision energies between 0-25V. The ions were mass selected with a window of 4-10 Da in order to see the iosotopic signature of the ions can be observed.

The gas phase ion molecule reactions were performed on the same Esquire Bruker mass spectrometer equipped with electrospray ionization (ESI) and modified in a way to allow the introduction of neutral reagent via the helium background gas inlet line (details discussed in chapter 5).

The theoretical isotope patterns for mass spectra were calculated using ‘‘Fluorine chemistry mass spec simulator’’[2] and ChemDraw. Mass peaks are quoted for ^{58}Ni, ^{48}Ti, ^{90}Zr, ^{180}Hf, ^{64}Zn, ^{59}Co, ^{187}Re and ^{93}Nb.

8.3 Synthesis of monofluoride complexes of Ni and Rh

$Ru(PPh_3)_3(CO)(H)F$[3] was already prepared in the group by T. Beweries and was borrowed from him.

8.2.1 2,3,5,6-tetrafluoro-4-dimethylaminopyridine

The ligand was prepared by the method mentioned in the literature.[4] MS (EI) $[M]^+$ 181. ^{19}F NMR ($CDCl_3$) δ –90.9 (m), δ –160.0 (m).

8.2.2 Synthesis of NiF{2-C_5NF_3(4-NMe_2)}(PEt_3)$_2$

2,3,5,6-tetrafluoro-4-dimethylaminopyridine (0.258 g, 1.33 mmol) was added to the cloudy red-purple suspension of $Ni(COD)_2$ (0.3 g, 1.1 mmol) and PEt_3 (295 mg, 2.5 mmol) in hexane and stirred for 2 h. The color of the solution changed to yellow. Volatiles were removed under vacuum and the oily residue was dissolved in hexane and filtered through cannula. The filtrate was concentrated under vacuum to 2 mL and was crystallized at –25^o C for 2 h to give NiF{$C_5NF_3(NMe_2)$}(PEt_3)$_2$. Yield 0.548 g (1.12 mmol, 97%) MS (LIFDI from toluene solution) *m/z* 488 [M^+] 100%. Anal. Calcd for $C_{19}H_{36}F_4N_2NiP_2$: C, 46.65; H, 7.42; N, 5.73. Found: C, 46.52; H, 7.40; N, 5.55. ^{1}H NMR (C_6D_6): δ 1.23 (m, 18H, CH_3), 1.42 (bm, 12H, CH_2), 2.8 (t, J_{FH} = 2.3 Hz, 6H, NMe_2). ^{19}F NMR (C_6D_6): δ –367.74 (t, J = 47.9 Hz, 1F), –91.28 (t, J = 28.5 Hz, 1F), –121.15 (d, J = 24.5 Hz, 1F) –164.33 (d, J = 28.7 Hz, 1F) ^{31}P NMR(C_6D_6): δ 12.79 (d, J_{PF} = 47.4 Hz).

8.2.3 Synthesis of 2,3,5,6-tetrafluoro-4-methoxypyridine

The ligand was prepared by the literature method.[4] ^{19}F NMR (CD_2Cl_2) δ –95.7 (s, 2F), δ –156.9 (s, 2F), ^{1}H NMR (CD_2Cl_2) δ 2.28 (t, J_{PF} = 2.95 Hz, 2H) MS (EI) *m/z* $[M]^+$ 194 MS (ESI from CH_3CN solution) *m/z* $[M+H]^+$ 195.

8.2.4 Synthesis of NiF{2-C_5NF_3(4-OMe)}(PEt_3)$_2$

2,3,5,6-tetrafluoro-4-methoxypyridine (240 µL, 1.33 mmol) was added to the cloudy red purple suspension of $Ni(COD)_2$ (0.3 g, 1.0 mmol) and PEt_3 (291 mg, 2.4 mmol) in hexane and stirred for 2 h. The color of the solution changed to yellow. Volatiles were removed under vacuum and the oily residue was dissolved in hexane and filtered through cannula. The filtrate was concentrated to 2 mL and was crystallized at –25^o C for 72 h to yield NiF{2-C_5NF_3(OMe)}(PEt_3)$_2$. Yield 0.2 g (0.52 mmol 48%) Anal. Calcd for $C_{18}H_{33}F_4NNiOP_2$: C, 45.44; H, 7.43; N, 3.01. Found: C, 45.44; H, 7.43; N, 3.04.

IR (KBr disc, cm^{-1}) 3405(b), 2969(s), 2936(s), 2876(w), 1605(s), 1572(w), 1552(w), 1524(bw), 1485.7(s), 1460.8(s), 1453.0(s), 1432.9(s), 1418.3(s), 1393.5(s), 1377(s), 1256(w), 1100.6(s), 1031.3(s), 1003.5(w), 911(w), 810.4(s), 763.8(s), 725.0(s), 709.6(w), 679.9(w), 632.1(w), 514.1(w), 490.4(w).

^{1}H NMR (C_6D_6): δ 1.19 (m, CH_3), 1.36 (b, CH_2), 3.73 (s, OMe). ^{19}F NMR (C_6D_6): δ –368.78 (t, J_{PF} = 45.7 Hz, 1F), –170.11 (d, J_{FF} = 28.5 Hz, 1F) –128.33 (d, J_{FF} = 28.0 Hz, 1F), –88.71 (t, J_{FF} = 28.5 Hz, 1F). ^{31}P NMR(C_6D_6): δ 13.05 (d, J_{PF} = 48.1 Hz).

MS (LIFDI from toluene solution) *m/z* 475 $[M]^+$ 100%.

8.2.5 $Ni(PEt_3)_2(C_5F_4N)F$

Complex **3** was synthesized by literature method.[5] MS (LIFDI) *m/z* 463 [M^+, %100].

8.2.5.1 Reaction of $Ni(PEt_3)_2(C_5F_4N)F$ (3) with Tetramethyl Ammonium Fluoride

To the solution of **3** in THF in two NMR tubes was added TMAF. TMAF is sparingly soluble in THF. The first NMR tube was left at room temperature and was checked for the product formation by NMR spectroscopy after each 24 h for 11 days. The second NMR tube was heated at 50 ^{o}C and was checked for the product formation after 4h, 8h and 18 h by NMR spectroscopy. It was observed that same product (**3** coordinated to TMAF) was formed in both NMR tube (product discussed in Chapter 2).

The same reaction of **3** was repeated in CD_3CN, and $NiF(PEt_3)(C_5F_4N)(CD_3CN)$ (**4**) was obtained.

$NiF(PEt_3)(C_5F_4N)(CD_3CN)$ (**4**) ^{31}P NMR (C_6D_6): δ 15.72 (s) and ^{19}F NMR (C_6D_6): δ –324.5 (d, J_{PF} = J 52.4) –174.9 (dd, J_{FF} =17. 5, 1F); –152.6(m), –133.03 (t, J_{FF} = 27.38, 1F), –88.44 (m).

8.2.5.2 Reaction of $Ni(PEt_3)_2(C_5F_4N)F$ with CsF

The above mentioned experiment was repeated for the reaction of **3** with CsF (used as a fluorinating agent instead of TMAF). It was observed that CsF behaved in similar way as TMAF. The progress of the reaction was followed by ^{31}P NMR and ^{19}F NMR spectroscopy (table 2.2).

8.2.5.3 Reaction of $Ni(PEt_3)_2(C_5F_4N)F$ with CsF and 18-crown ether

To the solution of $Ni(PEt_3)_2(C_5F_4N)F$ in THF was added a small amount of CsF and 18-crown ether. CsF is sparingly soluble in THF. ^{19}F NMR shows the formation of two compounds which could not be identified.

8.2.5.4 Reaction of $Ni(PEt_3)_2(C_5F_4N)F$ with TBAF

No reaction of **3** was observed when TBAF was used as a fluorinating agent.

8.2.6 $Ni(PEt_3)_2(C_5F_3HN)F$

Complex **5** was prepared by reported method.[5]

MS (LIFDI) m/z 445 [M^+, 100%]

8.2.7 $Ni(PEt_3)_2(C_6F_5)F$

Complex **6** was prepared by reported method.[5]

MS (LIFDI) m/z 480 [M^+, 100%]

8.2.8 Synthesis of $Rh(PPh_3)_3F$ [6]

The synthesis of $Rh(PPh_3)_3F$ is a three step process.

$[RhCl(1,5\text{-}COD)_2]$[6] and $Rh_2(1,5\text{-}COD)_2\mu(OH)_2$[7] were prepared by literature method.

$Rh_2(1,5\text{-}COD)_2\mu(OH)_2$ (1.15 g, 0.33 mmol) and PPh_3 (1.15 g, 4.25 mmol) were suspended in ether (8 mL) and added $Et_3N.3HF$ (37 μL, 0.23 mmol) was added to the reaction mixture. After stirring for 2 h, the orange solid was precipitated and filtered through cannula, washed with ether and dried over vacuum.

$$(COD)_2Rh_2(\mu\text{–}OH)_2 + 2/3Et_3N(HF)_3 + 6PPh_3 \xrightarrow[3\text{-}4\ H]{Et_2O,\ 20^oC} Ph_3P\text{—}\underset{\displaystyle PPh_3}{\overset{\displaystyle PPh_3}{Rh}}\text{—}F \quad \text{------ 8.1}$$

The complex was recrystallized by dissolving in warm benzene and then adding hexane to the warm benzene, left overnight. Solvent was decanted by cannula and the crystals were dried under vacuum. As per literature the purity of the complexes was checked by NMR but the compound cannot be purified because it is change to its isomer at room temperature.[6]

8.3 Difluoride complexes of Ti, Zr and Hf

8.3.1 Synthesis of $(Cp^*)_2TiF_2$

Complex **11** was synthesized by literature method.[8]

^1H NMR (C_6D_6): δ 1.92 (s) and ^{19}F NMR (C_6D_6): δ 74.69 (s)

MS (LIFDI from toluene solution) *m/z* 356 [M^+] 100%. MS (ESI from CH_3CN solution) *m/z* 395, $[M+K]^+$, 379 $[M+Na]^+$, 337 $[M–F]^+$.

8.3.2 Syntheis of $(Cp^*)_2ZrF_2$

The synthesis followed the method for $(Cp^*)_2TiF_2$.[8] A suspension of bis(pentamethylcyclopentadienyl) zirconium dichloride (0.295 g, 0.64 mmol) and sodium fluoride (0.81 g, 19.2 mmol) in methanol (25 mL) was refluxed for 3 hours under argon in a two-necked round bottomed flask. The reaction mixture was allowed to cool to the room temperature and filtered.

$$(C_5Me_5)_2ZrCl_2 + 2NaF \xrightarrow[\text{Reflexed for 3h}]{\text{MeOH}} (C_5Me_5)_2ZrF_2 + 2NaCl \quad \text{---------} \quad 8.2$$

The solvent was pumped off under vacuum. The resultant solid compound was recrystallized from hexane. Yield 0.15g (60%).

^{1}H NMR (C_6D_6): δ 1.96 (s) and ^{19}F NMR (C_6D_6): δ 28.72 (s)

MS (LIFDI from toluene solution) m/z 398 [M^+] 100%. MS (ESI from CH_3CN solution) *m/z* 437 [M+K]$^+$, 421 [M+Na]$^+$, 397 [M–H]$^+$ and 379 [M–F]$^+$

8.3.3 Synthesis of $(Cp^*)_2HfF_2$

A two necked round bottomed flask was charged with bis(pentamethylcyclopentadienyl) hafnium dichloride (0.37g, 0.64 mmol), sodium fluoride (0.81 g, 19.2 mmol) and 25 mL methanol. The mixture was reflux for three hours under argon. The colour changed from red brown to yellow orange. The reaction mixture was allowed to cool to the room temperature and filtered.

$$(C_5Me_5)_2HfCl_2 + 2NaF \xrightarrow[\text{Reflexed for 6h}]{\text{MeOH}} (C_5Me_5)_2HfF_2 + 2NaCl \quad \text{---------} \quad 8.3$$

The solvent was pumped off under vacuum. The resultant solid compound was recrystallized from hexane. Yield 0.15g (60%).

^{1}H NMR (C_6D_6): δ 1.99 (s) and ^{19}F NMR (C_6D_6): δ –17.51 (s)

MS (LIFDI from toluene solution) *m/z* 488 [M^+] 100%, MS (ESI from CH_3CN solution) *m/z* 501 [M+Na]$^+$, 487 [M–H]$^+$ and 469 [M–F]$^+$.

8.4 Hydride, Monofluoride and difluoride complexes ruthenium

8.4.1 Synthesis of $(PMe_3)_4RuH_2$

8.4.1.1.Method (i)

$[RuCl_2(COD)]_x$ (0.352 g, 1.25 mmol), NaOH (1.00 g, 25 mmol) and PMe_3 (0.738 g, 9.7 mmol) were taken in a schlenk tube and transfer degassed sec-butyl alcohol (80 mL) was added. The reaction mixture was left stirring under argon for 3 hours and allowed to cool to the room temperature.

$$[RuCl_2(COD)_x + 4PMe_3 + 2NaOH + 2\text{-butanol} \longrightarrow Ru(PMe_3)_4H_2 + 2NaCl + COD + 2\text{-butanone} \quad \text{------ 8.4}$$

Excess NaOH was dissolved in degassed water (100 mL), the solvent was decanted and the residue was washed with degassed methanol, dried under vacuum using schlenk line and redissolved in benzene. The solution was filtered and the compound was dried under vacuum. Yield 28%

^1H NMR (C_6D_6): δ –9.60 (m), ^{31}P NMR (C_6D_6): δ –0.25 (t, J_{PF} = 26.2 Hz), δ –7.79 (m).

8.4.1.2.Method (ii)

This method consists of three steps. In the first step the $[Ru(PMe_3)_4Cl_2]$ is synthesized by refluxing $RuCl_3.xH_2O$ (0.3 g, 1.2 mmol) and PMe_3 (1 mL, 9.8 mmol) in degassed distilled water (10 mL) and ethanol (60 mL) for 4 hours producing dark green solution. It was left overnight at room temperature and the solvent was pumped off under vacuum. The solid was extracted with toluene and recrystallized.[9]

$[Ru(PMe_3)_4Cl_2]$ (0.15 g, 0.31 mmol) and $NaBH_4$ (0.1 g, 2.7 mmol) formed a suspension in 10 mL of benzene. With dropwise addition of methanol to this suspension produces effervescence and the mixture was stirred for 1 hour at room temperature. The volatiles were removed by vacuum and the solid was extracted with hexane (10 mL) three times. The solvent was removed under vacuum and dried solid. This white solid is a mixture of $[Ru(PMe_3)_4H_2]$ and $[RuH(BH_4)(PMe_3)_3]$. The mixture was dissolved in benzene and PM_3 (50 µL) was added. Before filtration, the solution was stirred for half an hour and solvent was removed under vacuum giving brown oil. A pure sample of **15** was obtained by subliming the oil was sublimed at 65°C using a cold finger.[10] Yield 0.097 g, 17%.

8.4.1.3.Method (iii)

To a very dark mixture of $RuCl_3.nH_2O$ (0.754 g, 3.14 mmol) in 39 mL of THF was added solution of PMe_3 (4 mL, 38.6 mmol) in 30 mL of THF which resulted in the formation of a brown precipitate which was stirred for 1 hour. It was stirred for a further 2 hours after the addition of $[NBu_4]BH_4$ (2.44 g, 9.48 mmol) which gave a dark yellow solution with some precipitate of $[NBu_4]Cl$. After filtration the THF was removed under vacuum and residue was extracted with 50 mL of pentane 4 times (Note. extracting more than 4 times takes the

impurities from the residue). The solvent was pumped off and solid was dried completely (6 h) under vacuum. The resultant product was pure.[11] Yield 0.2 g, 14%

^{1}H NMR (C_6D_6): δ –9.60 (m), ^{31}P NMR (C_6D_6): δ –0.24 (m), –0.74 (m).

8.4.2 Synthesis of $(PMe_3)_4Ru(FHF)_2$

To the solution of *cis*-$[Ru(PMe_3)_4H_2]$ (0.2 g, 0.41 mmol) in THF(50 mL) was added a two-fold excess of $NEt_3 \cdot 3HF$ (0.335 g, 0.93 mmol). After stirring the reaction mixture for 1 hour, the solvent was pumped off. The residue was extracted with benzene, and the extract was dried under vacuum. Recrystallization from THF at –30 °C gave yellow crystals of **15**.[12]

^{19}F NMR (C_6D_6): δ (b, –315.1, 2F) (d, –175.7 , 2F), ^{1}H NMR (C_6D_6): δ 13.4

8.4.3 Synthesis of $(PMe_3)_4RuF_2$

$(PMe_3)_4Ru(FHF)_2$ (50 g, 0.1 mmol) was dissolved in THF and excess of TMAF was added. The mixture was stirred for 48 h and filtered. The solvent was pumped off under vacuum.

$$Ru(PMe_3)_4(FHF)_2 + 2Me_4NF \longrightarrow Ru(PMe_3)_4F_2 + 2[Me_4N][FHF] \quad \text{- - - - - - - - - - - -} \quad 8.5$$

^{19}F NMR (C_6D_6): δ –325.4) ^{31}P NMR (C_6D_6): δ 2.98 (quintet, J_{PF} = 30.9 Hz, J_{PF} = 30.9 Hz), 22.10 (m), 21.13(m). MS (LIFDI from toluene solution) m/z 444 [M^+] 100%.

8.4.4 Synthesis of $Ru(dppe)_2H_2$

8.4.4.1. Method (i)

Dimethyl sulfoxide (5 mL) was added to $RuCl_3.H_2O$ (1.0 g, 4.8 mmol) in a schlenk tube and refluxed (5 min). The volume was reduced by half by pumping off the solvent and 20 mL of acetone was add which resulted in a yellow precipitate. The liquid was removed by filtration, the yellow solid was washed with acetone and ether, and finally dried under vacuum to yield $[RuCl_2(Me_2SO)_4]$.[13]

To the solution of $[RuCl_2(Me_2SO)_4]$ (0.70 g. 1.45 mmol) in CH_2Cl_2 was added a solution of dppe (1.2 g, 3 mmol) in CH_2Cl_2 (7 mL) and the yellow solution was stirred for 1 hour. The solvent was removed under vacuum and the solid was washed with hexane. This solid is a mixture of cis and trans isomers of $[Ru(dppe)_2Cl_2]$ in a 3:1 ratio approximately. This solid was dissolved in in CH_2Cl_2 and a concentrated solution is prepared, which is layered carefully by hexane. The pure cis isomer crystallizes out and could be separated

from the trans isomer. The top solvent is decanted and the crystals are washed with small amount of cold ethanol and dried under vacuum.

To the solution of cis-[$Ru(dppe)_2Cl_2$] (0.6 g, 0.62 mmol) in a mixture of THF (10 mL) and ethanol (3 mL) was added NaOEt (0.17 g, 2.5 mmol) under argon and the mixture stirred for 15 h. The solvent was pumped off and the solid was again dissolved in benzene and filtered through celite. The solution was layered with hexane and cis-[$Ru(dppe)_2H_2$] precipitated as cream crystals. To purify the compound, it was dissolved CH_2Cl_2 and filtered through cannula. Upon addition of hexane to the solution the complex was then precipitated and was separated by filtration. The complex was washed with hexane and dried under vacuum. The NMR spectra was in close agreement with literature.[14]

8.4.4.2.Method (ii)

The compound **17** was synthesized by method similar to the first method of preparation of trans-[$Ru(PMe_3)_4H_2$].

8.4.5 Synthesis of $Ru(dppe)_2H(FHF)$

A three-fold excess of $NEt_3 \cdot 3HF$ (0.537 g, 3.33 mmol) was added to the solution cis-[$Ru(dppe)_2H_2$] (1.0 g, 1.11 mmol) in THF (50 mL) and left stirring for 1 hour. The solvent was pumped off and the residue was extracted with benzene. The solvent was removed and the compound was dried under vacuum. It was recrystallized from THF/hexane at –30 °C.[12]

8.4.6 Synthesis of cis-$[Ru(dppp)_2H_2]$

This complex was prepared in an identical fashion to the first method of synthesis of trans-[$Ru(PMe_3)_4H_2$].[15]

8.4.7 Synthesis of trans-$Ru(dppp)_2H(FHF)$

This complex was prepared by the same method as that used for the synthesis of $Ru(dppe)_2H(FHF)$.[12]

8.5 Complexes of Platinum

8.5.1 Synthesis of $Pt(PPh_3)_4$

A solution of potassium hydroxide (0.35 g, 6.2 mmol) in ethanol (8mL) and water (2ml) was added to the clear solution of triphenylphosphine (3.8 g, 14.5mmol) in ethanol (50 mL) at 65^o. To the alkaline solution of triphenylphosphine was added a solution of potassium

tetrachloroplatinate (II) (1.31 g, 3.2 mmol) in 12.5 mL of water slowly (in about 20 minutes) stirring at 65^{o}. The yellow product is precipitated as with the addition of the solution. It was cooled to room temperature and filtered, washed with warm ethanol (40 mL), cold water (15 mL) and cold ethanol (15 mL). It was dried under vacuum for 2 hours.[16] Yield 2.5 g (66%).

^{31}P NMR (C_6D_6): δ 26.58 (s).

8.5.2 Synthesis of $Pt(PPh_3)_2I_2$ (9) [17]

I_2 (0.01 g, 0.4 mmol) was added to the suspension of $Pt(PPh_3)_4$ (0.05 g, 0.39 mmol) in 20 mL of toluene, stirred for one hour and left standing for 1 h. The liquid was decanted and the product was dried under vacuum. Yield 0.3g (78%).

^{31}P NMR ($CDCl_3$): δ 12.00 (J_{Pt-P} = 2496 Hz)

MS (EI) *m/z* 846.0 $[M–I]^+$, 718.1 $[(M–HI_2)]^+$, 262.1$[PPh_3]^+$.

MS (ESI from CH_2Cl_2 solution) *m/z* 846.6 $[M–I]^+$, 719.7 $[M–I_2]^+$.

Note: When the reaction was carried in ethanol according to the literature $Pt(PPh_3)_2HI$ **(12)** was formed.

8.5.3 Synthesis of $Pt(PPh_3)_2FI$

$Pt(PPh_3)_2I_2$ (0.2 g, 0.2 mmol) was dissolved in 30 mL CH_2Cl_2 and stirred with AgF (0.019 g, 0.3 mmol) at 45-50^{o} for 3 h. The suspension was filtered through a sintered glass celite column, the filtrate was concentrated under vacuum and 30 mL hexane was added. The resulting white precipitate was collected and dried under vacuum. Yield 0.1 g, (60%).

^{19}F NMR (C_6D_6): δ –310.68 (t, J_{PtF} = 541.4 Hz, 1F). ^{31}P NMR (C_6D_6): δ 15.25 (d, J_{PtP} = 2746 Hz, J_{PF} = 19.2 Hz).

MS (LIFDI from toluene solution) *m/z* 865.05 $[M]^+$ 100%.

MS (ESI from CH_3CN solution) *m/z* 845.9 $[M–F]^+$, 777.1 $[(M–I)+K]^+$.

8.5.4 Synthesis of cis–$Pt(PPh_3)_2F_2$

$Pt(PPh_3)_2I_2$ (0.2 g, 0.2 mmol) was dissolved in 30 mL CH_2Cl_2 and stirred with AgF (0.019 g, 0.3 mmol) at room temperature for 3 h. A sintered glass celite column was used to filter the suspension. The volume of the filtrate was reduced under vacuum and hexane (30 mL) was added. The resulting white precipitate was collected and dried under vacuum.[18]

^{19}F NMR $CDCl_3$: δ –215.75 (AA´MXX´, $J_{P(cis)F}$ = 14.7 Hz, J_{FF} = 85.1 Hz). ^{31}P NMR $CDCl_3$: δ 4.45 (AA´MXX´, J_{PtF} = 3832 Hz, $J_{P(trans)F}$ = 179.4 Hz, $J_{P(cis)P}$ = 22.4 Hz)

8.5.5 Synthesis of trans–$Pt(PPh_3)_2F_2$

$Pt(PPh_3)_2FI$ (0.2 g, 0.2 mmol) was dissolved in 30 mL CH_2Cl_2 and stirred with AgF (0.019 g, 0.3 mmol) at room temperature for 3 h. The suspension was filtered through a sintered glass celite column, the filtrate was concentrated in vacuum and 30 mL hexane was added. The resulting white precipitate was collected and dried in vacuum.

^{19}F NMR (C_6D_6) δ –436.96 (J_{PtP} = 535.1, J_{PF} = 14.80 Hz).

8.5.6 Synthesis of $Pt(DMSO)_2Cl_2$

K_2PtCl_4 (1.24 g, 0.0008 mol) was dissolved in 10 mL of water at 50˚C. To this solution was added DMSO (0.37 mL, 0.004 mol) at 50˚C. The solid was precipitated as yellow crystals when the solution was allowed to cool at room temperature. The compound was filtered, washed with water, ethanol and ether, and dried under vacuum for 4 hours.[19]

8.5.7 Synthesis of [Pt(dien)Cl]Cl

To a stirring suspension of (0.4 g, 0.94 mmol) $Pt(DMSO)_2Cl_2$ in 60 mL methanol was added a solution of diethylenetriamine (0.097 g, 0.94 mmol) in methanol (10 mL) and the mixture was refluxed for 3 h which resulted in a clear solution. The solution was concentrated under vacuum to ca 5 mL and unreacted $Pt(DMSO)_2Cl_2$ was removed by filtration. To the filtrate was added 30 mL of chloroform and product was precipitated as a white gelatinous solid. It was filtered, washed with chloroform, ether and air dried.[20]

$$Pt(DMSO)_2Cl_2 + (NH_2CH_2)_2NH \longrightarrow [Pt((NH_2CH_2)_2NH)Cl]Cl + DMSO$$

MS (ESI from water/methanol 50:50 mixture) *m/z* 334.0 $[M–Cl]^+$

8.6 Difluoride complexes of Zn, Co and Ni

8.6.1 Synthesis of $[Zn(DMEA)_2F_2]$

DMEA (10 mmol, 1.07 mL) was added to the suspension of white powdered zinc difluoride (5 mmol, 0.52 g) in 50 mL of methanol stirred overnight at room temperature. The ZnF_2 began to dissolve giving a colourless solution. Unreacted ZnF_2 was removed by filtration

and filtrate was concentrated by evaporating the solvent under vacuum for 5-6 h. The white precipitate was collected by decanting the top liquid and further dried in the glove box. The decanted liquid portion was also in left in the glove box and crystals were seen after 5 days. Note: Plastic ware used to do all steps of the experiment.

Anal. Calcd. for $[Zn(DMEA)_2F_2]$ $C_8H_{32}F_2N_4O_4Zn$: C, 34.35; H, 8.65; N, 20.03. Found: C, 31.58; H, 9.11; N, 18.39

^1H NMR (CD_3OD): δ 2.84 (t, J_{PF} = 5.1 Hz, 4H), 2.47 (J_{PF} = 5.8 Hz, 4H) and 2.30 (s, 12H)

^{19}F NMR (CD_3OD): δ −152 (s).

MS (ESI from CH_3OH solution) *m/z* 259.1 $[M–F]^+$, 239.1 $[M–HF_2]^+$.

8.6.2 Co(DMEA)$_2$F$_2$]

DMEA (10 mmol, 1.07 mL) was added to the pink suspension of cobalt difluoride (5 mmol, 0.48 g) in 50 mL of methanol and left stirring at room temperature overnight. The color of the reaction mixture began to change from pink to red/purple in color which indication for the formation of complex. Unreacted CoF_2 was removed by filtration and filtrate was concentrated by evaporating the solvent at room temperature. The concentrated solution was further concentrated under vacuum for 3 h and was left in the glove box for 7 days to get the compound fully dry.

Note: Plastic ware used to do all steps of the experiment .

Exact mass (ESI from MeOH solution) $^{12}C_8{}^1H_{24}{}^{59}Co^{19}F_2{}^{14}N_4$ *m/z* calculated 273.1301, found 273.1294

MS (ESI from CH_3OH solution) *m/z* 295.0 $[M+Na-H]^+$, 273.0 $[M]^+$, 254.0 $[M–F]^+$, 233.0 $[M–2HF]^+$.

Anal. Calcd. for $[Co(DMEA)_2F_2]$ $C_8H_{24}CoF_2N_4$; C, 35.17; H, 8.85; N, 20.51 found C, 35.80; H, 8.40; N, 19.48

8.6.3 Ni(DMEA)$_2$F$_2$]

DMEA (10 mmol, 1.09 mL) was added to the suspension of greenish yellow powdered NiF_2 (5 mmol, 0.48 g) in 50 mL of methanol and stirred overnight at room temperature. The NiF_2 began to dissolve giving a bluish green solution. Unreacted nickel fluoride was removed by filtration and filtrate was concentrated by evaporating the solvent at room temperature. The

concentrated solution was further concentrated under vacuum for 3 h and was left in the glove box for 7 days to get the compound fully dry.

Note: Plastic ware used to do all steps of the experiment.

MS (ESI from CH_3OH solution) *m/z* 273.4 $[M+F]^+$, 253.3 $[M-F]^+$, 233.4 $[M-HF_2]^+$.

Anal. Calcd. for $[Ni(DMEA)_2F_2]$ $C_8H_{24}CoF_2N_4$; C, 35.20; H, 8.86; N, 20.52 found C, 26.66; H, 8.52; N, 14.42

8.7 Synthesis of Mn salt

8.7.1 $[Mn(CO)_5Br]$

Manganese carbonyl (1.53 g, 0.33 mol.) was dissolved in carbon tetrachloride (50 mL) and added bromine (2.46 g, 0.43 mol.). The reaction mixture was stirred at 40 ºC and manganese bromide was precipitated. The solid was washed with three portions of water **(**25 mL) and dried under vacuum.[21]

$$Mn_2(CO)_{10} \xrightarrow{Br_2} 2Mn(CO)_5 \qquad \text{8.7}$$

8.7.2 $[Mn(CO)_3(bpy)Br]$

$Mn(CO)_3(bpy)Br$ precipitates as fine orange crystals upon refluxing $Mn(CO)_5Br$ (5.5 mmol, 1.5g) and bipyridine (5.4 mmol, 0.84g) in ether for half an hour. Precipitation was completed by cooling the reaction mixture to -80 ºC. The liquid portion was filtered off and product was washed with cold diethyl ether (30mL) and dried under vacuum.[22]

8.7.3 Synthesis of $[Mn(CO)_3(bpy)(pic)]PF_6$

To the solution $Mn(CO)_3(bpy)Br$ (0.042) in THF was added picoline (0.28 mL) and $AgPF_6$ (0.031g) and refluxed for 1 hour. The solution was passed through a celite column and solvent was pump off under vacuum. The yellow product was washed with excess of hexane to get rid of the unreacted picoline and dried completely under vacuum.

$$Mn(CO)_3(bpy)Br + AgPF_6 + C_6H_7N \xrightarrow[THF]{\text{reflux for 1 h}} [Mn(CO)_3(bpy)(C_6H_7N)]PF_6 + AgBr \qquad \text{8.8}$$

^{31}P NMR (CD_3COCD_3); δ −130.84 (sept, J_{PF} = 707.6 Hz), ^{19}F NMR(CD_3COCD_3); δ −73.91 (d, J_{PF} = 707.5 Hz)

MS (ESI from CH_3CN solution) *m/z* 387.9 $[M]^+$, 294.9 $[M–Picoline]^+$

8.8 Halogen bonding

8.8.1 Hydrogen bonding of $(Cp^*)_2TiF_2$ with indole

In order to do the titration experiment, two stock solutions were prepared. The stock solution of **11** was prepared by dissolving 106 mg of compound in 5.8 mL of protio toluene and transferred to 10 NMR labeled tubes in approximately equal volumes. Another stock solution of indole was prepared by dissolving 1.001 g of indole in 1.375 mL of protio toluene. One sample in NMR tube was left without adding the titrant (indole) and to the rest of the nine tubes were added different volumes of titrant (mentioned in table 6.2). The volumes were corrected for weight.

8.8.2 Hydrogen bonding of $(Cp^*)_2TiF_2$ with HFIP

The stock solution of **11** was prepared by dissolving 57 mg of compound in 6.65 mL of protio toluene and the solution of HFIP was prepared by dissolving 0.911 g of HFIP in 0.469 mL of protio toluene.

Approximately equal amounts of the solution of the complex were transferred to 11 NMR tubes (already labeled) and weight of the solution in each NMR tube was recorded.

The volume was corrected for weight. One sample was left without adding the titrant (used as a reference). To the rest of NMR tube was added different amount of the titrant solution (mentioned in table 6.2).

8.8.3 Hydrogen bonding of $(Cp^*)_2ZrF_2$ with indole

The stock solution of $Cp^*)_2ZrF_2$ (**12**) was prepared by dissolving 54 mg of compound in 6.65 mL of protio toluene and transferred to 10 NMR labeled tubes in approximately equal volumes. Aother stock solution of indole was prepared by dissolving 0.762 g of indole in 1.007 mL of protio toluene. One sample in NMR tube was left without adding the titrant (indole) and to the rest of nine was added different volume of titrant. The volume was corrected for weight

8.8.4 Hydrogen bonding of $(Cp^*)_2ZrF_2$ with HFIP

The stock solution of $Cp^*)_2ZrF_2$ (**12**) was prepared by dissolving 58 mg of compound in 6.55 mL of protio toluene and transferred to 10 NMR labeled tubes in approximately equal

volumes. Another stock solution of indole was prepared by dissolving 0.35 g of indole in 0.675 mL of protio toluene. One sample in NMR tube was left without adding the titrant (indole) and to the rest of nine was added different volume of titrant.

LIST OF ABBREVIATIONS

Spectroscopy

NMR	Nuclear Magnetic Resonance spectroscopy
δ	chemical shift
Hz	Hertz
d	doublet
dd	doublet of doublet/s
dt	doublet of triplet/s
q	quintet
J	coupling constant
s	singlet
t	triplet
m	multiplet
quart	quartet
MS	mass spectroscopy
EI	electron impact
ESI	electrospray ionization
FI	field ionization
FD	field desorption
LIFDI	liquid injection field desertion ionization
FAB	fast atom bombardment
QIT	quadrupole ion trap
TOF	time of flight
CID	collision induced dissociation
MS^n	multistage mass spectrometer or tandem mass spectrometer
$[M]^+$	molecular ion
IR	infra-red
br	broad

w	weak
s	strong
m	medium
IM	ion molecule reactions

Chemicals

Me	$-CH_3$
Et	$-CH_2CH_3$
^{i}Pr	$-CH(CH_3)_2$
Bu^{t}	$-C(CH_3)_3$
R	alkyl, aryl
Ar	aryl
Ph	phenyl
thf	tetrahydrofuran
cod	1,5-cyclooctadiene
dppe	diphenylphosphinoethane
dppp	diphenylphosphinopropane
PMe_3	trimethylphosphine
TBAF	tetrabutylammonium fluoride
TMAF	tetramethylammonium fluoride
DMSO	dimethyl sulfoxide
Cp*	pentamethylcyclopentadienyl
DMEA	1, 1 N,N-dimethylethylene-1,2-diamine
HFIP	1,1,1,3,3,3 hexafluoroisopropanol
pic	picoline
dien	diethylenetriamine

Units

min	minute(s)
h	hour(s)
ms	millisecond

K	Kelvin
eq	equivalents
mol	mole(s)
ppm	parts per million
Hz	hertz
cm^{-1}	centimeter
Å	angstrom
°	degree
atm	atmosphere
mA	millampere
V	volt
ΔS^o	entropy
ΔH^o	enthalpy
ΔG^o	Gibbs free energy

Special terms

MCAs	multiply charged anions
RCB	repulsive columbic barrier
HB	hydrogen bonding

REFERENCES

Chapter 1

(1) Amii, H.; Uneyama, K. *Chem. Rev.* **2009**, *109*, 2119.

(2) Bennett, C.; Clayton, S.; Tovell, D. *Chem. Ind.* **2010**, 21.

(3) Burdeniuc, J.; Jedlicka, B.; Crabtree, R. H. *Chem. Ber. Recl.* **1997**, *130*, 145.

(4) Crabtree, R. H.; Mingos, D. M. P. *Comprehensive Organometallic Chemistry III*; Elsevier: Oxford, 2007; Vol. 1.

(5) McClinton, M. A.; McClinton, D. A. *Tetrahedron* **1992**, *48*, 6555.

(6) Burton, D. J.; Yang, Z. Y. *Tetrahedron* **1992**, *48*, 189.

(7) Treichel, P. M.; Chaudhari, M. A.; Stone, F. G. A. *J. Organomet. Chem.* **1963**, *1*, 98.

(8) Kiplinger, J. L.; Richmond, T. G.; Osterberg, C. E. *Chem. Rev.* **1994**, *94*, 373.

(9) Spannenberg, A.; Arndt, P.; Baumann, W.; Burlakov, V. V.; Rosenthal, U.; Becke, S.; Weiss, T. *Organometallics* **2004**, *23*, 3819.

(10) Hofmann, P.; Unfried, G. *Chem. Ber. Recl.* **1992**, *125*, 659.

(11) Cronin, L.; Higgitt, C. L.; Karch, R.; Perutz, R. N. *Organometallics* **1997**, *16*, 4920.

(12) Clot, E.; Eisenstein, O.; Jasim, N.; Macgregor, S. A.; McGrady, J. E.; Perutz, R. N. *Acc. Chem. Res.* **2011**, *44*, 333.

(13) Yahav, A.; Goldberg, I.; Vigalok, A. *J. Am. Chem. Soc.* **2003**, *125*, 13634.

(14) Kaspi, A. W.; Goldberg, I.; Vigalok, A. *J. Am. Chem. Soc.* **2010**, *132*, 10626.

(15) Vigalok, A. *Organometallics* **2011**, *30*, 4802.

(16) Racowski, J. M.; Gary, J. B.; Sanford, M. S. *Angew. Chem. Int. Ed.* **2012**, *51*, 3414.

(17) Hollingworth, C.; Gouverneur, V. *Chem. Commun.* **2012**, *48*, 2929.

(18) Nyffeler, P. T.; Duron, S. G.; Burkart, M. D.; Vincent, S. P.; Wong, C. H. *Angew. Chem. Int. Ed.* **2005**, *44*, 192.

(19) Engle, K. M.; Mei, T.-S.; Wang, X.; Yu, J.-Q. *Angew. Chem. Int. Ed.* **2011**, *50*, 1478.

(20) Lee, E.; Kamlet, A. S.; Powers, D. C.; Neumann, C. N.; Boursalian, G. B.; Furuya, T.; Choi, D. C.; Hooker, J. M.; Ritter, T. *Science* **2011**, *334*, 639.

(21) Vincent, S. P.; Burkart, M. D.; Tsai, C. Y.; Zhang, Z. Y.; Wong, C. H. *J. Org. Chem.* **1999**, *64*, 5264.

(22) Zemva, B. *Comptes Rendus De L Academie Des Sciences Serie Ii Fascicule C-Chimie* **1998**, *1*, 151.

(23) Gut, R.; Rueede, J. *J. Organomet. Chem.* **1977**, *128*, 89.

(24) Tramsek, M.; Zemva, B. *J. Fluorine Chem.* **2006**, *127*, 1275.

(25) Tramsek, M.; Goreshnik, E.; Lozinsek, M.; Zemva, B. *J. Fluorine Chem.* **2009**, *130*, 1093.

(26) Brewer, S. A.; Holloway, J. H.; Hope, E. G. *Journal of the Chemical Society-Dalton Transactions* **1994**, 1067.

(27) Coleman, K. S.; Holloway, J. H.; Hope, E. G. *Journal of the Chemical Society-Dalton Transactions* **1997**, 1713.

(28) Coleman, K. S.; Fawcett, J.; Holloway, J. H.; Hope, E. G.; Nassar, R. *J. Fluorine Chem.* **2001**, *112*, 185.

(29) Fawcett, J.; Harding, D. A. J.; Hope, E. G. *Dalton Transactions* **2010**, *39*, 5827.

(30) Pimentel, G. C. *J. Chem. Phys.* **1951**, *19*, 446.

(31) Emsley, J. *Chem. Soc. Rev.* **1980**, *9*, 91.

(32) Jasim, N. A.; Perutz, R. N.; Foxom, S. P.; Walton, P. H. *J. Am. Chem. Soc., Dalton Trans* **2001**, 1676.

(33) Jasim, N. A.; Perutz, R. N.; Archibald, S. J. *Dalton Trans.* **2003**, 2184.

(34) Jasim, N. A.; Perutz, R. N. *J. Am. Chem. Soc.* **2000**, *122*, 8685.

(35) Braun, T.; Perutz, R. N. *Chem Commun.* **2002**, 2749.

(36) Duthaler, R. O.; Hafner, A. *Angew. Chem. Int. Ed. Engl.* **1997**, *36*, 43.

(37) Murphy, E. F.; Murugavel, R.; Roesky, H. W. *Chem. Rev.* **1997**, *97*, 3425.

(38) Mankad, N. P.; Toste, F. D. *Chem. Sci.* **2012**, *3*, 72.

(39) Scharf, A.; Goldberg, I.; Vigalok, A. *Organometallics* **2012**, *31*, 1275.

(40) Ball, N. D.; Sanford, M. *J. Am. Chem. Soc.* **2009**, *131*, 3796.

(41) Robinson, P. S. D.; Khairallah, G. N.; Silva, G.; Lioe, H.; O'Hair, R. A. J. *Angew. Chem. Int. Ed.* **2012**, *51*, 3812.

(42) Parsons, A. T.; Senecal, T. D.; Buchwald, S. L. *Angew. Chem. Int. Ed.* **2012**, *51*, 2947.

(43) Cho, E. J.; Buchwald, S. L. *Org. Lett.* **2011**, *13*, 6552.

(44) Maimone, T. J.; Milner, P. J.; Kinzel, T.; Zhang, Y.; Takase, M. K.; Buchwald, S. L. *J. Am. Chem. Soc.* **2011**, *133*, 18106.

(45) *Mass Spectrometry of Inorganic, Coordination and Organometallic Compounds,*; Henderson, W.; McIndoe, J. S., Eds.; Wiley 2005.

(46) http://www.bdal.com/uploads/media/esquire6000.pdf.

(47) Yamashita, M.; Fenn, J. B. *J. Phys. Chem.* **1984**, *88*, 4451.

(48) Gaskell, S. J. *J. Mass Spectrom.* **1997**, *32*, 677.

(49) Milman, B. L. *Rapid Commun. Mass Spectrom.* **2003**, *17*, 1344.

(50) Wang, G.; Cole, R. G. *J. Am. Soc. Mass Spectrom.* **1996**, *7*, 1050.

(51) Pashynska, V. A.; Kosevich, M. V.; Van den Heuvel, H.; Claeys, M. *Rapid Commun. Mass Spectrom.* **2006**, *20*, 755.

(52) Bossee, A.; Fournier, F.; Tasseau, O.; Bellier, B.; Tabet, J. C. *Rapid Commun. Mass Spectrom.* **2003**, *17*, 1229.

(53) Henderson, W.; Cameron, E. *Inorg. Chim. Acta* **1999**, 183.

(54) Kaluderovic, G. N.; Vasiljevic, T. M.; Lausevic, M. D.; Gaballa, A. S.; Sabo, T. J. *Monatsh. Chem.* **2009**, *140*, 553.

(55) Gross, J. H.; Nieth, N.; Linden, H. B.; Blumbach, U.; Richter, F. J.; Tauchert, M. E.; Tompers, R.; Hofmann, P. *Anal. Bioanal. Chem.* **2006**, *386*, 52.

(56) Gross, J. H. *J. Am. Soc. Mass Spectrom.* **2007**, *18*, 2254.

(57) Beweries, T.; Brammer, L.; Jasim, N. A.; McGrady, J. E.; Perutz, R. N.; Whitwood, A. C. *J. Am. Chem. Soc.* **2011**, *133*, 14338.

(58) Nova, A.; Erhardt, S.; Jasim, N. A.; Perutz, R. N.; Macgregor, S. A.; McGrady, J. E.; Whitwood, A. C. *J. Am. Chem. Soc.* **2008**, *130*, 15499.

(59) Richard, A.; O'Hair, J. *Chem. Commun.* **2006**, 1469.

(60) Chen, Y. J.; Fenn, P. T.; Ng, C. Y. *Chem. Phys. Lett.* **2001**, *336*, 105.

(61) Fooladi, E.; Krapp, A.; Sekiguchi, O.; Tilset, M.; Uggerud, E. *Dalton Transactions* **2010**, *39*, 6317.

(62) Gerdes, G.; Chen, P. *Organometallics* **2003**, *22*, 2217.

(63) Robinson, P. S. D.; Khairallah, G. N.; da Silva, G.; Lioe, H.; O'Hair, R. A. J. *Angew. Chem. Int. Ed.* **2012**, *51*, 3812.

(64) Rijs, N. J.; O'Hair, R. A. J. *Dalton Trans.* **2012**, *41*, 3395.

(65) Rijs, N. J.; O'Hair, R. A. J. *Organometallics* **2010**, *29*, 2282.

(66) Rijs, N. J.; Sanvido, G. B.; Khairallaha, G. N.; O'Hair, R. A. J. *Dalton Trans.* **2010**, *39*, 8655.

(67) Scheller, M. K.; Compton, R. N.; Cederbaum, L. S. *Science* **1995**, *270*, 1160.

(68) Boxford, W. E.; Pearce, J. K.; Dessent, C. E. H. *Chem. Phys. Lett.* **2004**, *399*, 465.

(69) Boxford, W. E.; Dessent, C. E. H. *Phys. Chem. Chem. Phys.* **2006**, *8*, 5151.

(70) Wang, X. B.; Nicholas, J. B.; Wang, L. S. *J. Chem. Phys.* **2000**, *113*, 10837.

(71) Wang, L. S.; Wang, X. B. *Abstr. Pap. Am. Chem. Soc.* **2000**, *220*, 178.

(72) Wang, X. B.; Wang, L. S. *J. Phys. Chem. A* **2000**, *104*, 4429.

(73) Milner, E. M.; Nix, M. G. D.; Dessent, C. E. H. *Phys. Chem. Chem. Phys.* **2011**, *13*, 18379.

(74) Richmond, T. G. *Coord. Chem. Rev.* **1990**, *105*, 221.

(75) Jeffrey, G.; Saenger, A. W. *Hylrogrn Bonding in Biological Structures*; Springer: Berlin, 1991.

(76) Jeffery, G. A.; Saenger, A. W. *Hydrogen bonding in biological structures*; Springer: Berlin, 1994.

(77) Lee, J. C.; Peris, E.; Rheingold, A. L.; Crabtree, R. H. *J. Am. Chem. Soc.* **1994**, *116*, 11014.

(78) Yap, G. P. A.; Rheingold, A. L.; Das, P.; Crabtree, R. H. *Inorg. Chem.* **1995**, *34*, 3474.

(79) Wessel, J.; Lee, J. C.; Peris, E.; Yap, G. P. A.; Fortin, J. B.; Ricci, J. S.; Sini, G.; Albinati, A.; Koetzle, T. F.; Eisenstein, O.; Rheingold, A. L.; Crabtree, R. H. *Angew. Chem. Int. Ed. Engl.* **1995**, *34*, 2507.

(80) Peris, E.; Wessel, J.; Patel, B. P.; Crabtree, R. H. *J. Chem. Soc., Chem. Commun.* **1995**, 2175.

(81) Aullon, G.; Bellamy, D.; Brammer, L.; Bruton, E. A.; Orpen, A. G. *Chem. Commun.* **1998**, 653.

(82) Brammer, L.; Bruton, E. A.; Sherwood, P. *New J. Chem.* **1999**, *23*, 965.

(83) Brammer, L.; Bruton, E. A.; Sherwood, P. *Cryst. Growth Des.* **2001**, *1*, 277.

(84) Aakeroy, C. B.; Seddon, K. R. *Chem. Soc. Rev.* **1993**, *22*, 397.

(85) Ermer, O.; Eling, A. *J. Chem. Soc., Perkin Trans. 2* **1994**, 925.

(86) Seto, C. T.; Whitesides, G. M. *J. Am. Chem. Soc.* **1990**, *112*, 6409.

Chapter 2

(1) *Organofluorine Chemistry: Principles and Commercial Applications*; Banks, R. E.; Smart, B. E.; Tatlow, J. C., Eds.; Plenum New York abd London, 1994.

(2) Thrasher, J. S.; Strauss, S. H. In *ACS Symposium Series 555*; American Chemical Society: San Francisco, California, 1992.

(3) Macgregor, S. A.; Roe, D. C.; Marshall, W. J.; Bloch, K. M.; Bakhmutov, V. I.; Grushin, V. V. *J. Am. Chem. Soc.* **2005**, *43*, 15304.

(4) Doherty, N. M.; Hoffman, N. W. *Chem. Rev* **1991**, *91*, 553.

(5) Schaub, T.; Backes, M.; Radius, U. *Eur. J. Inorg. Chem.* **2008**, 2680.

(6) Braun, T.; Perutz, R. N.; Sladek, M. I. *Chem Commun* **2001**, 2254.

(7) Braun, T.; Perutz, R. N. *Chem Commun.* **2002**, 2749.

(8) Jasim, N. A.; Perutz, R. N.; Whitwood, A. C.; Braun, T.; Izundu, J.; Neumann, B.; Rothfeld, S.; Stammler, H.-G. *Organometallics* **2004**, *23*, 6140.

(9) Braun, T.; Parsons, S.; Perutz, R. N.; Voith, M. *Organometallics* **1999**, *18*, 1710.

(10) Yahav, A.; Goldberg, I.; Vigalok, A. *Inorg. Chem.* **2005**, *44*, 1547.

(11) Ball, N. D.; Sanford, M. *J. Am. Chem. Soc.* **2009**, *131*, 3796.

(12) Ball, N. D.; Kampf, J. W.; Sanford, M. *Dalton Trans* **2010**, *39*, 632.

(13) Nova, A.; Erhardt, S.; Jasim, N. A.; Perutz, R. N.; Macgregor, S. A.; McGrady, J. E.; Whitwood, A. C. *J. Am. Chem. Soc.* **2008**, *130*, 15499.

(14) Yahav, A.; Goldberg, I.; Vigalok, A. *J. Am. Chem. Soc.* **2003**, *125*, 13634.

(15) Herzog, A.; Liu, F. Q.; Roesky, H. W.; Demsar, A.; Keller, K.; Noltemeyer, M.; Pauer, F. *Organometallics* **1994**, *13*, 1251.

(16) Anbarasan, P.; Neumann, H.; Beller, M. *Angew. Chem. Int. Ed.* **2010**, *49*, 2219.

(17) Tang, P.; Ritter, T. *Tetrahedron* **2011**, *67*, 4 4 4 9.

(18) Murphy, V. J.; Hascall, T.; Chen, J. Y. *J. Am. Chem. Soc.* **1996**, *118*, 7428.

(19) Whittlesey, M. K.; Perutz, R. N.; Greener, B.; Moor, M. H. *Chem Commun.* **1997**, *187*.

(20) Jasim, N. A. Doctor of Philosophy, University of York, 2000.

(21) Banks, R. E.; Burgess, J. E.; Cheng, W. M.; Haszeldine, R. N. *J. Chem. Soc.* **1965**, 575.

(22) Dransfield, T. A.; Nazir, R.; Perutz, R. N.; Whitwood, A. C. *J. Fluorine Chem.* **2010**, *131*, 1213.

(23) http://www.nobelprize.org/nobel_prizes/chemistry/laureates/2002/.

(24) Cronin, L.; Higgitt, C. L.; Karch, R.; Perutz, R. N. *Organometallics* **1997**, *16*, 4920.

(25) Johnson, S. A.; Taylor, E. T.; Cruise, S. J. *Organometallics* **2009**, *28*, 3842.

(26) Doster, M. E.; Johnson, S. A. *Angew. Chem. Int. Ed.* **2009**, *48*, 2185.

(27) Schaub, T.; Backes, M.; Radius, U. *J. Am. Chem. Soc.* **2006**, *128*, 15964.

(28) Cariati, F.; Monica, G. L. *Inorg. Synth.* **1968**, *11*, 105.

(29) Tayim, H. A.; Aklj, N. S. *Inorg, Nucl. Chem.* **1974**, *36*, 1071.

(30) Gassman, P. G.; H., W. C.; David, M. W. *Organometallics* **1984**, *3*, 385.

(31) Piglosiewicz, I. M.; Kraft, S.; Beckhaus, R.; Hasse, D.; Saak, W. *Eur. J. Inorg. Chem.* **2005**, 938.

(32) Kraft, B. M.; Jones, W. D. *J. Am. Chem. Soc* **2002**, *124*, 8681.

(33) Jasim, N. A.; Perutz, R. N.; Foxom, S. P.; Walton, P. H. *J. Am. Chem. Soc., Dalton Trans* **2001**, 1676.

(34) http://home.cc.umanitoba.ca/~budzelaa/gNMR/gNMR.html.

(35) *NMR and chemistry, an introduction to modern NMR spectroscopy*; Akitt, J. W.; Mann, B. E., Eds.; nelson thornes: Cheltenham, 2002.

(36) Henderson, W.; Cameron, E. *Inorg. Chim. Acta* **1999**, 183.

(37) http://www.nobelprize.org/nobel_prizes/physics/laureates/1989/paul-lecture.html.

Chapter 3

(1) Cronin, L.; Higgitt, C. L.; Karch, R.; Perutz, R. N. *Organometallics* **1997**, *16*, 4920.

(2) Macgregor, S. A.; Roe, D. C.; Marshall, W. J.; Bloch, K. M.; Bakhmutov, V. I.; Grushin, V. V. *J. Am. Chem. Soc.* **2005**, *43*, 15304.

(3) Murphy, V. J.; Hascall, T.; Chen, J. Y. *J. Am. Chem. Soc.* **1996**, *118*, 7428.

(4) Jasim, N. A.; Perutz, R. N.; Foxom, S. P.; Walton, P. H. *J. Am. Chem. Soc., Dalton Trans* **2001**, 1676.

(5) Furuya, T.; Ritter, T. *J. Am. Chem. Soc*, **2008**, *130*, 10060.

(6) Ball, N. D.; Kampf, J. W.; Sanford, M. *Dalton Trans* **2010**, *39*, 632.

(7) Yahav, A.; Goldberg, I.; Vigalok, A. *Inorg. Chem.* **2005**, *44*, 1547.

(8) Whittlesey, M. K.; Perutz, R. N.; Greener, B.; Moor, M. H. *Chem Commun.* **1997**, *187*.

(9) Schaub, T.; Backes, M.; Radius, U. *Eur.J.Inorg.Chem.* **2008**, 2680.

(10) Schaub, T.; Fischer, P.; Steffen, A.; Braun, T.; Radius, U.; Mix, A. *J. Am. Chem. Soc.* **2008**, *130*, 9304.

(11) Braun, T.; Perutz, R. N. *Chem Commun.* **2002**, 2749.

(12) Amii, H.; Uneyama, K. *Chem. Rev.* **2009**, *109* 2119

(13) Doster, M. E.; Johnson, S. A. *Angew. Chem. Int. Ed.* **2009**, *48*, 2185.

(14) Johnson, S. A.; Huff, C. W.; Mustafa, F.; Saliba, M. *J. Am. Chem. Soc.* **2008**, *130* 17278.

(15) Schaub, T.; Backes, M.; Radius, U. *J. Am. Chem. Soc.* **2006**, *128*, 15964.

(16) Schaub, T.; Radius, U. *Chem. Eur. J.* **2005**, *11*, 5024.

(17) Jäger-Fiedler, U.; Arndt, P.; Baumann, W.; Spannenberg, A.; Burlakov, V. V.; Rosenthal, U. *Eur. J. Inorg. Chem.* **2005**, 2842.

(18) Steffen, A.; Sladek, M. I.; Braun, T.; Neumann, B.; Stammler, H.-G. *Organometallics* **2005**, *24*, 4057.

(19) Johnson, S. A.; Taylor, E. T.; Cruise, S. J. *Organometallics* **2009**, *28*, 3842.

(20) Braun, T.; Steffen, A.; Schorlemer, V.; Neumann, B.; Stammler, H. G. *Dalton Trans.* **2005**, 3331.

(21) Braun, T.; Schorlemer, V.; Neumann, B.; Stammler, H. G. *J. Fluorine Chem.* **2006**, *127*, 367.

(22) Henderson, W.; Cameron, E. *Inorg. Chim. Acta* **1999**, 183.

(23) Huang, W.-C.; Tsai, C.-C.; Chen, C.-L.; Chen, T.-Y.; Chen, Y.-P.; Lin, Y.-S.; Lu, P.-J.; Lin, C.-M.; Wang, S.-H.; Tsao, C.-W.; Wang, C.-Y.; Cheng,

Y.-L.; Hsieh, C.-Y.; Tseng, P.-C.; Lin, C.-F. *FASEB (Fed Am Soc Exp Biol)* **2011**, *25*, 3661.

(24) Gomer, R.; Inghram, M. G. *J. Am. Chem. Soc* **1955**, *77*, 500.

(25) Beckey, H. D. *Int. J. Mass spectrom. Ion Phys.* **1969**, *2*, 495.

(26) *Mass Spectrometry of Inorganic, Coordination and Organometallic Compounds,*; Henderson, W.; McIndoe, J. S., Eds.; Wiley 2005.

(27) Winkler, H. U.; Beckey, H. D. *Biochem. Biophys. Res. Commun.* **1972**, *46*, 391.

(28) *Field Desorption Mass Spectrometry,*; Prokai, L., Ed.; Marcel Dekker, 1990.

(29) Smith, D. F.; Schaub, T. M.; Rodgers, R. P.; Hendrickson, C. L.; Marshall, A. G. *Anal. Chem.* **2008**, *80*, 7379.

(30) Gross, J. H.; Nieth, N.; Linden, H. B.; Blumbach, U.; Richter, F. J.; Tauchert, M. E.; Tompers, R.; Hofmann, P. *Anal. Bioanal. Chem* **2006**, *386*, 52.

(31) www.linden-cms.de.

(32) Gross, J. H. *J. Am. Soc. Mass Spectrom.* **2007**, *18*, 2254.

(33) Dawson, J. H. J.; Guilhaust, M. *Rapid. Commun. Mass Spectrom.* **1989**, *3*, 155.

(34) Nova, A.; Erhardt, S.; Jasim, N. A.; Perutz, R. N.; Macgregor, S. A.; McGrady, J. E.; Whitwood, A. C. *J. Am. Chem. Soc.* **2008**, *130*, 15499.

(35) http://fluorine.ch.man.ac.uk/research/mstool.php.

(36) http://www.chem.ualberta.ca/~massspec/atomic_mass_abund.pdf.

(37) Dransfield, T. A.; Nazir, R.; Perutz, R. N.; Whitwood, A. C. *J. Fluorine Chem.* **2010**, *131*, 1213.

(38) Reade, S. P.; Nama, D.; Mahon, M. F.; Pregosin, P. S.; Whittlesey, M. K. *Organometallics* **2007**, *26*, 3484.

(39) Jasim, N. A.; Perutz, R. N.; Archibald, S. J. *Dalton Trans.* **2003**, 2184.

(40) Beweries, T.; Brammer, L.; Jasim, N. A.; McGrady, J. E.; Perutz, R. N.; Whitwood, A. C. *J. Am. Chem. Soc.* **2011**, *133*, 14338.

(41) Choi, J.; Wang, D. Y.; Kundu, S.; Choliy, Y.; Emge, T. J.; Krogh-Jespersen, K.; Goldman, A. S. *Science* **2011**, *332*, 1545.

Chapter 4

(1) Yamashita, M.; Fenn, J. B. *J. Phys. Chem.* **1984**, *88*, 4451.

(2) Gaskell, S. J. *J. Mass Spectrom.* **1997**, *32*, 677.

(3) Henderson, W.; Cameron, E. *Inorg. Chim. Acta* **1999**, 183.

(4) *Mass Spectrometry of Inorganic, Coordination and Organometallic Compounds,*; Henderson, W.; McIndoe, J. S., Eds.; Wiley 2005.

(5) Yamashita, M.; Fenn, J. B. *J. Phys. Chem.* **1984**, *88*, 4671.

(6) http://www.nobelprize.org/nobel_prizes/chemistry/laureates/2002/.

(7) Vanberkel, G. J.; Glish, G. L.; McLuckey, S. A. *Anal. Chem.* **1990**, *62*, 1284.

(8) Cooks, R. G.; Kaiser, R. E. *Acc. Chem. Res.* **1990**, *23*, 213.

(9) March, R. E. *J. Mass Spectrom.* **1997**, *32*, 351.

(10) http://www.nobelprize.org/nobel_prizes/physics/laureates/1989/paul-lecture.html.

(11) O'Hair, R. A.; *J. Chem. Commun.* **2006**, 1469.

(12) Hoffmann, E. d.; Stroobant, V. *Mass Spectrometry Principles and Application*; 3rd ed.; Wiley, 2007.

(13) Jennings, K. R. *Int. J. Mass spectrom.* **2000**, *200*, 479.

(14) Rijs, N. J.; Sanvido, G. B.; Khairallaha, G. N.; O'Hair, R. A. J. *Dalton Trans.* **2010**, *39*, 8655.

(15) Rijs, N. J.; O'Hair, R. A. J. *Organometallics* **2010**, *29*, 2282.

(16) Felder, T.; Rohrich, A.; Stephan, H.; Schalley, C. A. *J. Mass Spectrom.* **2008**, *43*, 651.

(17) Butschke, B.; Schwarz, H. *Organometallics* **2010**, *29*, 6002.

(18) Hammad, L. A.; Gerdes, G.; Chen, P. *Organometallics* **2005**, *24*, 1907.

(19) Rodgers, M. T.; Armentrout, P. B. *Mass Spectrom. Rev.* **2000**, *19*, 215.

(20) Ham, B. M.; Cole, R. B. *Anal. Chem.* **2005**, *77*, 4148.

(21) Boxford, W. E.; Dessent, C. E. H. *Phys. Chem. Chem. Phys.* **2006**, *8*, 5151.

(22) Wang, X. B.; Sergeeva, A. P.; Xing, X. P.; Massaouti, M.; Karpuschkin, T.; Hampe, O.; Boldyrev, A. I.; Kappes, M. M.; Wang, L. S. *J. Am. Chem. Soc.* **2009**, *131*, 9836.

(23) Boxford, W. E.; Pearce, J. K.; Dessent, C. E. H. *Chem. Phys. Lett.* **2004**, *399*, 465.

(24) Taylor, C. J.; Wu, B.; Dessent, C. E. H. *Int. J. Mass spectrom.* **2008**, *276*, 31.

(25) Burke, R. M.; Boxford, W. E.; Dessent, C. E. H. *J. Chem. Phys.* **2007**, *126*.

(26) http://fluorine.ch.man.ac.uk/research/mstool.php.

(27) Kaluderovic, G. N.; Vasiljevic, T. M.; Lausevic, M. D.; Gaballa, A. S.; Sabo, T. J. *Monatsh. Chem.* **2009**, *140*, 553.

(28) Jasim, N. A.; Perutz, R. N.; Archibald, S. J. *Dalton Trans.* **2003**, 2184.

(29) Du, L. S.; Schurko, R. W.; Lim, K. H.; Grey, C. P. *J. Phys. Chem.* **2001**, *105*, 760.

(30) Brown, G. M.; Walker, L. A. *Acta Cryst.* **1966**, *20*, 220.

Chapter 5

(1) Eller, K.; Schwarz, H. *Chem. Rev.* **1991**, *91*, 1121.

(2) O'Hair, R. A.; J. *Chem. Commun.* **2006**, 1469.

(3) Fornarini, S. *Mass Spectrom. Rev.* **1996**, *15*, 365.

(4) Stone, J. A. *Mass Spectrom. Rev.* **1997**, *16*, 25.

(5) Gross, M. L.; Lin, P. H.; Franklin, S. J. *Anal. Chem.* **1972**, *44*, 974.

(6) Reid, G. E.; O'Hair, R. A. J.; Styles, M. L.; McFadyen, W. D.; Simpson, R. J. *Rapid Commun. Mass Spectrom.* **1998**, *12*, 1701.

(7) Combariza, M. Y.; Vachet, R. W. *J. Am. Soc. Mass. Spectrom.* **2002**, *13*, 813.

(8) Combariza, M. Y.; Fermann, J. T.; Vachet, R. W. *Inorg. Chem.* **2004**, *43*, 2745.

(9) Combariza, M. Y.; Fahey, A. M.; Milshteyn, A.; Vachet, R. W. *Int. J. Mass spectrom.* **2005**, *244*, 109.

(10) Combariza, M. Y.; Vachet, R. W. *J. Am. Soc. Mass. Spectrom.* **2004**, *15*, 1128.

(11) Sellers-Hahn, L.; Russell, D. R. *J. Am. Chem. Soc.* **1990**, *112*, 5953.

(12) Simpson, M. J. Doctor of Philosophy, University of Birmingham, 2010.

(13) Gronert, S. *Mass Spectrom. Rev.* **2005**, *24*, 100.

(14) Rijs, N. J.; O'Hair, R. A. J. *Organometallics* **2010**, *29*, 2282.

(15) Rijs, N. J.; Sanvido, G. B.; Khairallaha, G. N.; O'Hair, R. A. J. *Dalton Trans.* **2010**, *39*, 8655.

(16) Annibale, G.; Brandolisio, M.; Pitteri, B. *Polyhedron* **1995**, *14*, 451.

(17) Price, J. D. H.; Williamson, A. N.; Schramm, R. F.; Wayland, B. B. *Inorg. Chem.* **1972**, *11*, 1280.

Chapter 6

(1) Vilar, R.; Mingos, D. M. P.; White, A. J. P.; Williams, D. *J. Angew. Chem., Int. Ed.* **1998**, *37*, 1258.

(2) Mareque Rivas, J. C.; Brammer, L. *New J. Chem.* **1998**, *22*, 1315.

(3) Jeffrey, J. C.; McCleverty, J. A.; Ward, M. D. *Angew. Chem., Int. Ed.* **1998**, *37*, 1279.

(4) Aakeroy, C. B.; Seddon, K. R. *Chem. Soc. Rev.* **1993**, *22*, 397.

(5) Subramanian, S.; Zaworotko, M. J. *Coord. Chem. Rev.* **1994**, *137*, 357.

(6) Crabtree, R. H. *The Organometallic Chemistry of the Transition Metals*; 3rd ed.; Wiley 2001.

(7) Jasim, N. A.; Perutz, R. N. *J. Am. Chem. Soc.* **2000**, *122*, 8685.

(8) Hille, B. In *Ionic Channels of Excitable Membranes*; Second Edition ed.; Sinauer Associates, Inc: Sunderland, Massachusetts, USA, 1992, p 607.

(9) Emsley, J.; Reza, N. M.; Dawes, H. M.; Hursthouse, M. B. *J. Chem. Soc., Dalton Trans.* **1986**, 313.

(10) Brammer, L.; Swearingen, J. K.; Bruton, E. A.; Sherwood, P. *Proc. Nat. Acad. Sci. USA* **2002**, *99*, 4956.

(11) Bentrup, U.; Feist, M.; Kemnitz, E. *Prog. Solid State Chem.* **1999**, *27*, 75.

(12) Berger, R.; Resnati, G.; Metrangolo, P.; Weber, E.; Hulliger, J. *Chem. Soc. Rev.* **2011**, *40*, 3496.

(13) Pimentel, G. C.; McClellan, A. L. *The Hydrogen Bond*; Reinhold Publishing corporation: New York, 1960.

(14) Vinogradov, S. N.; Linnell, R. H. *Hydrogen Bonding*; Van Nostrand Reinhold: New York, 1971.

(15) Kovacs, A.; Varga, Z. *Coord. Chem. Rev.* **2006**, *250*, 710.

(16) Huggins, M. L. *Angew. Chem. Int. Ed.* **1971**, *10*, 147.

(17) Jeffrey, G. A. *An Introduction to Hydrogen Bonding*; Oxford University: Oxford, 1997.

(18) Brammer, L.; Bruton, E. A.; Sherwood, P. *Cryst. Growth Des.* **2001**, *1*, 277.

(19) Peris, E.; Wessel, J.; Patel, B. P.; Crabtree, R. H. *J. Chem. Soc., Chem. Commun.* **1995**, 2175.

(20) Montoro, T.; Jouvet, C.; Lopezcampillo, A.; Soep, B. *J. Phys. Chem.* **1983**, *87*, 3582.

(21) Abraham, M. H.; Grellier, P. L.; Prior, D. V.; Taft, R. W.; Morris, J. J.; Taylor, P. J.; Laurence, C.; Berthelot, M.; Doherty, R. M.; Kamlet, M. J.; Abboud, J. L. M.; Sraidi, K.; Guiheneuf, G. *J. Am. Chem. Soc.* **1988**, *110*, 8534.

(22) Libri, S., University of Sheffield, 2011.

(23) Blanks, R. F.; Prausnitz, J. M. *J. Chem. Phys.* **1963**, *38*, 1500.

(24) Purcell, K. F.; Stikelea.Ja; Brunk, S. D. *J. Mol. Spectrosc.* **1969**, *32*, 202.

(25) Cativiela, C.; Garcia, J. I.; Mayoral, J. A.; Salvatella, L. *Can. J. Chem.* **1994**, *72*, 308.

(26) http://evans.harvard.edu/pdf/evans_pka_table.pdf.

(27) Metrangolo, P.; Resnati, G. *Chem. Eur. J.* **2001**, *7*, 2511.

(28) Metrangolo, P.; Pilati, T.; Resnati, G. *Crystengcomm* **2006**, *8*, 946.

(29) Brammer, L.; Espallargas, G. M.; Libri, S. *Crystengcomm* **2008**, *10*, 1712.

(30) Beweries, T.; Brammer, L.; Jasim, N. A.; McGrady, J. E.; Perutz, R. N.; Whitwood, A. C. *J. Am. Chem. Soc.* **2011**, *133*, 14338.

(31) Lu, J.; Zhang, B.; Deng, Q.; Wang, J.; Lu, Y.; Zhu, W. *Int. J. Quantum Chem* **2010**, *111*, 2352.

(32) Metrangolo, P.; Neukirch, H.; Pilati, T.; Resnati, G. *Acc. Chem. Res.* **2005**, *38*, 386.

(33) Wasilewska, A.; Gdaniec, M.; Polonski, T. *Crystengcomm* **2007**, *9*, 203.

(34) Libri, S.; Jasim, N. A.; Perutz, R. N.; Brammer, L. *J. Am. Chem. Soc.* **2008**, *130*, 7842.

(35) Valerio, G.; Raos, G.; Meille, S. V.; Metrangolo, P.; Resnati, G. *J. Phys. Chem. A* **2000**, *104*, 1617.

(36) Ammann, C.; Meier, P.; Merbach, A. E. *J. Magn. Reson.* **1982**, *46*, 319.

(37) Atkin, P. *The elements of physical chemistry*; 3rd ed.; Oxford University press: Oxford 2001.

(38) Atkin, P. *Physical chemistry*; 4th ed.; Oxford University Press: Oxford, 1990.

Chapter 8

(1) http://home.cc.umanitoba.ca/~budzelaa/gNMR/gNMR.html.

(2) http://fluorine.ch.man.ac.uk/research/mstool.php.

(3) Reade, S. P.; Nama, D.; Mahon, M. F.; Pregosin, P. S.; Whittlesey, M. K. *Organometallics* 2007, *26*, 3484.

(4) Banks, R. E.; Burgess, J. E.; Cheng, W. M.; Haszeldine, R. N. *J. Chem. Soc.* 1965, 575.

(5) Cronin, L.; Higgitt, C. L.; Karch, R.; Perutz, R. N. *Organometallics* 1997, *16*, 4920.

(6) Macgregor, S. A.; Roe, D. C.; Marshall, W. J.; Bloch, K. M.; Bakhmutov, V. I.; Grushin, V. V. *J. Am. Chem. Soc.* 2005, *43*, 15304.

(7) Uson, R.; Oro, L. A.; Cabeza, J. A.; Bryndza, H. E.; Srepro, M. P. *Inorg.Synth* 1985, *23*, 126.

(8) Gassman, P. G.; H., W. C.; David, M. W. *Organometallics* 1984, *3*, 385.

(9) Jones, R. A.; Wilkinson, G.; Colquohoun, I. J.; McFarlane, W.; Galas, A. M. R.; Hursthouse, M. B. *J. Chem. Soc., Dalton Trans.* 1980, 2480.

(10) Kohlmann, W.; Werner, H. *Z. Naturforsch B* 1993, *48*, 1499.

(11) Gusev, D. G.; Hubener, R.; Burger, P.; Orama, O.; Berke, H. *J. Am. Chem. Soc.* 1997, *119*, 3716.

(12) Jasim, N. A.; Perutz, R. N.; Foxom, S. P.; Walton, P. H. *J. Am. Chem. Soc., Dalton Trans* 2001, 1676.

(13) Evans, I. P.; Spencer, A.; Wilkinso, G. *J. Chem. Soc., Dalton Trans.* 1973, 204.

(14) Bautista, M. T.; Cappellani, E. P.; Drouin, S. D.; Morris, R. H.; Schweitzer, C. T.; Sella, A.; Zubkowski, J. *J. Am. Chem. Soc.* 1991, *113*, 4876.

(15) Lilie, J.; Shinohara, N.; Simic, M. G. *J. Am. Chem. Soc.* 1976, *98*, 6516.

(16) Cariati, F.; Monica, G. L. *Inorg. Synth.* 1968, *11*, 105.

(17) Tayim, H. A.; Aklj, N. S. *Inorg, Nucl. Chem.* 1974, *36*, 1071.

(18) Yahav, A.; Goldberg, I.; Vigalok, A. *Inorg. Chem.* 2005, *44*, 1547.

(19) Price, J. D. H.; Williamson, A. N.; Schramm, R. F.; Wayland, B. B. *Inorg. Chem.* 1972, *11*, 1280.

(20) Annibale, G.; Brandolisio, M.; Pitteri, B. *Polyhedron* 1995, *14*, 451.

(21) Abel, E. W.; Wilkinson, G. *J. Chem. Soc.* 1959, 1501.

(22) Staal, L. H.; Oskam, A.; Vrieze, K. *J. Organomet. Chem.* 1979, *170*, 235.